UNIVERSITY OF SOUTHAMPTON

LIQUID CRYSTALLINITY AND THE ROLE OF MOLECULAR FLEXIBILITY

by

Ian David Fletcher

A dissertation submitted in partial
fulfilment of the requirements for
the degree of Doctor of Philosophy
at the University of Southampton

Department of Chemistry

July 1993

UNIVERSITY OF SOUTHAMPTON

ABSTRACT

FACULTY OF SCIENCE

CHEMISTRY

Doctor of Philosophy

LIQUID CRYSTALLINITY AND THE ROLE OF MOLECULAR FLEXIBILITY

by Ian David Fletcher

The work presented in this thesis examines the relationship between the structure of several new series of dimeric liquid crystals and the occurence of liquid crystalline behaviour. The alkyl spacer is shown to have a critical influence on the mesogenicity of these compounds. Chapter 1 introduces the reader to the liquid crystal phase and outlines the experimental techniques used to characterise its structure. A novel series of dimeric liquid crystals is presented in chapter 2, the α,ω-bis(4-alkylphenylimino-benzylidene-4'-oxy)alkyldiynes. The influence of a central diacetylene unit in the alkyl spacer on liquid crystalline behaviour is highlighted. Compared to the rich smectic polymorphism of their saturated analogues only smectic A and C behaviour is observed. In chapter 3 two series of racemic dimeric liquid crystals with branched terminal alkyl chains are reported and as expected their clearing temperatures are lower than those of their straight chain analogues. Their chiral analogues were also synthesised and in one series exhibit blue phase liquid crystalline behaviour; this is the first reported instance for dimeric systems. Chapter 4 investigates the mesogenicity of the 4-*n*-alkyloxycinnamic acids when linked together or to a 4-cyanobiphenyl group via a flexible spacer. Chapter 5 investigates the symmetry of a reported biaxial nematic liquid crystal. A deuterium NMR experiment is outlined which shows how it is possible to obtain a direct measure of the biaxiality of nematic phases exhibited by thermotropic liquid crystals. Finally, chapter 6 presents the liquid crystalline behaviour of novel disc-rod dimers when mixed with the electron acceptor TNF. In this chapter we also present results of X-ray diffraction and deuterium NMR studies of discotic dimers when mixed with varying amounts of TNF.

CONTENTS

Acknowledgements

I would like to thank my supervisor, Professor G.R. Luckhurst, for his continued support, guidance and above all patience which have seen me through to completing this thesis.

I must also thank Doctor G.S. Attard and my industrial supervisor, Doctor S.K. Heeks at the G.E.C. Hirst Research Centre, Wembley, for the interest they have taken in my work and for the help and advice they have given me whenever possible.

I am grateful to Andrew Blatch for carrying out countless X-ray diffraction experiments, to Steve Roskilly for the surface tensor calculations which appear in chapter 5, and to Mark Tearle for allowing me to use the deuterium NMR results which are described in chapter 6. I would like to express my thanks to Chris Dunn, Andrew Douglass and Jason Hughes for proofreading various parts of this thesis. I must also mention Peter Barnes and Flávio Bezerra dos Santos for helping to make my time in the lab such a memorable one.

I am very grateful to Professor H. Finkelmann for allowing me to visit his research group at the Makromolekulare Institut, Freiburg, Germany, where I prepared the cinnmaic acid derivatives prsented in chapter 4.

I would like to express my gratitude to Doctor Kolinski at the G.E.C. Hirst Research Centre, Wembley, for carrying out the non-linear optics measurements discussed in chapter 2. I must also thank Doctor Coates at Merck Ltd.,Poole, for allowing me to carry out the Cano wedge experiments which appear in chapter 3.

Finally, I am grateful to the SERC for the award of a CASE studentship.

CHAPTER 1

Molecular structure and the liquid crystalline state

1. Introduction to liquid crystals

For a long time it was thought that there were only three states of matter, that is solid, liquid and gas. However, between the solid and the liquid states there is a state known as the liquid crystal phase which has now become well-established as a distinct state of matter [1]. The discovery of the liquid crystal state in 1888 was, like many discoveries, made by accident. An Austrian botanist, trying to determine the structure of cholesterol, noticed that the derivative cholesteryl benzoate had two distinct melting points; it first melted to a turbid liquid at 145.5°C which only on further heating to 178.8°C became clear [2]. Subsequent analysis of cholesteryl benzoate was made by Lehmann, a German physicist well-known for his studies of melting behaviour, who showed the *in between phase* or mesophase to have properties common to both the liquid and crystal phases [3]. For example, the mesophase flowed like a liquid yet was birefringent, that is to say showed double refraction, a property common to crystals. This combination of properties, on the one hand mechanically liquid-like and on the other optically crystal-like, led to the name liquid crystal - a term which has remained ever since it was first assigned at the turn of the century.

Compounds which form the liquid crystal phase are also known as mesogens and are principally divided into two types. (i) Lyotropic liquid crystal compounds have a polar head group attached to an alkyl chain and hence are amphiphilic. The phases they form are based on micellar aggregates of amphiphilic molecules, whose structure, although has a temperature dependence, is mainly related to their concentration in a single or multi-solvent system. The study of lyotropic liquid crystals will not be

dealt with in this thesis and so for a detailed treatment the reader is referred to the review in [4]. (ii) Thermotropic liquid crystal compounds form phases which are based on specific molecular arrangements which have a temperature dependence. Thus when a thermotropic liquid crystal compound melts a transition to a mesophase occurs which on further heating can undergo transitions to other mesophases before clearing into the isotropic liquid. It should be noted, however, that the distinction between lyotropic and thermotropic liquid crystals is not clear and compounds known as amphitropic liquid crystals can exhibit both types of mesophase.

Thermotropic liquid crystals tend to have a high degree of shape anisotropy and this is important for the forces which stabilise the liquid crystal phases. Consequently thermotropic liquid crystal phases are most commonly formed from rod-like or disc-like molecules or even exotic combinations of both [5]. Not all liquid crystal compounds form phases above the melting point (enantiotropic phase) but instead it is often necessary to supercool the isotropic liquid below the melting point with the hope that a liquid crystal phase will form (monotropic phase) before freezing occurs.

2. The molecular structure of liquid crystal phases

In this section we describe the structural features of the liquid crystal phases pertinent to the work described in the following chapters. A detailed summary of the many thermotropic liquid crystal phases is given in [6,7].

2.1. *The nematic phase (N)*

The nematic phase is the most disordered of the liquid crystal phases formed by rod-like molecules. In this phase the molecular centres of gravity are disordered at long range as in a liquid, that is there is no positional order, but there exists in any one domain a statistical parallel arrangement of the molecular long axes along an axis known as the director, **n**, giving long range orientational order (see figure 1).

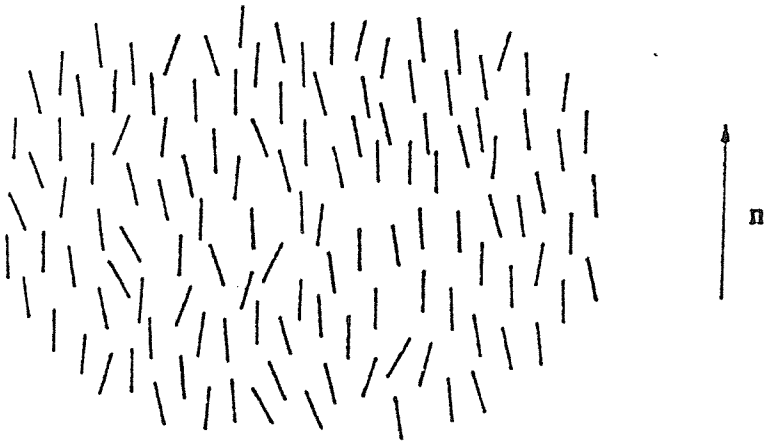

Figure 1. A snapshot of the molecular order in the nematic phase.

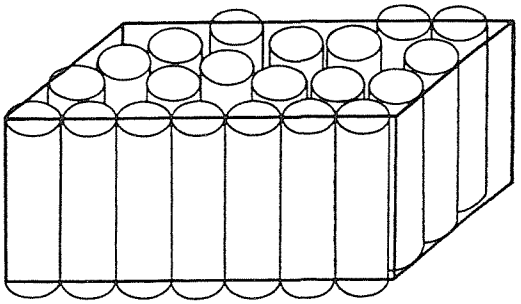

Figure 2. The layered arrangement of the molecules in the smectic A phase.

2.2. *The smectic A phase (S_A)*

The smectic A phase is the least ordered of all the smectic phases formed by rod-like molecules. In the smectic A phase the molecules are randomly arranged in layers and the director is orthogonal to the layer planes (see figure 2). There exists unhindered rotational motion about the molecular long axis and there is no long range positional order in the planes of the smectic layers. The layers are liquid-like in nature and are therefore free to slide over each other; movement of molecules between the layers also occurs readily. The lamellar thickness is different to the most extended molecular conformation and this can be attributed to various factors, such as a degree of terminal chain compression or the molecules may be tilted in random directions. It is also possible for bilayers to form of which there are two types: if the lamellar thickness is 0.5 times the molecular length the layers are said to be intercalated and if it is roughly 1.5 times then the layers are termed interdigitated (see chapter 3 for a more detailed account).

2.3. *The smectic B phases (S_B)*

There are two smectic B phases: the hexatic B and the crystal B (see figure 3). The hexatic B phase is similar to the smectic A phase in that the molecules are arranged in layers. However, unlike the smectic A phase where there is no positional ordering within the layer the molecules in the hexatic B phase have short range positional order and are ordered on a hexagonal net. The molecules in the hexagonal nets have three dimensional bond orientational order, that is the net is arranged in the same orientation from layer to layer but there are no real positional correlations of the molecules between the layers. The dimensions of the hexagonal net are small, such that the molecules lie close to one another, and molecular motion tends to be cooperative rather than free as for the smectic A phase. As a result this phase has greater orientational order than the smectic A phase but again there is no long range positional order.

The crystal B phase is highly ordered in three dimensions such that not only is the hexagonal, closed-packed arrangement within a given layer very long range but also the hexagonal net is correlated over an extremely large number of layers. In consequence, the phase is structurally crystal-like and not simply a liquid crystal phase; it is thus referred to as a crystal B phase. However, some of the physical properties of the crystal B phase are more consistent with those of a true liquid crystal than those of a crystal. For example, the phase exhibits shear and flow properties and the transitions to and from the phase are always reversible and do not undergo supercooling. These characteristics are not found when we consider a crystal, but are all normally observed when dealing with a liquid crystal. The thermodynamic transition between the two B phases has been shown to be very weakly first order or second order in nature.

2.4. *The smectic C phase (S_C)*

The smectic C phase is structurally similar to the smectic A phase except that the director is tilted by some angle, θ, to the layer normal (see figure 4). The tilt angle, θ_t, is constant over large volume elements. There is short range order of the molecular centres of mass within the layer, but there is no long range correlation between the layers apart from that of the tilt angle. The smectic layers have a liquid-like, unstructured arrangement of the molecules. The tilt angle varies from compound to compound, and may, for a given compound either vary with temperature over the range of the phase, for example following a smectic C to smectic A transition, or stay relatively constant, for example following a smectic C to nematic or isotropic transition.

2.5. *The smectic F and I phases (S_F, S_I)*

In the smectic F phase the molecules are packed in layers with their long axes tilted with respect to the layer planes. The molecules have short range positional order and

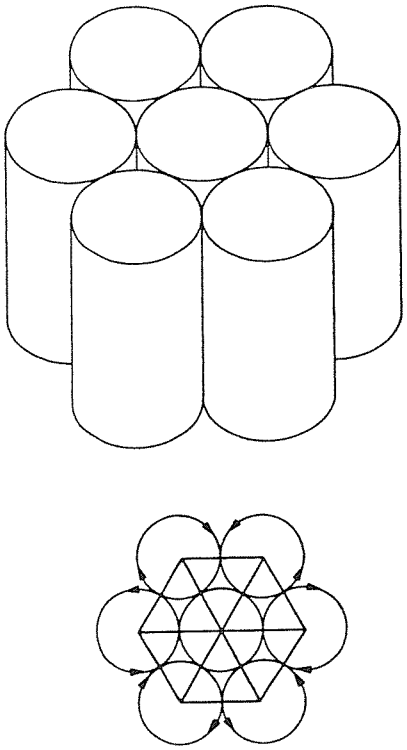

Figure 3. The hexagonal close-packed arrangement of the molecules in the smectic B phase.

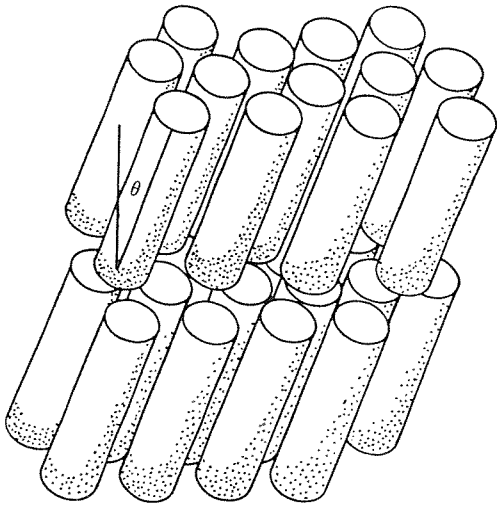

Figure 4. The tilted arrangement of the molecules in the smectic C phase.

are arranged on pseudo-hexagonal nets which are not correlated between the layers. Indeed the layers are free to slide over each other. They are however, not free to rotate relative to one another and so the phase has extensive bond orientational ordering. The smectic I phase is structurally similar to the smectic F phase. The phases differ, however, in their tilt directions. The molecules in the smectic F phase tilt towards the sides of the heaxgonal net whereas those of the smectic I phase tilt towards the apices (see figure 5).

2.6. *The smectic G and J phases (S_G, S_J)*

The molecules in the smectic G and J phases are packed in layers such that their molecular long axes are tilted with respect to the layer normal. Further, the molecules in the layers lie on a pseudo-hexagonal net which is well-correlated between the layers and consequently gives rise to a three dimensional structure. Thus the smectic G and J phases are in essence crystal phases and can be considered as the tilted analogues of the crystal B phase. Molecular rotation is restricted as the molecules in the pseudo-hexagonal nets lie too close to one another. In consequence, the molecules are envisaged as having co-operative movement about their long axes. Although the smectic G and J phases would appear to be very similar they do, however, differ in one aspect; they have different tilt directions. The molecules in the smectic G phase tilt towards an edge of the pseudo-hexagonal net, whereas in the smectic J case the tilt direction is towards an apex of the net. Hence the smectic G and J phases can be regarded as the crystal analogues of the smectic F and I phases, respectively.

2.7. *The chiral nematic phase (N^*)*

The chiral nematic phase can be formed in one of two ways - by liquid crystal chiral molecules or by dissolving a chiral molecule into a nematic host. Locally the phase order is still like a nematic phase, that is there is only long range orientational order

(*a*) (*b*)

Figure 5. The different tilt directions of the hexagonal net in the smectic F and I phases. (*a*) Tilt direction to the side of the hexagonal net for the smectic F phase and (*b*) tilt direction to the apex of the hexagonal net for the smectic I phase.

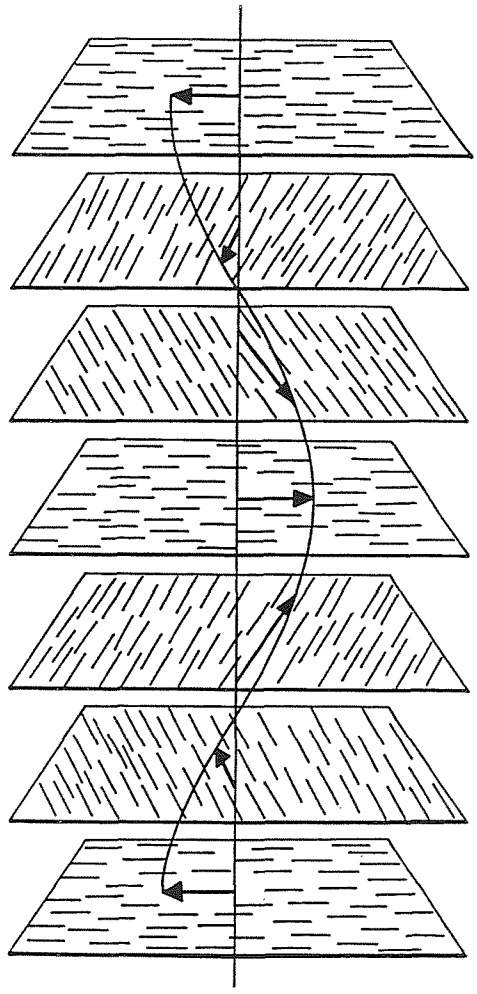

Figure 6. A schematic representation of the helical arrangement of the director in the chiral nematic phase. The arrow denotes the director **n**.

and the molecular orientation has a preferred orientation described by a director, **n**. However, the director is not constant in space and is twisted along a helical axis (see figure 6). The helix is periodic and (since the states **n** and -**n** are equivalent) the spatial period is equal to half the pitch, p. Due to the helix the optical properties of the chiral nematic phase are considerably different to those of the nematic phase. Chiral nematic phases show selective reflection of light; the maximum of this reflection lies at the wavelength λ_{max}:

$$\lambda_{max}=p.n,$$

where n is an average refractive index of one quasi-nematic layer. The helical pitch does not change very much with temperature and the chiral nematic phase is said to have a constant colour. However, if, for example, a smectic A phase transition is approached the reflected colour rapidly changes as the helix unwinds.

2.8. *The blue phases*

Blue phases (BPs) are liquid crystalline phases which exist over a very short temperature range between chiral nematic phases of small pitch and the isotropic phase. There are, at present, three BPs which exist in the phase sequence

$$N^* \text{ — BPI — BPII — BPIII — I.}$$

The BPs are chiral and have optical properties similar to chiral nematics, for example selective reflection, yet are of low birefringence. The BPI and BPII phases have a double twist structure. This structure is more stable than the helical (or single twist) structure of chiral nematic liquid crystals. Instead of having one helical axis the director in this double twist structure rotates in a helical fashion about every axis perpendicular to a line (see figure 7). At the centre of the cylinder the director is parallel to the cylinder axis. In figure 7(*a*) the cylinder axis is perpendicular to the plane of the page and the helical axes are in the plane. Figure 7(*b*) shows that the

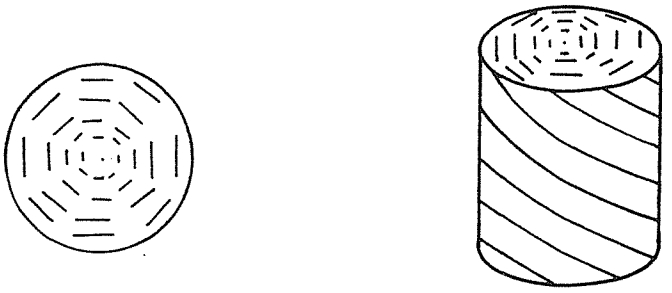

(*a*) (*b*)

Figure 7. The double twist cylinder. (*a*) A cross-sectional view with the director parallel to the cylinder axis. (*b*) A side-on view showing the director to be twisted by 45° between the centre and the outside of the cylinder.

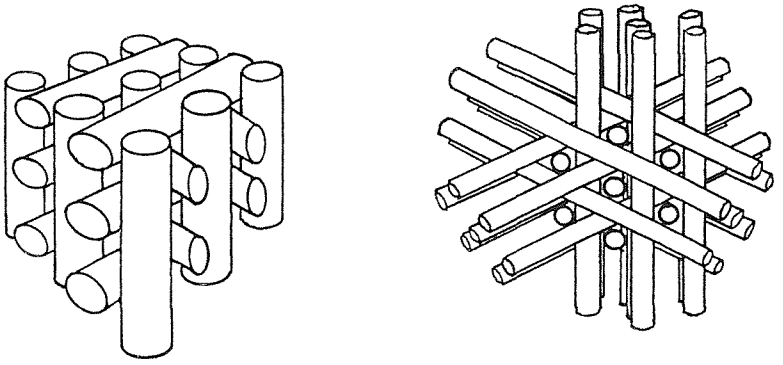

(*a*) (*b*)

Figure 8. The arrangement of the double twist cylinders in (*a*) a simple cubic lattice and in (*b*) a body-centred lattice.

director has twisted by 45° between the centre and outside of the cylinder. Although this structure is more stable than the more common single twist structure it is only stable over short distances from the centre of any cylinder. This distance is of the order of a short pitch chiral nematic liquid crystal (~500nm). Most chiral nematic liquid crystals have pitches larger than 500nm and so the double twist structure rarely occurs. To be able to fit these double twist cylinders into a three dimensional structure so that the edges match is topologically impossible: the system is said to be frustrated and disclinations, defects in the orientational arrangement of the director, are necessary in order to relieve the elastic strain energy. These defects tend to make the structure less stable than the single twist structure without defects. However, for roughly a 1°C temperature range between the chiral nematic and isotropic phases it is found that the double twist structure is slightly more stable than the single twist struture. As mentioned previously there are two known structures composed of double twist cylinders (see figure 8). These structures possess a regular array of defects at planes where double twist cylinders with different directors meet. Both structures have a cubic defect arrangement. In figure 8(*a*) the defects are positioned at the corners of the cube and in 8(*b*) they are in the corners and in the centre of the cube. The defects are thus arranged in a lattice just like molecules in a crystal. The blue phases are fluid lattices of defects and just like normal crystal lattices they can also give Bragg-like reflection. This property was used to derive the lattice constants for the BPI and BPII phases. BPs are not normally blue in colour as the reflected light depends upon the the spacing between the lattice planes and the angle between the light beam and the lattice planes (Bragg's law: $2d\sin\theta = n\lambda$). The most convincing evidence for the existence of the three BPs has been shown by DSC measurements. The transitions between all three phases is first order although the size of the entropy changes ($\Delta S/R$) is very small. For example consider the data for cholesteryl oleate [8]:

N^*—6.6 x 10^{-3}—BPI—4.4 x 10^{-3}—BPII—0.18—I.

The extent of the molecular ordering in the BPs is thus very similar to that of the chiral nematic phase.

The structure of BPIII is as yet unknown. The BPIII phase selectively reflects circularly polarised light and also exhibits rotatory power with a strength between that of the isotropic phase and BPI or BPII. Thermodynamically the BPIII phase is more similar to the BPII phase than the isotropic phase. However, visually it is more like an isotropic phase than the bright texture of BPII. There are several models for the possible phase structure of BPIII but as yet none has been proven.

2.9. *The discotic nematic phase (N_D)*

The discotic nematic phase is the least ordered of the phases formed by disc-like mesogens (see figure 9). It has long range orientational order where the symmetry axis (the disc normal) tends to lie parallel to a preferred direction called the director. The entropy change ($\Delta S/R$) for the N_D-I transition is typically smaller than that of its calamitic counterpart with $\Delta S/R$ being roughly 0.1 and this reflects the smaller degree of orientational order present in this phase. The discotic chiral nematic phase has also been reported, where now the side chains contain asymmetric centres.

2.10. *The columnar nematic phase (N_c)*

The columnar nematic phase has been reported for a binary system containing a specific concentration of 2,4,7-trinitro-9-fluorenone and [(1,2,3,5,6-pentakis-(phenylethynyl)benzene-4-oxy]nonane or tridecane (both components are not liquid crystalline) [9]. The charge transfer interaction between them leads to the formation of columns which have short range positional order and long range orientational order (see figure 10). The length of the columns, which is governed by a balance of enthalpic and entropic constraints, tends to be approximately ten molecules long. The clearing entropy change for the nematic columnar phase is of the same magnitude as that of the calamitic nematic phase with $\Delta S/R$ being about 0.4.

Figure 9. The arrangement of the molecules in a discotic nematic phase.

Figure 10. The arrangement of the molecules in a columnar nematic phase. A binary mixture of electron donor (black) and electron acceptor (grey) molecules induces the formation of the columns via charge transfer interactions.

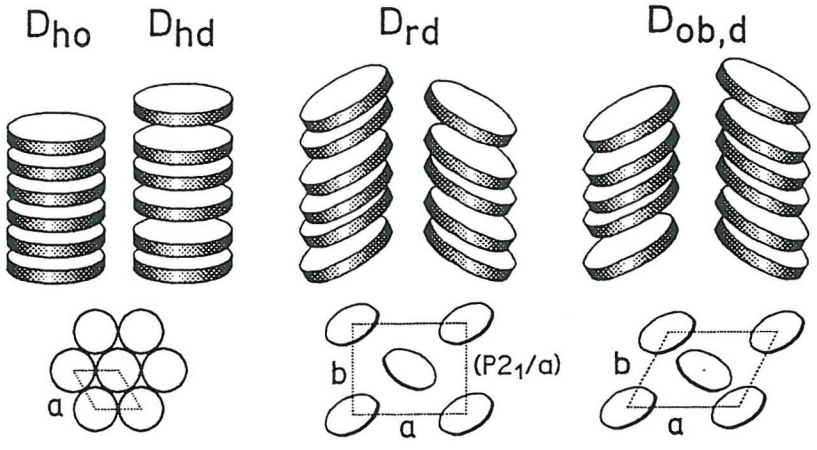

Figure 11. The structures of the discotic columnar phases with their space groups.

2.11. *The discotic columnar phases*

In the discotic columnar phases the molecules are stacked in columns which are in turn arranged into two dimensional arrays. These phases (labelled D) are classified according to the symmetry of the two dimensional unit cell of the mesophase and also to the way the molecules are stacked in the columns (see figure 11). Thus the indices h, r and ob refer, respectively, to hexagonal, rectangular and oblique arrangements of columns, while the letters o and d denote phases in which the molecules are ordered or disordered within the columns, respectively. The D_r and D_{ob} phases are comprised of columns in which on average the molecules are tilted with respect to the column axis and hence they are biaxial. The D_r phases are more complex than the D_{ob} phase: there are three D_{rd} phases each differing in their space groups, that is $P2_1/a$, P2/a and C2/m.

3. The characterisation of liquid crystal phases

There are now a range of tools available to liquid crystal researchers which can be used to characterise and distinguish the nature of the ever increasing number of liquid crystal phases. Of these there are three standard experimental techniques: polarising microscopy, differential scanning calorimetry and X-ray diffraction. All three methods have been used to help assign the liquid crystal phases reported in this thesis. In addition, we shall discuss the technique of conoscopy to help the reader understand the discussion in chapter 5 as it is important in the determination of the symmetry of liquid crystal phases. We should add deuterium nuclear magnetic resonance spectroscopy to this list as it is a powerful analytical method which is very sensitive to the degree of order in liquid crystal phases; it is described in chapter 5.

3.1. *Polarising microscopy*

The polarising microscope is the same as any common microscope except that the sample, sandwiched between two glass slides, is placed between a pair of crossed polarisers. Normally no light emerges from crossed polarisers as the light emerging from the first polariser is completely absorbed by the second polariser (or analyser) and the field of view appears dark. In addition an isotropic material does not have any effect since the polarisation of the light is unchanged as it travels through the sample. Liquid crystals are birefringent materials: uniaxial substances have two refractive indices - one parallel to the director and one perpendicular to it. The x and y components of polarised light, which are at an angle of 0° or 90° with respect to the director, pass through a uniaxial material without their direction of polarisation being altered. However, polarised light, which is incident at angles other than 0° and 90° is doubly refracted (birefringence). The light ray is split into ordinary and extraordinary rays whose polarisation direction differs by 90°. The rays thus travel through the material with different velocities and the emergent light ray, which is now out of phase, is said to have become elliptically polarised. Such polarised light is constantly rotating and will be parallel to the polarisation axis of the analyser twice during each cycle, hence some of the light will be observed. In general the presence of a liquid crystal causes the field of view to appear bright whereas with no liquid crystal it is dark. The ordering of the director is different in each liquid crystal phase and as a result interacts with polarised light in a different way. The resultant liquid crystal phase textures are the microscopic images of polarised light interacting with a specific director arrangement. Using a heating stage it is possible to observe the transitions between the optical textures as the temperature is changed. Those textures which are produced on cooling directly from the isotropic liquid are known as natural textures. However, those textures which are obtained from a preceding phase are called paramorphotic as the phase texture inherits some of its features from its predecessor.

The characterisation of the optical textures reported in this thesis was carried out on an Olympus BH-2 polarising microscope connected to a TMS90 Linkam hot stage.

3.1.1. *The nematic phase*

The nematic phase possesses three optical textures: the threaded texture, the schlieren texture and the marbled texture. The threaded texture is composed of flexible filaments which are observed to float freely in the fluid. These filaments or threads, from which the term nematic is derived, are disclinations. The schlieren texture is the most common nematic texture and consists of point singularities which possess two or four brushes. The marbled nematic texture is a homogeneous texture which exhibits sharp, straight bordered areas which impart a rock-like appearance to the preparation. All three textures are highly mobile, brightly coloured and flash when subjected to mechanical stress.

3.1.2. *The smectic A phase*

The smectic A phase exhibits two optical textures: the homeotropic and the focal-conic fan textures and these can be exhibited simultaneously. Under the polarising microscope the homeotropic texture appears black where the director is arranged orthogonally to the glass slides. The focal-conic fan texture is formed from bâtonnets which separate out from the nematic or isotropic phase and coalesce to form the focal-conic fan texture.

3.1.3. *The smectic B phases*

Polarising microscopy observations show both smectic B phases to exhibit mosaic textures when formed directly from the isotropic liquid. Both phases also exhibit paramorphotic focal-conic and homeotropic textures when formed from the smectic A phase; the backs of the focal-conic fans for the B phases are smoother than those of the smectic A phase which highlights the increased order of the director in the phase. The focal-conic fan texture is different for each B phase at the smectic A

transition. For the smectic A to hexatic B transition no transition bars (bright threads on the backs of the focal-conic fans) are usually observed but they are for the crystal B case. In addition the focal-conic fans are more angled for the crystal B rather than curved for the hexatic B phase.

3.1.4. *The smectic C phase*

The smectic C phase has two optical textures: the schlieren texture and the focal-conic texture, both of which can be exhibited simultaneously. Unlike the schlieren texture of the nematic phase only four point singularities are observed for the smectic C schlieren. For the smectic C phase the focal-conic fans tend to have a broken or sanded appearance compared to the smectic A phase.

3.1.5. *The smectic F and I phases*

The smectic F and I phases have very similar optical textures. When the smectic F phase separates directly from the isotropic liquid it can exhibit two types of texture - the mosaic texture and a texture which may be of the cylindrical, spherulitic or fan type. The mosaic texture is not a true mosaic, but instead shows mosaic platelets separated by fine lines which contain schlieren-like brushes. The texture is thus of a schlieren-mosaic nature. For the smectic I phase there are also two types of optical texture - the broken focal-conic fan and the schlieren textures. The broken focal-conic fan texture is almost identical to that of the smectic F phase but the schlieren texture has a distinct difference. The schlieren texture of the smectic I phase has typical schlieren brushes. However, for the smectic F phase, although the schlieren areas are still retained, the texture is crossed with fine mosaic lines giving a schlieren-mosaic texture.

3.1.6. *The smectic G and J phases*

The smectic G phase can exhibit a range of optical textures. The natural texture of the smectic G phase separates from the isotropic liquid via a dendritic growth pattern which leads to a mosaic texture. On cooling from the nematic phase the smectic G phase forms as large splinter-shaped particles or lancets which coalesce to form a mosaic texture composed of oblong platelets. The smectic G phase also has several other paramorphotic textures which are principally based on focal-conic fan and homeotropic or schlieren textures. There are two types of focal-conic fan textures shown by the smectic G phase: the patchwork or broken fan and the arced-broken fan textures. The patchwork texture has a chequered pattern and is normally obtained by cooling smectic A, C or F phases. The broken, arced, focal-conic fan texture of the smectic G phase is only observed on cooling the smectic B phase where the backs of the fans break into parallel arcs. A large number of mosaic textures are also exhibited by the smectic G phase and these are dependent on the nature of the preceding phase. In general, the mosaic textures have a similar type of structure to that of the B phases, where in each individual platelet the molecules have a preferential tilt direction. On cooling from the smectic C or F phases the mosaic platelets are quite large and highly coloured. However, if the smectic G phase is cooled from a homeotropically aligned B phase the mosaic platelets are small and ill-defined and are also not especially highly coloured.

As regards the optical textures of the smectic J phase it is not known at present if they are any different to those of the smectic G phase.

3.1.7. *The chiral nematic phase*

The helical structure of the chiral nematic phase has a profound effect on the optical texture. The chiral nematic phase has two optical textures: the focal-conic fan and Grandjean textures. The focal-conic fan texture is essentially the same as that for the smectic A phase and this is a result of the 'quasi-layered' structure of the chiral

nematic phase. If this phase is sheared then a planar texture called the Grandjean texture is formed. This is also known as the oily streak texture as it is composed of thick, bright disclination lines which float over the selectively reflected coloured background. The Grandjean texture is very mobile and flashes when subjected to mechanical stress.

3.1.8. *The blue phases*

If a blue phase (BPI or BPII) is cooled extremely slowly a texture composed of what looks like multicoloured single crystals (platelet texture) is formed. In the case of BPI the single crystals in this texture appear to have straight edges, whereas for BPII the edges have a more undulated appearance. Under a polarising microscope BPIII appears as a very faint, amorphous grey phase, which has been called the fog, the blue fog, the grey fog and the foggy phase before BPIII became the standard term.

3.1.9. *The discotic nematic phase*

From polarising microscopy observations the discotic nematic phase texture is of the schlieren type and visually no different from that of a calamitic nematogen.

3.1.10. *The columnar nematic phase*

The optical texture of this phase is similar to that of the schlieren nematic phase exhibited by calamitic compounds.

3.1.11. *The discotic columnar phases*

On slow cooling the optical texture of the D_{ho} phase appears as flower-like hexagons

from the isotropic liquid which then merge on further cooling into a mosaic of birefringent and homeotropic domains. Conversely the D_{hd} phase texture does not have a mosaic texture but instead focal-conic or fan-shaped textures are observed. Of the D_{rd} phases the $D_{rd(C2/m)}$ phase has typically a mosaic texture similar to that of the smectic G phase. However the $P2_1/a$ analogue has no typical textures and indeed fingerprint, striated and broken fan-shaped textures are all possible. As regards the $D_{ob,d}$ phase there are as yet no typical optical textures.

3.2. *Differential scanning calorimetry (DSC)*

This technique records the energy necessary to establish a zero temperature difference between a substance under examination and a reference material (usually an empty pan) as the temperature or time is changed. The two pans are subjected to identical temperature regimes in an environment which is heated or cooled at a controlled rate. In the DSC system the sample and reference pans are each provided with identical heaters. In consequence, it is possible to apply a null-balance principal. We can think of the system as being divided into two control loops. One mantains an average temperature control, such that the temperature of the sample and reference pans may be increased or decreased at a preset rate. The other loop ensures that if a temperature difference occurs between the sample and reference pans, due to exothermic or endothermic changes within the sample, the power input is adjusted to remove this difference. As a result the temperatures of the sample and reference pans are always kept the same by an automatic adjustment of the heater power. The signal, which is equal to the difference between the heat input to the sample and that to the reference pans, dq/dT, is recorded with respect to temperature or time.

There are two types of transition exhibited by liquid crystals and these are classified as being either first or second order in nature. In the case of first order transitions, for example a nematic to isotropic transition, the transition entropy and enthalpy changes are discontinuous, that is they are non-zero at the transition. Second order

transitions, for example a smectic C to smectic A transition, are continuous changes where the transition entropy and enthalpy are zero at the transition. First order transitions are shown as a peak in the DSC curve whereas second order changes occur as a step (see figure 12). The onset temperature can be obtained as shown in the figure and the area under the peak for a first order transition is proportional to the transitional enthalpy. From this the enthalpy and entropy changes per mole of material can be obtained. For second order transitions there is no enthalpy change but the change in the heat capacity at constant pressure can be obtained (see figure 12). The transition temperature is arbitrarily assigned as the point at which the change in specific heat capacity is one half its maximum value. In this thesis all measurements were carried out on a Perkin-Elmer DSC7 and sample weights were typically 3-5mg. Indium and zinc standards were used to calibrate dq/dT and temperature. The heating and cooling rates were $10°Cmin^{-1}$ unless stated otherwise. By taking multiple measurements the error in the transition temperatures was taken as $\pm 1°C$ and the thermodynamic data $\pm 5\%$.

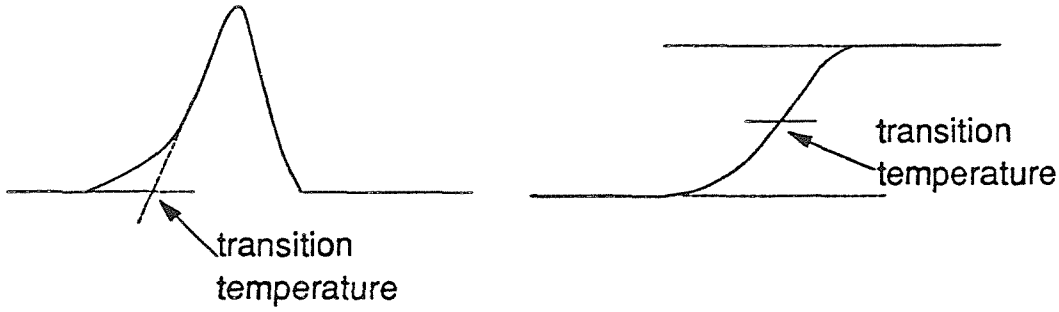

(*a*) (*b*)

Figure 12. DSC traces for (*a*) a first order transition and (*b*) a second order transition between two phases.

3.3. *X-ray diffraction*

X-ray diffraction provides a means of obtaining the local order in liquid crystal phases, where the diffraction patterns give information on periodic distances. The diffraction patterns result from interference between the diffracted X-ray waves. Waves, whose amplitudes are in-phase, combine so as to enhance one another and this is termed constructive interference. Conversely, waves, whose amplitudes are out-of-phase, cancel each other and this is known as destructive interference. The phases of waves, which are reflected by a common source are related directly to their path lengths. Figure 13 shows the reflection of two X-rays from several layers of molecules. Clearly the difference in the path length between the two rays is simply AB+BC. From simple trigonometry we find AB and BC to be equivalent and equal to $d\sin\theta$. It follows, therefore, that X-rays are in-phase when their path length difference, $2d\sin\theta$, is an integer number of wavelengths. Thus bright reflections occur when

$$n\lambda = 2d\sin\theta,$$

where n is an integer, λ is the wavelength of the X-rays, θ is the angle of incidence of the X-rays and d is the diffraction space. This relationship is known as Bragg's law and in an X-ray diffraction experiment, where the wavelength of the X-rays is known, 2θ is measured (see figure 13). For the first order Bragg reflection $n=1$ and using this the diffraction space can be easily calculated.

X-ray diffraction experiments can be carried out with aligned or powder liquid crystal samples. Powder liquid crystal samples are composed of many different domains. The powder diffraction pattern of, for example, a smectic A phase consists of an inner sharp ring, which corresponds to small angle diffraction, and an outer diffuse ring, which is known as the wide angle diffraction. The inner ring corresponds to the layer spacing and the outer one to the side-by-side molecular distances. For an aligned smectic A phase the diffraction pattern consists of an inner pair of sharp diffraction spots at small angle and at wide angle a diffuse pair of arcs (see figure 14).

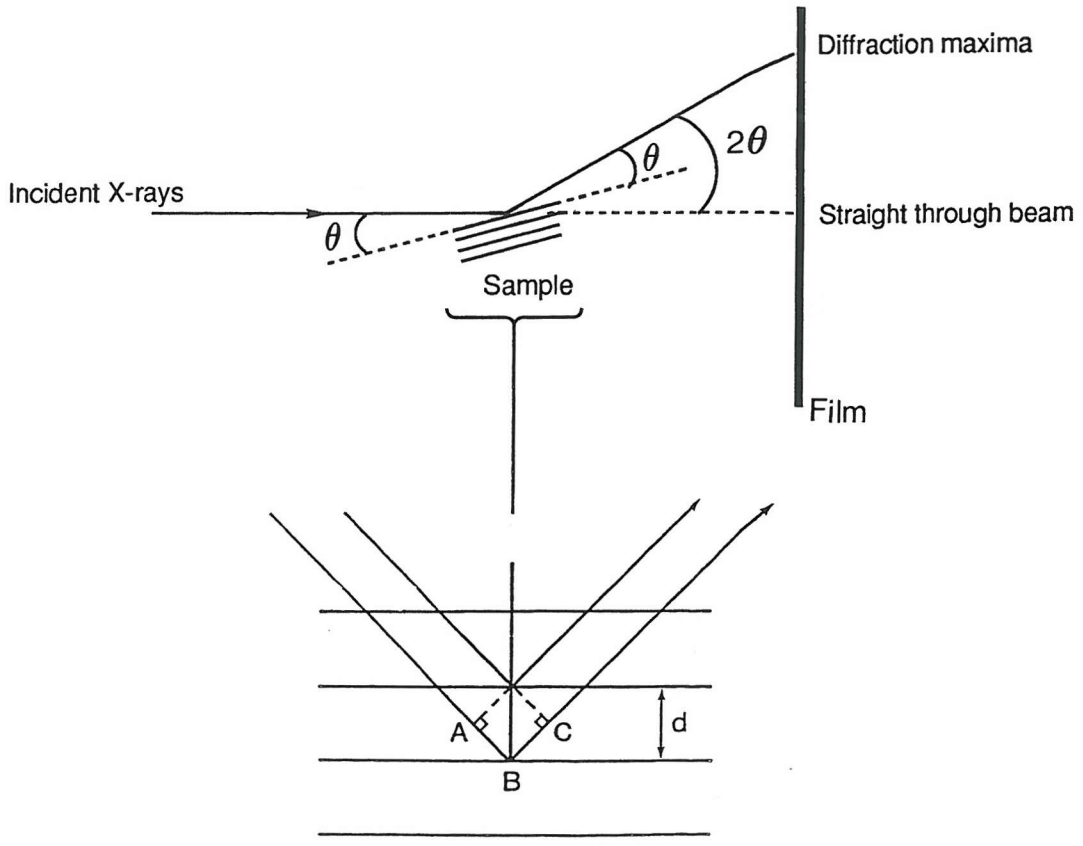

Figure 13. A schematic representation of the reflection of X-rays from a stack of lattice planes.

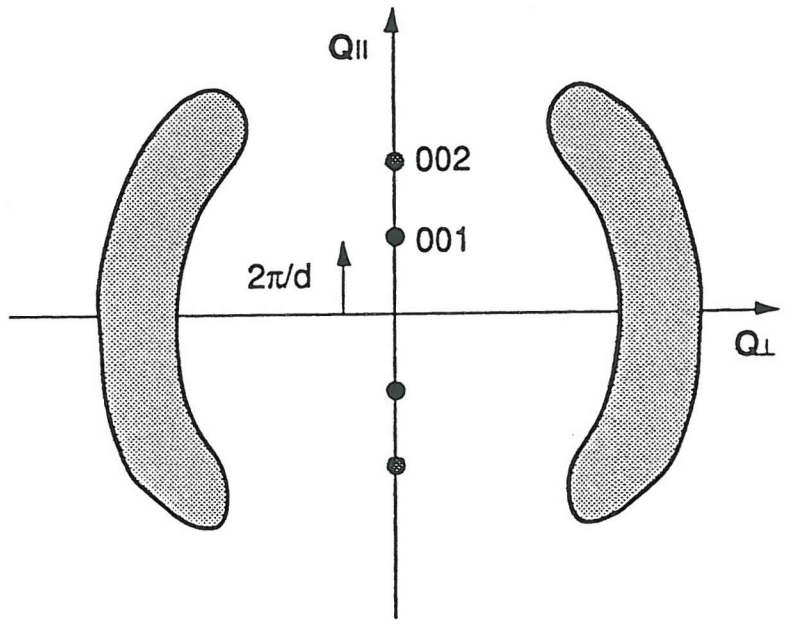

Figure 14. The diffraction pattern for an aligned smectic A phase.

The X-ray diffraction experiments in this thesis were carried out with a home-made Guinier-type diffraction camera using Cu-$K_{\alpha 1}$ radiation (λ=0.154nm). A magnetic field was used to align the nematic phase.

3.4. *Conoscopy*

Microscopy is the observation of a samples' magnified image in polarized light and allows the examination of the samples' optical character in one direction only, that is that parallel to the objective. Conoscopy differs from orthoscopy in that an interference figure or directions image is observed instead of the magnified image of the object when a strongly convergent beam of light is passed through the sample; this allows the simultaneous examination of the samples' optical character in many directions. The polarizing microscope can be used as a conoscope by inserting a Bertrand lens into the optical tube above the objective so that the back focal plane of the objective can be examined (see figure 15). Light passing through the polariser P is concentrated by the condenser C,N upon the object X. The divergent rays pass through the objective and converge again in the upper focal plane U of the objective to form a real image, each point of which is the focal point of light which has passed in a definite direction through the sample, hence the name directions image. Two important parameters are necessary for the observation of good interference figures in conoscopic work: one is the size of the microscope aperture and the other is the sample thickness. The former should be as wide as possible and the latter should be between 25-100μm. In addition the liquid crystal sample should be well-aligned so that the optic axis of the phase is parallel to the observation direction. Hence homeotropic alignment is required. For uniaxial liquid crystals the interference figure appears as a dark, blurred Maltese cross with concentric interference rings (see figure 16(*a*)). Any one convergent light ray incident at an angle other than 0° or 90° to an anisotropic sample is doubly refracted. The ordinary and extraordinary light waves produced travel through the sample at different velocities. If the phase difference between them, when they emerge from the sample, is exactly one wavelength or an integer of wavelengths the two waves are said to be out-of-phase. In consequence,

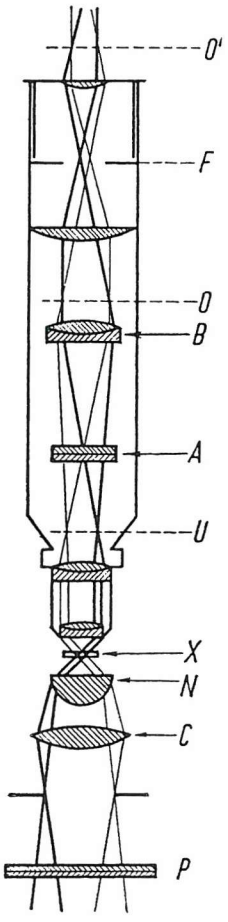

Figure 15. The microscope used as a conoscope. Rays which pass through the sample X in the same direction are emphasised equally in the figure. Where such rays are brought into focus, that is at U and F, an interference figure is formed. Where rays which emanate from the same point on the sample are focussed, that is at O and O', an object image is formed, P, A and B are the polariser, analyser and Bertrand lens, respectively.

(*a*)

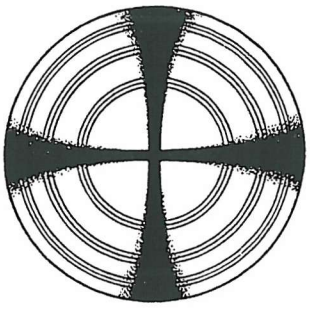

(*b*)

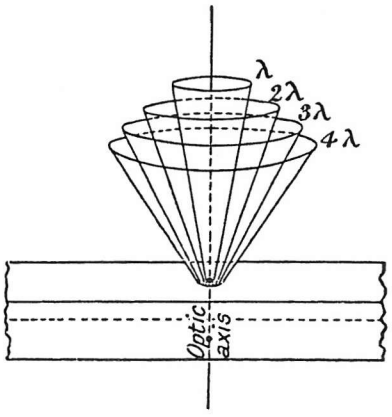

(*c*)

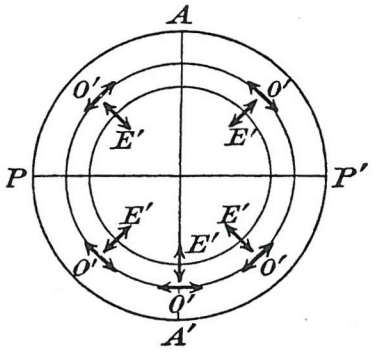

Figure 16. (*a*) An interference figure for a uniaxial phase. (*b*) Concentric cones of equal retardation around the optic axis of a uniaxial phase. (*c*) The vibration directions of the ordinary (O') and the extraordinary rays (E') with respect to the polariser (P, P') and analyser (A, A').

they interfere destructively and darkness results. Conversely, if the emergent waves have a phase difference which is multiples of half wavelengths they are said to be in-phase. They interfere constructively and brightness occurs. Thus a pattern of bright and dark rings, the so-called isochromes, is formed around the optic axis (see figure 16(*b*)). For uniaxial systems the extraordinary rays vibrate in planes which include the sample axis (see figure 16(*c*)). The ordinary rays, however, vibrate perpendicuarly to the extraordinary rays or tangentially to the interference rings (see figure 16(*c*)). Areas in the interference figure with vibration directions parallel to the polarisers, that is north-south and east-west, undergo extinction and darkness results producing the interference figure of a cross. This figure is also called an isogyre (sites of identical vibration directions). In the central portion of the interference figure the rays are parallel to the optic axis, they do not undergo double refraction and hence here, the figure appears black. On rotating the microscope stage the Maltese cross remains in the same position and does not break up indicating that the optic axis is in line with the microscope axis.

Biaxial phases produce interference figures in much the same way as in the uniaxial case except now the effect of two optic axes must be taken into account. In order to obtain a monodomain sample both the major axis and one of the minor axes must be aligned in a preferred direction. This can be achieved by chemically treating the surface of the glass slides together with an external field; one method must align one axis (for example the major axis) homeotropically and the other must align one axis (one of the minor axes) homogeneously. Conoscopic investigations on monodomain biaxial liquid crystals produce an interference figure as shown in figure 17(*a*). It consists of two eyes or melatopes, which mark the points of emergence of the optic axes from the sample, and are surrounded by interference rings. The inner rings are nearly circular and surround each eye individually whereas the outer ones are initially figure of eight-like before becoming oval shaped. In the extinction position two isogyres pass through the melatopes; they are narrow at their centres and broad in the middle of the figure forming a cross. When the microscope stage is rotated by 45° the cross opens up and splits into two hyperbolic brushes which are centred on the melatopes. The original cross is reformed on a further rotation of 45°. The isogyres

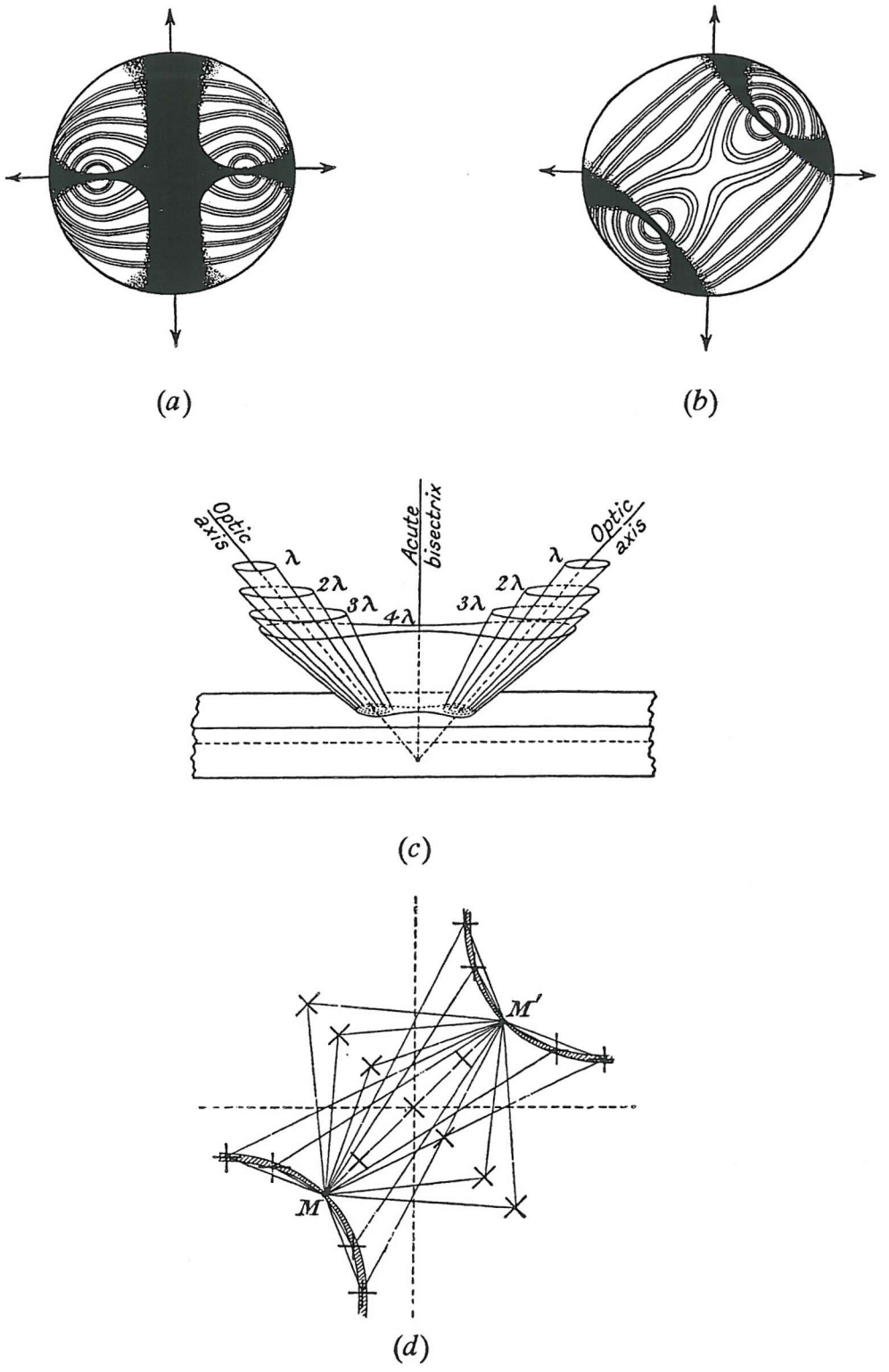

Figure 17. A biaxial phase in (*a*) the extinction position and (*b*) after a rotation of 45°. (*c*) The surfaces of equal retardation around the optic axes of a biaxial phase. (*d*) The determination of the positions of the isogyres for a biaxial phase.

revolve in a direction opposite to the movement of the microscope stage. The degree to which these brushes split gives an indication of the degree of phase biaxiality. Figure 17(*b*) shows the case for maximum biaxiality. The isochromes and isogyres are formed in exactly the same way as for uniaxial systems. The overlap of the isochromes produced by each melatope causes the formation of the figure of eight-like and oval shaped patterns (see figure 17(*c*)). The determination of the positions of the isogyres in figure 17(*b*) is shown in figure 17(*d*). MM' are the points of emergence of the optic axes. At any point on the figure, the directions of vibration may be found by joining the point to each melatope and bisecting the angles included between the lines thus drawn [10]. It is seen that when the trace of the optical axial plane is 45° from the crossed polars as shown, the directions of vibration parallel to those of the polars fall on curves which coincide with the shape of the isogyres in figure 17(*b*), whilst when it is parallel to the crossed polars, the isogyres form a cross as in figure 17(*a*).

4. Structure-property relationships of dimeric liquid crystals

Dimeric liquid crystals have now become well-established not only because of their fundamental interest but also as their properties are used to model the behaviour of thermotropic, semi-flexible, liquid crystalline polymers [11]. Symmetric, dimeric liquid crystals are typically composed of two mesogenic groups linked together by a flexible chain, or spacer, as shown in figure 18. The mesogenic groups can also have terminal substituents. As we shall see the types of spacer and terminal groups have a profound effect on the liquid crystalline properties of this class of liquid crystal.

Figure 18. A schematic representation of a symmetric dimeric liquid crystal.

4.1. *The nature of the spacer*

The spacer group plays a significant role in determining the liquid crystalline properties of the dimer. When Vorländer synthesised the first dimeric liquid crystals, the α,ω-bis(4-alkyloxyphenyl-4'-azophenyl)alkanedioates (see structure (1)), he discovered the strong dependence of the clearing temperatures on the number of methylene units in the spacer. This was particularly apparent when comparing the enantiotropic oxalic acid derivative, whose clearing temperature was so high that it decomposed before reaching it, and the monotropic malonic acid derivative, whose liquid crystal to isotropic transition was so low that it could only be estimated by mixture experiments [12].

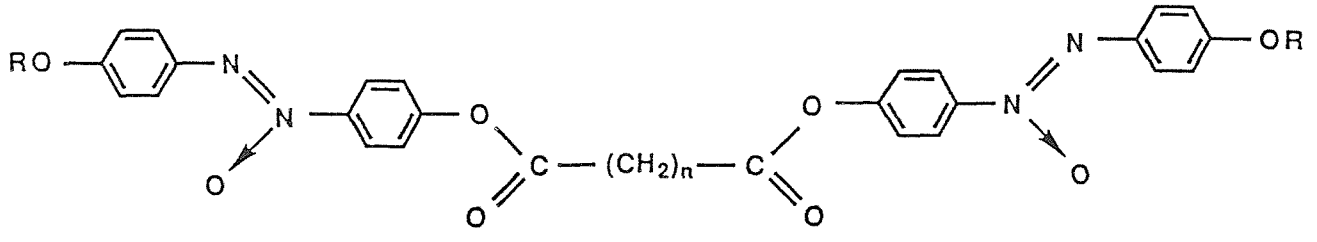

(1)

A strong odd-even effect becomes apparent when comparing the T_{NI} values on varying the number of methylene units, n, in the spacer chain for a homologous series. Figure 19 illustrates this common property as exemplified by the α,ω-bis(4'-cyanobiphenyl-4-yloxy)alkanes [13]. The T_{NI} values for the even membered homologues lie on a decreasing curve, whereas those for the odd membered homologues lie on a curve which at first rises before falling steadily; the T_{NI} values for the even membered homologues are consistently higher than those for the odd membered homologues. As a result the odd-even effect for T_{NI} is large at the beginning and then attenuates on increasing n. Simplistically this can be rationalised by considering molecules in their all *trans* conformation. It is seen that dimers with an odd number of methylene units assume a conformation in which the terminal mesogenic units lie at approximately 108° to each other, whereas even membered

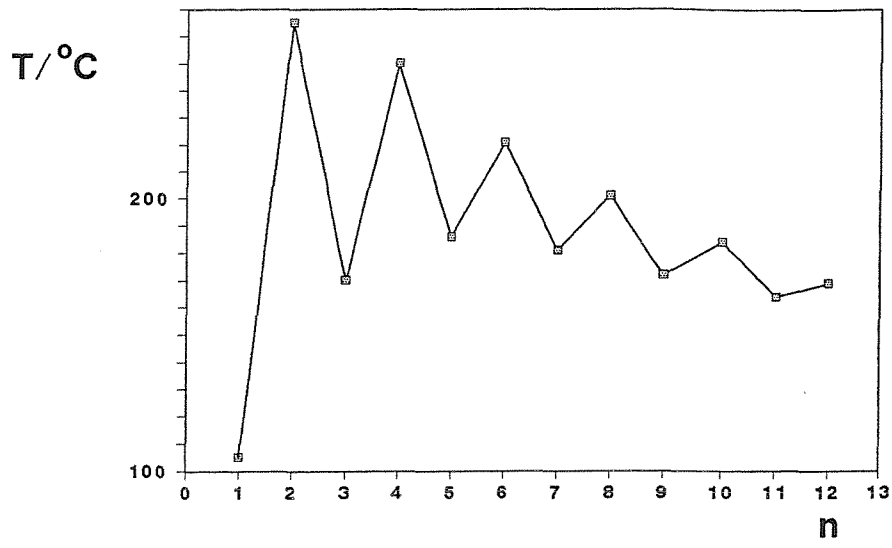

Figure 19. The influence of the number of carbon atoms in the spacer, *n*, on the nematic to isotropic transition temperature for the α,ω-bis-(4'cyanobiphenyl-4-yloxy)alkanes.

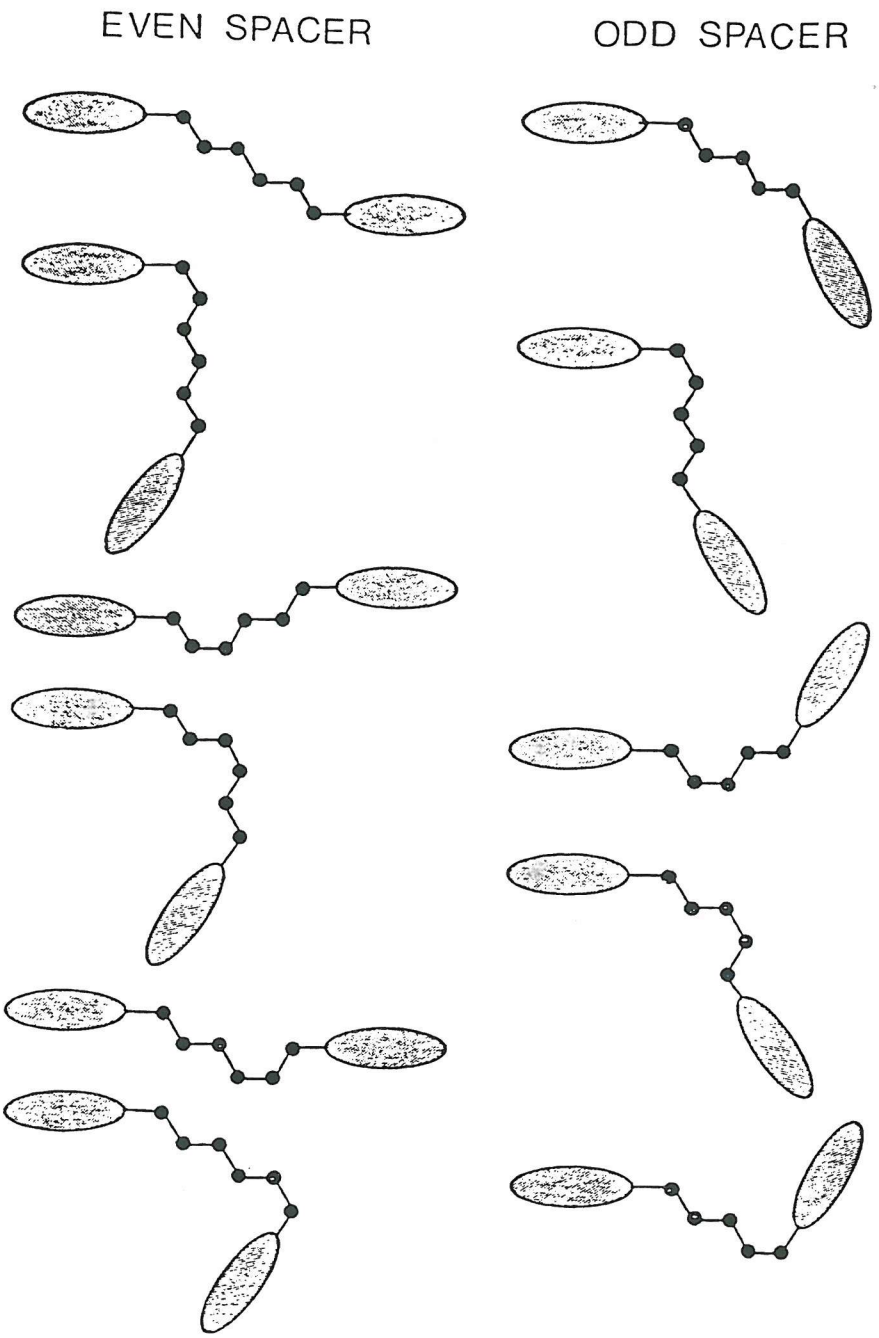

Figure 20. The effect of incorporating a *gauche* linkage in the spacer for an even and odd membered dimeric liquid crystal.

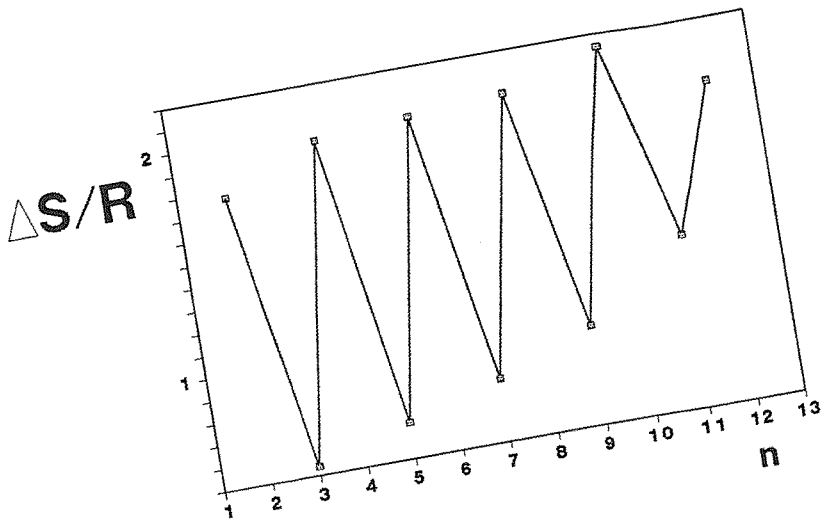

Figure 21. The influence of the number of carbon atoms in the spacer, n, on the nematic to isotropic entropy change for the α,ω-bis(4'-cyanobiphenyl-4-yloxy)alkanes.

spacers allow the mesogenic groups to lie parallel to one another. This is rather too simplistic a view since the spacer is flexible. Instead it is better to think of even membered spacers giving rise to significantly more conformations which allow a parallel arrangement of the mesogenic groups as compared to odd membered spacers. This is illustrated by figure 20 which shows the effect of incorporating a *gauche* linkage in the spacer for an odd and an even membered spacer. Conformations for which the mesogenic groups are parallel enhance the molecular anisotropy and hence stabilise liquid crystalline behaviour. The clearing temperature falls as the length of the spacer increases since the spacer tends to act as a diluent and progressively reduces the anisotropy of molecular polarisability. The initial rise in the clearing temperatures for the odd membered homologues can be attributed to an increase in molecular anisometry brought about by an increase in the length of the spacer despite the bent conformation which is subsequently offset by an increase in the number of bent conformations.

The nematic to isotropic entropy change (plotted as the dimensionless quantity $\Delta S/R$) alternates strongly as the spacer length is increased. Unlike the odd-even effect for the clearing temperature the odd-even effect for the clearing entropy change does not attenuate on increasing the length of the spacer. Figure 21 shows the effect of the length of the spacer on the nematic to isotropic entropy change, $\Delta S_{NI}/R$, for the α,ω-bis(4'-cyanobiphenyl-4-yloxy)alkanes [13]. The magnitude of $\Delta S_{NI}/R$ for the even membered spacers is considerably higher than that for the odd membered homologues and this reflects the difference in molecular order between liquid crystal phases composed of odd or even membered molecules. Clearly liquid crystal phases composed of dimeric molecules whose mesogenic groups lie parallel to each other are more ordered than dimeric molecules whose mesogenic groups are bent with respect to each other. As the clearing entropy change represents an order to disorder change the entropy change is larger for an even membered than for an odd membered dimeric liquid crystal. The values for the odd and even membered homologues tend to lie on two steadily rising curves and reflect the concomitant increase in molecular weight.

Creed and coworkers [14] have studied the effect of the spacer on the transition temperatures for dimeric liquid crystals by using three different five-membered spacer groups, that is pentamethylene, diethylene oxide and disiloxane, and keeping the terminal mesogenic group, 4'-cyanobiphenyl-4-yloxy or 4-pentyloxyphenylcinnamate, constant (see structures (2) and (3), respectively).

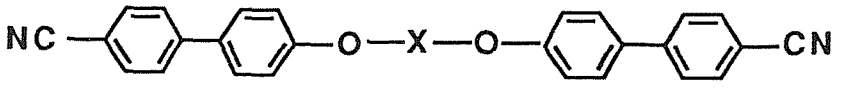

(2)

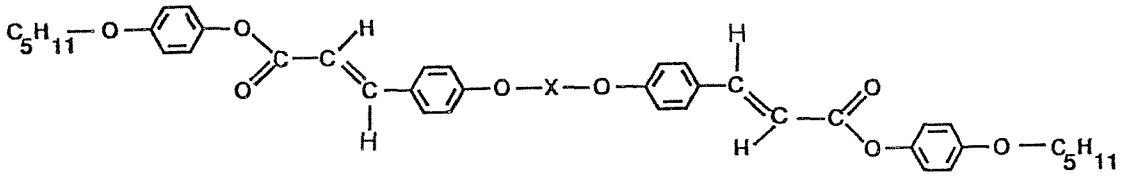

(3)

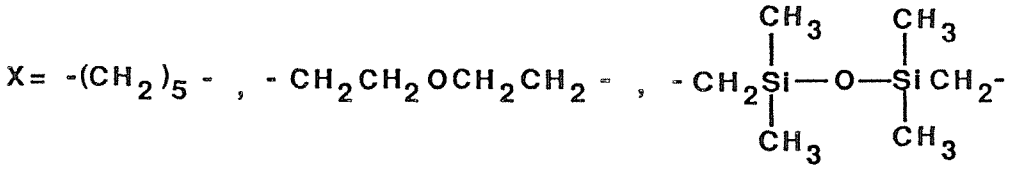

They discovered that the T_{NI} increases from the disiloxane spacer to the diethylene oxide and then to the pentamethylene spacer (compounds with the disiloxane spacer were not liquid crystalline although compound 6 was reported to show a strongly monotropic nematic phase on rapid cooling at ~70°C (see the table)). This trend reflects the energy barrier to rotation between the *trans* and *gauche* conformers for the relevant bonds in the spacer, that is Si-O < C-O < C-C. Further, if we consider the conformational structure of the spacer groups it is seen that the pentamethylene

A comparison of the thermodynamic data for the 4'-cyanobiphenyl-4-yloxy (1-3) and the 4-pentyloxyphenylcinnamate systems (4-6) containing either a pentamethylene (PM), diethylene oxide (EO) or disiloxane spacer (DS). The bond angles are also given for the spacer chains which are taken from bond angle simulations in the gas phase and disallow for intermolecular interactions.

Compound	Spacer	*T*/°C		ΔH/kJmol^{-1}		ΔS/R	
		†C-I C-N	N-I	†C-I C-N	N-I	†C-I C-N	N-I
1	PM	138.3	184.1	22.7	1.9	6.6	0.5
2	EO	146.5	153.5	44.9	2.1	12.9	0.6
3	DS	†138.9		†40.5		†11.8	
4	PM	130.4	178.3	38.5	1.8	11.5	0.5
5	EO	113.2	163.9	73.3	2.2	22.8	0.6
6	DS	122.6	~70	65.8		20.0	

Group	Bond angle/°
Ar-O-C	118
O-C-O	109
C-O-C	114
$(Me)_2Si$-O-$Si(Me)_2$	144
O-Si-C	107
C-C-C	114

spacer cannot allow the mesogenic groups to lie parallel to one another. In the all *trans* conformation the rigid cores are bent by roughly 108° with respect to the spacer axis and this decreases the orientational order in the system. Conversely the ethylene oxide spacer has a preference for conformations with *gauche* linkages. As a result the mesogenic groups can lie parallel to one another and the increased orientational order is reflected in the relatively higher nematic to isotropic entropy change (see the table). The difference in the nematic to isotropic transition temperatures is a consequence of the differing intermolecular forces between the pentamethylene and ethylene oxide spacers. The disiloxane spacer group prefers the *trans* geometry, but due to the alternating bond lengths and bond angles (as well as the low E_{tg}) along the chain it has difficulty in adopting a parallel arrangement of the mesogenic groups and hence forming a liquid crystalline phase.

The geometry of the link between the spacer and mesogenic groups has also been shown to be important in stabilising the liquid crystal phase [15]. For example, the bond angle for a methylene link, C-$\hat{C}$-C, is approximately 108° whereas for an ether link, C-$\hat{O}$-C, it is approximately 120°. The nematic to isotropic transition temperatures of the α,ω-bis(4'-cyanobiphenyl-4-yloxy)alkanes have been compared to those of the α,ω-bis(4-cyanobiphenyl-4-yl)alkanes (see structures (4*a*) and 4(*b*), respectively). The total number of atoms in the spacer, n, was compared for the $n=6$ and 7 homologues of both series. In both cases T_{NI} was higher for the ether linked dimers and the difference was greatest for the $n=7$ homologues (ether link $n=6$ $T_{NI}=250$°C, $n=7$ $T_{NI}=186$°C: methylene link $n=6$ $T_{NI}=230$°C, $n=7$ $T_{NI}=115$°C). As the link angle decreases so the odd-even effect is predicted to increase and this results largely from a reduction in the liquid crystallinity of the odd membered dimer. In figure 22 the all *trans* conformation for the $n=7$ homologue is shown schematically for both the methylene linked and ether linked dimers. From this it is clear that the methylene linked dimer gives an all *trans* conformation in which the mesogenic groups lie at a larger angle to one another than is the case for the ether linked dimer. It is this effect which leads to a reduction in the liquid crystallinity of the odd membered dimer. Conversely, the difference in the all *trans* conformation of the even membered dimers is not so great, that is both have a parallel arrangement of their

mesogenic groups, and this is reflected in their similar nematic to isotropic transition temperatures.

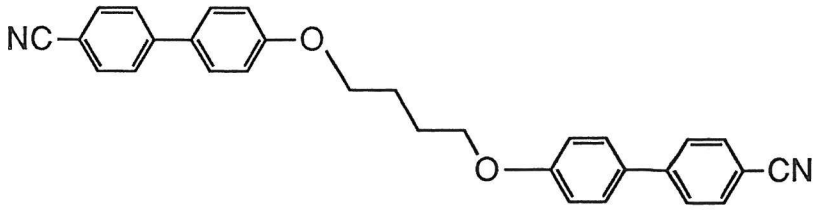

(4*a*)

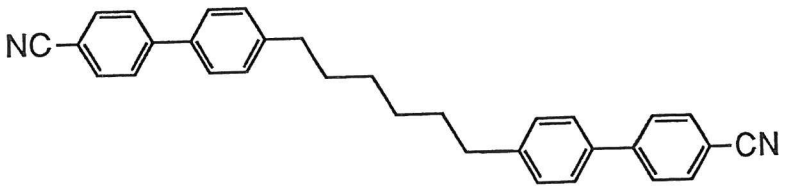

(4*b*)

(*a*)

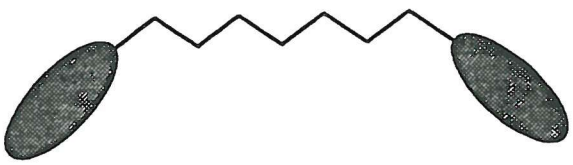

(*b*)

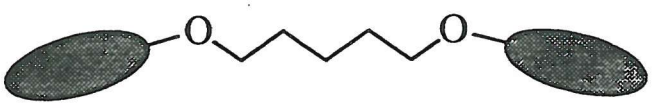

Figure 22. The difference in molecular shape for (*a*) methylene and (*b*) ether linked dimers with an odd number of atoms in the spacer.

4.2. *The nature of the mesogenic group and terminal substituents*

With a view to examining the properties of the mesogenic group in a dimeric liquid crystal Griffin *et al.* [16] synthesised three series of dimeric liquid crystals, all with a terminal cyano group (see structure (5)).

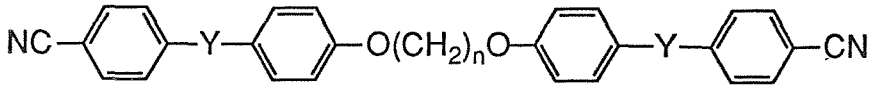

(5)

Y= imine, ester and nothing (biphenyl; see also [13]); n=2-12.

All of the compounds studied were enantiotropic nematic liquid crystals with the exception of the n=3 member of the biphenyl series. The T_{NI} values for the three series of dimers generally follow the order imines > esters > biphenyls (as is observed for monomers).

Imrie [17] has also conducted a study to examine the effect of lateral substitution at the mesogenic group on the nematic to isotropic transition temperature for liquid crystal dimers. The substituted compounds of structure (6) were compared with their analogues shown by structure (7).

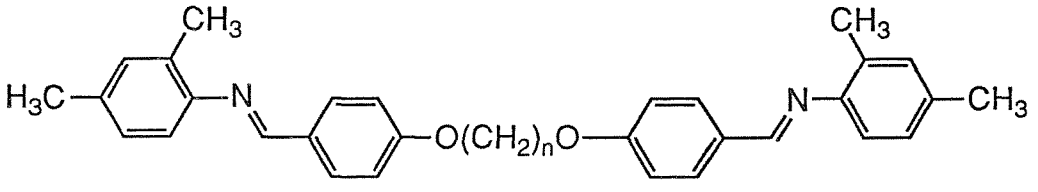

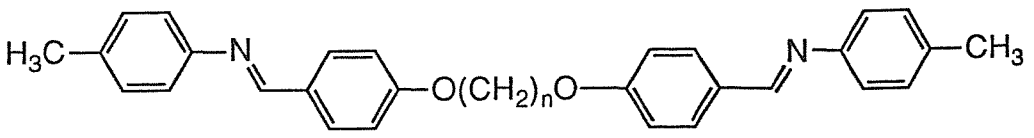

(7)

It is seen that lateral substitution results in a large decrease in both T_{CN} and T_{NI} as expected [18]. Interestingly, the reduction in the nematic to isotropic transition temperature is larger for compounds containing odd membered spacers and this leads to an increased odd-even effect; this is more pronounced for shorter spacer lengths. The entropy change at the nematic to isotropic transition is less for the laterally substituted series and this would imply an increase in the molecular biaxiality with a tendency towards second order transitional behaviour.

Jin and coworkers [19-22] have carried out a number of studies which have focussed on the nature of the terminal substituents in dimeric liquid crystals and their subsequent structure-property relationships (see structures (8)-(10)).

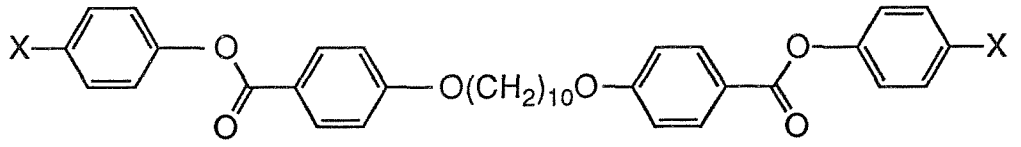

(8)

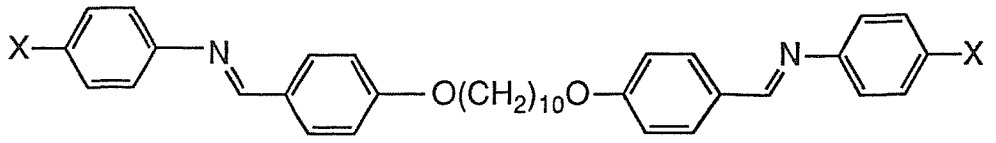

(9)

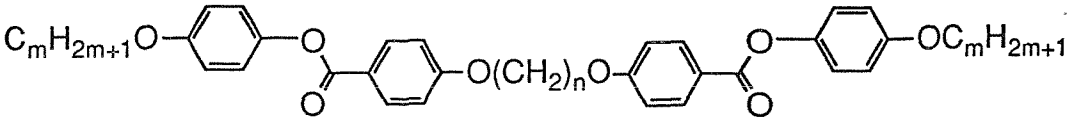

(10)

X= H, CH_3, Cl, CHO, NO_2, CN and C_6H_5; m= 1-7; n=5,6 and 10.

All of the compounds of structures (8) and (9) form enantiotropic nematic mesophases. The ability of the substituents, X, to stabilise a nematic phase and raise T_{NI} is in the order

$$H < CH_3 < Cl < CHO < NO_2 < CN < C_6H_5.$$

Either an enhanced polarizability, increased polarity or lengthening of the rigid core or a combination thereof are the most important factors for the stabilisation of the nematic phase. The influence of the substituent on the nematic to isotropic transition temperatures was found to be in accord with the behaviour of analogous nematogens with a single rigid core [18]. On varying the alkyloxy terminal chain for the compounds of structure (10) Jin *et al.* [22] did not find an odd-even effect for the clearing temperatures. However, the change in enthalpy and entropy at the clearing temperature showed a clear dependence on the number of carbon atoms in the

terminal chains. All of the compounds were liquid crystalline exhibiting different mesophases, in an irregular fashion, depending on the lengths of both the spacer and the terminal chains. Date *et al.* [23] have shown that increasing the length of the terminal alkyl chains for compounds of structure (7) enhances the tendency for smectic polymorphism as the chains are thought to help separate the molecules into layers. It was concluded that if smectic behaviour was to be observed at all then the terminal chain length must be greater than half the length of the spacer.

5. Struture-property relationships of trimeric liquid crystals

Symmetric, trimeric liquid crystals are typically composed of three anisometric units linked together by two flexible spacers as shown schematically in figure 23.

Figure 23. A schematic representation of a symmetric trimeric liquid crystal.

Furuya and coworkers [24] have prepared and compared two short series of trimeric liquid crystals, namely the 1,4-bis((ω-4'-cyanobiphenyl-4-yloxy)alkyloxy)benzenes and the 4,4'-bis((ω-4'-cyanobiphenyl-4-yloxy)alkyloxy)biphenyls (see structures (11) and (12), respectively).

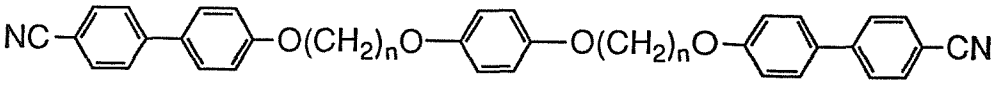

(11)

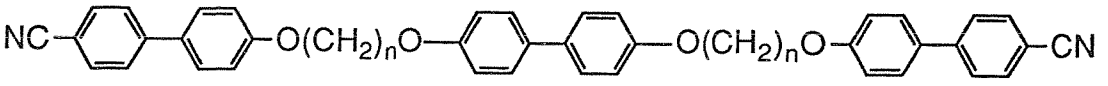

(12)

The only mesophase detected was an enantiotropic nematic phase. For trimeric molecules, they concluded, a smaller rigid core (phenyl compared to biphenyl) enhances the odd-even effect, such that for odd members of methylene units in the spacer chain, no mesophase forms at all; a larger more rigid central core would seem to be able to stabilise a mesophase regardless of how many mehthylene units there are in the spacer chains since an increase in molecular anisometry leads to an enhancemant of liquid crystalline behaviour [18]. Comparing the results of the trimeric species shown by structure (12) with those obtained for its dimeric analogue [13] we see a marked difference in T_{NI} as shown in figure 24. This is an obvious result of the increase in shape anisotropy. Similarly, the change in entropy at the transition, ΔS_{NI}, is also seen to increase when comparing the dimers with their trimeric analogues as shown in figure 25; this difference increases across the series. This can be rationalised in terms of the greater long range orientational order for the trimeric molecule as compared to its dimeric counterpart as well as its larger molecular weight.

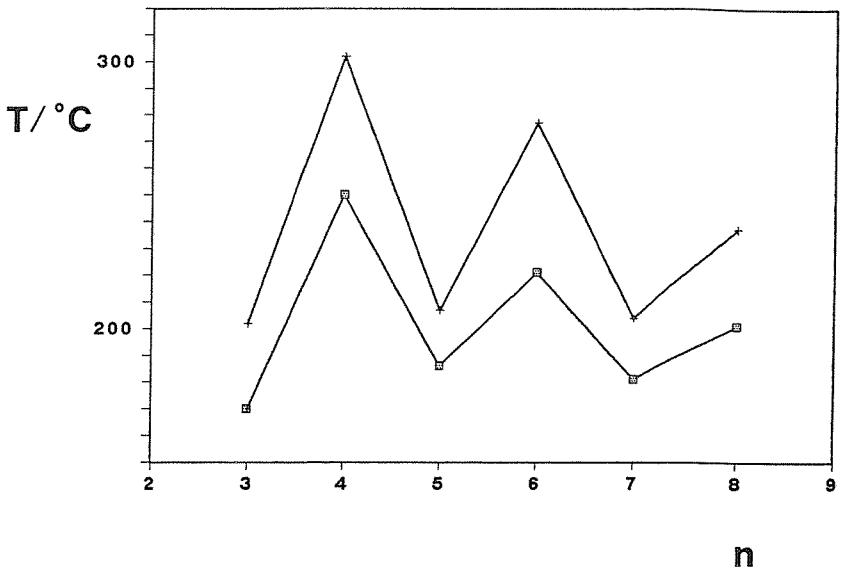

Figure 24. The influence of the number of carbon atoms in the spacer, *n*, on the nematic to isotropic transition temperature for the trimeric 4,4'-bis((ω-4'-cyanobiphenyl-4-yloxy)alkyloxy)biphenyls (+) as compared to the dimeric α,ω-bis(4'-cyanobiphenyl-4-yloxy)alkanes (■).

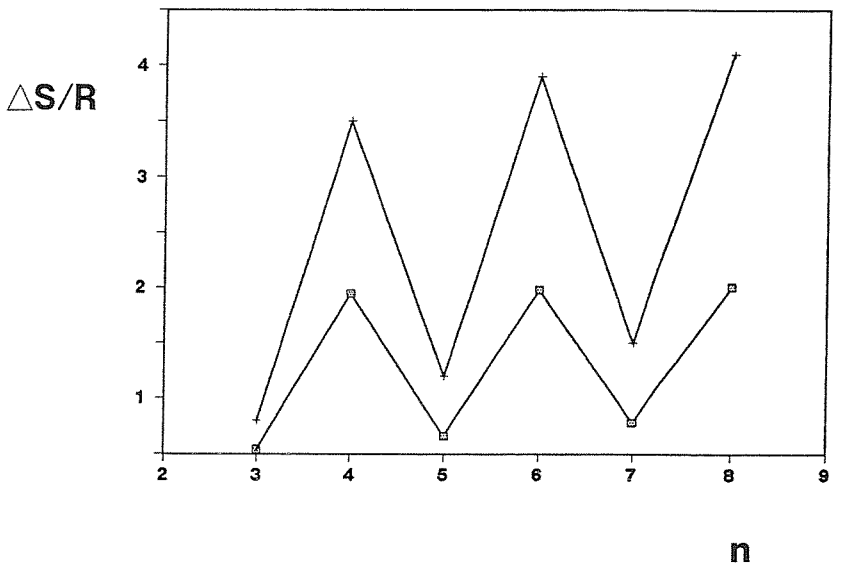

Figure 25. The influence of the number of carbon atoms in the spacer, *n*, on the nematic to isotropic entropy change for the trimeric 4,4'-bis((ω-4'-cyanobiphenyl-4-yloxy)biphenyls (+) as compared to the dimeric α,ω-bis(4'-cyanobiphenyl-4-yloxy)alkanes (■).

Attard and Imrie [25] have studied the effect of attaching a lateral chain to a central phenyl ring in a trimeric liquid crystal (see structure (13)). A nematic phase was exhibited no matter how many carbon atoms, *n*, were in the lateral chain. They reported the *n*-alkyl-2,5-bis(4'-cyanobiphenyl-4-butyloxy)benzoates and showed the possibility of obtaining monotropic smectic phases in addition to the nematic phase, which is the only phase reported for the unsubstitued trimer.

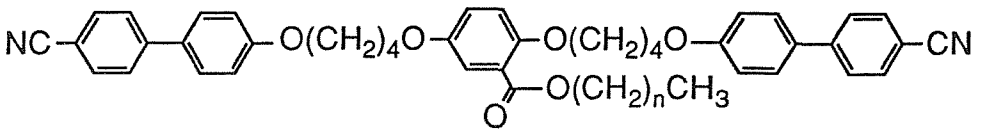

(13)

The melting point of the butyloxy homologue is lowered by the attachment of a lateral chain which is expected (see the analogue in [24]). The melting points for the series show a regular dependence on the length of the lateral chain, whereas the nematic to isotropic transition temperatures gradually decrease as the lateral chain length increases; the n=7-11 members of the series all show monotropic nematic phases. The entropy changes associated with the nematic to isotropic transition, for the reported trimers, are independent of the length of the lateral chain and are significantly lower than the values measured for the unsubstituted trimer; this would suggest that the lateral chain perturbs the anisotropic interactions between the anisometric groups and thereby reduces the degree of long range orientational order in the system. In addition the lateral chain tends to increase the molecular biaxiality leading to weaker first order transitional entropy changes.

6. Structure-property relationships of dimeric and trimeric liquid crystals containing disc-like units

Despite the discovery of the discotic nematic phase in 1977 [26] there are few reports in the literature of dimeric or trimeric liquid crystals which contain disc-shaped mesogens. The first report of symmetric discotic twins was the α,ω-bis[(1,2,3,5,6-pentakis(heptanoyloxy)benzene-4-]alkanoates [27] shown by structure (14).

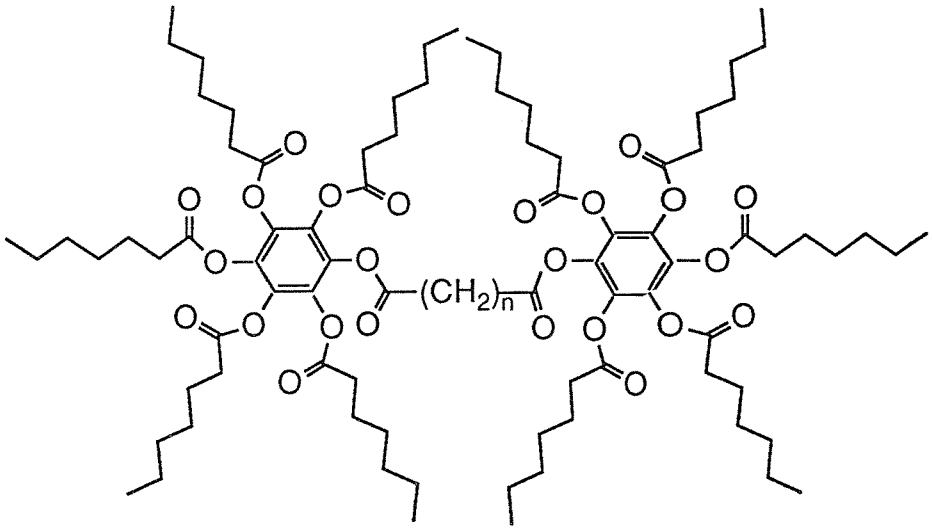

(14)

R= -$C_6H_{13}CO_2$

Two homologues were synthesised, where n=8 and 18. It was found for the short chain twin that no mesophase was formed yet the long chain homologue formed a discotic columnar phase. The phase was not characterised fully but was probably of the discotic hexagonal type. It was argued that the spacer length controls the liquid crystal properties of the discotic twins. Further, the assumption was made that the two discs prefer to stack in adjacent columns and so it follows that only particularly long spacers are capable of bridging the gap between the columns to form a discotic mesophase.

Praefcke *et al.* [28] have prepared and characterised several homologues of structure (15).

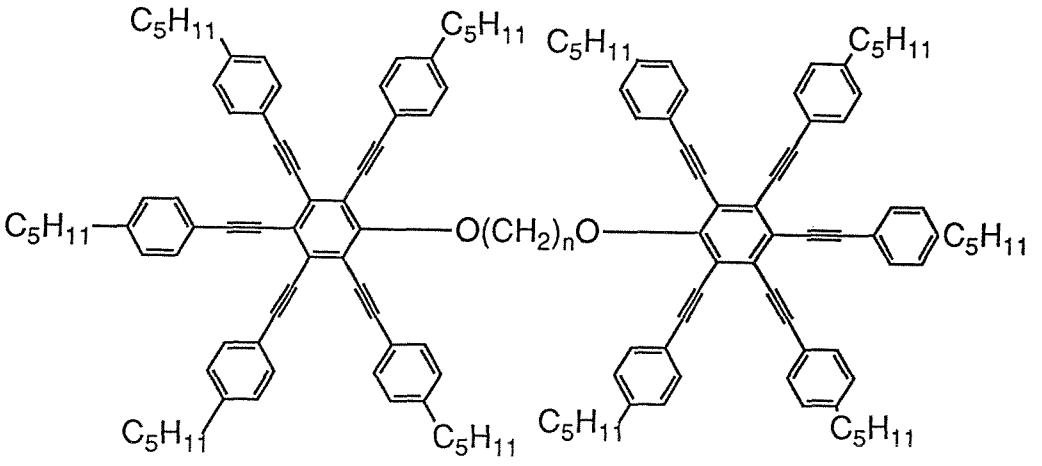

(15)

n= 8-12

All of the homologues were found to exhibit the discotic nematic phase and this is thought to be a consequence of the large core size. The clearing temperatures showed an odd-even effect. A conoscopy study of the n=12 homologue has reported the discotic nematic phase to have a weak optical biaxiality [29]. Indeed the entropy change for the discotic nematic to isotropic transition is very small (ΔS/R=0.1 for the n=10-12 homologues).

In an example of a non-symmetric dimeric liquid crystal containing a disc-like unit Möller *et al.* [30] have conducted an elegant study of discotic charge transfer twins. Charge transfer complexes are normally produced by two component mixtures of an electron donor and an electron acceptor. These compounds consist of a triphenylene unit (acting as electron donors) linked via a flexible spacer to a 2,4,7-trinitro-9-fluorenone unit (acting as an electron acceptor) (see structure (16)).

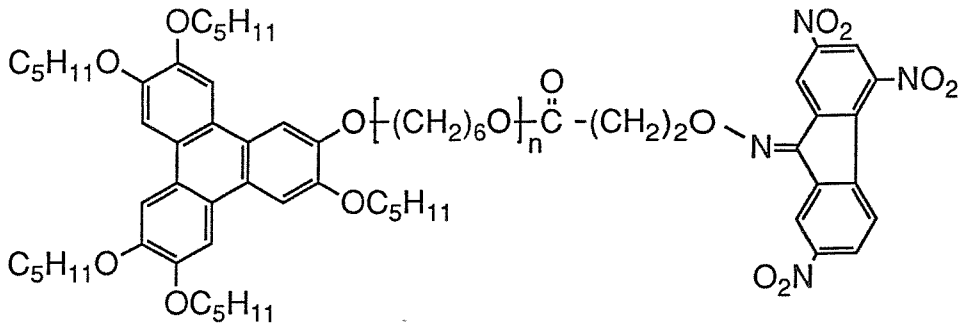

(16)

n=0,1.

By linking the electron donor and acceptor units in this way problems such as immiscibility are overcome. Both the n=0 and 1 homologues are liquid crystalline and exhibit a type of discotic phase up to 265°C and 242°C, respectively. In addition they both have glass transitions at room temperature. X-ray analysis indicates that the phase contains molecules which are arranged in columns such that the electron donor and acceptor molecules alternate along the column and neighbouring columns are connected together via the flexible spacer.

Kreuder *et al.* [31] have attempted to produce a thermotropic, biaxial nematic phase by preparing two types of trimeric systems: one based on two terminal disc-like units and a terminally linked rod-like bridge and the other on two terminal disc-like units and a laterally linked rod-like bridge (see structures (17) and (18), respectively). The thermotropic, biaxial nematic phase has been predicted to exist for mixtures of rod-like and disc-like nematogens [32]. However, experimentally the components separate into their constituent phases. By linking disc-like and rod-like units together through flexible spacers it was hoped that a material would be formed which had biaxial properties.

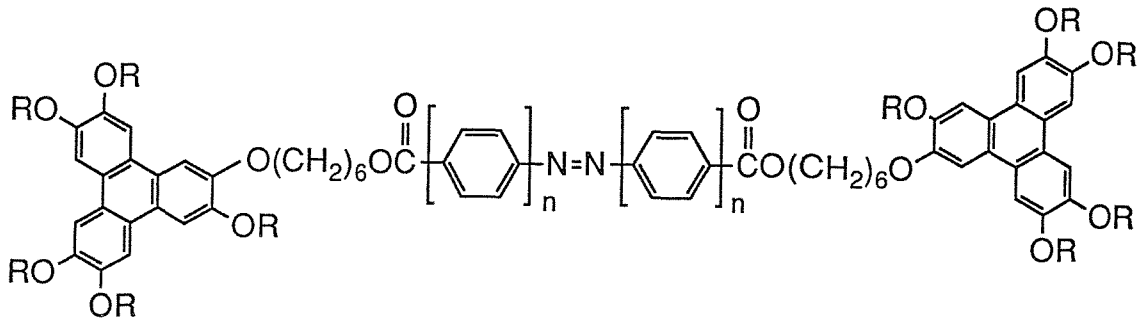

(17)

R= -C_5H_{11}, n=2.

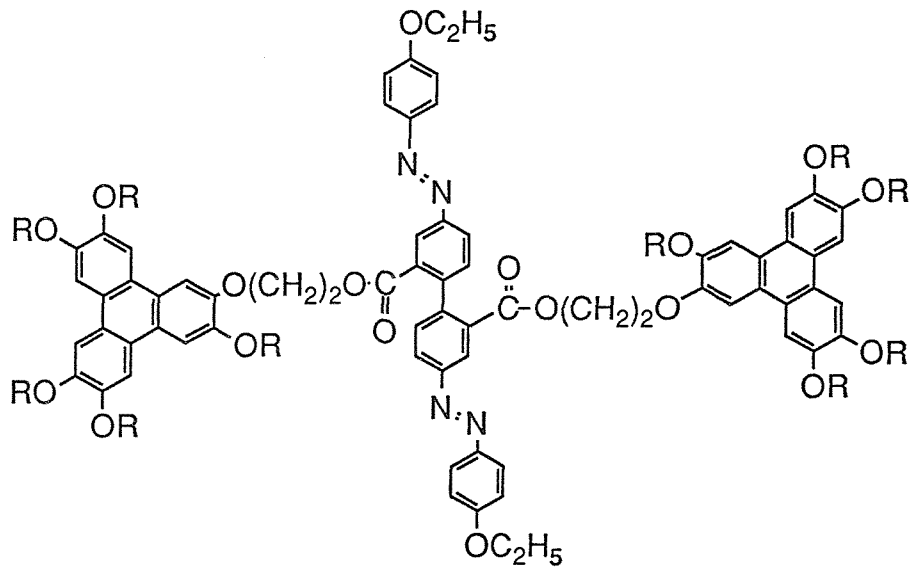

(18)

R= -C_5H_{11}.

Compound (18) has a high melting point (167°C) and is not liquid crystalline; even supercooling the isotropic liquid by 120°C does not produce a mesophase. However, compound (17) forms a highly ordered mesophase which is characterised by a layer structure, typical for smectic phases, and a regular stacking of the disc-like units

observed for discotic phases. There was no report of any biaxial phase behaviour for this material.

References

[1] Templer, R., and Attard, G., 1991, *New Scientist*, 4 May, p.25.

[2] Reinitzer, F., 1888, *Monatsheft. Chem.*, **9**, 421. For an English translation see 1989, *Liq. Crystals*, **5**, 7.

[3] Lehmann, O., 1889, *Z. Phys. Chem.*, **4**, 462.

[4] Ringsdorf, H., Schlarb, B., and Venzmer, J., 1988, *Angew. Chem.*, **27**, 113.

[5] Demus, D., 1989, *Liq. Crystals*, **5**, 75.

[6] Gray, G.W., and Goodby, J.W.G., 1984, *Smectic Liquid Crystals-Textures and Structures* (Leonard Hill).

[7] Demus, D., and Richter, L., 1978, *Textures of Liquid Crystals* (VEB Deutscher Verlag für Grundstoffindustrie).

[8] Voets, G., Martin, H., and van Dael, W., 1989, *Liq. Crystals*, **5**, 871.

[9] Praefcke, K., Singer, D., Kohne, B., Ebert, M., Liebmann, A., and Wendorff, J.H., 1991, *Liq. Crystals*, **10**, 147.

[10] Hartshorne, N.H., and Stuart, A., 1970, *Crystals and the Polarising Microscope* (Pitman Press), p.335.

[11] Griffin, A.C., and Britt, T.R., 1981, *J. Am. chem. Soc.*, **103**, 4957.

[12] Vorländer, D., 1927, *Z. Phys. Chem.*, **126**, 449.

[13] Emsley, J.W., Luckhurst, G.R., Sage, I., and Shilstone, G.N., 1984, *Molec. Crystals liq. Crystals Lett.*, **102**, 223.

[14] Creed, D., Gross, J.R.D., Sullivan, S.L., Griffin, A.C., and Hoyle, C.E., 1987, *Molec. Crystals liq. Crystals*, **149**, 185.

[15] Barnes, P.J., Douglass, A.G., Heeks, S.K., and Luckhurst, G.R., 1993, *Liq. Crystals*, **13**, 603.

[16] Griffin, A.C., Vaidya, S.R., Hung, R.S.L., and Gormann, S., 1985, *Molec. Crystals liq. Crystals*, **1**, 131.

[17] Imrie, C.T., 1989, *Liq. Crystals*, **6**, 391.

[18] Gray, G.W., 1979, *The Molecular Physics of Liquid Crystals*, edited by G.R. Luckhurst and G.W. Gray (Academic Press), Chap.1.

[19] Jin, J.-I., 1983, *Polymer Preprints (Japan)*, **32**, 935.

[20] Jin, J.-I., Chang, Y.-S., Lenz, R.W., and Ober, C., 1983, *Bull. Korean*

chem. Soc., **4**, 193.

[21] Jin, J.-I., Kang, J.-S., Jo, B.-W., and Lenz, R.W., 1983, *Bull. Korean chem. Soc.*, **4**, 176.

[22] Jin, J.-I., Oh, H.-T., and Park, J.-H., 1986, *J. chem. Soc., Perkin Trans. II*, 343.

[23] Date, R.W., Imrie, C.T., Luckhurst, G.R., and Seddon, J.M., 1992, *Liq. Crystals*, **12**, 203.

[24] Furuya, H., Asahi, K., and Abe, A., 1986, *Polymer J.*, **18**, 779.

[25] Attard, G.S., and Imrie, C.T., 1989, *Liq. Crystals*, **6**, 387.

[26] Chandrasekhar, S., Sadashiva, B.K., and Suresh, K.A., 1977, *Pramana*, **9**, 471.

[27] Lillya, C.P., and Murthy, Y.L.N., 1985, *Molec. Crystals liq. Crystals Lett.*, **2**, 121.

[28] Praefcke, K., Kohne, B., Gündogan, B., Singer, D., Demus, D., Diele, S., Pelzl, G., and Bakowsky, U., 1991, *Molec. Crystals liq. Crystals*, **198**, 393.

[29] Praefcke, K., Kohne, B., Singer, D., Demus, D., Pelzl, G., and Diele, S., 1990, *Liq. Crystals*, **7**, 589.

[30] Möller, M., Tsurkruk, V., Wendorff, J.H., Bengs, H., and Ringsdorf, H., 1992, *Liq. Crystals*, **12**, 17.

[31] Kreuder, W., Ringsdorf, H., Herrmann-Schönherr, O., and Wendorff, J.H., 1987, *Angew. Chem. Int. Ed. Engl.*, **26**, 1249.

[32] Tinh, N.H., Destrade, C., and Gasparoux, H., 1979, *Phys. Lett.* A, **72**, 251.

CHAPTER 2

The properties of some novel liquid crystalline diacetylenes

1. Introduction

Materials scientists have shown increasing interest in diacetylene compounds ever since Wegner [1] discovered their solid state, topotactic polymerization to polydiacetylenes. Polydiacetylenes have an extended, π-conjugated, polarizable molecular chain and have been shown to be excellent candidates for third order optical non-linearity [2,3]: a process which leads to the frequency tripling of light and has huge potential in future high speed optical devices [4].

To be of value in such applications polydiacetylene materials must have acceptable mechanical properties that enable the fabrication of large, high quality crystals or defect-free thin films. Although versatile polydiacetylene materials are not without their drawbacks [5]. During the polymerization process crystal lattice defects and dislocations can occur causing the polymer to form as microcrystallites. The task of growing defect-free crystals of the monomer from solution or from the melt and the conversion of these into high quality polymer single crystals can be difficult. Furthermore the polymerization of diacetylenes in Langmuir-Blodgett multilayers is problematical as the layers are prone to collapse [6].

One possible solution to the problem of producing high quality polymer single crystals is thought to be offered by the properties of liquid crystals. It is well-known that the nematic liquid crystal phase can be aligned by external fields or pretreated glass slides to produce a monodomain [7]. On cooling a monodomain nematic into a smectic phase a high quality crystal can be obtained. By polymerizing diacetylene

compounds in this state a means of producing highly ordered, bulk polydiacetylene samples could be realized. It was with this in mind that we decided to investigate the liquid crystalline properties of a new series of diacetylene compounds. But before we go on to consider the structure-property relationships of liquid crystalline diacetylene compounds and the design of the compounds presented in this chapter it is necessary to outline the theory behind the polymerisation of diacetylenes as well as the theory of non-linear optics.

2. Solid state polymerization of diacetylenes to polydiacetylenes

The solid state polymerization of diacetylenes to polydiacetylenes proceeds via a topotactic reaction, in which the growing polymer retains the order of the monomer crystal. A strict geometrical arrangement of the monomer units governs the reaction, that is, the molecules must be packed in a reactive configuration, such that the reaction path is precisely defined by the crystal structure. The polymerization process, which may be initiated either thermally or by ultraviolet or ionizing radiation (X-rays or γ-rays), follows a 1,4-addition mechanism, through the formation of diradicals which autocatalyse the growth of the polymer chain [1]. The monomer molecules form linear arrays which are converted into a planar, fully conjugated polymer backbone which has a metallic lustre. The monomers undergo very specific rotation and translation on their lattice sites during the polymerization process and as a consequence the crystallographic position and symmetry of the monomer units are preserved. It has been shown that the separation of the centres of gravity of the diacetylenes along the stack axis (d in figure 1) must be less than 0.4nm in the crystal lattice [8]. A minimum value of 0.34nm is imposed as this is twice the van der Waals radius for triply-bonded carbon atoms. Further the angle (γ in figure 1) between the diacetylene units and the stack axis has also been shown to be important and should be between 32° and 62° [8].

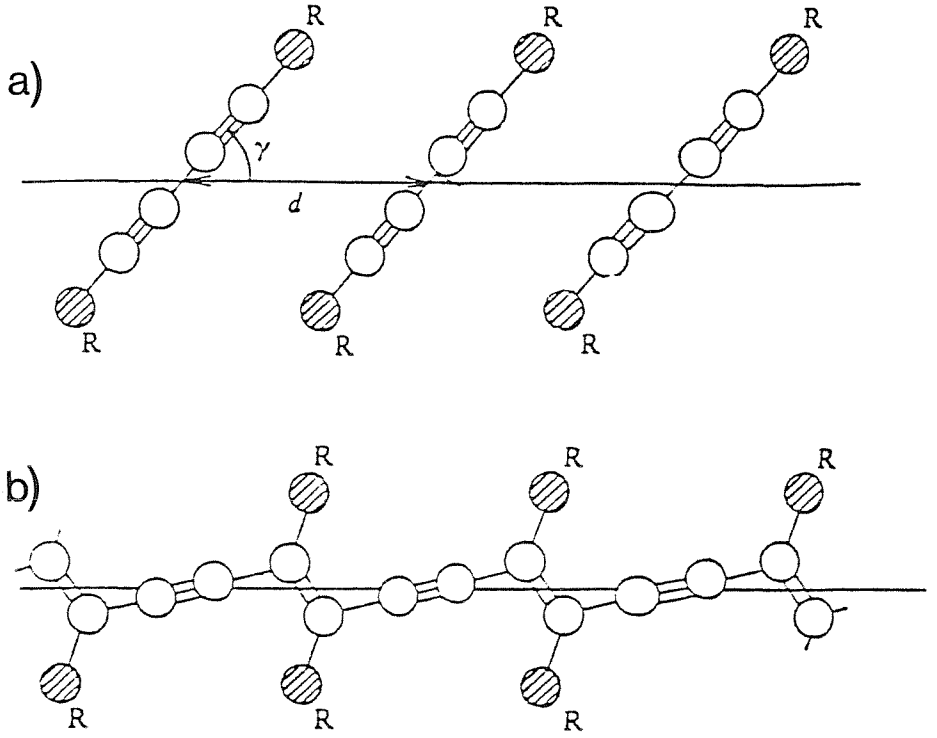

Figure 1. A schematic representation of the solid-state polymerisation of diacetylenes. (*a*) Monomer array, (*b*) conjugated polymer. γ represents the angle between the diacetylene molecule and the stack axis and d is the distance between adjacent molecules.

3. Theory of non-linear optics

When a light wave passes through a material, the electric field associated with this wave causes a redistribution of the weakly bound electrons surrounding the atomic nuclei. The displacement of the negative charge relative to the positively charged nuclei results in an induced dipole moment, and the material is said to have become polarized. The induced dipole moment per unit volume is called the polarization, **P**, and is for most substances linearly proportional to the applied field, **E**, for small values of this field so that

$$\mathbf{P}=\epsilon_o \chi^{(1)} \mathbf{E}, \tag{1}$$

where ϵ_o is the permittivity of free space and $\chi^{(1)}$ is the linear electric susceptibility.

When the electric field of the light wave is no longer small, as in the case of laser radiation, equation (1) needs to be modified. If the material is not significantly altered by the field, a power expansion can be used to describe the induced polarization according to

$$\mathbf{P}=\epsilon_o (\chi^{(1)} \mathbf{E} + \chi^{(2)} \mathbf{E}.\mathbf{E} + \chi^{(3)} \mathbf{E}.\mathbf{E}.\mathbf{E} + ...), \tag{2}$$

where $\chi^{(2)}$ and $\chi^{(3)}$ are the second and third order non-linear electric susceptibilities, respectively. One consequence of these higher order terms is that light can be produced having frequencies (and therefore wavelengths) different from the incident wave. The conversion of incident light to twice or three times the fundamental frequency is known as second or third order harmonic generation, respectively.

The $\chi^{(2)}$ and $\chi^{(3)}$ coefficients in equation (2) are highly symmetry dependent. Odd order coefficients, such as $\chi^{(1)}$ and $\chi^{(3)}$ are non-vanishing for all materials, but even order coefficients such as $\chi^{(2)}$ are zero only for centrosymmetric crystals. However, the symmetry of centrosymmetric materials can be broken by the application of an external field, a technique known as *poling*. As the compounds considered here are

centrosymmetric molecules we shall only consider the investigation of third harmonic generation ($\chi^{(3)}$).

4. Structure-property relationships of diacetylene liquid crystalline compounds

Liquid crystal researchers have been attracted to the diacetylene unit as a means of extending molecular anisotropy and polarizability [9,10]. For example consider the 1,4-bis(4-*n*-alkylphenyl)butanes (1). All members of this series are not liquid crystalline and yet the 1,4-bis(4-*n*-alkylphenyl)buta-1,3-diynes (2), possess an enantiotropic nematic phase [9].

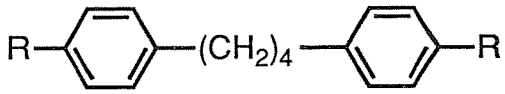

(1)

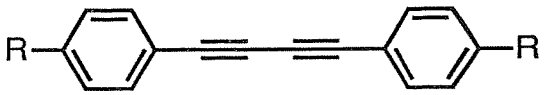

(2)

Fouquey *et al.* [11] have reported studies on molecules based on the diphenyldiacetylene core with nitro and secondary alkylamino substituents, so-called push-pull diacetylenes as the amino substituent is electron donating and the nitro is electron withdrawing (see structure (3)). The resultant dipole is important for second

order non-linear optics.

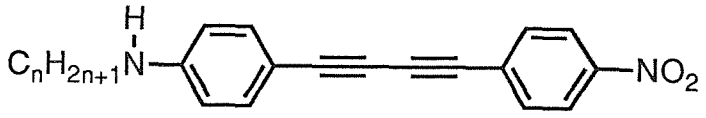

(3)

The mesomorphic properties of homologues with chain lengths of n=6-12 reflect those of a typical homologous series; for short chains, n=6-8, only a nematic phase is observed, whereas for longer chains, n=9-11, smectic behaviour appears together with a nematic phase and then exists alone for the n=12 homologue. The melting and clearing temperatures both show a pronounced odd-even effect.

The compounds considered thus far possess a diacetylene unit attached directly to a mesogenic group and consequently tend to have high melting points. This has the disadvantage of raising the melting point to the detriment of liquid crystalline behaviour. One way of lowering the melting point is to incorporate a degree of flexibility into the molecule. The liquid crystalline properties of compounds containing a central diacetylene unit linked to cholesteryl groups via a flexible spacer have been reported (see structure (4)) [12].

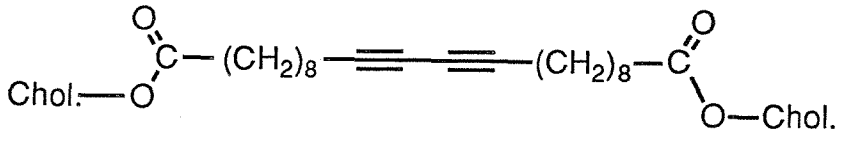

(4)

This compound possesses a monotropic smectic phase. The phase could not be characterized by polarizing microscopy alone (the optical texture was highly birefringent but without any specific features) and only after careful analysis of X-ray data was it considered to be an interdigitated smectic A phase.

In this chapter we report the synthesis and characterization of a new homologous series of diacetylene liquid crystalline compounds, the α,ω-bis(4-*n*-alkylphenyliminobenzylidene-4'-oxy)alkyldiynes (see structure (5)), where the diacetylene and mesogenic units are linked together via flexible spacers. This class of compound was chosen for several reasons. It was of interest to examine the change in the liquid crystalline behaviour of the analogous, α,ω-bis(4-alkylphenyliminobenzylidene-4'-oxy)alkanes [13] when a central diacetylene unit is incorporated into the spacer. We also synthesised α,ω-bis(4-cyanobiphenyl-4'-oxy)deca-4,6-diyne (see structure (6)) to again examine the effect of the diacetylene unit on the liquid crystalline behaviour of the well-characterised α,ω-bis(4-cyanobiphenyl-4'-oxy)alkanes [14]. We hoped the compounds to display nematic and smectic behaviour, which is the case for the analogous compounds with a fully saturated spacer, as only a nematic to smectic phase sequence can produce a monodomain crystalline sample of the diacetylene compound when cooled in the presence of an external field. Ultimately we wished to polymerize the diacetylene compounds to polydiacetylenes and to obtain an indication of their third order non-linear susceptibilities.

(5)

(6)

5. Experimental

5.1. *Synthesis of materials*

The α,ω-bis(4-alkylphenyliminobenzylidene-4'-oxy)alkyldiynes were prepared as shown in the scheme. For the purpose of simplification these compounds will be abbreviated to $(m.On)_2DA$, where m is the length of the terminal alkyl chain, O represents an oxygen atom, n is the number of methylene units in the spacer linking the diacetylene unit to the mesogenic group and DA stands for diacetylene. Thus it follows that α,ω-bis(4-decylphenyliminobenzylidene-4'-oxy)deca-4,6-diyne is abbreviated to $(10.O3)_2DA$. α,ω-bis(4'-cyanobiphenyl-4-yloxy)deca-4,6-diyne is abbreviated to $(CB.O3)_2DA$, where CB represents cyanobiphenyl.

The synthetic procedure for the $(m.O3)_2DA$ series is outlined using α,ω-bis(4-decylphenyliminobenzylidene-4'-oxy)deca-4,6-diyne as an example.

5.1.1. *Synthesis of deca-4,6-diyne-1,10-diol*

The Glaser coupling reaction [15] was employed in this step. Ammonium chloride (130g; 2.25mol) and cuprous chloride (75g; 7.5 x 10^{-1}mol) were added to distilled

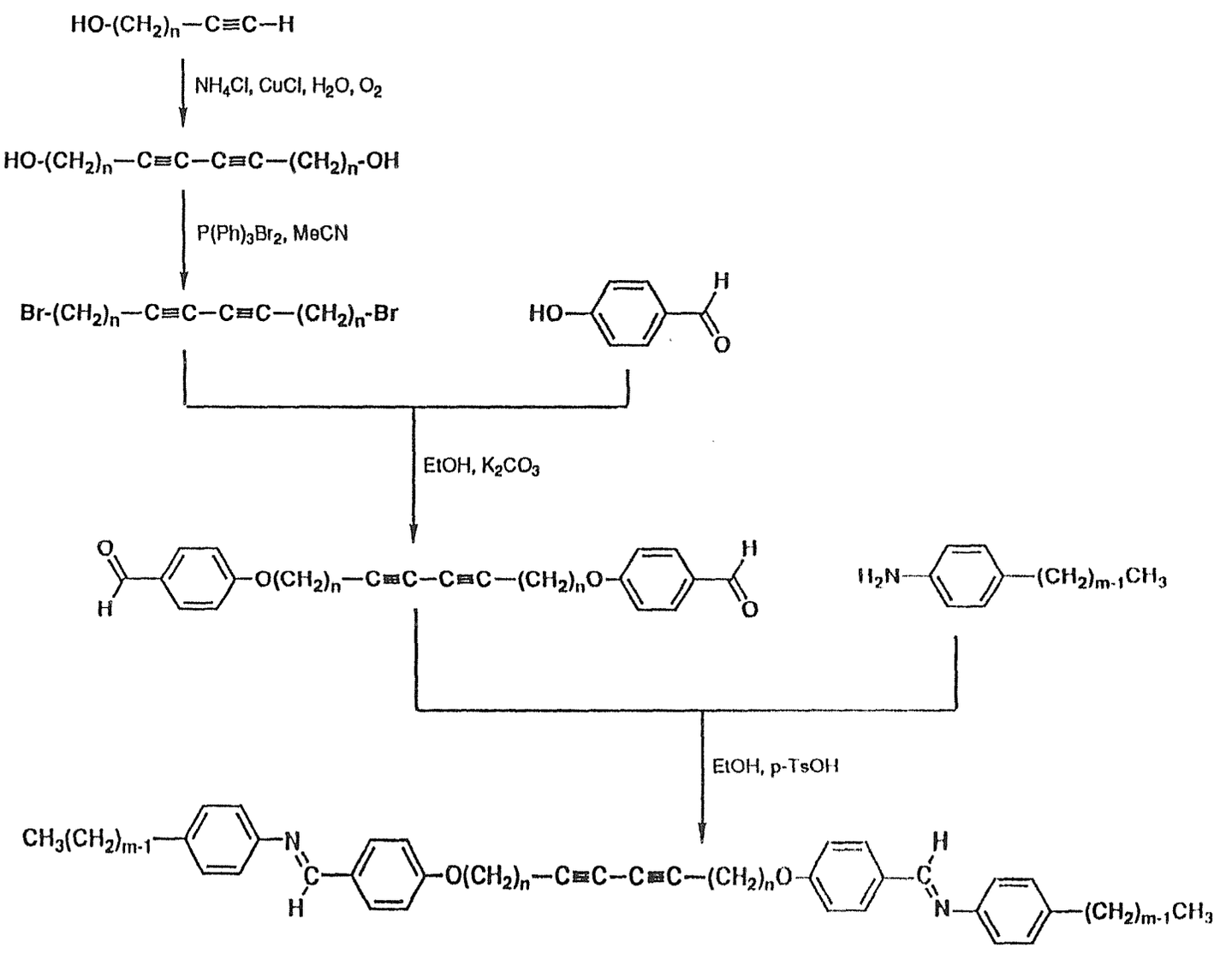

The reaction scheme for the synthesis of the $(m.On)_2$DA series.

water (200ml) in a 500ml, two neck, round bottom flask fitted with a bubbler and the mixture aerated with oxygen for 20min. 4-Pentyne-1-ol (25g; 2.9 x 10^{-1}mol) was then added and the reaction mixture left to stir overnight. The dark green reaction solution was observed to change to a dark brown colour. The mixture was extracted with ethyl acetate (3 x 100ml). The combined extracts were washed with distilled water (100ml), saturated sodium chloride solution (100ml), two molar sulphuric acid and dried overnight using anhydrous sodium sulphate. The sodium sulphate was filtered off and the ethyl acetate removed on the rotary evaporator to yield a yellow oil. Yield: 15g (60%). The oil was kept in solution to prevent crystallization and potential subsequent photochemical polymerization (it was found by error that this turned into a white, crystalline product which polymerized rapidly and turned dark blue in colour).

IR (NaCl disc, neat): ν 2161.3, 2257.3 (-C≡C-C≡C-), 3379.8cm^{-1} (-OH).
^{1}H NMR ($CDCl_3$): δ 1.2-1.4 (q, 4H), 1.9-2.1 (t, 4H), 3.0-3.2 (t, 4H), 3.3ppm (s, 2H).

5.1.2. *Synthesis of deca-4,6-diyne-1,10-dibromide* [16]

Dibromotriphenylphosphorane (78.5g; 1.9 x 10^{-1}mol) was added to 150ml of dry acetonitrile (over CaH_2) in a 500ml, three neck, round bottom flask fitted with a calcium chloride guard tube and thermometer to monitor the exothermicity of the reaction. Deca-4,6-diyne-1,10-diol (10g; 6.02 x 10^{-2}mol) dissolved in anhydrous acetonitrile (50ml) was added dropwise over a 15min period and the mixture left to stir for about an hour and a half. The dibromotriphenylphosphorane was seen to dissolve for a short while before triphenylphosphine oxide, a by-product, was precipitated. The temperature of the reaction mixture increased by about 6°C during the course of the reaction. The deposited triphenylphosphine oxide was filtered off and the acetonitrile removed on a rotary evaporator to yield a solid. Dry diethyl ether (250ml) was added to the solid and the mixture stirred for half an hour. The solid was filtered off and the diethyl ether removed on a rotary evaporator to yield a yellow oil. The yellow oil was refluxed with decolourising charcoal for 15min in dry

diethyl ether. The decolourising charcoal was filtered off through a fluted filter paper and the diethyl ether removed to give a colourless liquid. Yield: 9.7g (56%).

IR (NaCl disc, neat): ν 648.3, 695.5, 722.8 (C-Br), 2161.3, 2257.3cm^{-1} (-C≡C-C≡C-).
^{1}H NMR ($CDCl_3$): δ 1.5-1.8 (t, 4H), 1.9-2.2 (q, 4H), 3.0-3.2ppm (t, 4H).

5.1.3. *Synthesis of deca-4,6-diyne-1,10-oxybenzaldehyde*

Deca-4,6-diyne-1,10-dibromide (4g; 1.38 x 10^{-2}mol), 4-hydroxybenzaldehyde (4.21g; 3.45 x 10^{-2}mol) and anhydrous potassium carbonate (11.4g; 8.28 x 10^{-2}mol) were refluxed in absolute ethanol (125ml) for 24h in a 250ml conical flask fitted with a Leibig condenser and a calcium chloride guard tube. The reaction mixture was allowed to cool and then poured into distilled water (400ml) chilled in an ice bath and left to stir. A waxy orange solid precipitated; this was filtered off and dried *in vacuo*. Yield: 4.8g (93%), mp 106°C.

IR (NaCl disc, film): ν 1680.3 (C=O), 2217.0cm^{-1} (-C≡C-C≡C-).
^{1}H NMR ($CDCl_3$): δ 1.9-2.1 (t, 4H), 2.2-2.6 (q, 4H), 3.9-4.1 (t, 4H), 6.8-7.0 (d, 4H), 7.6-7.8 (d, 4H), 9.7ppm (s, 2H).

5.1.4. *Synthesis of α,ω-bis(4-decylphenyliminobenzylidene-4'-oxy)deca-4,6-diyne*

Deca-4,6-diyne-1,10-oxybenzaldehyde (1g; 2.67 x 10^{-3}mol) was dissolved in hot absolute ethanol (30ml) together with a few crystals of 4-toluenesulphonic acid in a 50ml conical flask fitted with a calcium chloride guard tube. Freshly distilled 4-*n*-decylaniline (1.31g; 5.61 x 10^{-3}mol) was added and the reaction mixture left to stir for 4h. A creamy yellow precipitate formed which was filtered off and recrystallized twice from ethyl acetate to yield white crystals and were dried *in vacuo*. Yield: 0.91g (42%).

IR (NaCl disc, film): ν 1510.6, 1571.9 1594.1 (-C=N-), 2214.1cm^{-1} (-C≡C-C≡C-).

^{1}H NMR ($CDCl_3$): δ 0.9-1.1 (t, 6H), 1.3-1.9 (m, 32H), 2.0-2.3 (q, 4H), 2.5-2.8 (q, 8H), 4.1-4.3 (t, 4H), 6.9-7.1 (d, 4H), 7.2-7.3 (m, 8H), 7.4-7.5 (d, 4H), 8.5ppm (s, 2H).
MS (EI): 587.5, 691.6, 804.7 (M^+).
Elemental analysis: calculated C 83.58%, H 8.96%, N 3.48%; found C 83.94%, H 9.00%, N 3.50%. Elemental analyses of randomly selected compounds are presented in table 1.

5.1.5. *Attempted synthesis of octa-3,5-diyne-1,8-oxybenzaldehyde*

The method described in 5.1.3 failed to yield the desired product for this reaction; a black oil was obtained which after examination by ^{1}H NMR (δ 4.45; d, -C=C-H) showed the presence of ethenic protons which infer the occurence of a dehydrobromination reaction and the formation of a stable, highly conjugated molecule (see figure 2).

In an attempt to increase the nucleophilicity of the 4-hydroxybenzaldehyde reagent the sodium salt was made [17] and reacted with octa-3,5-diyne-1,8-dibromide. Sodium metal (0.25g; 1.1 x 10^{-2}mol) was added to an excess of ethanol (35ml) in a 100ml conical flask fitted with a Leibig condenser and calcium chloride guard tube. Once the evolution of hydrogen had ceased 4-hydroxybenzaldehyde (1.4g; 1.1 x 10^{-2}mol) was added and the mixture left to stir for 20min. Octa-3,5-diyne-1,8-dibromide (1g; 3.82 x 10^{-3}mol) was then added and the reaction mixture refluxed for 6h. After cooling the mixture was poured into a large excess of distilled water in an ice-bath and left to stir. A black oil settled on the surface of the water. ^{1}H NMR (δ 4.45; d, -C=C-H) again showed the presence of ethenic protons indicating the possible occurence of a dehydrobromination reaction.

5.1.6. *Synthesis of α,ω-bis(4'-cyanobiphenyl-4-yloxy)deca-4,6-diyne*

Deca-4,6-diyne-1,10-dibromide(1g;3.45x10^{-3}mol),4-hydroxy-4'-cyanobiphenyl(1.42g;

Table 1. Elemental analysis data (calculated values in parentheses) for some randomly selected $(m.On)_2DA$ compounds.

Compound	Analytical data		
	C	H	N
$(5.O3)_2DA$	83.77% (83.13%)	7.78% (7.83%)	4.11% (4.22%)
$(10.O3)_2DA$	83.94% (83.58%)	9.09% (8.96%)	3.52% (3.50%)
$(12.O4)_2DA$	83.17% (83.78%)	9.52% (9.46%)	3.19% (3.15%)
$(10.O1)_2DA$	82.97% (83.42%)	8.66% (8.56%)	3.65% (3.74%)
$(CB.O3)_2DA$	82.88% (83.08%)	5.45% (5.39%)	2.65% (2.69%)

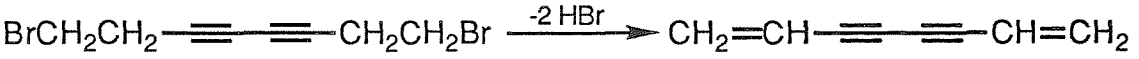

Figure 2. The double dehydrobromination of octa-3,5-diyne-1,8-oxybenzaldehyde.

7.24 x 10^{-3}mol) and anhydrous potassium carbonate (2.87g; 2.1 x 10^{-2}mol) were refluxed in 60ml of Analar acetone for 24h. The reaction mixture was filtered while still hot to remove any excess potassium carbonate and potasium bromide formed in the reaction. The filtrate was washed several times with hot Analar acetone. The acetone was removed on a rotary evaporator to yield a solid which was recrystallized from toluene and dried *in vacuo*. Yield 1.35g (76%).

IR (NaCl disc, nujol): ν 2215.4 (-C≡C-C≡C-), 2296.5cm^{-1} (C≡N).
^{1}H NMR ($CDCl_3$): δ 1.9-2.2 (q, 4H), 2.4-2.6 (t, 4H), 4.0-4.2 (t, 4H), 6.9-7.1 (d, 4H), 7.4-7.6 (d, 4H), 7.7ppm (s, 8H).
MS (EI): 520 (M^+).

5.2. *Polymerization of diacetylenes to polydiacetylenes*

Crystalline powders of two compounds, $(14.O3)_2$DA and $(CB.O3)_2$DA, were polymerized by exposure to UV radiation (RS 555-279 UV exposure unit) for 48h. $(14.O3)_2$DA was chosen as a representative member of the $(m,O3)_2$DA series, whereas $(CB.O3)_2$DA was chosen as it was the only compound to possess a nematic phase, which could be aligned in a cell. Both compounds gradually turned dark blue in colour with a slight metallic sheen indicative of a polydiacetylene. The extent of polymerisation was not characterised.

5.3. *Measurement of third harmonic generation*

5.3.1. *Experimental set-up*

The Kurtz powder technique [18] allows the rapid assessment of material non-linear optical efficiency and avoids the long and expensive growth of optical quality single crystals. The experimental apparatus is shown schematically in figure 3. A powdered sample of the material of interest is contained in a cell and illuminated with laser

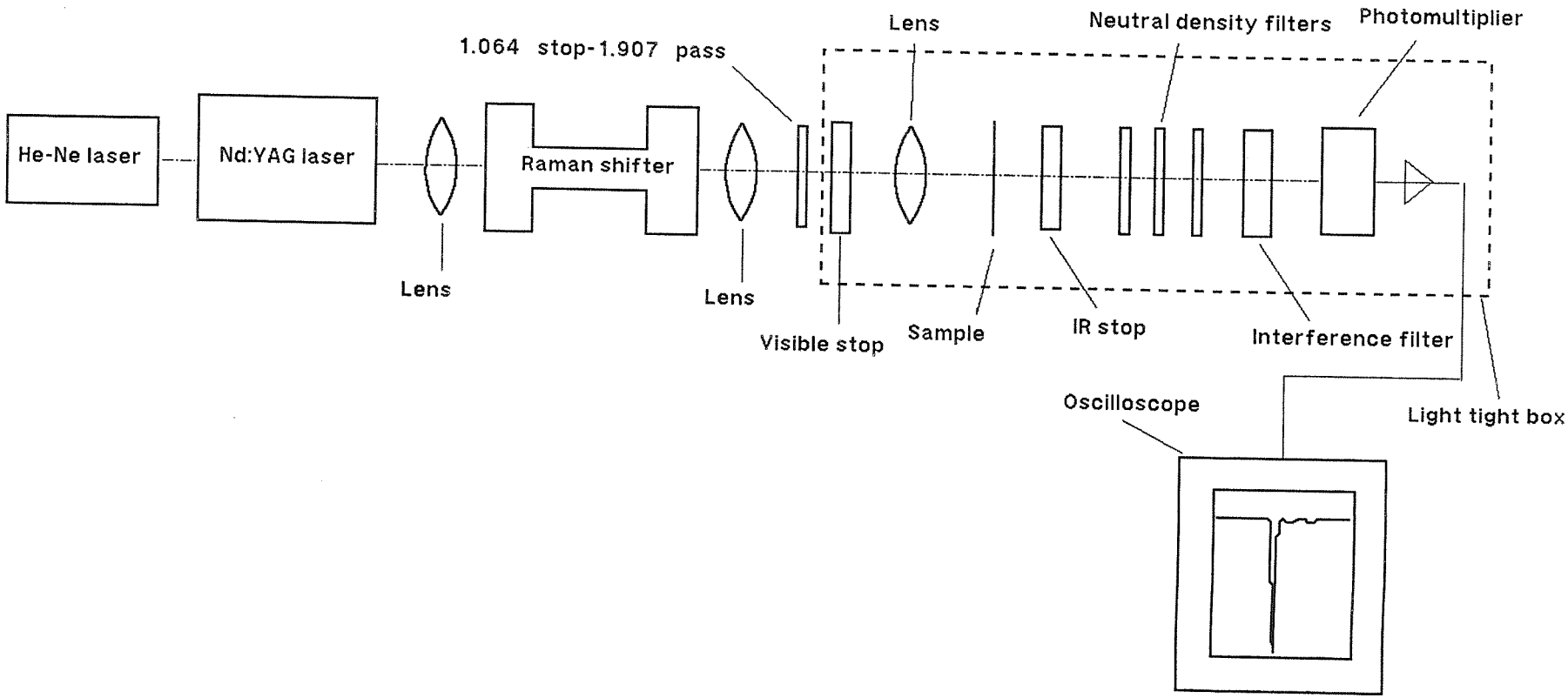

Figure 3. The experimental apparatus for the measurement of third harmonic generation.

light from a continuous wave He-Ne laser (power ~1mW) collinear with a Q-switched Nd:YAG laser. The pulse duration was 25ns (FWHM). The laser wavelength of 1.064μm was converted to 1.907μm by means of a high pressure (40bar) hydrogen Raman shifter. The laser light is then focussed through a combination of 1.064μm stop-1.907μm pass and visible stop filters onto the sample positioned on a stage in a light tight box. The scattered light passes through infrared absorbing glass (to remove any residual fundamental light) and an interference filter (which only transmits the third harmonic wavelength at 636nm) before being detected by a photomultiplier tube connected to an oscilloscope. The photomultiplier is positioned at an angle of approximately 30° with respect to the sample.

For film measurements the same set up is employed with the photomultiplier positioned immediately behind the sample. A crude film was produced by simply melting the monomeric sample on a glass slide covering with a cover slip and polymerizing with UV radiation as described previously. The signal was checked for its third harmonic purity by substituting interference filters either side of the third harmonic wavelength. A lack of signal confirms that the signal is narrow-band and third harmonic.

Glass cells (3μm thick, polyimide alignment layers to achieve homogeneous alignment with respect to the glass slide) were filled with $(CB.O3)_2DA$ in the hope of aligning the monotropic nematic phase. After filling and allowing the sample to crystallise the cells were irradiated with UV light for 48h after which a blue film was observed.

6. Results and discussion

6.1. *The $(m.O3)_2DA$ series*

The transition temperatures, enthalpies and entropies for this series are summarized in table 2. The first three homologues of this series are not liquid crystalline. There

Table 2. The transition temperatures, enthalpies and entropies for the $(m.O3)_2DA$ series.

m	T/°C			ΔH/kJmol^{-1}			ΔS/R		
	†C-I ‡C-S_A C-S_C	$S_{G/J}$-S_C	†S_A-I S_C-I	†C-I ‡C-S_A C-S_C	$S_{G/J}$-S_C	†S_A-I S_C-I	†C-I ‡C-S_A C-S_C	$S_{G/J}$-S_C	†S_A-I S_C-I
1	†190			†43.8			†11.4		
2	†180			†24.4			†6.6		
3	†178			†29.0			†7.8		
4	†177		†(169)	†14.6		†(13.1)	†4.2		†(3.7)
5	‡173		†179	‡19.2		†15.8	‡5.3		†4.3
6	176		177	28.7		19.3	7.9		5.2
7	170		181	23.3		17.0	6.4		4.6
8	167		178	27.1		20.8	7.5		5.6
9	164		181	23.8		23.2	6.6		6.2
10	164	(155)	181	17.9	∮	23.7	5.1	∮	6.4
12	158	(153)	178	11.6	(5.5)	21.8	3.3	(1.6)	5.9
14	148	(147)	170	27.4	(3.1)	34.8	7.8	(0.9)	6.3

∮ Could not be determined by DSC due to crystallization.

Parentheses indicate a monotropic transition.

is a general decrease in the melting point as the terminal chain length is increased which is expected. The melting point decreases further for the m=4 homologue which is the first liquid crystalline compound; it possesses a monotropic smectic A phase exhibiting a focal-conic fan texture with homeotropic regions. The m=5 homologue has an enantiotropic smectic A phase. For the m=6-9 homologues only a smectic C phase is exhibited on both heating and cooling. The texture of this phase is characterized by broken focal-conic regions surrounded by schlieren nematic (see plate 1). The schlieren texture flashes when subjected to mechanical stress and on closer inspection is observed to possess brushes with only a four point singularity characteristic of a smectic C phase [19]. From X-ray diffraction experiments of $(10.O3)_2DA$ the tilt angle for the smectic C phase has been calculated to be 35° (all *trans* molecular length from CPK models: 56Å, measured layer spacing: 45Å). On increasing the terminal chain length still further (m=10,12 and 14) a monotropic smectic phase is observed (see plate 2). The focal-conic fans become lined and the nematic schlieren changes to a mosaic platelet appearance which is very reminiscent to the smectic G or J phase texture shown in [13]. It was not possible to examine the structure of this phase by X-ray diffraction as it crystallised soon after it was formed and so its assignment as a smectic G or J phase is based solely on its optical texture.

Figure 4 shows a plot of the transition temperatures versus the terminal alkyl chain length, m, for the $(m.O3)_2DA$ series. It is clear from this figure that the melting points progressively decrease leading to an increase in the mesophase stability across the series. The clearing temperatures show no real trend except for the early homologues which exhibit a weak odd-even effect.

Figure 5 shows the effect of changing the terminal alkyl chain length on the transition temperatures for the α,ω-bis(4-alkylphenyliminobenzylidene-4'-oxy)decanes (m.O10O.m) [13], that is the analogous compounds to the $(m.O3)_2DA$ series except the chain linking the 4-alkylphenyliminobenzylidene units is fully saturated. We can think of the $(m.O3)_2DA$ series as being trimeric in nature since the diacetylene unit is rigid whereas the m.O10O.m series is dimeric. The clearing and melting temperatures of the trimeric series are considerably higher than those of the dimeric

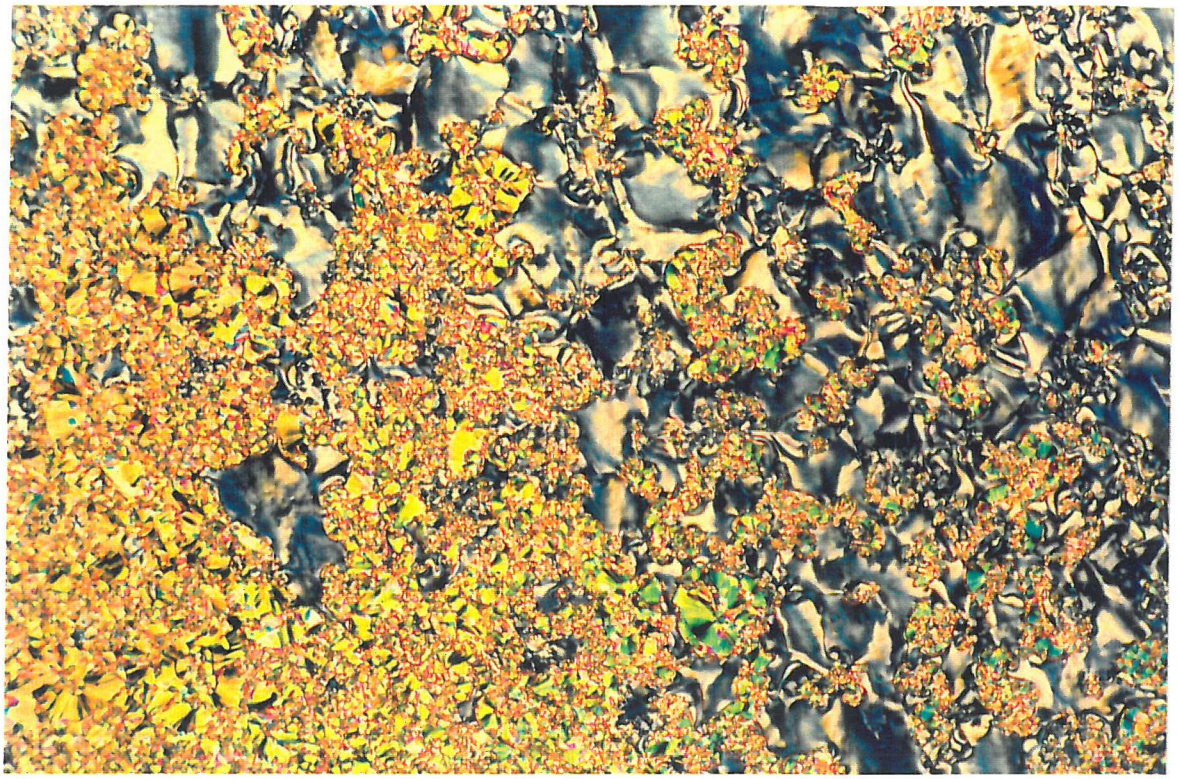

Plate 1. The smectic C phase texture of $(10.O3)_2DA$ on cooling from the isotropic phase. 176°C, magnification x200.

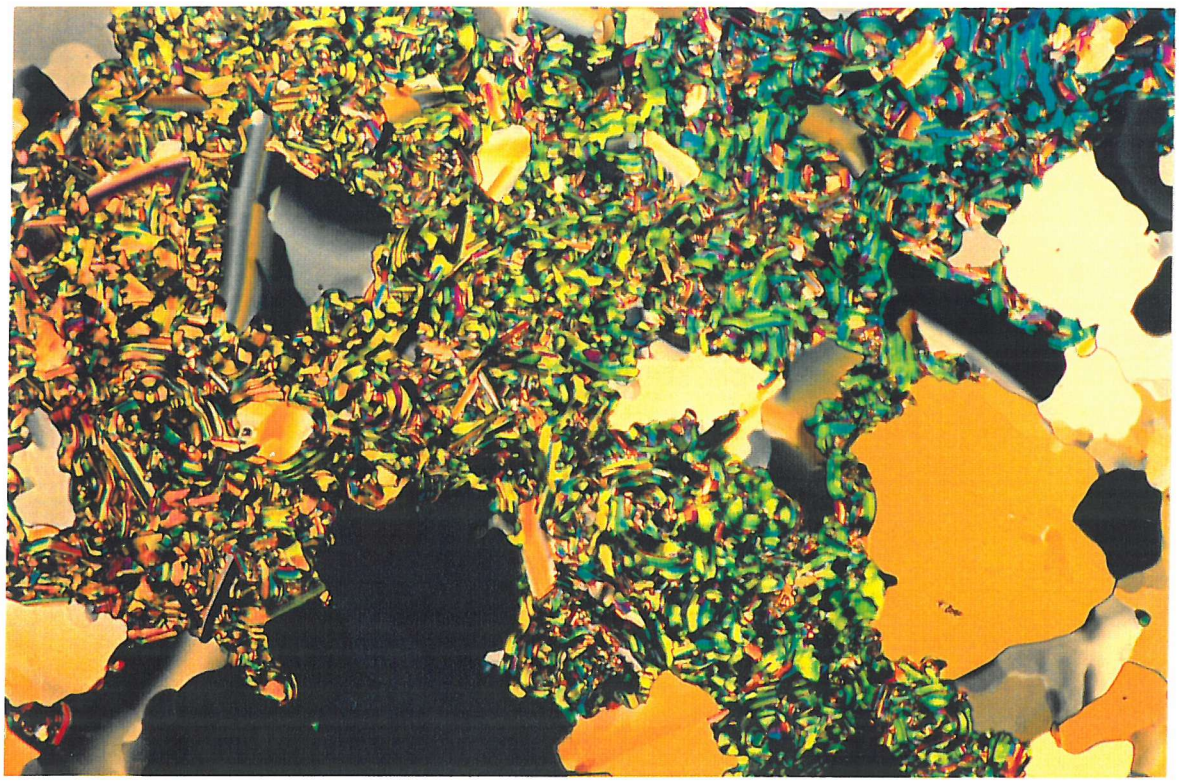

Plate 2. The smectic G/J phase texture of $(10.O3)_2DA$ on cooling from the smectic C phase. 158°C, magnification x200.

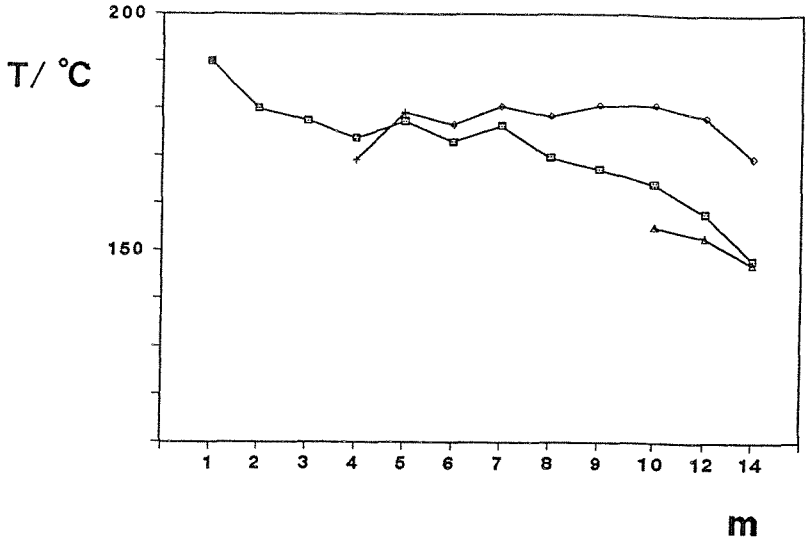

Figure 4. The influence of the number of carbon atoms in the terminal alkyl chain, *m*, on the transition temperatures of the $(m.O3)_2DA$ series. C- (■), S_A-I (+), S_C-I (◇), $S_{G/J}$-S_C (△).

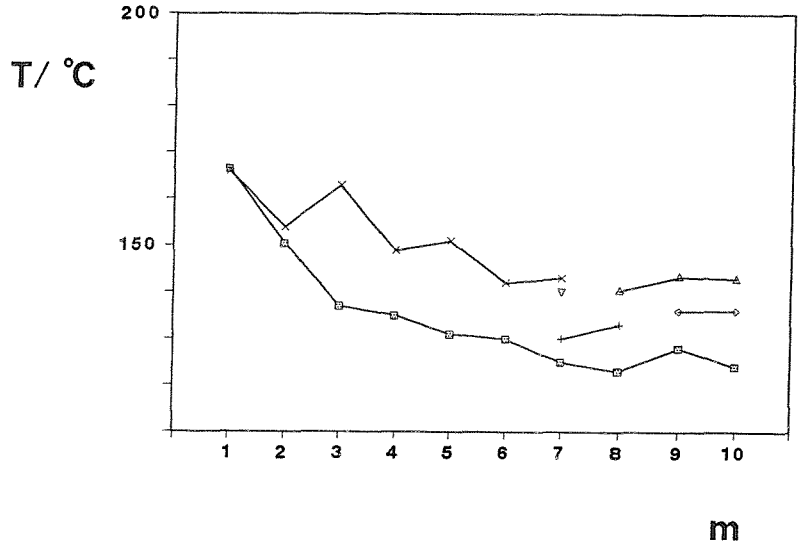

Figure 5. The influence of the number of carbon atoms in the terminal alkyl chain, *m*, on the transition temperatures of the *m*.O10O.*m* series. C- (■), N-I (×), $S_{G/J}$-S_A (+), S_A-N (△), S_F-S_A (◇), S_A-I (▽).

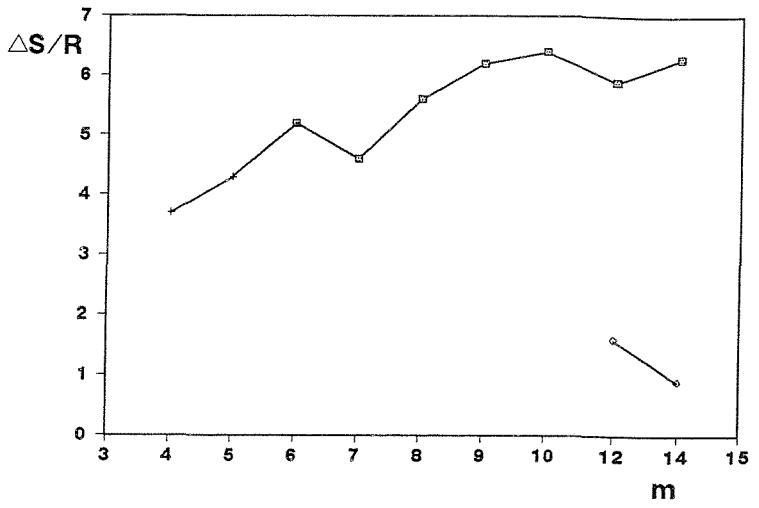

Figure 6. The influence of the number of carbon atoms in the terminal alkyl chain, *m*, on the mesophase entropy changes for the $(m.O3)_2DA$ series. S_A-I (+), S_C-I (■), $S_{G/J}$-S_C (◇).compounds.

The dimeric series has a greater polymorphism than the $(m.O3)_2DA$ compounds and there is also an enhanced odd-even effect for the clearing temperatures as shown in figure 5.

The change in the transitional entropy versus the alkyl chain length, *m*, for the $(m.O3)_2DA$ series is illustrated by figure 6. There is a general increase in the transitional entropy across the series but no real odd-even effect. The values for the S_C-I entropy change are typically larger than those for the dimeric compounds reported in [13]. The $\Delta S/R$ values for the $S_{G/J}$-S_C transition, for $m=12$ and 14, are small as the transitions occur close to the freezing point. For $m=10$ the value could not be measured since it occurs just as crystallization sets in.

The introduction of a central diacetylene unit clearly has a strong effect on the

mesophasic behaviour. The $m=4$ and 5 homologues only show smectic A behaviour but when $m \geq 6$ a crossover point is reached such that only smectic C behaviour is observed.

6.2. *The $(m.O1)_2DA$ series*

Thermodynamic data for two homologues of the $(m.O1)_2DA$ series are shown in table 3. Both homologues possess smectic C and smectic G/J phases; the phase assignment was based on similar optical textures to those of the $(m.O3)_2DA$ series. The smectic C range is larger for $(10.O1)_2DA$ than for $(10.O3)_2DA$ and, as expected, is smaller than for $(12.O1)_2DA$ [20]. The entropy changes for the S_C-I transitions are similar to those for the $(m.O3)_2DA$ series. If we compare the liquid crystal phase behaviour of $(10.O1)_2DA$ with that of its analogue, 10.O6O.10, some interesting differences arise. The liquid crystal phase transitions of the two compounds are

$(10.O1)_2DA$	C 121°C ($S_{G/J}$ 114°C) S_C 178 I,
10.O6O.10	C 103°C S_F 149°C S_C 171°C S_A 180°C I.

First, we see that 10.O6O.10 possesses a smectic A phase as well as the smectic F and C phases. Secondly, $(10.O1)_2DA$ has a higher melting point yet its clearing temperature is similar to that of 10.O6O.10. Thirdly, we notice that the smectic C phase of $(10.O1)_2DA$ is 7°C more stable on heating than that of 10.O6O.10.

6.3. *The $(m.O4)_2DA$ series*

The transition temperatures, enthalpies and entropies for four members of the $(m.O4)_2DA$ series are shown in table 3. Of the four homologues synthesized none was liquid crystalline. We can rationalise this behaviour in the following way; since the diacetylene unit is rigid we see that there is an odd number of atoms (5) linking it to the 4-alkylphenyliminobenzylidene unit. Figure 7 shows the effect of odd and

Table 3. The transition temperatures, enthalpies and entropies of some members of the $(m.O1)_2DA$ and $(m.O4)_2DA$ series as well as those of $(CB.O3)_2DA$.

Compound	T/°C			ΔH/kJmol^{-1}			ΔS/R		
	†C-I C-S_C	$S_{G/J}$-S_C	†N-I S_C-I	†C-I C-S_C	$S_{G/J}$-S_C	†N-I S_C-I	†C-I C-S_C	$S_{G/J}$-S_C	†N-I S_C-I
$(10.O1)_2DA$	121	(114)	178	31.2	(1.3)	19.9	10.5	(0.4)	5.4
$(12.O1)_2DA$	115	122	181	53.6	1.9	23.8	17.8	0.6	6.5
$(1.O4)_2DA$	†155			†53.3			†15.2		
$(6.O4)_2DA$	†129			†49.9			†15.1		
$(10.O4)_2DA$	†126			†65.1			†19.8		
$(12.O4)_2DA$	†116			†71.1			†22.1		
$(CB.O3)_2DA$	†204		†(196)	†65.1		†(4.8)	†16.3		†(2.9)

Parentheses indicate a monotropic transition.

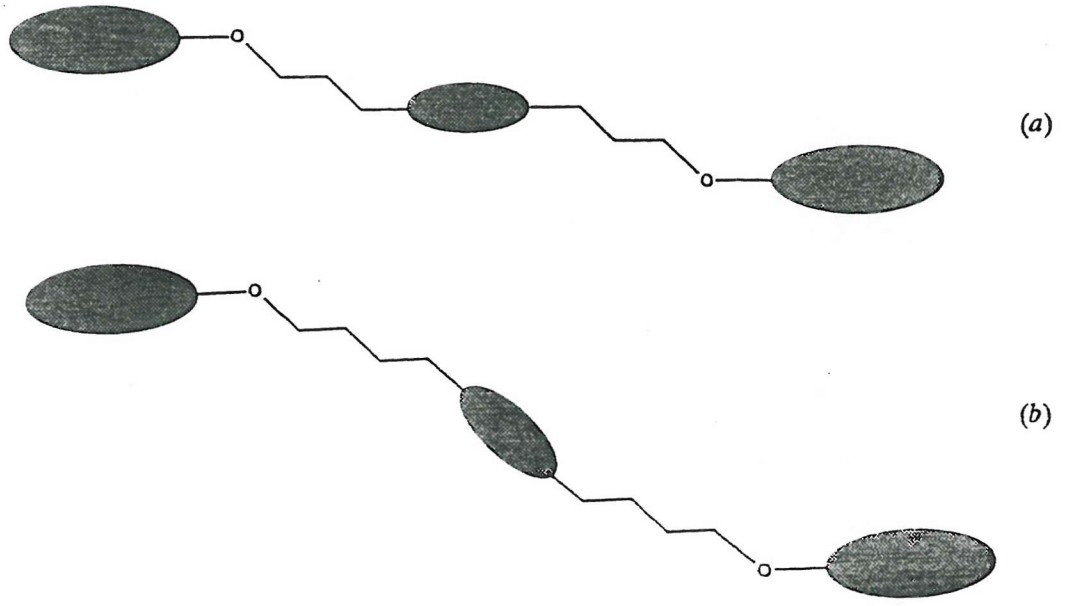

Figure 7. A schematic representation of a trimeric (m.On)$_2$DA molecule with (a) an even membered and (b) an odd membered oxymethylene spacer between the central diacetylene unit and the terminal mesogenic group.

even numbered spacers in the all *trans* conformation on the geometry of a (m.On)$_2$DA molecule. For an even-membered spacer (see figure 7(a)) we see that the diacetylene unit is parallel to the terminal mesogenic units. Conversely, in figure 7(b) the diacetylene unit is tilted with respect to the mesogenic units. The odd-membered spacer chain proves crucial and has the effect of destroying liquid crystallinity in these compounds. If we compare these compounds with the analogous m.O12O.m series we see that the latter compounds have lower melting points and show liquid crystalline behaviour [13].

The 1,4-bis((ω-4,4'-cyanobiphenyloxy)alkoxy)benzenesshow similar behaviour, where instead of a central diacetylene unit now a phenyl ring is placed in the spacer between two mesogenic units: liquid crystalline behaviour was only observed for even membered spacers [21].

6.4. *(CB.O3)$_2$DA*

$(CB.O3)_2DA$ possesses a monotropic nematic phase; its transition temperatures and thermodynamic data are shown in table 3. Comparing the transition temperatures with those of its analogue, CB.O10O.CB (C 165.8°C N 185.4°C I) [14], we see that the replacement of butane by a diacetylene unit has the effect of raising T_{NI} by 11°C but also the melting point by 39°C. The entropy change for the nematic to isotropic transition is larger than that for the α,ω-bis(4-cyanobiphenyl-4'-oxy)alkanes [14] but similar to the 1,4-bis((ω-4,4'-cyanobiphenylyloxy)alkoxy)benzeneswhere a phenyl ring is inserted into the spacer [21].

6.5. *The third harmonic signals of (14.O3)$_2$DA and (CB.O3)$_2$DA*

The third harmonic signals for $(14.O3)_2DA$ and $(CB.O3)_2DA$ are shown in table 4 where they are compared with the well-known third harmonic generators PTS-PDA (*para*-toluenesulphonate polydiacetylene) and fused quartz. The third harmonic signal of $(14.O3)_2DA$, shown in plate 3(*b*), is approximately half that of PTS-PDA; $(CB.O3)_2DA$ has a signal two orders of magnitude smaller. Plate 3(*a*) shows the effect of replacing the 636nm filter with a 620nm filter: the signal disappears to noise proving that the signal in plate 3(*b*) is purely third harmonic and not a result of frequency mixing. The third harmonic signal transmitted by the film of $(CB.O3)_2DA$ (see plate 4) is much larger than that of its powder analogue (any absorption was not taken into account). This is clear since more of the third harmonic signal is detected. However the result is intersting as it is considerably larger than that of fused quartz (see table 4). The estimated $\chi^{(3)}$ value for the film of $(CB.O3)_2DA$ was calculated using the following equation:

$$\chi^{(3)}_{film} = (2/\pi)\,\chi^{(3)}_{quartz}\,\sqrt{(I_{3w,film}/I_{3w,quartz})} \cdot (l_{c,quartz}/d_{film}), \qquad (3)$$

where $\chi^{(3)}_{quartz}$ is $3.9 \times 10^{-22} m^2V^{-2}$, $l_{c,quartz}$ (the coherence length of quartz) is 18.24μm,

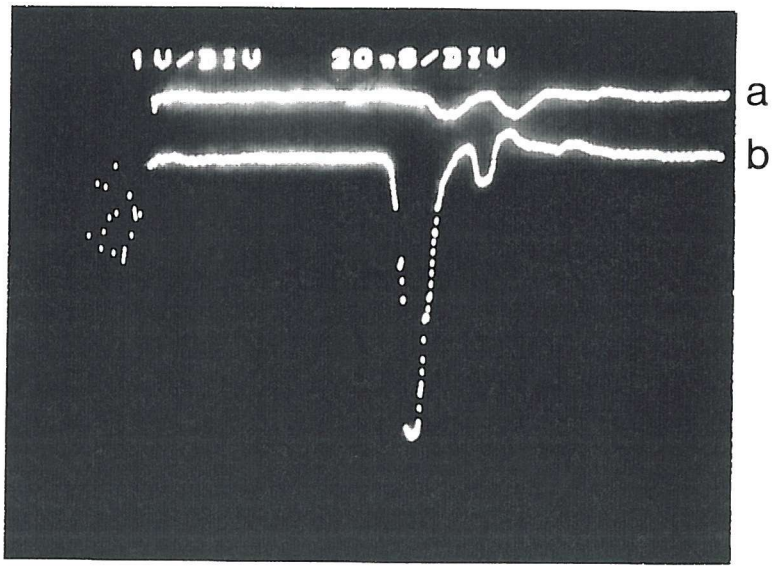

Plate 3. The third harmonic signal from a powder sample of $(CB.O3)_2DA$ (*b*) and the effect of replacing the 636nm filter with a 620nm filter (*a*).

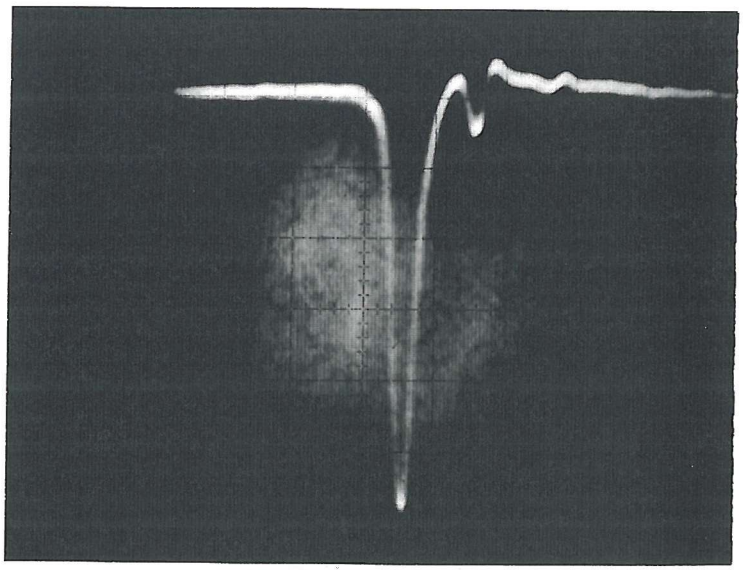

Plate 4. The third harmonic signal from a film of $(CB.O3)_2DA$.

Table 4. The relative strengths of the third harmonic signals for powder samples of the compounds studied compared to that of PTS-PDA. The estimated $\chi^{(3)}$ value for the film of $(CB.O3)_2DA$ is also given and compared to that of fused quartz.

Material	THG signal
$(CB.O3)_2DA$ powder	$3.1 \times 10^3 mV$
$(14.O3)_2DA$ powder	$1.7 \times 10^5 mV$
PTS-PDA powder	$3.0 \times 10^5 mV$
$(CB.O3)_2DA$ film	$9.2 \times 10^{-20} m^2V^{-2}$
Fused quartz	$3.9 \times 10^{-22} m^2V^{-2}$

$I_{3w,film}$ is the measured signal (in mV), $I_{3w,quartz}$ is 350mV, and d_{film} is the estimated film thickness of 6.25μm as measured by a multi-channel analyser (an instrument used to determine the thickness of the air space in liquid crystal cells at G.E.C., H.R.C.).

Unfortunately no third harmonic generation was detected from the cells containing $(CB,O3)_2DA$ since the film laser-damaged easily; this could be due to local heating by the laser.

7. Conclusions

A new series of liquid crystalline compounds, the $(m.On)_2DA$ series, has been reported. In comparison to the analogous *m*.O*n*O.*m* series of compounds the central diacetylene unit has a profound effect on the liquid crystalline behaviour of the

compounds. It has been inferred that an odd number of atoms between the diacetylene unit and the Schiff base destroys liquid crystallinity, whereas an even number favours liquid crystalline behaviour. The incorporation of a diacetylene unit in the spacer causes a rise in both the melting and clearing transitions for the liquid crystalline compounds reported. Unlike the rich polymorphism of the *m*.O*n*O.*m* series the liquid crystalline (*m*.O*n*)$_2$DA compounds tend to exhibit smectic C behaviour for $m \geq 6$ which is probably due to packing constraints in the layers. For short chain homologues of the (*m*.O3)$_2$DA series, i.e. $m = 4$ and 5, a smectic A phase is observed, whereas long chain homologues ($m = 10,12$ and 14) show a monotropic smectic G or J phase in addition to a smectic C phase.

Two compounds, (14.O3)$_2$DA and (CB.O3)$_2$DA, were polymerized by UV radiation to their parent polydiacetylenes and exhibited large third harmonic generation in powder form. A crude film of polymerized (CB.O3)$_2$DA had a third harmonic signal two orders of magnitude greater than that of fused quartz, a well-known third harmonic generator.

References

[1] Wegner, G., 1969, *Z. Naturforsch.*, **24b**, 824.

[2] Kubodera, K., and Kobayashi, H., 1990, *Molec. Crystals liq. Crystals*, **182A**, 103.

[3] Tomaru, S., Kubodera, K., Zembutsu, S., Takeda, K., and Hasegawa, M., 1987, *Electronics Lett.*, **23**, 595.

[4] Ulrich, D.R., 1987, *Polymer*, **28**, 533.

[5] Baker, G.L., and Etemad, S., 1987, *SPIE Advances in Non-linear Polymers and Inorganic Crystals, Liquid Crystals and Laser Media*, **824**, 102.

[6] Tieke, B., Wegner, G., Naegele, D., and Ringsdorf, H., 1976, *Angew. Chem. Int. Ed. Engl.*, **15**, 764.

[7] Kelker, H., and Hatz, R., 1980, *Handbook of Liquid Crystals* (Verlag Chemie), p.174.

[8] Bloor, D., 1986, *Molec. Crystals liq. Crystals*, **93**, 183.

[9] Grant, B., Clecak, N.J., and Cox, R.J., 1979, *Molec. Crystals liq. Crystals*, **51**, 209.

[10] Grant, B., 1978, *Molec. Crystals liq. Crystals*, **48**, 175.

[11] Fouquey, C., Lehn, J.M., and Malthête, J., 1987, *J. chem. Soc., chem. Commun.*, 1424.

[12] Le Moigne, J., Soldera, A., Guillon, D., and Skoulios, A., 1989, *Liq. Crystals*, **6**, 627.

[13] Date, R.W., Imrie, C.T., Luckhurst, G.R., and Seddon, J.M., 1992, *Liq. Crystals*, **12**, 203.

[14] Emsley, J.W., Luckhurst, G.R., Shilstone, G.N., and Sage, I., 1984, *Molec. Crystals liq. Crystals*, **149**, 185.

[15] Furniss, B.S., Hannaford, A.J., Rogers, V., Smith, P.W.G., and Tatchek, A.R. (editors), 1978, *Vogel's Textbook of Practical Organic Chemistry*, 4th Edn, (Wiley), p.351.

[16] Machinek, R., and Lüttke, W., 1975, *Synthesis*, 255.

[17] Donahoe, H.B., Benjamin, L.E., Fennoy, L.V., and Greiff, D., 1960, *J. org. Chem.*, **26**, 474.

[18] Kurtz, S.K., and Perry, T.T., 1968, *J. appl. Phys.*, **39**, 3798.

[19] Goodby, J.W., and Gray, G.W., 1984, *Smectic Liquid Crystals - Textures and Structures* (Leonard Hill).

[20] Gray, G.W., 1979, *The Molecular Physics of Liquid Crystals*, edited by G.R. Luckhurst and G.W. Gray (Academic Press), Chap. 1.

[21] Furuya, H., Asahi, K., and Abe, A., 1986, *Polymer J.*, **18**, 779.

CHAPTER 3

Dimeric liquid crystals with chiral terminal chains

1. Introduction

The cholesteric phase was discovered in 1888 [1] and has continued to fascinate researchers ever since. The cholesteric phase which is produced by derivatives of cholesterol is structurally equivalent to the chiral nematic phase formed by rod-like molecules which contain chiral centres. Chiral centres can be introduced into a rod-like molecule by the addition of suitably branched alkyl chains. In addition to creating a chiral centre and so influencing the phase behaviour a branched chain also effects the transitional behaviour. The effect of branched alkyl chains on liquid crystalline behaviour has been examined systematically in [2] for low molar mass liquid crystals. It was observed that a methyl branch at the α-carbon of a terminal alkyl chain decreases the nematic to isotropic transition temperature considerably. As the methyl branch is moved progressively away from the mesogenic core so the effect on T_{NI} becomes less significant. The methyl branch in the α-position tends to reduce the length-to-breadth ratio to a greater extent than a methyl branch further away from the mesogenic core; it is this decrease in the molecular anisotropy that leads to the reduced thermal stability of liquid crystal phases. It should be noted that alkyl chain branching also lowers the melting point but to a much smaller extent compared to the reduction in T_{NI}. Interestingly, as the branching centre is moved progressively away from the mesogenic core an enhancement in the thermal stability of the smectic C phase is observed [3]. This is thought to result from the steric asymmetry of branched systems such that when the molecules pack together they preferentially do so in a tilted fashion.

For dimeric liquid crystals it is possible to introduce a branch into either the flexible

spacer linking the two mesogenic groups or into one or both of the terminal alkyl chains. There are several reports of dimers which possess chiral spacers [4-6]. The effect of a branched spacer on the clearing transition temperatures is exemplified by the bis-azomethines which possess a central (*R*)-3-methyladipoyl group (see structure (1)) as the flexible spacer [6]; they have been compared with their unbranched analogues in [7]. Both series of compounds exhibited extensive smectic behaviour as the terminal alkyl chains were lengthened. For the unbranched compounds the onset of smectic behaviour began with the $n=3$ homologue whereas the $n=4$ homologue was the first compound to exhibit smectic properties for the branched compounds. It was observed that the clearing temperatures for the compounds with a branched spacer were on average 30°C lower compared to their straight chain analogues.

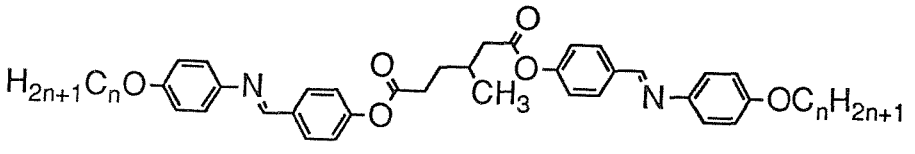

(1)

There are few reports of dimers containing chiral terminal chains. One study was based on the molecule shown by structure (2) [8]. This compound has a ferroelectric smectic C phase and has the phase sequence, C 122°C S_C^* 139°C S_A 155°C I. The pitch was determined to be 2.5μm at the S_C^*-S_A transition.

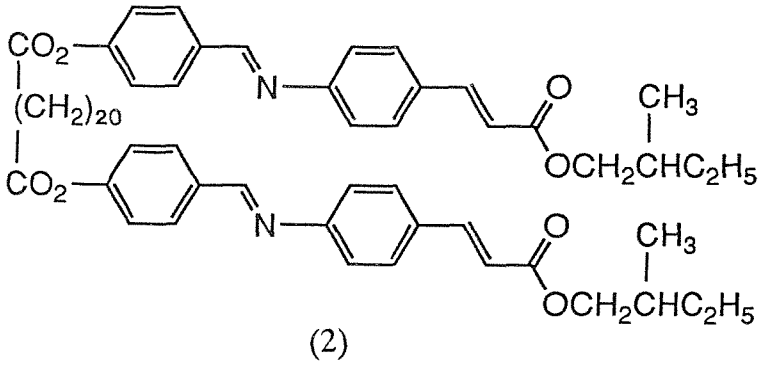

(2)

The liquid crystal phases formed by dimeric molecules are considerably more ordered orientationally than the analogous phases exhibited by monomeric compounds. Thus the elastic constants of even membered dimers should be higher than those of odd membered dimers. As a result the chiral nematic phases of dimeric liquid crystals should exhibit enhanced chirality since low orientational order should lead to an increase in the twisting power of the material. To enhance our knowledge of dimeric liquid crystals with chiral terminal chains we present two new homologous series of dimeric liquid crystals based on 2-methylbutan-1-ol: firstly, the α,ω-bis(4-(2-methylbutyl)phenyliminobenzylidene-4'-oxy)alkanes and second the α-(4-(2-methylbutyl)phenyliminobenzylidene-4'-oxy)-ω-(4'-cyanobiphenyl-4-yloxy)alkanes. All of the racemic compounds were synthesised together with a selection of their chiral analogues. The symmetric dimers were chosen as their monomeric analogues are already known [9] and further the structurally isomeric, straight chain analogues of these dimers, the α,ω-bis(4-pentylphenyliminobenzylidene-4'-oxy)alkanes, have been studied in detail [10]. Similarly the α-(4-alkylphenyliminobenzylidene-4'-oxy)-ω-(4'-cyanobiphenyl-4-yloxy)alkanes are well-characterised [11]. To gauge the effect of branching in the terminal chain more fully for the non-symmetric dimers the remaining homologues of the structurally isomeric α-(4-pentylphenyliminobenzylidene-4'-oxy)-ω-(4'-cyanobiphenyl-4-yloxy)alkanes were synthesised as only the n=3-6 homologues were reported in [11].

2. Experimental

For convenience we shall denote the α,ω-bis(4-(2-methylbutyl)phenyliminobenzylidene-4'-oxy)alkanes and the α-(4-(2-methylbutyl)phenyliminobenzylidene-4'-oxy)-ω-(4'-cyanobiphenyl-4-yloxy)alkanes by the mnemonics 2MB.O*n*O.2MB and 2MB.O*n*O.CB, respectively. Here 2MB denotes the 2-methylbutyl group, CB cyanobiphenyl and n is the number of carbon atoms in the alkyl spacer. The straight chain analogues of 2MB.O*n*O.CB, the α-(4-pentylphenyliminobenzylidene-4'-oxy)-ω-(4'-cyanobiphenyl-4-yloxy)alkanes, are abbreviated to 5.O*n*O.CB, where 5 represents the number of carbon atoms in the terminal chain. The chiral analogues of

2MB.O*n*O.2MB and 2MB.O*n*O.CB are abbreviated to (*R*)2MB.O*n*O.(*R*)2MB and (*R*)2MB.O*n*O.CB, respectively, where *R* is the absolute configuration of the 2-methylbutyl substituent.

The syntheses of the racemic and chiral 2MB.O*n*O.2MB and 2MB.O*n*O.CB series (and 5.O*n*O.CB series) are outlined in schemes 1 and 2, respectively. The syntheses of (*R*)2MB.O6O.(*R*)2MB and (*R*)2MB.O6O.CB are given in the following experimental methods.

2.1. *Synthesis of (R)-(+)-2-methylbutyl-4-toluenesulphonate*

30g (3.4 x 10^{-1}mol) of (*S*)-(-)-2-methylbutan-1-ol ($[\alpha]_D^{23}$ = -5.8°, neat) was dissolved in pyridine (300ml) and cooled in an ice bath in a 500ml conical flask. To this 4-toluenesulphonyl chloride (129.8g; 6.8 x 10^{-1}mol) was added. The reaction mixture was stirred for half an hour and left overnight in the fridge. The mixture was diluted with an excess of water and stirred for two hours in an ice bath. The mixture was then extracted with diethyl ether (3 x 100ml). The extracts were washed with cold 6M hydrochloric acid until the presence of pyridine had been irradicated, then with distilled water and dried with anhydrous sodium sulphate and potassium carbonate. After filtration the ether was evaporated to yield a colourless liquid. Yield 76.26g (92%).

IR (NaCl disc, neat): ν 1097.4, 1184.3, 1356.2cm^{-1} (O=S=O).
^{1}H NMR ($CDCl_3$): δ 0.7-1.8 (m, 11H), 2.4 (s, 3H), 3.7-3.8 (d, 2H), 7.3-7.4, (d, 2H), 7.7-7.8ppm (d, 2H).
$[\alpha]_D^{20}$ = +4.94° (*c*, 0.89) $CHCl_3$. Literature value +4.4° (*c*, 1.4) $CHCl_3$ [9].

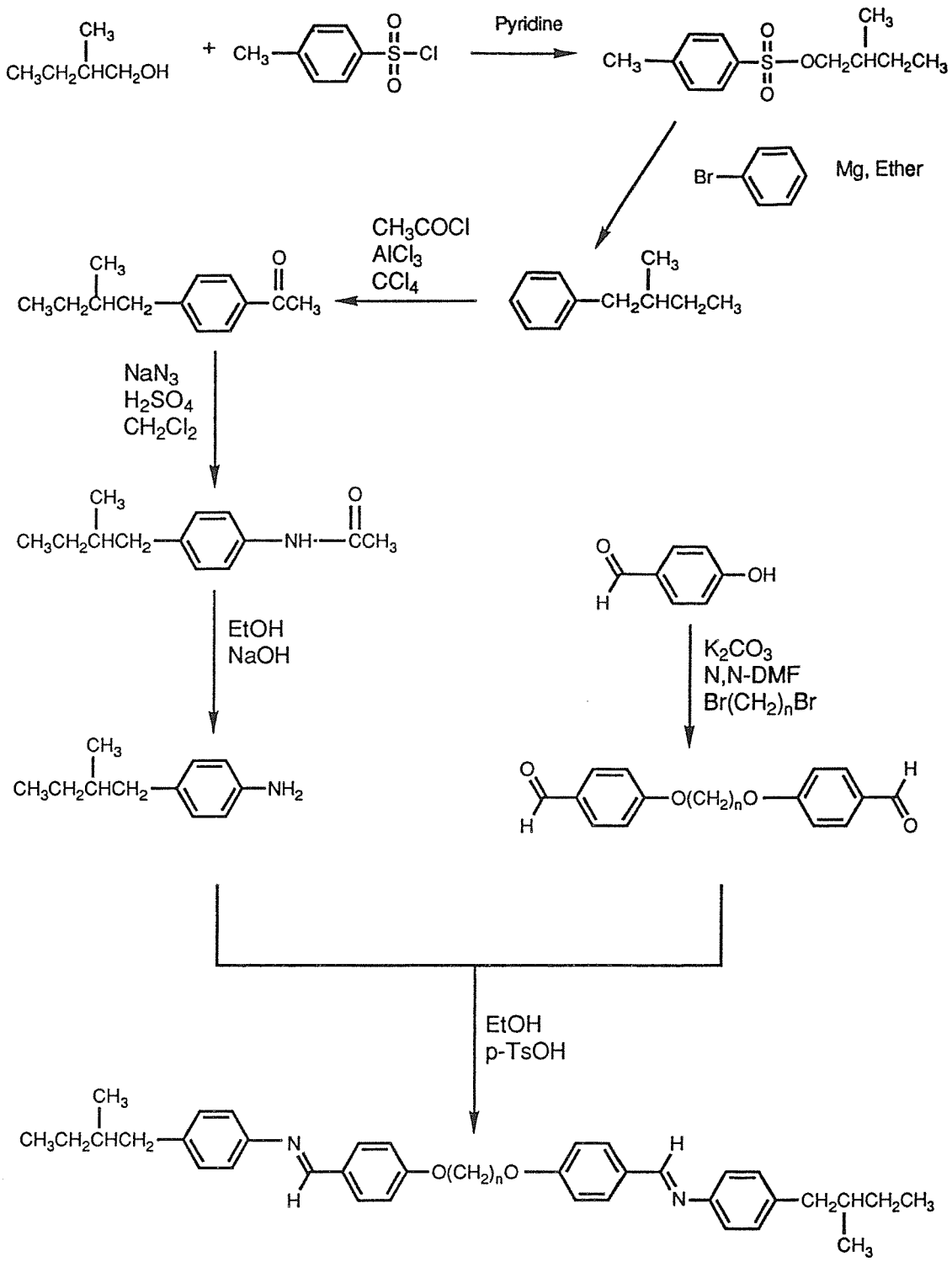

Scheme 1. The synthetic route to the α,ω-bis(*R*)-(+)-(4-(2-methylbutyl)phenyliminobenzylidene-4'-oxy)alkanes.

2.2. *Synthesis of (R)-(+)-4-(2-methylbutyl)benzene*

Phenyl magnesium bromide was prepared from bromobenzene (24.38g; 1.55 x 10^{-1}mol) and magnesium turnings (3.72g; 1.55 x 10^{-1}mol) in sodium-dried diethyl ether (200ml) in a 500ml, three neck, round bottom flask fitted with a Leibig condenser, calcium chloride guard tube and dropping funnel. The reagent was cooled in an ice bath and (*R*)-(+)-2-methylbutyl-4-toluenesulphonate (76.26g; 3.1 x 10^{-1}mol) was added in a dropwise fashion. When the addition was complete the reaction was stirred for two hours, refluxed for two hours and left to stand overnight. Aqueous 1M sulphuric acid was added until a clear solution formed. The mixture was separated and the aqueous layer extracted with diethyl ether (3 x 100ml). The combined organic layers were washed with sodium bicarbonate, water and dried with anhydrous magnesium sulphate. The solvent was evaporated and the product distilled on a Kugelrohr apparatus. A colourless liquid was collected from the fraction boiling at 90-98°C (1mb). Yield 45.4g (39%).

IR (NaCl disc, neat): ν 1494.8, 1604.9cm^{-1} (Aromatic C=C).
^{1}H NMR ($CDCl_3$): δ 0.8-1.8 (m, 9H), 2.1-2.8 (2q, 2H), 7.1 (s, 5H).
$[\alpha]_D^{20}$ = +6.15° (*c*, 2.6) $CHCl_3$. Literature value +9.4° (*c*, 5) $CHCl_3$ [9].

2.3. *Synthesis of (R)-4-(+)-(2-methylbutyl)acetophenone*

(*R*)-(+)-4-(2-methylbutyl)benzene (25g; 1.69 x 10^{-1}mol) was added dropwise to a stirred mixture of anhydrous aluminium (III) chloride (27g; 2.0 x 10^{-1}mol) and acetyl chloride (13.3g; 1.69 x 10^{-1}mol) in carbon tetrachloride (200ml) in a 500ml, round bottom, three neck flask fitted with a Leibig condenser and calcium chloride guard tube cooled in an ice bath. During the addition the temperature of the reaction mixture was kept between 0-5°C to avoid formation of the *ortho* derivative. The ice bath was removed and the mixture stirred for an additional hour at room temperature. The mixture was then poured cautiously (exothermic hydrolysis of the complex) into a 500ml beaker containing concentrated hydrochloric acid (250ml) and

ice (500g). A heterogeneous mixture resulted of which only the lower, organic layer was kept. This was washed with 2M hydrochloric acid (2 x 100ml) to remove the aluminium salts, then with sodium bicarbonate (100ml) and finally with distilled water (100ml) before being dried overnight with 4Å molecular sieves. The solvent was removed on a rotary evaporator and the residue distilled. The fraction which distilled at 108°C (1mb) was collected. Yield 22.6g (71%).

IR (NaCl disc, neat): ν 1684.1cm^{-1} (C=O).
^{1}H NMR ($CDCl_3$): δ 0.6-1.8 (m, 9H), 2.0-2.8 (m, 5H), 7.15 (d, 2H), 7.8ppm (d, 2H).
$[\alpha]_D^{20}$ = +5.82° (*c*, 3.35) $CHCl_3$.

2.4. *Synthesis of (R)-(+)-4-(2-methylbutyl)acetanilide*

Sodium azide (5.3g; 8.3 x 10^{-2}mol) was added in small portions to a stirred solution of (*R*)-(+)-4-(2-methylbutyl)acetophenone (15.61g; 8.2 x 10^{-2}mol) in 70% sulphuric acid in a 250ml, two neck, round bottom flask fitted with a Leibig condenser and bubbler. To prevent foaming dichloromethane (40ml) was added before the sodium azide. During the reaction the temperature of the reaction mixture was kept between 15-20°C by a water bath. Nitrogen was evolved and the mixture became slightly viscous. The mixture was stirred for a further two hours and then poured into a mixture of chilled water (200ml) and dichlormethane (100ml). The resulting heterogeneous mixture was poured into a separating funnel. The lower organic layer was separated and kept and the aqueous layer was extracted with dichlormethane (2 x 50ml). The combined organic layers were washed with 50ml of 2M sodium bicarbonate solution and distilled water. The volume of the dichlormethane was reduced by half leaving about 50ml which was poured into 200ml of petroleum ether (60-80°C). The resulting white, crystalline precipitate was filtered off and dried *in vacuo*. Yield 8.94g (53%); mp 119°C.

IR (NaCl disc, film): ν 1598.1, 3455.4 (N-H), 1660.2cm^{-1} (C=O).
^{1}H NMR ($CDCl_3$): δ 0.8-1.8 (m, 9H), 2.0 (s, 4H), 2.2-2.7 (d, 2H), 7.0-7.1 (d, 2H), 7.4-

7.5ppm (d, 2H).
$[\alpha]_D^{20}$ = +18.3° (*c*, 9.6) $CHCl_3$.

2.5. *Synthesis of (R)-(+)-4-(2-methylbutyl)aniline*

(*R*)-(+)-4-(2-methylbutyl)acetanilide (8.94g; 4.4 x 10^{-1}mol) and 40g of sodium hydroxide pellets, dissolved in 26ml of distilled water, were refluxed in ethanol (70ml) for five and a half hours in a 250ml round bottom flask fitted with a Leibig condenser. The mixture was cooled and part of the solvent removed by rotary evaporation until the volume was about 40ml. This was then poured into a mixture of 150ml of water and 200g of ice. The resulting heterogeneous mixture was poured into a separating funnel and extracted with toluene (2 x 100ml). The combined organic extracts were washed with distilled water (2 x 100ml) and dried with anhydrous potassium carbonate. The solvent was removed by rotary evaporation and the residue distilled with a Kugelrohr apparatus. The fraction which distilled at 124°C (1mb) was collected. Yield 6.12g (85%).

IR (NaCl disc, neat): ν 1622.0, 3368.0, 3429.1cm^{-1} (Ar. N-H).
^{1}H NMR ($CDCl_3$): δ 0.8-2.0 (m, 9H), 2.1-2.8 (2q, 2H), 3.4 (s, 2H), 6.4-6.6 (d, 2H), 6.8-7.0ppm (d, 2H).
$[\alpha]_D^{20}$ = +14.05° (*c*, 6.3) $CHCl_3$. Literature value +13.5° (*c*, 6.3) $CHCl_3$ [9].

2.6. *Synthesis of α,ω-bis(4-formylphenyl-4'-oxy)hexane* [12]

1,6-Dibromohexane (4g; 1.65 x 10^{-2}mol), 4-hydroxybenzaldehyde (4.24g; 3.5 x 10^{-2}mol) and anhydrous potassium carbonate (13.68g; 9.9 x 10^{-2}mol) were refluxed in 30ml of dry *N,N*-dimethylformamide (4Å molecular sieves) for three hours in a 100ml conical flask fitted with a Leibig condenser and calcium chloride guard tube. The reaction mixture was allowed to cool and then poured into 100ml of distilled water and stirred. The resulting precipitate was filtered off, dried *in vacuo* and recrystallized

twice from ethanol. The resulting off-white crystalline product was again dried *in vacuo*. Yield 3.82g (71%). All the other homologues were synthesised in the same way except for the undecyl and dodecyl homologues which were refluxed in absolute ethanol for 24h as a polymerisation reaction occurs in the higher boiling *N,N*-dimethylformamide solvent [10]. All the yields were in excess of 60%. Table 1 gives a list of the melting points and compares them with those of [12].

IR (NaCl disc, film): ν 1684.4cm^{-1} (C=O).
^{1}H NMR ($CDCl_3$): δ 1.2-2.0 (m, 8H), 4.0 (t, 4H), 7.0 (d, 4H), 7.8 (d, 4H), 9.8ppm (s, 1H).

2.7. *Synthesis of α,ω-bis(R)-(+)-(4-(2-methylbutyl)phenyliminobenzylidene -4'-oxy)hexane*

(*R*)-(+)-4-(2-methylbutyl)aniline (0.5g; 3.07 x 10^{-3}mol) was added to a hot solution of α,ω-bis(4-formylphenyl-4'-oxy)hexane (0.47g; 1.46 x 10^{-3}mol) with a few crystals of 4-toluenesulphonic acid in absolute ethanol (30ml) in a 50ml conical flask fitted with a calcium chloride guard tube. While cooling, the reaction mixture was stirred for five hours. A creamy yellow precipitate formed which was filtered off and recrystallized twice from dry ethyl acetate to give white crystals which were dried *in vacuo*. Yield 0.61g (68%). The yields of the remaining homologues were all in excess of 65%. The optical rotations of the other homologues are shown in table 2.

IR (NaCl disc, film): ν 1509.2, 1571.4, 1596.3, 1624.0cm^{-1} (C=N).
^{1}H NMR ($CDCl_3$): δ 0.8-1.0 (t, 4H), 1.1-1.9 (m, 22H), 2.1-2.8 (2q, 4H), 3.9 (t, 4H), 6.7 (d, 4H), 6.9 (s, 8H), 7.6 (d, 4H), 8.1ppm (s, 2H).
MS (EI): 469, 616 (M^+).
$[\alpha]_D^{20}$ = +17.5° (*c*, 1.04) $CHCl_3$.

Table 1. The melting points of the α,ω-bis(4-formylphenyl-4'-oxy)alkanes compared to those of [12].

n	Melting point/°C	Lit. melting point/°C
3	130-131	130
4	102-104	103-104
5	80-81	80-81
6	107-108	106-107
7	63-65	62-64
8	84-86	82-83
9	82-84	81-83
10	78-80	78-80
11	82-84	82-84
12	70-71	68-71

Table 2. The observed optical and calculated molecular rotations of the (*R*)2MB.O*n*O.(*R*)2MB and (*R*)2MB.O*n*O.CB compounds.

Compound	$[\alpha]_D^{20}$/°	$[M]_D^{20}$/°
(*R*)2MB.O4O.(*R*)2MB	19.1	112.3
(*R*)2MB.O6O.(*R*)2MB	17.5	107.8
(*R*)2MB.O8O.(*R*)2MB	8.7	56.0
(*R*)2MB.O6O.CB	8.5	46.2
(*R*)2MB.O7O.CB	14.4	80.4
(*R*)2MB.O8O.CB	19.9	113.8
(*R*)2MB.O9O.CB	40.2	235.6

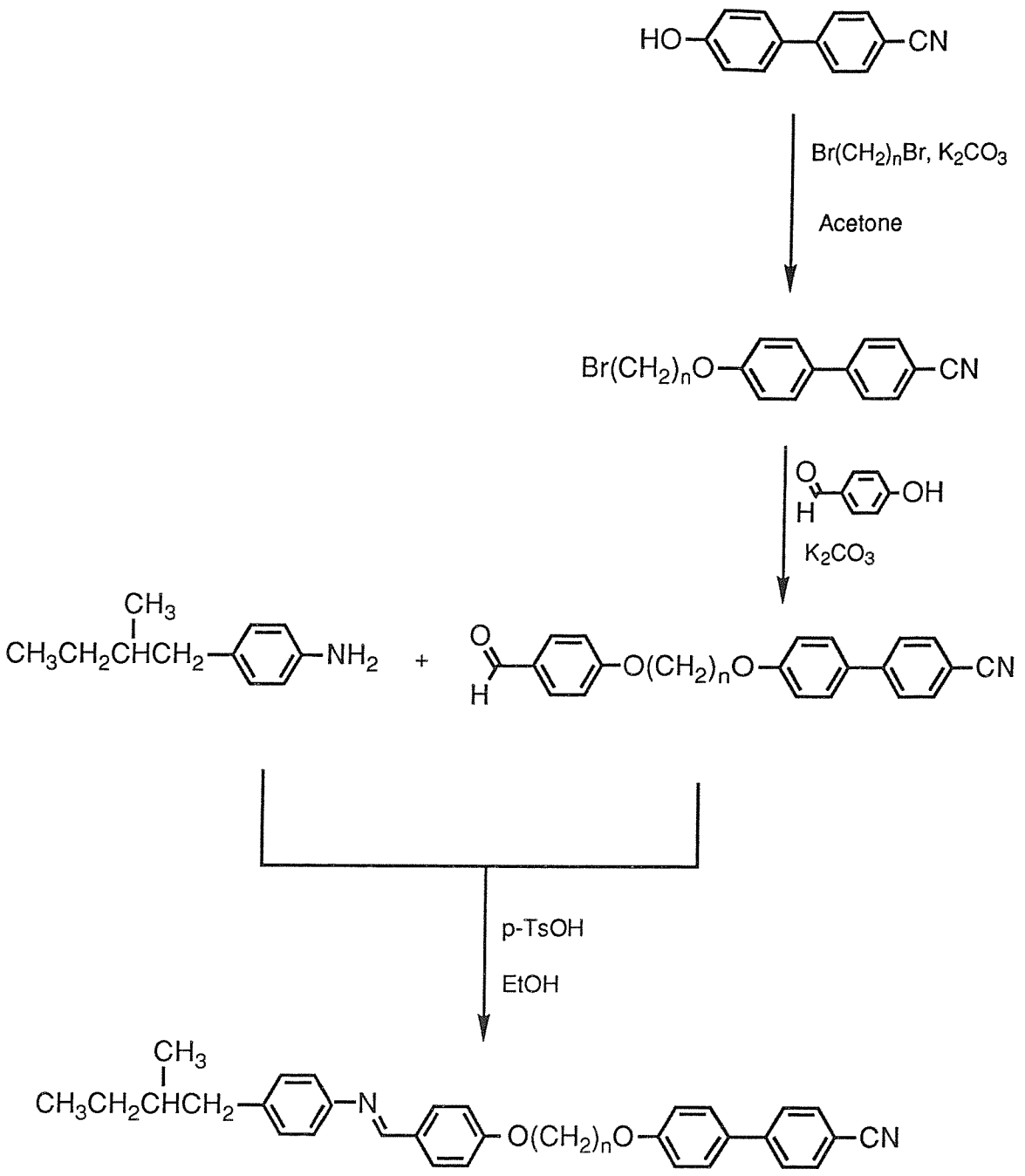

Scheme 2. The synthetic route to the α-(*R*)-(+)-(4-(2-methylbutyl)phenyl-iminobenzylidene-4'-oxy)-ω-(4'-cyanobiphenyl-4-yloxy)alkanes.

2.8. *Synthesis of α-bromo-ω-(4'-cyanobiphenyl-4-yloxy)hexane*

4-Hydroxy-4'-cyanobiphenyl (2g; 1.03 x 10^{-2}mol), 1,6-dibromohexane (25g; 1.03 x 10^{-1}mol) and anhydrous potassium carbonate (10.32g; 7.5 x 10^{-2}mol) were refluxed in Analar acetone (150ml) for 24h in a 250ml conical flask fitted with a Leibig condenser and calcium chloride guard tube. The reaction mixture was filtered while still hot to remove excess potassium carbonate and any potassium bromide formed in the reaction; these solids were washed several times with hot acetone. The acetone was removed by rotary evaporation and the excess 1,6-dibromohexane recovered on a Kugelrohr apparatus (90°C, 1mb). The remaining solid residue was recrystallized twice from methanol and dried *in vacuo*. Yield 2.89g (79%). The remaining homologues were all obtained in yields in excess of 75%; their transition temperatures are shown in table 3.

IR (NaCl disc, film): ν 643.8 (C-Br), 2221.7cm^{-1} (C≡N).
^{1}H NMR ($CDCl_3$): δ 1.5-2.0 (m, 8H), 3.4 (t, 2H), 4.0 (t, 2H), 7.0 (d, 2H), 8.1 (d, 2H), 8.2 (s, 4H).

2.9. *Synthesis of α-(4'-cyanobiphenyl-4-yloxy)-ω-(4-formylphenyl-4'-oxy)hexane*

α-Bromo-ω-(4'-cyanobiphenyl-4-yloxy)hexane (1g; 2.93 x 10^{-3}mol), 4-hydroxybenzaldehyde (0.4g; 3.23 x 10^{-3}mol) and anhydrous potassium carbonate (1.22g; 8.79 x 10^{-3}mol) were refluxed in Analar acetone (50ml) for 24h in a 50ml conical flask fitted with a Leibig condenser and calcium chloride guard tube. The reaction mixture was filtered while still hot to remove excess potassium carbonate and any potassium bromide formed in the reaction. The residue was washed several times with hot acetone. The acetone was removed on a rotary evaporator and the crude solid remaining was recrystallized twice from ethanol and dried *in vacuo*. Yield 0.84g (72%). The yields of all the other homologues were in excess of 65% and the transition temperatures of all the homologues are shown in table 4.

Table 3. The phase behaviour of the α-bromo-ω-(4'-cyanobiphenyl-4-yloxy)alkanes.

n	T/°C	
	C-I	N-I
3	107	(40)
4	66	(63)
5	84	(65)
6	70	(65)
7	79	(66)
8	84	(65)
9	74	(72)
10	77	(68)
11	78	(68)
12	77	(69)

Parentheses indicate a monotropic transition.

Table 4. The phase behaviour of the α-(4'-cyanobiphenyl-4-yloxy)-ω-(4-formylphenyl-4'-oxy)alkanes.

n	T/°C	
	C-I †C-N	N-I
3	108	
4	†115	141
5	104	(82)
6	†85	126
7	94	(87)
8	†111	116
9	†89	94
10	†93	106
11	97	(88)
12	†97	103

Parentheses indicate a monotropic transition.

IR (NaCl disc, film): ν 1686.5 (C=O), 2220.7cm^{-1} (C≡N).
^{1}H NMR ($CDCl_3$): δ 1.4-2.1 (m, 8H), 4.0-4.2 (m, 4H), 7.1 (d, 4H), 7.8 (d, 2H), 7.9 (s, 4H), 8.0 (d, 2H), 9.8 (s, 1H).

2.10. *Synthesis of α-(R)-(+)-(4-(2-methylbutyl)phenyliminobenzylidene-4'-oxy)-ω-(4'-cyanobiphenyl-4-yloxy)hexane*

(*R*)-(+)-4-(2-methylbutyl)aniline (0.5g; 3.07 x 10^{-3}mol), prepared as described in section 2.5 was added to a stirred solution of α-(4'-cyanobiphenyl-4-yloxy)-ω-(4-formylphenyl-4'-oxy)hexane (1.27g; 3.18 x 10^{-3}mol) and a few crystals of 4-toluenesulphonic acid in hot absolute ethanol in a 50ml conical flask fitted with a calcium chloride guard tube. The reaction mixture was stirred for five hours while cooling. A creamy yellow precipitate formed which was filtered off and recrystallized twice from dry ethyl acetate to give white crystals which were dried *in vacuo*. Yield 1.14g (66%). The yields of all the other homologues were in excess of 65%. The optical rotations of the other homologues are shown in table 2.

IR (NaCl disc, film): ν 1506.2, 1571.9, 1602.5 (C=N), 2248.0cm^{-1} (C≡N).
^{1}H NMR ($CDCl_3$): δ 0.8-1.2 (t, 2H), 1.2-2.0 (m, 15H), 2.3-2.7 (2q, 2H), 3.9-4.2 (m, 4H), 6.8-7.4 (m, 8H), 7.5-8.0 (m, 8H), 8.4 (s, 1H).
MS (EI): 487, 544 (M^+).
$[\alpha]_D^{20}$ = +8.5° (*c*, 0.87) $CHCl_3$.

2.11. *Measurement of the optical rotation*

The optical rotations of the chiral compounds were measured with an AA-100 polarimeter (Optical Activity Ltd.). A solution of a weighed amount of the compound in dry chloroform was made up in a 2ml volumetric flask. A polarimeter tube (column length 5cm) was filled with the solution and carefully placed horizontally in the polarimeter. Before taking measurements the *zero* position of the instrument was

determined with the empty polarimeter tube. The specific rotation for a solution of an optically active substance at a temperature T for the sodium D line is given by

$$[\alpha]_D^T = 100\alpha/lc,$$

where α is the measured optical rotation in degrees, l is the length of the column of liquid in decimetres and c is the number of grams of the substance dissolved in 100ml of the solution. The optical rotation can also be expressed by the molecular rotation, that is the optical rotation per mole of material, which is given by

$$[M]_D^T = [\alpha]_D^T \times M / 100,$$

where M is the molecular weight of the compound.

2.12. *Measurement of the chiral pitch*

Chiral pitch measurements were made using two techniques: the Cano wedge method [13] and UV-VIS spectroscopy (Philips PU8730 series). The Cano wedge method was used for the monotropic chiral nematogen (*R*)2MB.O6O.(*R*)2MB as it could not be determined by UV-VIS spectroscopy due to crystallisation. UV-VIS spectroscopy was used to determine the pitches of the (*R*)2MB.O*n*O.CB compounds. Using the Cano wedge method pitch measurements were made on three and five per cent w/w mixtures of the test compound in E7 (C -10°C N 61°C I, Merck Ltd., Poole, U.K.). The cells were constructed from two glass plates which were coated with ITO, to obtain planar alignment, and are inclined at a small angle. By measuring the average distance between two disclinations (d), as observed by polarising microscopy (see plate 5 later), the helical twisting power (HTP) for the mixture can be obtained using the formula

$$HTP = 15.273 / (d \times c \times \sin\theta),$$

where 15.273 is a microscope scaling constant, c is the percentage w/w concentration and θ is the angle of the wedge. The pitch, p, is related to HTP by

$$HTP = 100 / (p \times c).$$

The pitch for the pure material is found by extrapolating the values obtained for the three and five per cent w/w mixtures to 100 per cent.

To measure the pitch by UV-VIS spectroscopy a heating block (Linkam hot stage) with a small aperture was placed in a UV-VIS spectrometer such that it was orthogonal to the incident UV light. The sample was placed between two glass slides and fixed to the heating block. The sample was then heated (Linkam TMS90 temperature controller unit) into the chiral nematic phase when it was sheared to obtain the Grandjean texture, that is to obtain a planar texture such that the director was parallel to the glass slides. The transmitted light was measured between wavelengths of 0.3-0.8μm.

3. Results and discussion

3.1. *The 2MB.OnO.2MB series*

The transition temperatures, enthalpies and entropies for the racemic 2MB.O*n*O.2MB series are given in table 5. It can be seen from the table that smectic A and nematic mesophases are exhibited by this series. From polarizing optical microscopy the smectic A phase was characterized by the coexistence of the focal-conic fan and homeotropic textures. The nematic phase was recognised from its schlieren texture which has both four and two point singularities and flashed when submitted to mechanical stress. Figure 1 shows the effect on the transition temperatures of varying the number of methylene units, n, in the flexible spacer for this series. There is a strong odd-even effect for the clearing transition temperatures which attenuates across the series. It is also evident that the odd membered

Table 5. The transition temperatures, enthalpies and entropies of the racemic 2MB.O*n*O.2MB series.

n	*T*/°C			Δ*H*/kJmol^{-1}		Δ*S*/R	
	C-	S_A-N	^1S_A-I N-I	C-	^2S_A-I N-I	C-	^3S_A-I N-I
3	136			39.7		11.7	
4	156		[1]183	32.2	[2]9.86	9.1	[3]2.60
5	124		†(91)	35.3		10.7	
6	154	‡(148)	(151)	42.6	4.47	12.2	1.27
7	147		†(96)	37.0		11.4	
8	132		133	38.6	3.95	11.7	1.17
9	108		†(94)	38.5		12.2	
10	121		120	52.3	4.61	16.2	1.39
11	110		†(95)	42.0		13.2	
12	119		(114)	65.3		20.2	

† Observed only by polarising microscopy by supercooling isolated droplets.

‡ Not possible to measure by DSC.

Parentheses indicate a monotropic transition.

homologues of this series are all strongly monotropic; indeed the nematic to isotropic transition temperatures of these homologues can only be observed by polarizing optical microscopy by supercooling isolated droplets. The n=4,8 and 10 homologues are the only enantiotropic homologues of this series. The n=4 and 6 homologues exhibit smectic behaviour (S_A); the S_A phase for both homologues shows strong homeotropic alignment for thin samples, an effect which occurs also for the smectic A phases of the monomeric analogues [9]. The remaining homologues all possess a nematic phase. An X-ray investigation of the smectic A phase of the n=4 homologue showed the small angle reflection to correspond to a periodicity of 33.7Å which is close to the all *trans* molecular length of 35Å calculated from CPK molecular models. This result indicates that the molecules are arranged in monolayers and that there is no significant interpenetration of the molecules between the layers. The effect of a branched terminal chain on the liquid crystalline behaviour is clearly highlighted by a comparison of the phase behaviour for the structurally isomeric unbranched 5.O*n*O.5 series (see figure 2) [10]. We see that the 5.O*n*O.5 series has higher clearing temperatures and exhibits a greater smectic polymorphism than the 2MB.O*n*O.2MB series. This can be explained in terms of the lateral methyl groups in the 2MB.O*n*O.2MB series which increase the length-to-breadth ratio of the molecule and hence lead to a lowering of the clearing temperatures. Further, the lateral methyl groups also sterically hinder the intermolecular interactions important for smectic phase formation. Figure 3 shows a plot of the difference between the melting and clearing temperatures for the 5.O*n*O.5 and 2MB.O*n*O.2MB series versus the length of the spacer, n (the data, which correspond to $T_{2MB.OnO2MB}$-$T_{5.OnO.5}$, are also summarised in table 6). There is an odd-even effect for the clearing temperatures which attenuates slightly across the series. The difference in the melting points also decreases across the series. We see that the difference in the clearing temperature is greatest for the odd membered homologues. The entropy changes at the clearing transition for the n=4,6,8, and 10 homologues of the 2MB.O*n*O.2MB series are all lower than their analogous, unbranched terminal chain homologues [10]. Figure 4 compares the entropy changes at the transition for the n=4,6,8 and 10 homologues of the 2MB.O*n*O.2MB series with the analogous compounds from the 5.O*n*O.5 series [10]. From this figure we see that the entropy changes for the unbranched chain

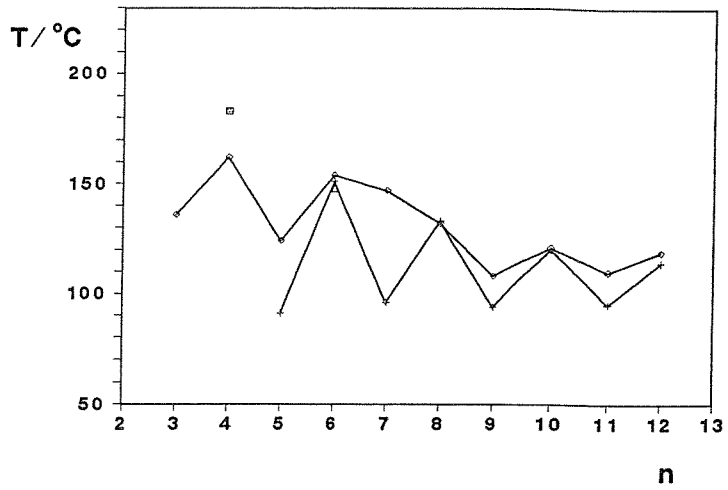

Figure 1. The influence of the length of the alkyl spacer, *n*, on the transition temperatures of the α,ω-bis(4-(2-methylbutyl)phenyliminobenzylidene-4'-oxy)alkanes. C- (◇), S_A-I (■), S_A-N (△), N-I (+).

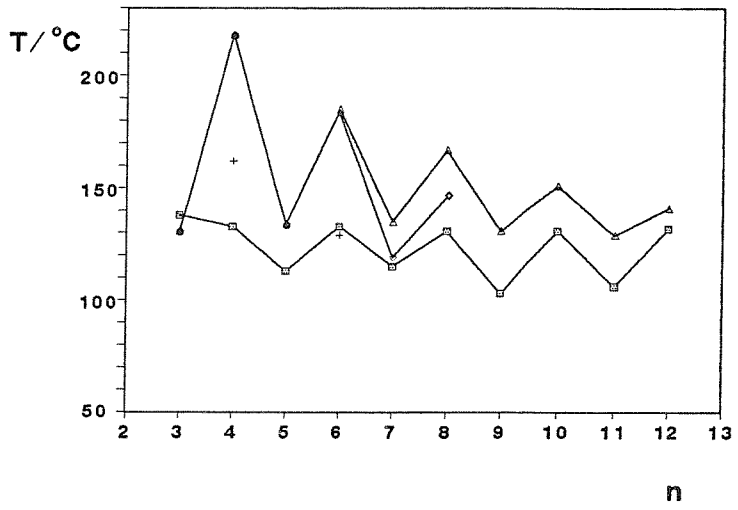

Figure 2. The influence of the length of the alkyl spacer, *n*, on the transition temperatures of the α,ω-bis(4-pentylphenyliminobenzylidene-4'-oxy)alkanes. C- (■), S_A-I (•), S_A-N (+), S_B-S_A (◇), N-I (△).

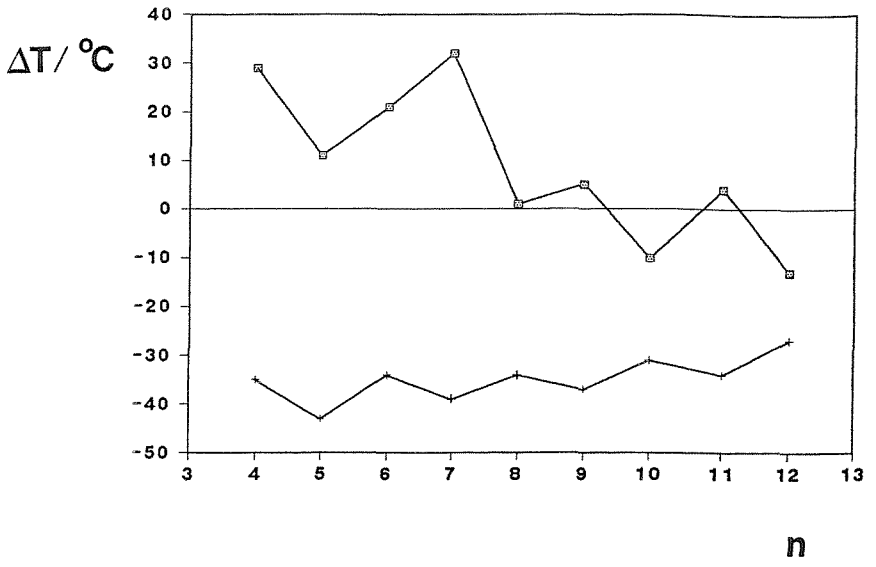

Figure 3. The difference between the melting (■) and clearing (+) temperatures of the 2MB.O*n*O.2MB and 5.O*n*O.5 series (the data correspond to $T_{2MB.OnO.2MB}$-$T_{5.OnO.5}$).

Table 6. The difference between the melting and clearing temperatures of the 2MB.O*n*O.2MB and 5.O*n*O.5 series (the data correspond to $T_{2MB.OnO.2MB}$-$T_{5.OnO.5}$).

n	ΔT_C/°C	ΔT_{NI}/°C
4	29	-35
5	11	-43
6	21	-34
7	32	-39
8	1	-34
9	5	-37
10	-10	-31
11	4	-34
12	-13	-27

compounds are almost twice as much for the nematic to isotropic transition with the values being about 50% greater for the smectic A to isotropic transition. The lower entropy changes for the branched compounds are a result of the lower orientational order in these systems, whereas the low smectic A to isotropic entropy changes can be rationalised in terms of low translational order.

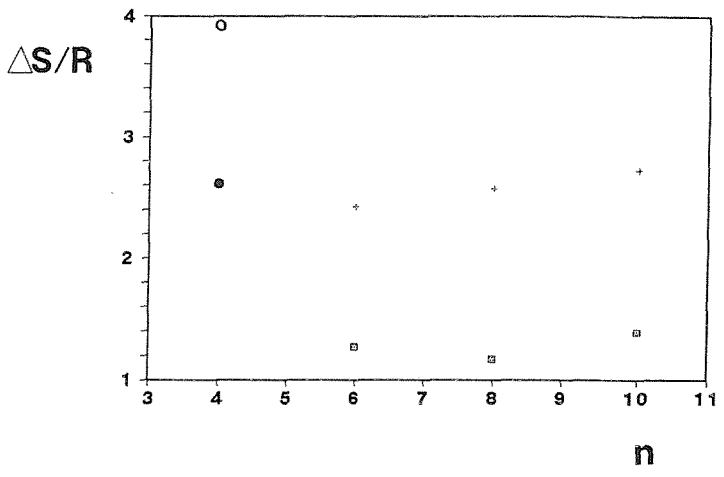

Figure 4. The influence of the length of the alkyl spacer, *n*, on the clearing entropy changes of the α,ω-bis(4-(2-methylbutyl)phenyliminobenzylidene-4'-oxy)alkanes (S_A-I (•), N-I (■)) compared to the α,ω-bis(4-pentylphenyliminobenzylidene-4'-oxy)alkanes (S_A-I (∘), N-I (+)).

3.2. *The (R)2MB.OnO.(R)2MB series*

In table 7 the transition temperatures, enthalpies and entropies are listed for the n=4, 6 and 8 homologues of the (*R*)2MB.O*n*O.(*R*)2MB series. We see that the data are similar to those of the racemic analogues, as expected. On cooling the n=6 and 8 homologues a focal-conic fan texture is obtained which, when sheared, gives an oily streak texture known as the Grandjean texture indicative of a chiral nematic phase. On cooling the chiral nematic phase of the n=6 homologue a change to a focal-conic fan and homeotropic texture occurs at the chiral nematic to smectic A transition temperature (see plate 1). On slow cooling (5°Cmin^{-1}) the unwinding of the chiral nematic helix can be observed. On heating back to the smectic A to chiral nematic transition bright threads appear which thicken as the temperature is increased (see plate 2). The web-like texture then coalesces into the Grandjean texture. Similar effects were observed for the chiral, monomeric analogues [9]. The sense of the chiral helix was determined to be dextrorotatory by contact preparations with the laevorotatory compound cholesteryl benzoate (C 150°C Ch 178°C I, Eastman Kodak Co., Rochester, U.S.A.) which showed a nematic phase at the junction of the two components. This result does not agree with the Gray and McDonnell rules [14] which state that for an *R* absolute configuration the sense of the chirality should be laevorotatory when the chiral centre is an even number of atoms away from the mesogenic core and when it is an odd number of atoms away dextro rotation should occur. The pitch of (*R*)2MB.O6O.(*R*)2MB was determined to be 0.2μm using the Cano wedge method. The value for the ethoxy monomeric derivative has been reported to be 0.2μm [9].

Table 7. The transition temperatures, enthalpies and entropies for the (*R*)2MB.O*n*O.(*R*)2MB series.

n	*T*/°C			Δ*H*/kJmol^{-1}			Δ*S*/R		
	C-	S_A-N^*	^1S_A-I N^*-I	C-	S_A-N^*	^2S_A-I N^*-I	C-	S_A-N^*	^3S_A-I N^*-I
4	153		^{1}182	38.4		^{2}11.5	10.8		^{3}3.04
6	149	(138)	(148)	49.3	(0.82)	(1.58)	14.1	(0.24)	(0.45)
8	127		131	42.0		4.27	12.6		1.27

Parentheses indicate a montropic transition.

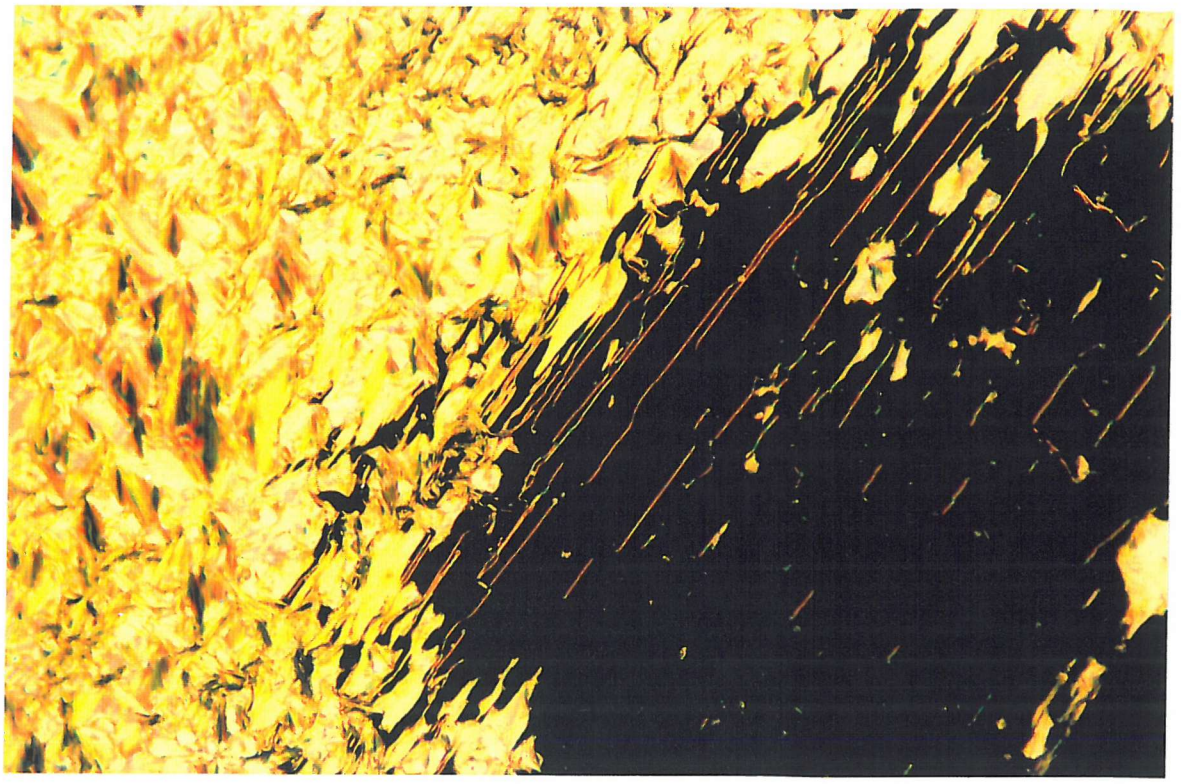

Plate 1. The focal-conic fan and homeotropic textures of the smectic A phase of 2MB.O6O.2MB just after the transition from the chiral nematic phase. 145°C, magnification x100.

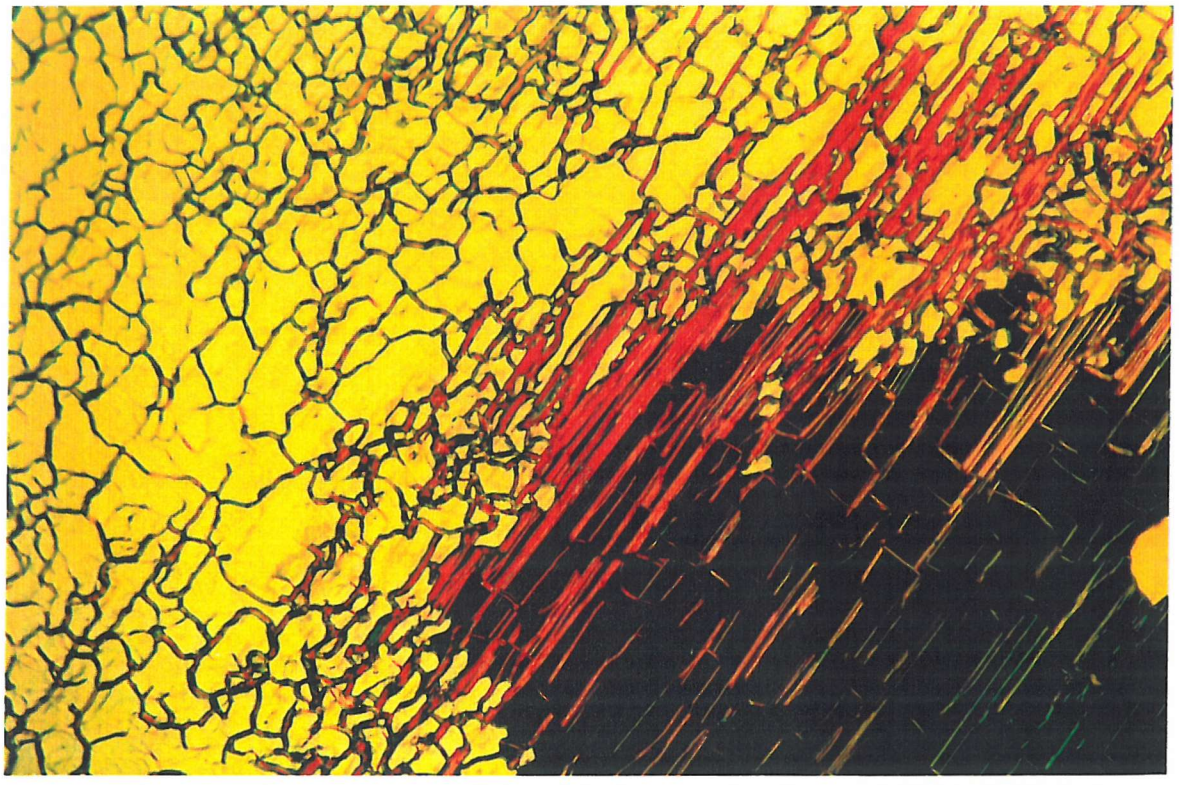

Plate 2. The Grandjean texture of the chiral nematic phase of 2MB.O6O.2MB on reheating the smectic A phase. The plate shows the thickening of the bright threads in the homeotropic region of plate 1. 146°C, magnification x100.

3.3. *The 5.OnO.CB series*

The n=3-6 homologues of this series were reported in [11]. Table 8 lists the data for the transition temperatures, enthalpies and entropies of this series of compounds. Figure 5 shows the effect of changing the length of the flexible spacer chain, n, on the transition temperatures for this series. We see that the n=3, 5 and 6 homologues are both smectogenic and nematogenic, although there is an unassigned smectic phase in addition to the smectic A phase for the n=3 and 6 homologues. The unidentified smectic phases (S_1) exhibited by the n=3 and 6 homologues were only observed fleetingly on rapid cooling before crystallization occurred [11]. Smectic behaviour disappears for the n=7 homologue before reappearing for the n=8-12 homologues. The disappearance of smectic behaviour for the n=7 homologue is thought to result from the inability of the mesogenic cores and alkyl chains to separate into microphases which is necessary for the formation of smectic phases [10]. The occurence of smectic behaviour for dimers composed of a Schiff base and a cyanobiphenyl group, for which the spacer is longer than the terminal chain, has been rationalised in terms of a specific mixed mesogenic group interaction, thought to be charge transfer in origin [15], such that an intercalated smectic phase is formed [11, 16]. It was found in [11] that when the terminal chain can be accommodated in the space between the mesogenic groups an intercalated smectic phase was formed with a periodicity approximately half the molecular length (see figure 6(*a*)). When the terminal chain could no longer be accommodated in the space between the mesogenic groups an interdigitated arrangement of the molecules resulted where the periodicity was now approximately 1.8 times the molecular length (see figure 6(*b*)). The interdigitated structure is thought to result from an interaction between the polar and polarisable cyanobiphenyl groups and the effect of molecular inhomogeneity produced by the long terminal chains. Powder X-ray investigations of the smectic A phases of the n=6,9 and 12 homologues indicated that the phases were intercalated as they each gave periodicities approximately half that of the calculated all *trans* molecular length (CPK atomic models) (see table 9). The n=9-12 homologues possess a smectic B phase as indicated by the smoothness of the focal-conic fans and the appearance of fine, bright threads across the backs of the fans at

Table 8. The transition temperatures, enthalpies and entropies of the 5.O*n*O.CB series.

n	*T*/°C				Δ*H*/kJmol^{-1}				Δ*S*/R			
	C-	$^{1}S_1$-S_A S_B-S_A	$^{2}S_1$-N S_A-N	$^{3}S_A$-I N-I	C-	$^{4}S_1$-S_A S_B-S_A	$^{5}S_1$-N S_A-N	$^{6}S_A$-I N-I	C-	$^{7}S_1$-S_A S_B-S_A	$^{8}S_1$-N S_A-N	$^{9}S_A$-I N-I
3	117		^{2}(53)	124	36.7		^{5}0.04	0.90	11.3		^{8}0.01	0.27
4	127			222	37.6			7.54	11.3			1.83
5	102		(74)	155	31.5		^{5}†	1.89	10.1		^{8}†	0.53
6	113	^{1}(87)	(109)	199	33.4	^{4}†	†	7.70	10.4	^{7}†	†	1.96
7	91			152	48.5			1.40	16.0			0.39
8	102		144	178	34.8		0.50	6.22	11.2		0.16	1.66
9	93	100	111	149	49.2	0.4	0.60	2.07	16.2	0.13	0.19	0.59
10	104	106	163	166	39.1	3.0	2.90	7.23	12.5	0.94	0.82	1.98
11	82	102	135	147	32.2	0.1	1.90	3.46	10.9	0.04	0.56	0.99
12	102	105		^{3}156	44.9	2.2		^{6}14.1	14.4	0.72		^{9}3.96

† Not measured in [16].

S_1 is an unidentified phase in [11,16].

Parentheses indicate a monotropic transition.

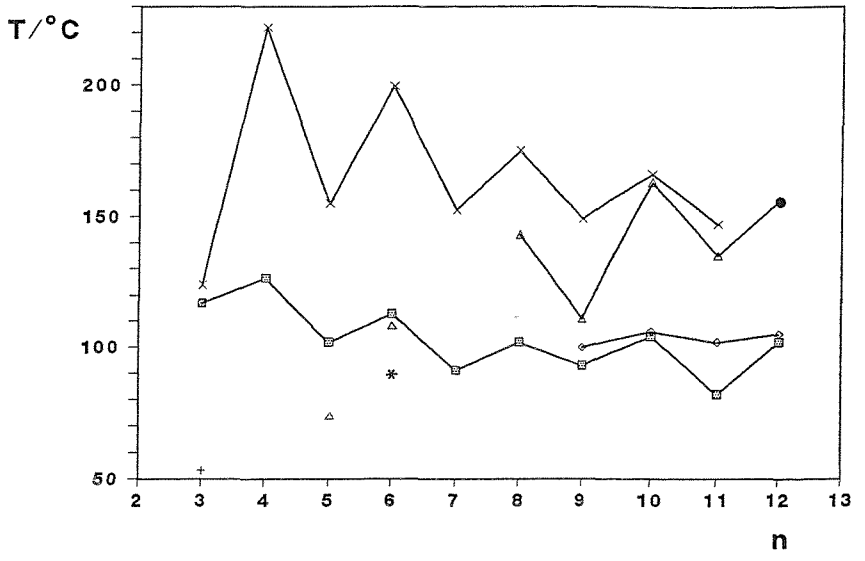

Figure 5. The influence of the length of the alkyl spacer, *n*, on the transition temperatures of the α-(4-pentylphenyliminobenzylidene-4'-oxy)-ω-(4'-cyanobiphenyl-4-yloxy)alkanes. C- (■), S_1-S_A (*), S_B-S_A (◇), S_1-N (+), S_A-N (△), S_A-I (•), N-I (×).

the transition to the smectic A phase. A powder X-ray investigation of the smectic B phase of the $n=12$ homologue showed the periodicity to increase to 24.8Å indicating an increase in the order within the layers (all *trans* molecular length is 44Å as claculated from CPK atomic models; the layer spacing in the smectic A phase is 21.9Å). The wide angle reflection is sharper than that for the smectic A phase which indicates that the phase is a hexatic B; there is no fine structure from the densitometer scan as expected for a crystal B phase.

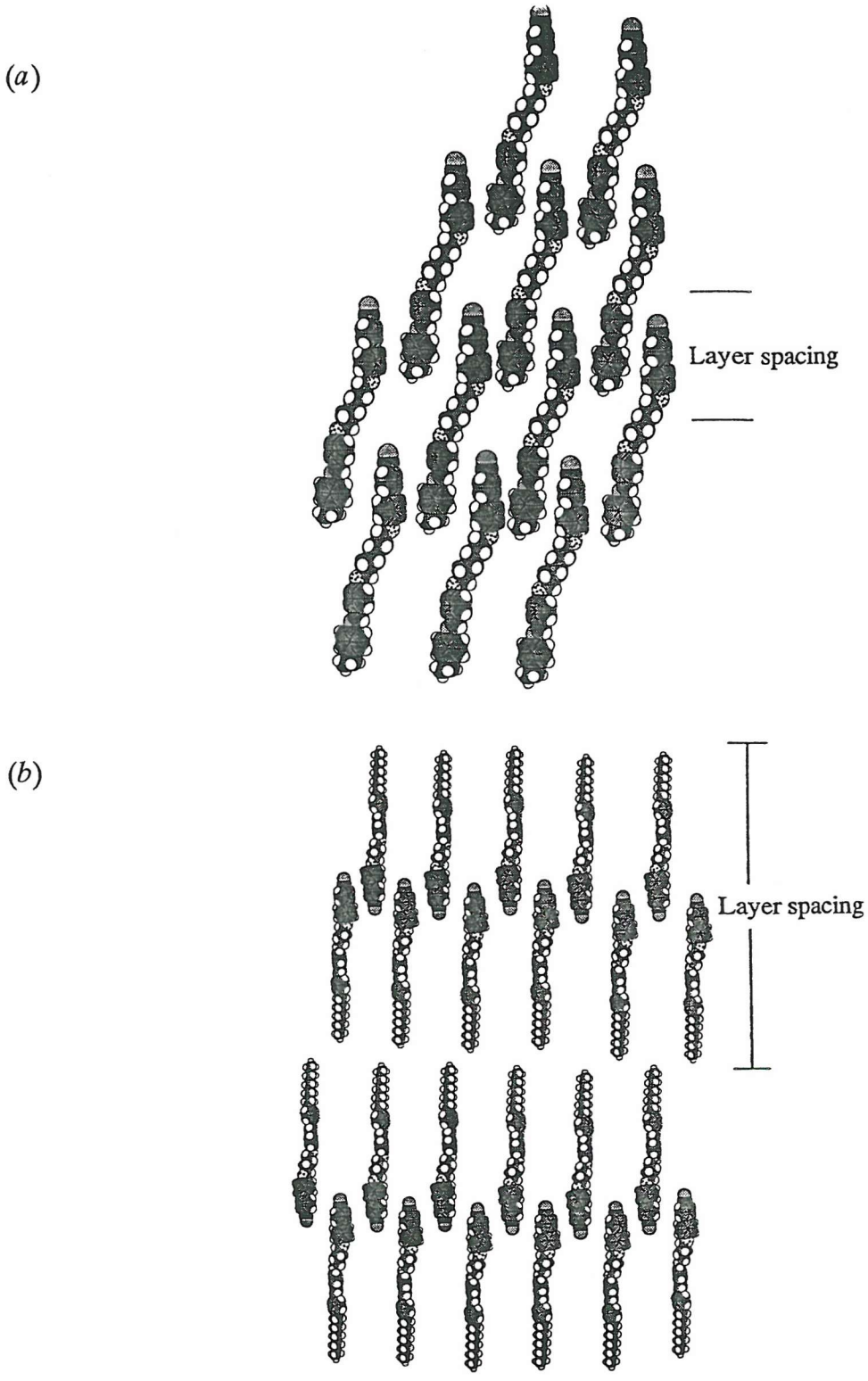

Figure 6. A schematic representation of the molecular structure in (*a*) the intercalated and (*b*) the interdigitated smectic A phase [11].

Table 9. The layer spacings, *d*, of some members of the 2MB.O*n*O.2MB and 5.O*n*O.5 series as measured by X-ray diffraction. The values are compared to their all *trans* molecular lengths, *l*, calculated from CPK atomic models. The error in the measured layer spacings is ±0.4Å.

Compound	*l*/Å	*d*/Å	*d*/*l*
2MB.O8O.CB	39	18.9	0.49
2MB.O11O.CB	40	21.4	0.54
2MB.O12O.CB	41	21.6	0.53
†5.O6O.CB	38	19.5	0.49
5.O9O.CB	41	20.1	0.49
5.O12O.CB	44	21.9	0.50
‡5.O12O.CB	44	24.8	0.56

† Taken from [11].

‡ Smectic B phase.

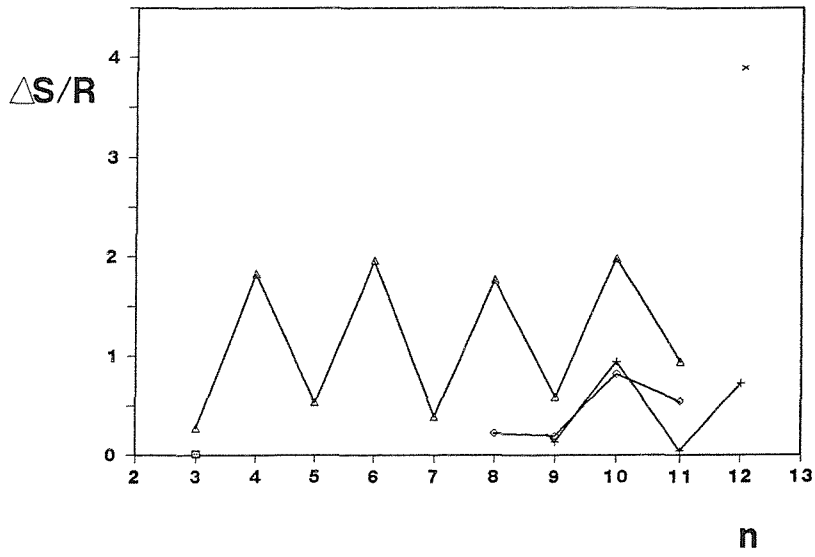

Figure 7. The influence of the length of the alkyl spacer, *n*, on the transitional entropy changes of the *α*-(4-pentylphenyliminobenzylidene-4'-oxy)-*ω*-(4'-cyanobiphenyl-4-yloxy)alkanes. S_B-S_A (+), S_1-N (■), S_A-N (◇), N-I (△), S_A-I (×).

Figure 7 shows a plot of the entropy changes versus n for the liquid crystal transitions of the 5.OnO.CB series. We see that the nematic to isotropic transition entropies exhibit a pronounced odd-even effect and reflect the influence of the spacer. The smectic A to nematic transition entropies show a slightly weaker odd-even effect of the same sense as the nematic to isotropic entropy changes. The magnitude of the smectic A to nematic entropy changes are consistent with McMillan's theory [17] which states that the larger the nematic range the more the nematic to smectic A entropy change tends to second order, that is the weaker the entropy change. The smectic B to smectic A entropy changes show a stronger odd-even effect.

3.4. *The 2MB.OnO.CB series*

In table 10 the transition temperatures, enthalpies and entropies of the 2MB.OnO.CB series are presented. All of the homologues are enantiotropic mesogens except for the $n=3$ member which is weakly monotropic; this is in stark contrast to the 2MB.OnO.2MB series, where only the even membered homologues are liquid crystalline. Figure 8 shows the effect of changing the length of the spacer, n, on the liquid crystalline properties of this series. We see that, with the exception of the $n=12$ homologue, all homologues exhibit a nematic to isotropic transition. Further this transition is seen to show a marked odd-even effect across the series. The $n=6$-12 homologues all possess a smectic A phase. As the series is ascended the smectic A to nematic transition temperature also has an odd-even effect. The smectic A to nematic transition temperatures for the odd and even membered homologues lie on two gradually increasing curves such that for the $n=12$ homologue the smectic A phase clears directly into the isotropic liquid. The effect of the methyl branch on the transition temperatures for this series is illustrated by figure 9 which shows a plot of the difference in the melting and clearing temperatures versus the length of the spacer, n, for the 5.OnO.CB and 2MB.OnO.CB series (the data correspond to $T_{\text{2MB.O}n\text{O.CB}}$-$T_{\text{5.O}n\text{O.CB}}$ and are summarized in table 11). Apart from the $n=3$ homologue we see that the melting points are lower for the 5.OnO.CB series. The difference in the clearing temperatures has an odd-even effect which attenuates across the series.

Table 10. The transition temperatures, enthalpies and entropies of the racemic 2MB.O*n*O.CB series.

n	*T*/°C			Δ*H*/kJmol^{-1}			Δ*S*/R		
	C-	S_A-N	^1S_A-I N-I	C-	S_A-N	^2S_A-I N-I	C-	S_A-N	^3S_A-I N-I
3	92		(80)	25.0		(0.3)	8.28		(0.09)
4	148		200	32.0		3.98	9.16		1.01
5	104		121	31.2		0.46	9.96		0.14
6	137	(102)	178	29.3	(0.44)	4.23	8.60	(0.14)	1.13
7	97	(70)	130	48.0	(3.85)	0.64	15.6	(1.35)	0.19
8	124	140	163	32.4	2.20	4.97	9.81	0.64	1.37
9	109	(100)	133	40.0	(3.66)	1.25	12.6	(1.18)	0.37
10	114	149	151	41.4	3.46	2.92	12.9	0.99	0.83
11	84	116	127	28.4	2.84	2.36	9.57	0.88	0.71
12	112		^{1}145	48.4		^{2}13.8	15.1		^{3}3.97

Parentheses indicate a monotropic transition.

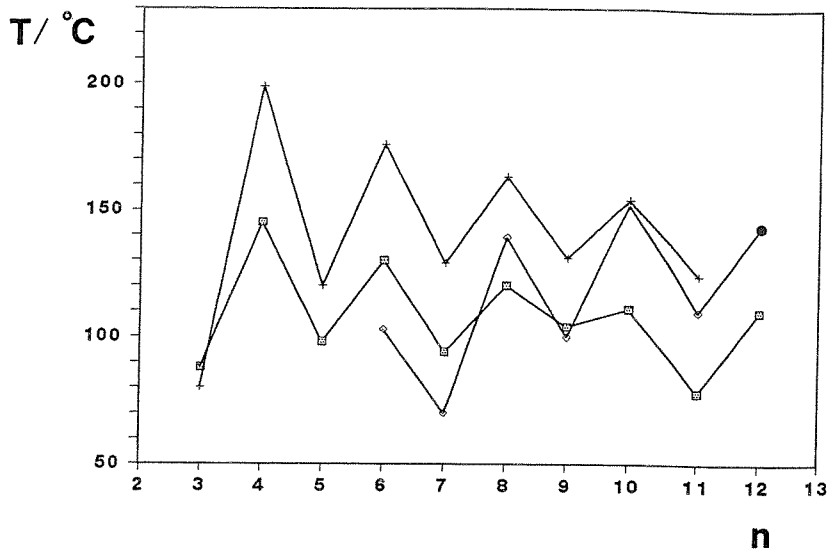

Figure 8. The influence of the length of the alkyl spacer, *n*, on the transition temperatures of the α-(4-(2-methylbutyl)phenyliminobenzylidene-4'-oxy)-ω-(4'-cyanobiphenyl-4-yloxy)alkanes. C- (■), N-I (+), S_A-N (◇), S_A-I (•).

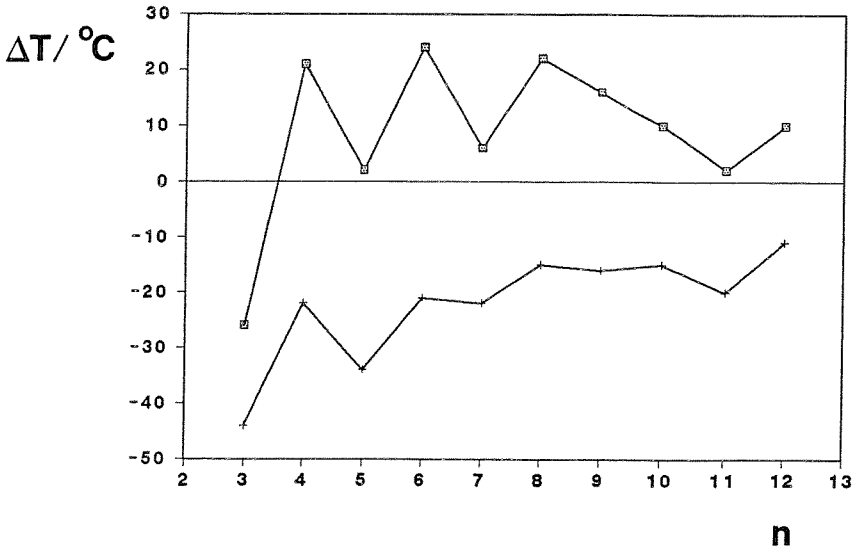

Figure 9. The difference between the melting (■) and clearing temperatures (+) of the 2MB.O*n*O.CB and 5.O*n*O.CB series (the data correspond to $T_{2MB.OnO.CB}$- $T_{5.OnO.CB}$).

As in figure 3 the difference in the clearing temperatures is greatest for homologues with odd membered spacers.

Figure 10 shows the effect of changing the length of the central methylene spacer, n, on the transition entropy. We see that the nematic to isotropic entropy changes exhibit an odd-even effect and their magnitudes are all smaller than the values of their straight chain counterparts. The smectic A to nematic entropy changes for the n=6-9 homologues also show an odd-even effect, such that an odd membered spacer gives a high entropy change for the smectic A to nematic transition whereas an even membered spacer chain gives a low entropy change for the smectic A to nematic transition. Further, there is an increasing trend for the strength of this transition across the series. This is strange as the nematic range is large for the n=7 homologue yet it has the highest smectic A to nematic entropy change. Coversely the n=8 homologue has a small nematic range yet its nematic to smectic A entropy change is about half that of the n=7 compound. This result appears to contravene McMillan's theory [17].

Powder X-ray investigations of the smectic A phases of the n=8, 11 and 12 homologues all gave a periodicity approximately half that of the all *trans* molecular length as calculated from CPK molecular models (see table 9). These results indicate that the phase has an intercalated structure. The periodicities reported here support the observation in [11, 16] that when the terminal chain can be easily accommodated between the mesogenic groups an intercalated smectic A phase forms. Smectic behaviour disappears altogether when it is not possible for the mesogenic cores and alkyl chains to separate significantly into microphases and hence stabilise smectic mesomorphism; this results in nematic behaviour.

Table 11. The difference between the melting and clearing temperatures of the 2MB.O*n*O.CB and 5.O*n*O.CB series (the data correspond to $T_{2MB.OnO.CB}$-$T_{5.OnO.CB}$).

n	ΔT_C/°C	ΔT_{NI}/°C
3	-26	-44
4	21	-22
5	2	-34
6	24	-21
7	6	-22
8	22	-15
9	16	-16
10	10	-15
11	2	-20
12	10	-11

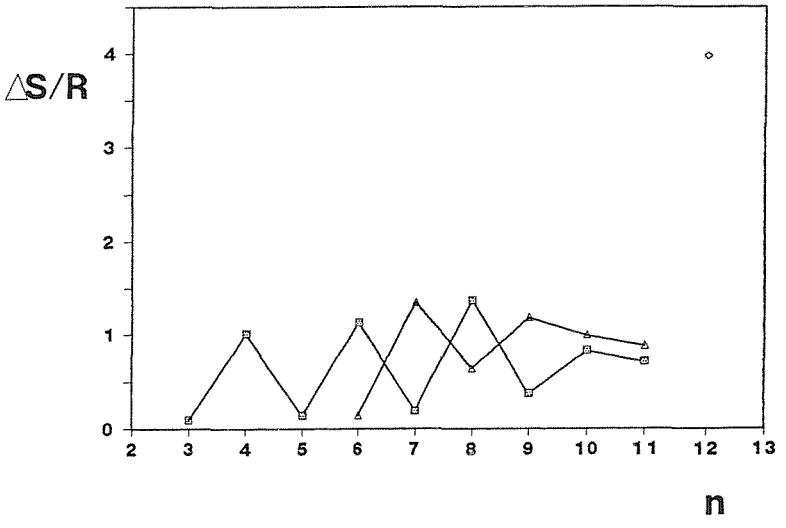

Figure 10. The influence of the length of the alkyl spacer, *n*, on the transitional entropy changes of the α-(4-(2-methylbutyl)phenyliminobenzylidene-4'-oxy)-ω-(4'-cyanobiphenyl-4-yloxy)alkanes. N-I (■), S_A-N (△), S_A-I (◇).

3.5. *The (R)2MB.OnO.CB series*

Table 12 presents the transition temperatures, enthalpies and entropies for the phase behaviour of the n=6-9 homologues of the (*R*)2MB.O*n*O.CB series. Figure 11 shows the effect of the number of methylene units, n, in the flexible spacer on the transition temperatures. All four homologues are liquid crystalline and the transition temperatures as well as the clearing entropy changes versus the length of the spacer, n, (see figure 12) agree closely with those of the analogous racemic compounds, as expected. On cooling the isotropic liquid for the n=6 and 8 homologues the focal-conic fan texture of the chiral nematic phase forms which when sheared then shows the oily streaks characteristic of the Grandjean texture. In contrast the n=7 homologue shows a different behaviour: when viewed in transmission mode by polarising microscopy on slow cooling (0.2°Cmin^{-1}), the isotropic liquid is seen to exhibit a homeotropic blue colour of low birefringence before a platelet texture composed of blue and green plates quickly grows; this is indicative of blue phase II (see plate 3). On further cooling another platelet texture composed of blue and red plates forms which is characteristic of blue phase I (see plate 4). The n=9 homologue exhibits blue phase I which is composed of red and blue plates. The blue phases are seen only on cooling and exist only for several degrees before the chiral nematic phase forms; they could not be detected by DSC, indeed the entropy changes between them are reported as being very small [18]. If the blue phase is submitted to mechanical stress the Grandjean texture forms. At the chiral nematic to smectic A transition bâtonnets form which coalesce into the smectic A focal-conic fan texture. Based on this observation there was no indication that the smectic A phase was of the twist grain boundary type (TGB) [19]. The sense of the chiral helix in the chiral nematic phase was determined to be dextrorotatory for all four compounds by contact preparations with cholesteryl benzoate (see plate 6). The pitch measurements obtained by UV spectroscopy were 0.6μm, 0.5μm, 0.6μm and 0.5μm for the n=6,7,8 and 9 homologues respectively. The pitch of the n=6 homologue was also determined to be 0.6μm by the Cano wedge method. These results support the observation of blue phases for the n=7 and 9 homologues as they tend to be exhibited by chiral compounds with pitches of 0.5μm or less [18].

Table 12. The transition temperatures, enthalpies and entropies for the (*R*)2MB.O*n*O.CB series.

n	*T*/°C					
	C-	S_A-N^*	†(N^*-BPI)	†(BPI-BPII)	†(BPII-I) †(BPI-I)[1]	N^*-I
6	137	(104)				176
7	97	(74)	(131.5)	(131.7)	(132.6)	133
8	128	143				165
9	110	102	(131.1)		(133.3)[1]	134

n	Δ*H*/kJmol^{-1}			Δ*S*/R		
	C-	S_A-N^*	N^*-I	C-	S_A-N^*	N^*-I
6	32.0	(0.68)	4.48	9.40	(0.22)	1.22
7	45.8	(4.33)	0.68	14.9	(1.50)	0.23
8	36.3	1.94	5.08	10.9	0.56	1.51
9	45.2	(3.84)	1.32	14.2	(1.23)	0.42

† Transition observed only by polarizing microscopy on slow cooling (0.2°Cmin^{-1}).

Parentheses indicate a monotropic transition.

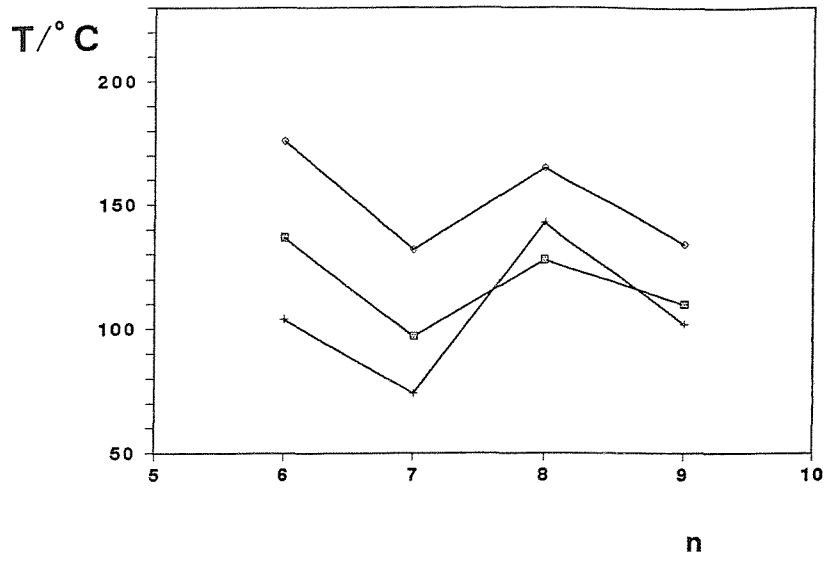

Figure 11. The influence of the length of the alkyl spacer, *n*, on the transition temperatures of the *α*-(*R*)-(+)-(4-(2-methylbutyl)phenyliminobenzylidene-4'-oxy)-*ω*-(4'-cyanobiphenyl-4-yloxy)alkanes. C- (■), S_A-N (+), N-I (◇).

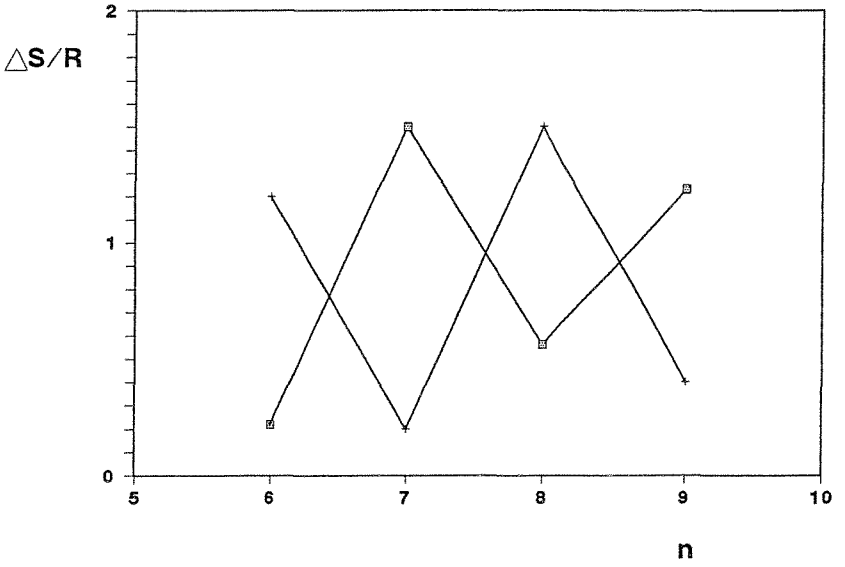

Figure 12. The influence of the length of the alkyl spacer, *n*, on the transitional entropy changes of the *α*-(*R*)-(+)-(4-(2-methylbutyl)phenylimino-benzylidene-4'-oxy)-*ω*-(4'-cyanobiphenyl-4-yloxy)alkanes. S_A-N (■), N-I (+).

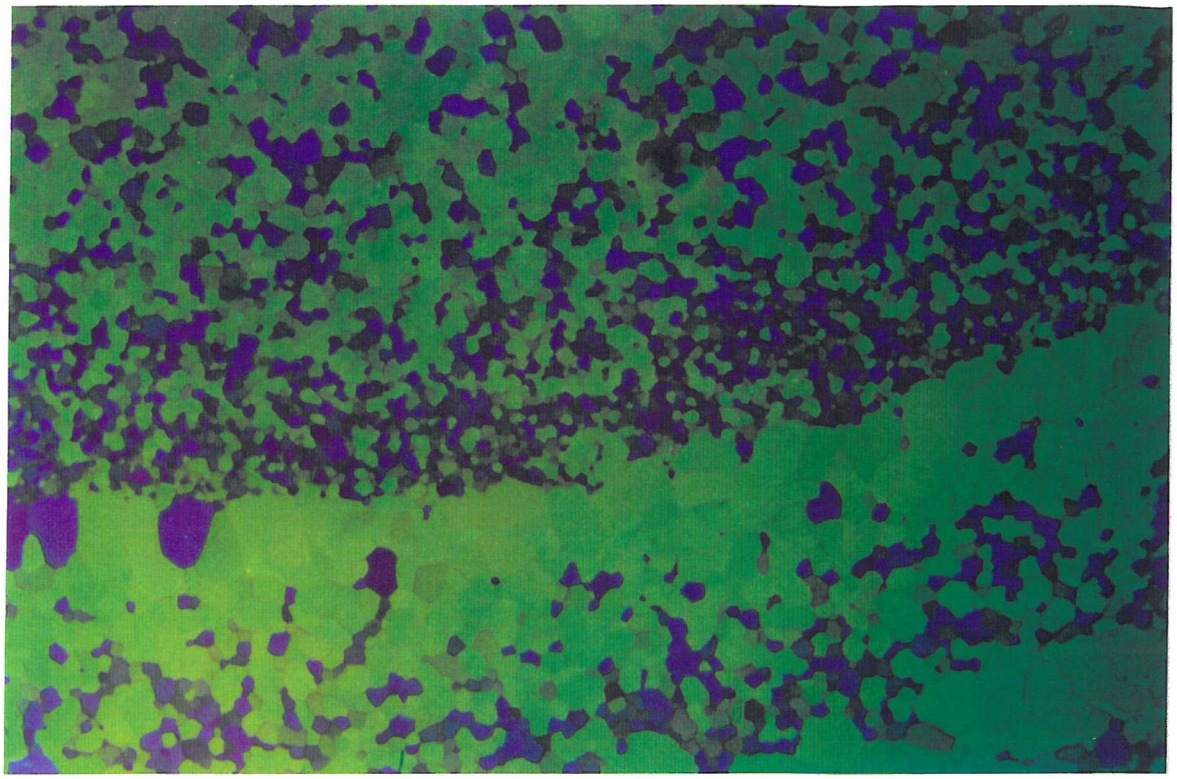

Plate 3. The blue phase II platelet texture of 2MB.O7O.CB on cooling from the isotropic phase. 132.5°C, magnification x200.

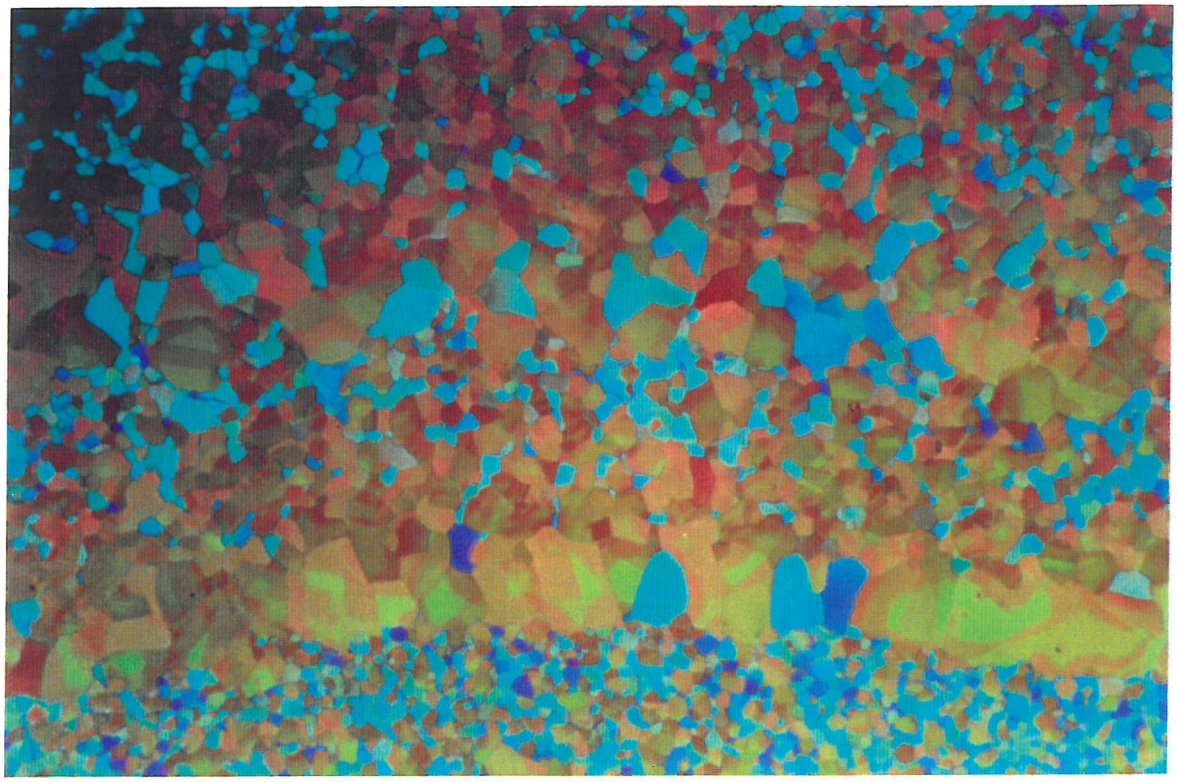

Plate 4. The blue phase I platelet texture of 2MB.O7O.CB on cooling from blue phase II. 132.1°C, magnification x200.

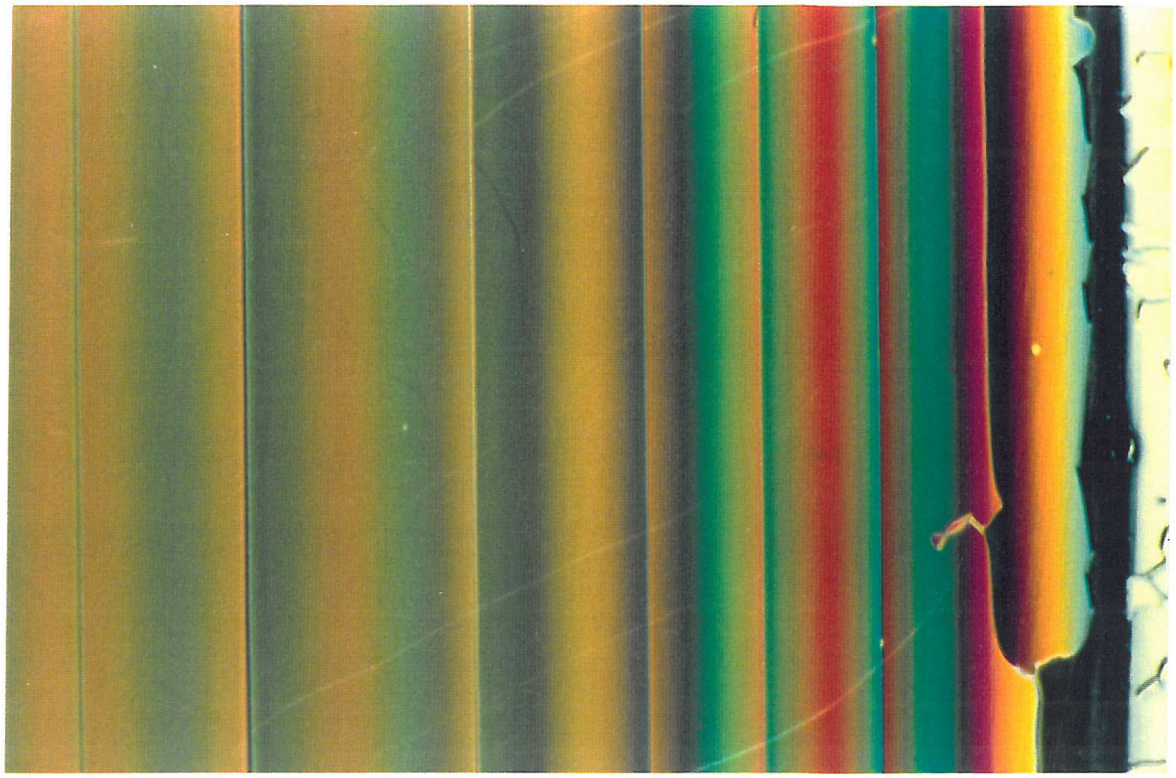

Plate 5. The disclination lines produced by a Cano wedge. Five per cent w/w mixture of 2MB.O6O.2MB in E7. Magnification x200.

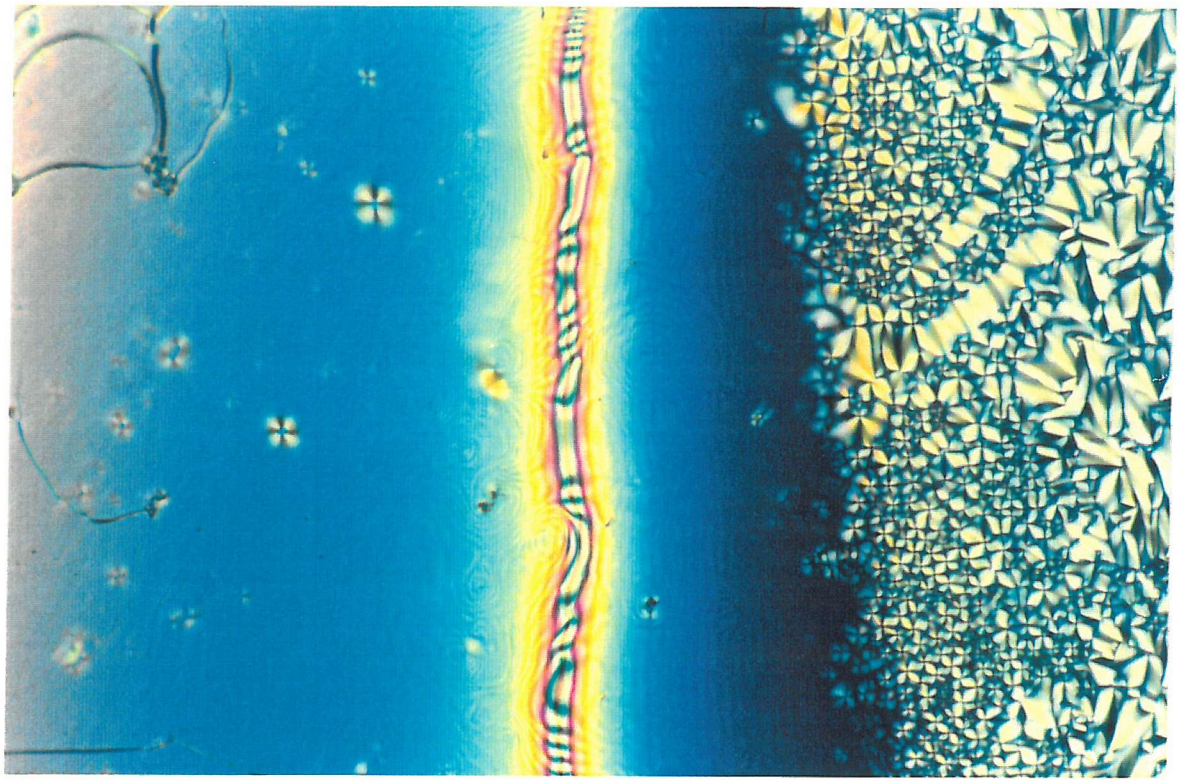

Plate 6. The contact preparation of (*R*)2MB.O6O.CB and cholesteryl benzoate. From left to right: the Grandjean texture of the chiral nematic phase (dextrorotatory twist sense) of (*R*)2MB.O6O.CB, the nematic phase, and the focal-conic fan texture of the cholesteric phase (laevorotatory twist sense) of cholesteryl benzoate. 172°C, magnification x200.

4. Conclusions

In this chapter we have presented two new series of dimeric compounds containing terminal alkyl chains with methyl branches. The symmetric branched dimers have enhanced clearing temperatures compared to their monomeric analogues as expected [9]. However, in comparison with their dimeric, unbranched chain analogues they have lower clearing temperatures and transition entropies. Indeed, the clearing temperatures of homologues with an odd membered spacer are very monotropic and can only be observed by supercooling isolated droplets. Further the smectic behaviour of the 2MB.O*n*O.2MB series is also reduced in comparison with their straight chain analogues. The pitch of (*R*)2MB.O6O.(*R*)2MB is similar to that of its monomeric analogue 2O.MB and this implies that the chiral nematic phases of these dimers do not possess enhanced chirality.

The clearing temperatures and entropies of the non-symmetric branched dimers are lower than those of their straight chain analogues but the difference is not as great as that between the symmetric dimers, as expected. Powder X-ray diffraction studies of the n=8, 11 and 12 homologues of the 2MB.O*n*O.CB series show their smectic A phases to be intercalated which supports observations of similar compounds reported in [11]. The smectic A phases of the n=6, 9 and 12 homologues of the 5.O*n*O.CB series also had layer periodicities approximately half that of the all *trans* molecular length (CPK atomic models) as measured by X-ray diffraction; thus these are also intercalated phases. The chiral nematic phases exhibited by the chiral analogues of the 2MB.O*n*O.CB series have pitches which are larger than that of (*R*)2MB.O6O.(*R*)2MB. The odd membered homologues of this series are the most interesting as they are the first reported dimers to exhibit blue phases.

References

[1] Reinitzer, F., 1888, *Monatsheft.*, **9**, 435.

[2] Gray, G.W., and Harrison, K.J., 1971, *Symp. Faraday Soc.*, **5**, 54.

[3] Coates, D., 1987, *Liq. Crystals*, **2**, 63.

[4] Heppke, G., Lötzsch, D., and Oestreicher, F., 1987, *Z. Naturforsch.*, **42a**, 279.

[5] Barberá, J., Omenat, A., Serrano, J.L., and Sierra, T., 1989, *Liq. Crystals*, **5**, 1775.

[6] Barberá, J., Omenat, A., and Serrano, J.L., 1989, *Molec. Crystals liq. Crystals*, **166**, 167.

[7] Howell, O.T., 1992, Ph.D. Thesis, Southampton University.

[8] Shiraishi, K., Kato, K., and Sugiyama, K., 1990, *Chem. Lett.*, 971.

[9] Dolphin, D., Muljiani, Z., Cheng, J., and Meyer, R.B., 1973, *J. chem. Phys.*, **58**, 413.

[10] Date, R.W., Imrie, C.T., Luckhurst, G.R., And Seddon, J.M., 1992, *Liq. Crystals*, **12**, 203.

[11] Attard, G.S., Date, R.W., Imrie, C.T., Luckhurst, G.R., Roskilly, S.J., Seddon, J.M., and Taylor, L., *Liq. Crystals* (in the press).

[12] Donahoe, H.B., Benjamin, L.E., Fennoy, L.V., and Greiff, D., 1960, *J. org. Chem.*, **26**, 474.

[13] Cano, R., 1968, *Bull. Soc. Fr. Minéral. Cristallog.*, **91**, 20.

[14] Gray, G.W., and McDonnell, D.G., 1976, *Molec. Crystals liq. Crystals*, **37**, 189.

[15] Park, J.W., Bak, C.S., and Labes, M.M., 1975, *J. Am. chem. Soc.*, **97**, 4398.

[16] Hogan, J.L., Imrie, C.T., and Luckhurst, G.R., 1988, *Liq. Crystals*, **3**, 645.

[17] McMillan, W.J., 1972, *Phys. Rev.* A, **6**, 936.

[18] Crooker, P.P., 1989, *Liq. Crystals*, **5**, 751.

[19] Goodby, J.W., Waugh, M.A., Stein, S.M., Chin, E., Pindak, R., and Patel, J.S., 1989, *J. Am. chem. Soc.*, **111**, 8119.

CHAPTER 4

The mesogenicity of cinnamic acid

1. Introduction

The liquid crystalline behaviour of the 4-*n*-alkyloxycinnamic acids has been known for a long time [1]. As for the 4-*n*-alkyloxybenzoic acids [2] and the 6-*n*-alkyloxy-2-naphthoic acids [2] hydrogen bonding via the carboxylic acid group, as shown by IR spectroscopy [3], enables the 4-*n*-alkyloxycinnamic acids to associate into dimers (see structure (1) which leads to an increased length-to-breadth ratio. The 4-*n*-alkyloxycinnamic acids show enantiotropic nematic phase character up to the octyloxy homologue before smectic C behaviour is introduced in addition to a nematic phase, for the n=9 and 10 homologues (see chapter 5).

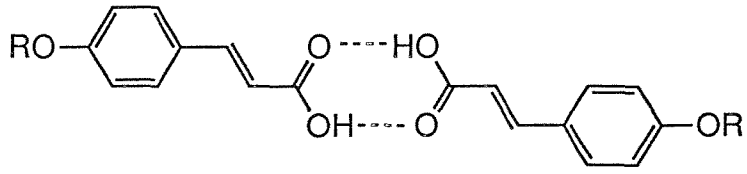

(1)

4-Methoxycinnamic acid has been used to study the photoreactive properties of liquid crystalline dimers. Ikeda *et al.* [4] have synthesised four α,ω-bis(4-methoxycinnamoate)polyoxyethylenes (*n*EGMC where n=2-5, see structure (2)), where the cinnamic acid moieties were incorporated at either end of an ethylene oxide spacer . They reported these materials to be liquid crystalline. 5EGMC had an optical texture similar to a smectic B phase but the phases of the other homologues

could not be identified conclusively by polarising microscopy. The transition temperatures, enthalpies and entropies are summarised in table 1. From these results we see that the melting points for the $n=4$ and 5 homologues are low as are their clearing temperatures. The entropy changes for the $n=2$ and 3 homologues are interesting; the melting entropy change is considerably smaller than the clearing entropy change. However it was concluded that the first transition was not a crystal to crystal transition since the phase was mobile and so it was reported as being liquid crystalline.

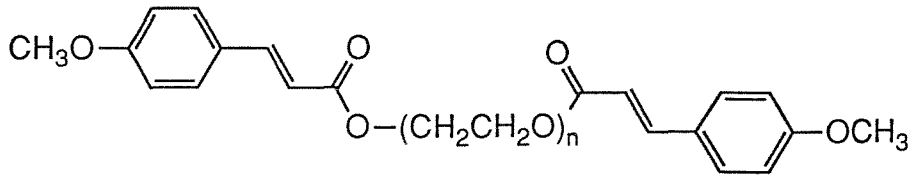

(2)

The ethylene oxide spacer has an energetic preference for *gauche* rather than for *trans* conformations about the carbon-carbon bond in $-CH_2CH_2OCH_2CH_2-$ segments which reduces the statistical probability of conformers with maximum elongation [5]. Conversely, dimers possessing flexible spacers composed of methylene units have been shown to have a strong, statistical preference for the all *trans* conformation in the liquid crystalline phase [6]. Compounds possessing ethylene oxide spacers generally have lower clearing temperatures compared to their methylene unit analogues. For example, the nematic to isotropic transition temperatures for the α,ω-bis(4'-cyanobiphenyl-4-yloxy)alkanes have been compared with those of the α,ω-bis(4'-cyanobiphenyl-4-yloxy)polyoxyethylenes in [7]. The $n=5$, 8 and 11 homologues of the former series were compared, respectively, with the diethylene oxide, triethylene oxide and tetraethylene oxide spacers in the latter series. The T_{NI} values were 32°C, 90°C and 94°C lower than the $n=5$, 8 and 11 homologues, respectively.

To compare the effect of a methylene spacer with the results reported in [4] we have

Table 1. The transition temperatures, enthalpies and entropies of the α,ω-bis(4-methoxycinnamoate)polyoxyethylenes (*n*EGMC), where *n* denotes the number of ethylene oxide units in the spacer.

*n*EGMC	T_m/°C	T_c/°C	ΔH_m/kJmol^{-1}	ΔH_c/kJmol^{-1}	ΔS_m/R	ΔS_c/R
2EGMC	56	72	2.8	27.2	5.4	9.5
3EGMC	72	83	17.1	37.8	6.0	12.8
4EGMC	24	29	22.1	4.6	8.9	1.8
5EGMC	16	26	27.9	3.5	11.5	1.4

The subscripts m and c denote the melting and clearing transitions, respectively.

synthesised some symmetric, dimeric compounds containing cinnamic acid moieties, the α,ω-bis(4-alkyloxycinnamoate)alkanes. We have also varied the length of the terminal alkyl chain since increasing its length has the effect of increasing the molecular length-to-breadth ratio as well as decreasing the melting point. The mnemonic used for these compounds is $(m\text{O.C})_2n$, where m and n denote the number of carbon atoms in the terminal and spacer chains, respectively, and C stands for cinnamoate. To gauge the mesogenicity of the cinnamic acid moiety more closely we have also synthesised some non-symmetric, dimeric compounds containing cinnamic acid as one group and cyanobiphenyl as the other; these are the α-(4-alkyloxycinnamoate)-ω-(4'-cyanobiphenyl-4-yloxy)alkanes. These compounds were chosen because the α,ω-bis(4'-cyanobiphenyl-4-yloxy)alkanes are well-known [6] and further the α-(4-alkylphenyliminobenzylidene-4'-oxy)-ω-(4'-cyanobiphenyl-4-yloxy)alkanes have also been studied in detail [8] and so comparisons between the three series are possible. The mnemonic used here is mO.CnO.CB, which is similar to that of the symmetric, dimeric compounds, where CB denotes cyanobiphenyl.

2. Experimental

The synthetic route for the $(m\text{O.C})_2n$ compounds is shown in scheme 1 and we describe the synthesis of $(2\text{O.C})_2 8$ as an example. Scheme 2 outlines the synthesis of the mO.CnO.CB compounds and in the descriptions of the synthetic steps 2O.C7O.CB is employed as an example.

2.1. *Synthesis of α,ω-bis(4-ethoxycinnamoate)octane*

4-Ethoxycinnamic acid (5g; 2.6 x 10^{-2}mol), which was synthesised as outlined in chapter 5, was dissolved in 50ml of anhydrous dimethyl sulphoxide (DMSO) in a 100ml conical flask and warmed to 30°C on a water bath. 1,8-Diazabicyclo[5.4.0]undec-7-ene (DBU) (3.2g; 1.2 x 10^{-2}mol) was added and the mixture stirred for 30min after which 1,8-dibromooctane (3.3g; 1.2 x 10^{-2}mol) was

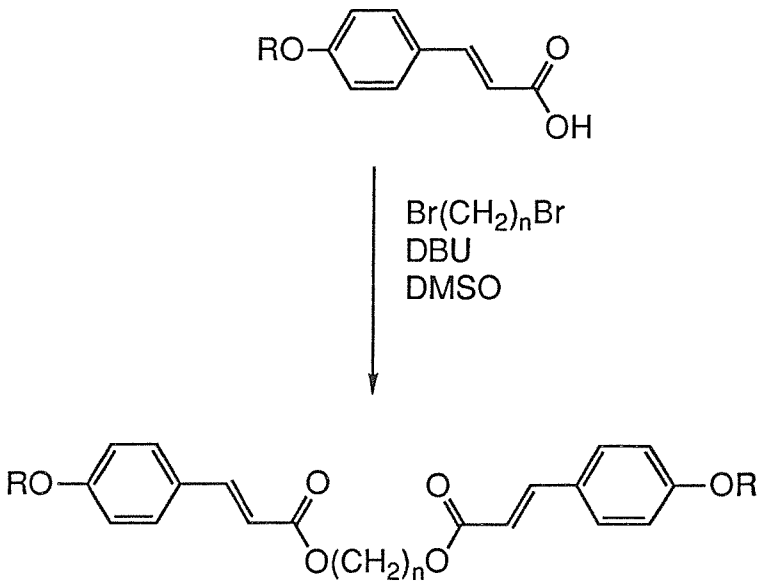

Scheme 1. The synthetic pathway to the α,ω-bis(4-alkyloxycinnamoate)alkanes.

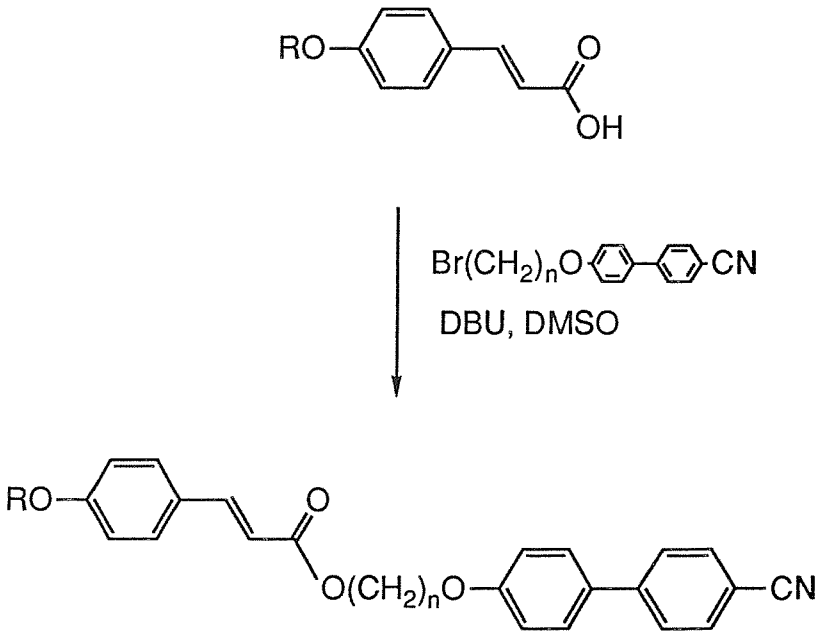

Scheme 2. The synthetic pathway to the α-(4-alkyloxycinnamoate)-ω-(4'-cyanobiphenyl-4-yloxy)alkanes.

added and the mixture left to stir for 5h. The reaction mixture was then poured into water and extracted with diethylether. The combined extracts were washed with saturated sodium carbonate solution to remove the excess 4-ethoxycinnamic acid and then evaporated to give a white solid. The crystalline white solid was recrystallised twice from methanol to yield white crystals which were dried *in vacuo*. Yield 3.9g (71%).

IR (NaCl disc, film): ν 1631.0 (cinnamic C=C), 1698.7cm^{-1} (C=O).
^{1}H NMR ($CDCl_3$): δ 1.2-1.8 (m, 18H), 3.9-4.3 (m, 8H), 6.2-6.4 (d, 2H), 6.8-7.0 (d, 4H), 7.4-7.6 (d, 4H), 7.7-7.8ppm (d, 2H).
MS (EI): 175, 494 (M^+).

2.2. *Synthesis of α-(4-ethoxycinnamoate)-ω-(4'-cyanobiphenyl-4-yloxy)heptane*

4-Ethoxycinnamic acid (0.53g; 2.76 x 10^{-3}mol) was dissolved in 30ml of anhydrous dimethyl sulphoxide in a 50ml conical flask. DBU (0.46g; 3.04 x 10^{-3}mol) was added and the mixture stirred on a water bath at 30°C for 30min. α-(Bromo)-(4'-cyanobiphenyl-4-yloxy)heptane (0.93g; 2.51 x 10^{-3}mol) (prepared as in chapter 3) was added and the mixture left to stir for 5h. The mixture was then poured into water and extracted with diethylether. The extracts were washed with saturated sodium carbonate solution to remove the excess 4-ethoxycinnamic acid and were then evaporated to give a white solid. This was recrystallised twice from methanol to yield white crystals which were dried *in vacuo*. Yield 0.53g (44%).

IR (NaCl disc, film): ν 1632.1 (C=C), 1705.4 (C=O), 2221.8cm^{-1} (C≡N).
^{1}H NMR ($CDCl_3$): δ 1.3-2.0 (m, 13H), 3.9-4.3 (m, 6H), 6.2-6.4 (d, 1H), 6.8-7.1 (m, 4H), 7.4-8.8ppm (m, 9H).
MS (EI): 175, 483 (M^+).

3. Results and discussion

3.1. *The (mO.C)$_2$n compounds*

Table 2 lists the transition temperatures, enthalpies and entropies of a selection of compounds from the (mO.C)$_2n$ series showing a range of spacer and termial chain lengths. None of the compounds examined showed liquid crystalline behaviour. Indeed the melting points of these compounds are too high to allow any liquid crystalline phases to be revealed even on supercooling. Mixture studies performed on (2O.C)$_2$8 with I-35 (C 29°C N 108°C I, Merck Ltd., Poole, U.K.) gave a virtual T_{NI} 55°C below the melting point which is outside the supercooling range of isolated droplets for this compound; this would suggest that these compounds are not too far from being liquid crystalline. Clearly the liquid crystalline properties of cinnamic acid are destroyed on inserting a flexible polymethylene spacer between two cinnamic acid moieties. We can think of an associated dimer of cinnamic acid as having a rod-shaped mesogenic core the anisometric properties of which are important for liquid crystalline behaviour. Breaking this core in half with a flexible spacer reduces the anisometry and destroys the liquid crystalline properties.

3.2. *The 1O.CnO.CB series*

In this series of compounds the number of carbon atoms in the spacer was varied between n=3-12. The spacer was seen to have a significant effect on the transition temperatures, enthalpies and entropies and these are summarised in table 3. For this series of compound we should remember that an odd number of carbon atoms in the alkyl part of the spacer leads to a molecular shape, which in the all *trans* conformation, allows the cinnamic acid group to lie approximately parallel to the cyanobiphenyl group since the -CO.O- and -O- linking units, that is three atoms, must be included when calculating the total spacer length. Thus we expect to see an enhancement of liquid crystal behaviour for alkyl spacers composed of an odd number of carbon atoms relative to the even membered homologues. Figure 1 shows

Table 2. The transition temperatures, enthalpies and entropies for members of the $(m\text{O.C})_2n$ series.

Compound	T_{CI}/°C	ΔH_{CI}/kJmol^{-1}	ΔS_{CI}/R
$(2OC)_2 2$	122	35.0	10.6
$(10OC)_2 2$	64	92.0	12.8
$(10OC)_2 4$	80	75.2	15.7
$(6OC)_2 6$	73	32.7	11.4
$(2OC)_2 8$	92	46.5	15.3
$(4OC)_2 8$	76	54.2	18.7
$(2OC)_2 9$	47	42.5	16.0

Table 3. The transition temperatures, enthalpies and entropies for the 1O.C*n*O.CB series.

n	*T*/°C		Δ*H*/kJmol^{-1}		Δ*S*/R	
	†C-N C-I	N-I	†C-N C-I	N-I	†C-N C-I	N-I
3	157	(149)	51.1	(4.7)	14.3	(1.4)
4	128	‡(52)	51.6		15.5	
5	147	(134)	45.7	(4.2)	13.1	(1.2)
6	115	‡(71)	58.9		18.3	
7	†122	128	†36.2	5.9	†11.0	1.8
8	101	(83)	47.6	(5.8)	15.3	§
9	122	(110)	52.2	(6.1)	15.9	(1.9)
10	88	(82)	44.4	(0.9)	15.2	(0.3)
11	125	(103)	56.9	(6.1)	17.2	(2.0)
12	82	(81)	47.5	(1.0)	16.1	(0.3)

‡ Observed only by polarizing microscopy by supercooling isolated droplets.

§ Not possible to measure by DSC.

Parentheses indicate a monotropic transition.

the effect of the number of carbon atoms, n, on the phase behaviour of the 1O.CnO.CB series. We see that all the homologues exhibit a nematic phase which was characterised by two and four point singularities and which flashed when stressed mechanically. For n=3-6 there is a huge odd-even effect; indeed the T_{NI} values for the n=4 and 6 homologues are so low that a nematic phase could only be detected by supercooling isolated, droplets of the material. The T_{NI} values for the even membered homologues lie on a steadily increasing curve. Conversely for the odd membered homologues the T_{NI} values steadily fall on increasing the spacer length and except for the n=7 homologue they are all monotropic nematogens. Figure 2 shows the effect of the spacer chain length, n, on the nematic to isotropic entropy change. It was not possible to measure this entropy change for the n=4,6 and 8 homologues as their T_{NI}s were too far below the melting point. For the odd membered homologues we see that the entropy change for the nematic to isotropic transition steadily rises across the series; the entropy changes (ΔS/R) are typical for dimeric compounds with an even number of atoms between the mesogenic units [7]. The n=10 and 12 homologues have very low nematic to isotropic entropy changes which are again typical of dimeric compounds whose mesogenic units are separated by an odd numbered spacer [7]. When taken together with the corresponding values for the n=9 and 11 homologues there is a considerable odd-even effect. Figure 3 shows a comparison of the effect of the total number of atoms in the spacer, n, on the nematic to isotropic transition temperatures for the α,ω-bis(4'-cyanobiphenyl-4-yloxy)alkanes (BC.O)$_2n$) [6] and the α-(4'-cyanobiphenyl-4-yloxy)-ω-(4-cyanophenyloxy)-alkanes (CNPh.OnO.CB) [7] together with those for the 1O.CnO.CB series. We see that the T_{NI} values for the 1O.CnO.CB series lie well below those of the (BC.O)$_2n$ series and this reflects the greater anisotropy of the latter series. However, they are very similar to those of the three compared homologues of the CNPh.OnO.CB series; particularly the n=6 and 8 homologues.

Figure 1. The influence of the length of the alkyl spacer, *n*, on the transition temperatures of the *α*-(4-methoxycinnamoate)-*ω*-(4'-cyanobiphenyl-4-yloxy)alkanes. C- (■), N-I (+).

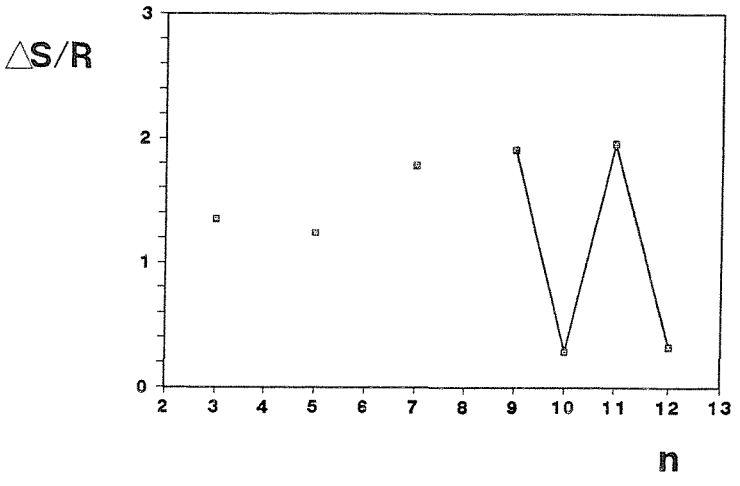

Figure 2. The influence of the length of the alkyl spacer, *n*, on the transitional entropy changes of the *α*-(4-methoxycinnamoate)-*ω*-(4'-cyanobiphenyl-4-yloxy)alkanes. N-I (■).

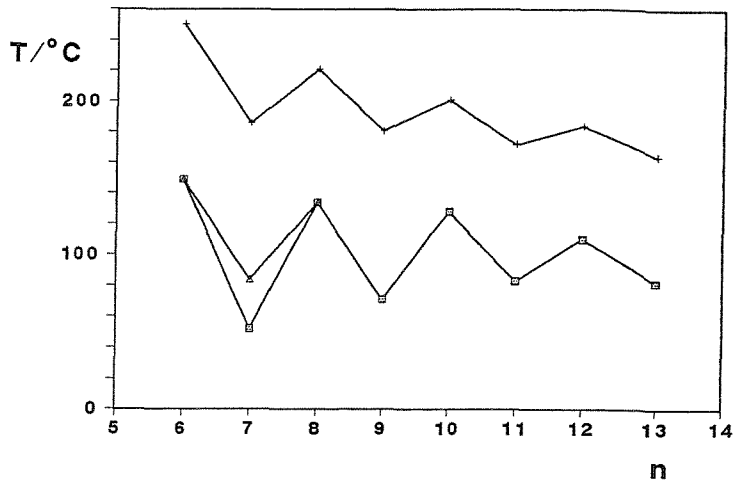

Figure 3. A comparison of the influence of the length of the alkyl spacer, n, on the nematic to isotropic transition temperatures of the α,ω-bis(4'-cyanobiphenyl-4-yloxy)alkanes (+), the α-(4'-cyanobiphenyl-4-yloxy)-ω-(4-cyanophenyloxy)alkanes (△) and the α-(4-methoxycinnamoate)-ω-(4'-cyanobiphenyl-4-yloxy)alkanes (■).

3.3. *The mO.C7O.CB series*

It was observed for the 1O.CnO.CB series that the n=7 homologue was the only enantiotropic nematogen and so it was of interest to see how the terminal chain affected the transition temperatures as its length was increased. Table 4 lists the transition temperatures, enthalpies and entropies for the mO.C7O.CB series and figure 4 shows the influence of the length of the terminal chain on the transition temperatures. We see that the n=1-8 homologues possess a nematic phase and that, interestingly, the n=2 and 3 homologues also exhibit monotropic, smectic A behaviour; the n=9 and 10 homologues only possess a smectic A phase. The smectic

Table 4. The transition temperatures, enthalpies and entropies for the *m*O.C7O.CB series.

m	*T*/°C			Δ*H*/kJmol^{-1}			Δ*S*/R		
	†C-I ‡C-S_A C-N	S_A-N	†S_A-I N-I	†C-I ‡C-S_A C-N	S_A-N	†S_A-I N-I	†C-I ‡C-S_A C-N	S_A-N	†S_A-I N-I
1	122		128	36.2		5.9	11.0		1.8
2	118	(101)	125	49.1	(1.5)	6.8	15.1	(0.48)	2.1
3	†126	(101)	(117)	†40.9	(2.7)	(6.3)	†12.3	(0.86)	2.0
4	†118		(116)	†39.2		(6.7)	†12.1		2.1
5	104		114	46.4		5.6	14.8		1.8
6	96		114	51.1		5.8	16.6		1.8
7	90		110	45.8		5.6	15.2		1.8
8	95		111	55.3		6.1	18.1		1.9
9	‡80		†107	‡43.7		†8.3	‡14.9		†2.6
10	‡91		†108	‡50.9		†7.4	‡16.8		†2.3

Parentheses indicate a monotropic transition.

A phase was characterised by the coexistence of the focal-conic fan and homeotropic textures. The clearing temperatures exhibit a weak odd-even effect across the series. As expected the melting points gradually decrease as the terminal chain is lengthened. Figure 5 shows the effect of the alkyl chain length, n, on the smectic A to nematic and clearing entropy changes. The nematic to isotropic entropy change, for which there is no real odd-even effect, has values typical for dimeric liquid crystals with an even spacer.

The disappearance and then reappearance of smectic A behaviour has been reported for the α-(4-alkylphenyliminobenzylidene-4'-oxy)-ω-(4'-cyanobiphenyl-4-yloxy)alkanes [8,9]. This behaviour is thought to be charge transfer in origin [10] and has been rationalised in terms of two specific mesogenic core interactions: one is a mixed mesogenic core interaction whereby the two different anisometric units lie next to one another giving rise to an intercalated smectic A phase and the other is an interaction between two cyanobiphenyl groups yielding an interdigitated smectic A phase (see figure 6 in chapter 3). The formation of these two smectic A phase types is dependent, as expected, on the length of the terminal alkyl chain. If the terminal chain can be accommodated in the space between the two anisometric units then an intercalated smectic A phase forms. Long terminal chains help stabilise the conventional smectic A modification by pushing the two different anisometric groups apart. They cannot be accommodated in the space between the layers which is dictated by the length of the spacer. Indeed X-ray experiments performed on 2O.C7O.CB indicate that the smectic A phase is intercalated as the small angle reflection gave a periodicity of 16.6Å (the all *trans* molecular length is 35Å as calculated from a CPK atomic model). This result is interesting as it is hard to see how charge transfer can exist between a cinnamic acid moiety, which is not particuarly electron rich, and a cyanobiphenyl group. The formation of such an intercalated phase could in this case be driven by entropy: a mixing of the cores would lead to a rise in entropy. For the $n=10$ homologue (the all *trans* molecular length is 44Å as calculated from a CPK atomic model) the small angle reflection gave a periodicity of 43Å which indicates that the phase was that of a conventional monolayer smectic A. It would seem that the disappearance of smectic behaviour for

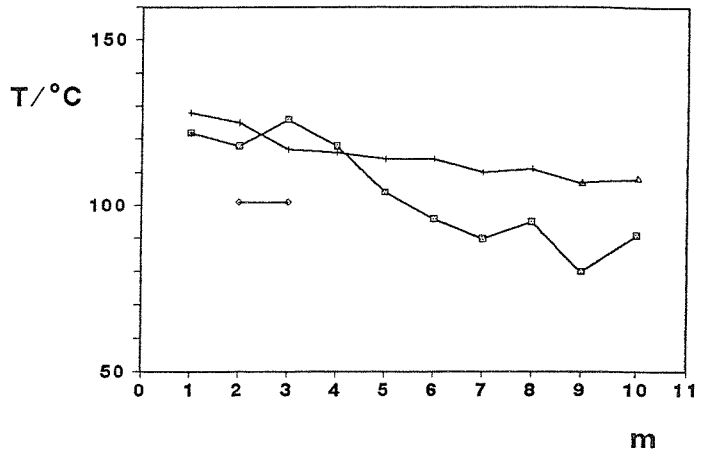

Figure 4. The influence of the length of the terminal chain, *m*, on the transition temperatures of the α-(4-alkyloxycinnamoate)-ω-(4'-cyanobiphenyl-4-yloxy)heptanes. C- (■), S_A-N (◇), N-I (+), S_A-I (△).

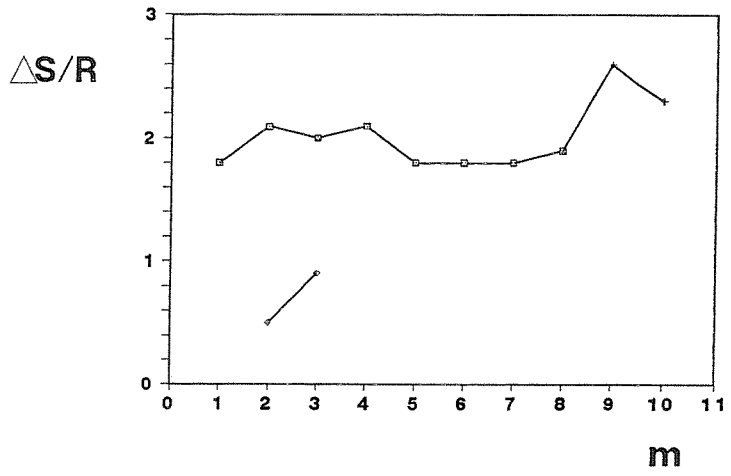

Figure 5. The influence of the length of the terminal chain, *m*, on the transitional entropy changes of the α-(4-alkyloxycinnamoate)-ω-(4'-cyanobiphenyl-4-yloxy)heptanes. N-I (■), S_A-N (◇), S_A-I (+).

intermediate chain lengths is due to the absence of any interactions which can stabilise smectic behaviour.

4. Conclusions

In this chapter we have presented two new series of dimeric compounds containing cinnamic acid moieties. Symmetric dimers containing cinnamic acid moieties linked together by a polymethylene spacer were not liquid crystalline no matter what the length of the spacer or terminal chains. Mixture studies of $(2O.C)_2 8$ with I-35 indicated that its virtual nematic to isotropic transition temperature was approximately 55°C below the melting point. However, when a methoxycinnamic acid moiety is linked via a flexible spacer to a cyanobiphenyl group mesophase behaviour is observed particularly for spacers which contain an even number of atoms in total. Further, as the terminal chain length is increased some interesting parallels arise with non-symmetric liquid crystal dimers [8,9]. For short terminal chains, $n=2$ and 3, a smectic A phase is formed which has an intercalated molecular arrangement. Smectic behaviour disappears for intermediate chain lengths before reappearing again for the $n=9$ and 10 homologues when a conventional smectic A phase is formed. Clearly the cinnamic acid moiety is very weakly mesogenic being similar to that of cyanophenyl. However, when it is linked to a strong mesogen, such as cyanobiphenyl, it tends to display similar liquid crystalline behaviour to that of the Schiff base portion of a cyanobiphenyl-Schiff base non-symmetric dimer.

References

[1] Gray, G.W., and Jones, B., 1954, *J. org. Chem.*, 1467.

[2] Demus, D., and Zaschke, H., 1974, *Flüssige Kristalle in Tabellen I* (VEB Deutscher Verlag für Grundstoffindustrie, Leipzig), p.57.

[3] Azima, A., Brown, C.W., and Mitra, S.S., 1975, *Spectrochim. Acta*, **31A**, 1475.

[4] Ikeda, T., Ikeda, T., Sasaki, T., Lee, B., Kurihara, S., and Tazuke, S., 1991, *Liq. Crystals*, **9**, 457.

[5] Creed, D., Gross, J.R.D., Sullivan, S.L., Griffin, A.C., and Hoyle, C.E., 1987, *Molec. Crystals liq. Crystals*, **149**, 185.

[6] Emsley, J.W., Luckhurst, G.R., Sage, I., and Shilstone, G.N., 1984, *Molec. Crystals liq. Crystals Lett.*, **102**, 223.

[7] Imrie, C.T., 1989, Ph.D. Thesis, Southampton.

[8] Attard, G.S., Date, R.W., Imrie, C.T., Luckhurst, G.R., Roskilly, S.J., Seddon, J.M., and Taylor, L., 1993, *Liq. Crystals* (in the press) and references therein.

[9] Hogan, J.L., Imrie, C.T., and Luckhurst, G.R., 1988, *Liq. Crystals*, **3**, 645.

[10] Park, J.W., Bak, C.S., and Labes, M.M., 1975, *J. Am. chem. Soc.*, **97**, 4378.

CHAPTER 5

The symmetry of the nematic phase of 2,3,4-tri-*n*-hexyloxycinnamic acid

1. Introduction

The isotropic liquid has properties such as orientational order, magnetic susceptibility and dielectric permittivity which are all directional independent. Thus using the principal axis of the system, *xyz* (see figure 1), we find that these properties have the same values in all three directions. In a monodomain, uniaxial phase such properties have the same values in the x and y directions but a different value in the z direction. For a monodomain, biaxial phase these physical properties have different values in all three directions. The symmetries of the isotropic, uniaxial and biaxial phases are equivalent to a sphere, a cylinder with a circular cross-section and a cylinder with an elliptical cross-section, respectively (see figure 1).

The terms uniaxial and biaxial, when applied to phase symmetry, originate from certain optical properties of the phase. For a uniaxial phase there is only one axis (the optic axis) along which a plane polarised light wave can travel without its state of polarisation being changed. Similarly for a biaxial phase there are just two axes along which a plane polarised light wave can travel without its state of polarisation being altered.

Figure 2 illustrates schematically the difference in the ordering of the molecules in uniaxial nematic and biaxial nematic phases. We know that nematic phases are typically formed by lath-like molecules. Their molecular long axes tend to point parallel to a common axis called the director and they have long range orienational order. If the rotation of the molecules along their axes is fairly free, such that the

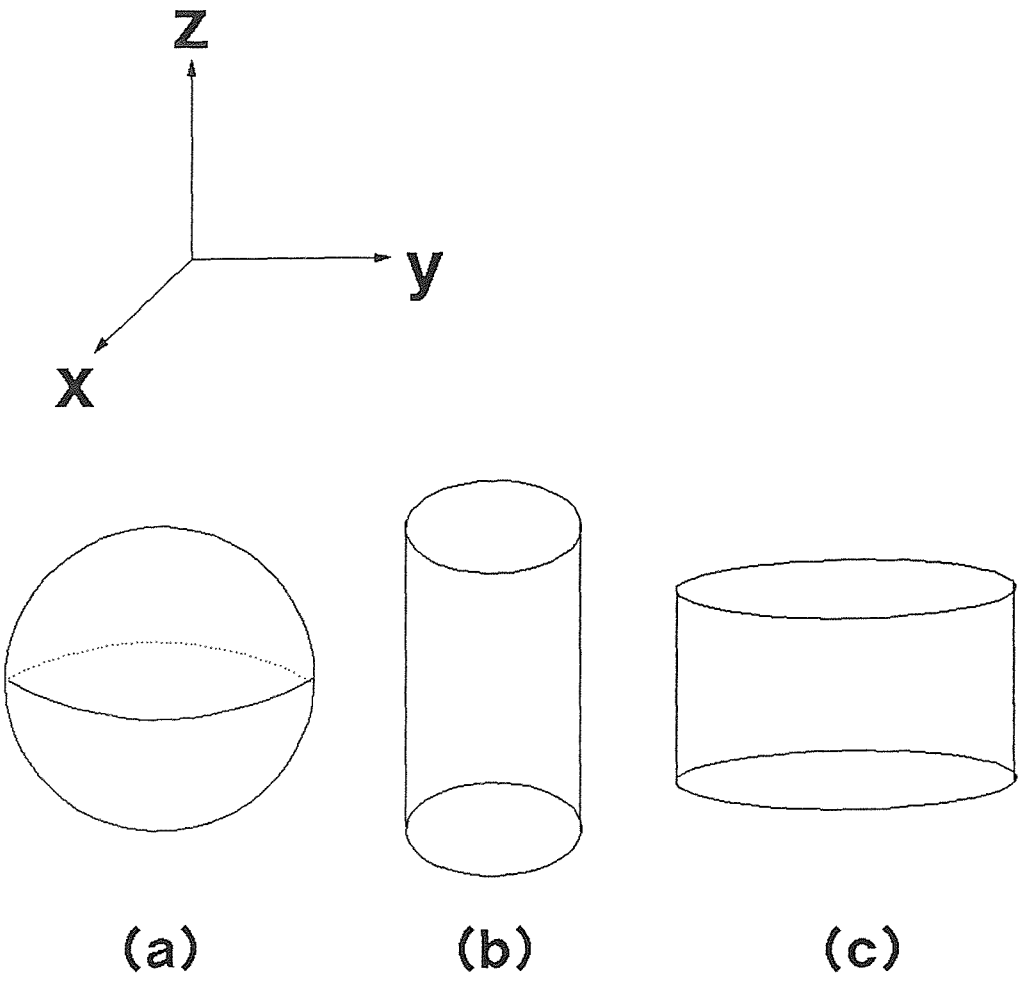

Figure 1. The schematic representations of the phase symmetries for (*a*) an isotropic phase, (*b*) a uniaxial phase and (*c*) a biaxial phase.

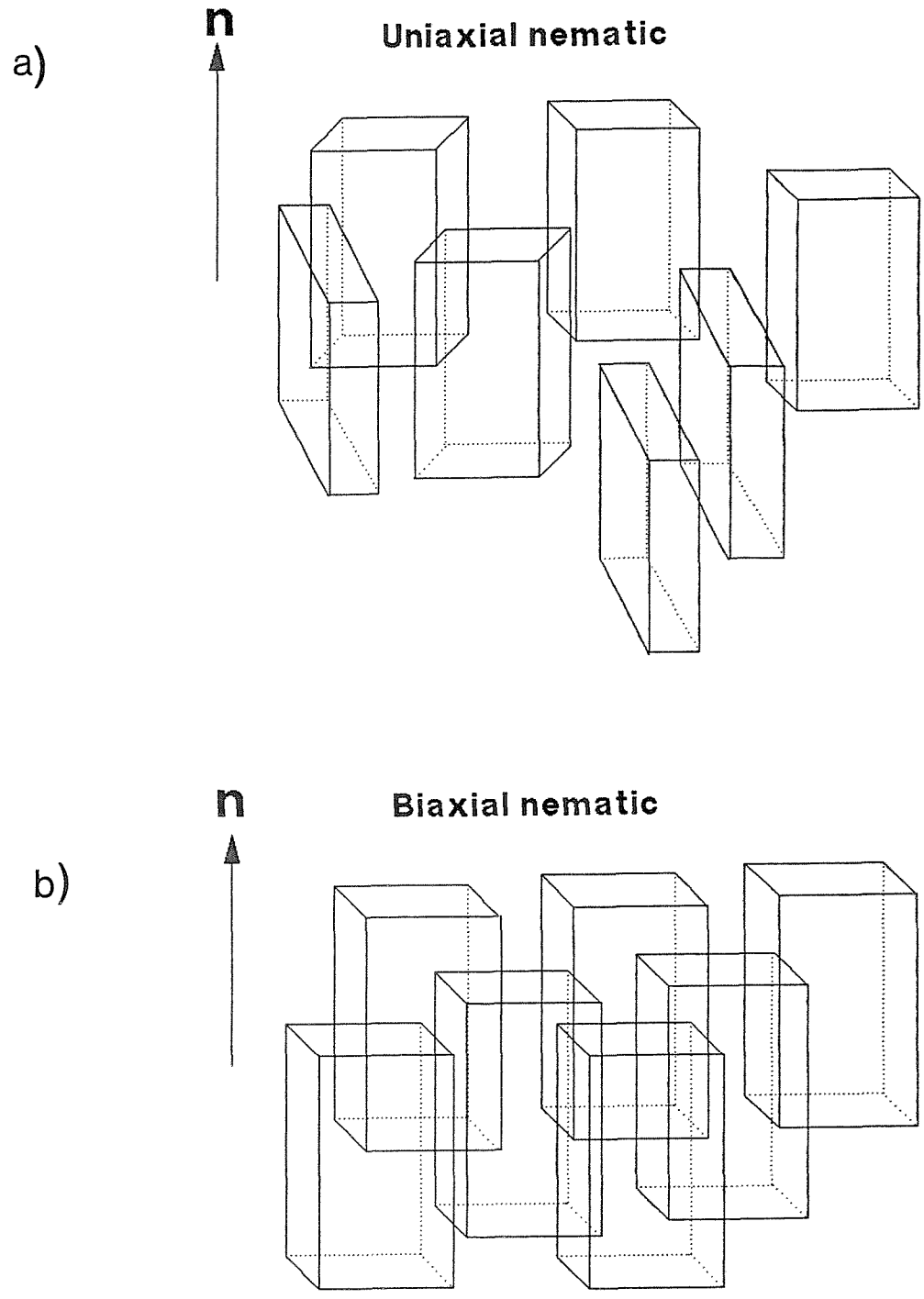

Figure 2. The molecular arrangements in (*a*) a uniaxial and (*b*) a biaxial nematic phase.

ordering of the nematic phase along the x and y molecular axes is the same, the nematic phase is said to be uniaxial (see figure 2(a)). However if the molecular rotation around the z axis becomes preferred in a certain direction, i.e. the precession of the molecular long axis has an elliptical orientational distribution function and not a circular one, the ordering along the x and y axes is now different and a biaxial nematic phase results (see figure 2(b)).

The majority of calamitic liquid crystals are composed of molecules which do not possess the cylindrical symmetry we usually suppose for them. One important consequence of this symmetry reduction is that the mesogens are expected to exhibit both the uniaxial nematic (N_U) and the biaxial nematic (N_B) phases. According to molecular field theory proposed by Freiser in 1970 [1] the phase sequence on cooling the sample should be

$I\text{-}N_U\text{-}N_B$.

The uniaxial nematic to isotropic phase transition is predicted to be first order while the biaxial to uniaxial nematic transition is predicted to be second order. Computer simulations have shown that as the molecular biaxiality increases so the strength of the uniaxial nematic to isotropic transition weakens and the two transitions approach each other until the maximum molecular biaxiality is reached when the isotropic phase undergoes a second order transition directly into the biaxial nematic phase [2,3].

Although the theory predicting the existence of a biaxial nematic phase was originally developed for thermotropic liquid crystals the first biaxial nematic phase was actually observed for a lyotropic liquid crystal formed from potassium laurate, 1-decanol and water [4]. The phase symmetry was determined using conoscopy and the magnitude of the phase biaxiality was quantified with deuterium NMR spectroscopy. The origin of the biaxial phase is thought to result from the biaxiality of the constituent micelles which appear to adopt extreme values; the phase diagram shows the phase to exist between calamitic and discotic nematic phases. To date there have been few accounts

of low molar mass, thermotropic, biaxial nematic liquid crystals. The first was not until 1986 when Malthête *et al.* [5] reported that 4-[3′,4′,5′-tri(*p*-*n*-dodecyloxybenzyloxy)]-benzoyloxy 4″-*p*-*n*-dodecyloxy-benzoyloxybiphenyl (see structure (1)) exhibits both uniaxial and biaxial nematic phases. The biaxial phase was identified on the basis of its optical texture which showed zig-zag disclination lines [6] and from its X-ray diffraction pattern. In contrast to theoretical predictions the phase sequence was isotropic to biaxial nematic to uniaxial nematic with decreasing temperature. In addition the N_B-I entropy change ($\Delta S/R$) was found to be 0.18 which is first order. The assignment of the first phase as a biaxial nematic is now thought to be a smectic phase [7].

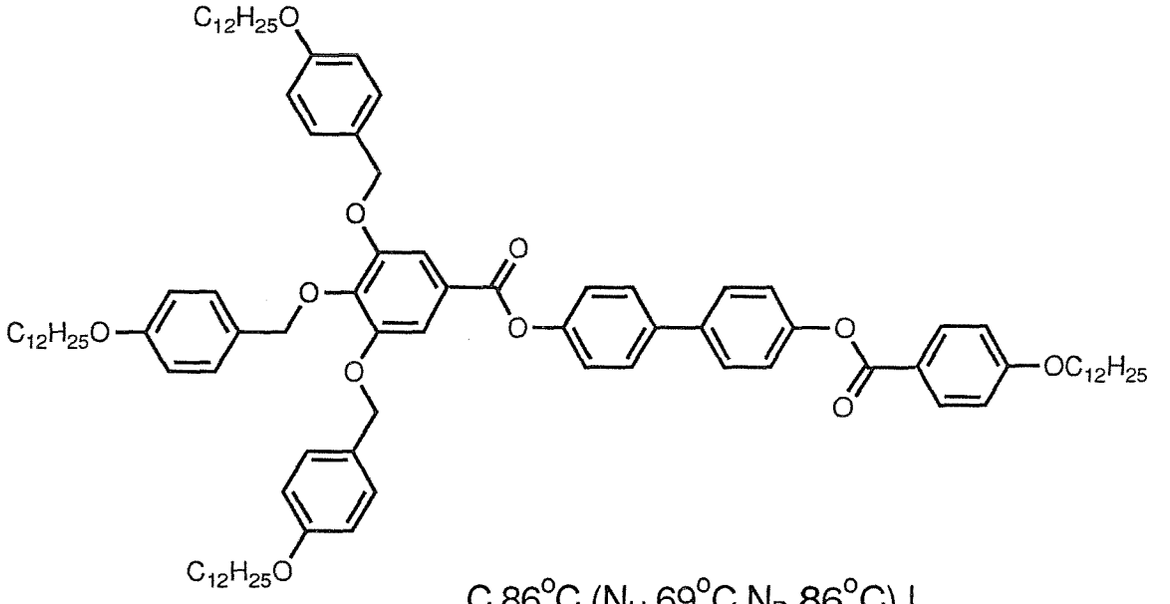

(1)

Later in 1988 Chandrasekhar *et al.* [8] claimed the existence of a monotropic, biaxial nematic phase for the copper complex with structure (2). The biaxial nematic phase for this compound, which undergoes a transition directly into the isotropic phase, was identified by conoscopy.

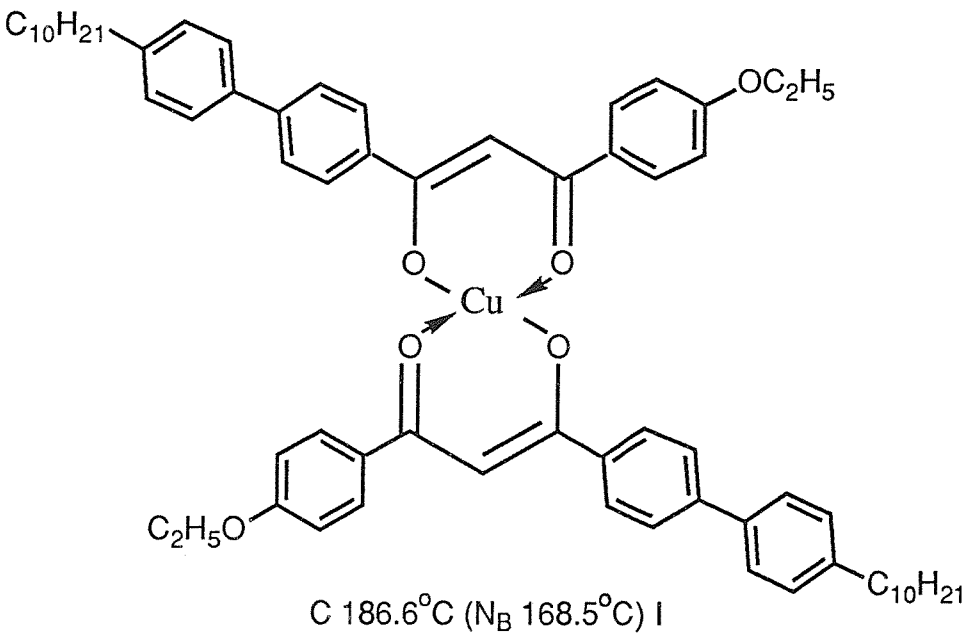

C 186.6°C (N_B 168.5°C) I

(2)

Considerable interest in thermotropic, biaxial nematic systems has been shown by Praefcke and his group [7,9,10]. On the basis of conoscopic studies they reported structures (3) and (4) to possess a biaxial nematic phase [9]. In both cases there was a direct transition from the isotropic to the biaxial nematic phase and the entropy change ($\Delta S/R$) for the transition for compounds (3) and (4) was 0.09 and 0.11, respectively. They have also reported 2,3,4-tri-*n*-hexyloxycinnamic acid to exhibit biaxial nematic phase behaviour (see structure (5)) [7,10]. The phase assignment was made on the basis of conoscopic observations and its unusual X-ray diffraction pattern. Conoscopic observations showed the cross, produced in the extinction position, to split into two hyperbolic brushes on rotation of the microscope stage. However, the centres of the brushes only moved apart slightly and remained close to the middle of the field of view. This is in contrast to the conoscopic observations in [4] where the centres of the brushes were seen to approach the edges of the field of view. The X-ray diffraction pattern shown in [10] has three pairs of diffuse maxima: at small angle one pair is perpendicular and one pair is parallel to the field

direction and at wide angle there is a pair perpendicular to the field direction. Normally the X-ray diffraction pattern of a nematic phase shows two pairs of diffuse maxima: one at small angle parallel and one at wide angle perpendicular to the field direction which correspond to the end-to-end and side-by-side molecular stacking distances, respectively. An X-ray study in [11] suggested that the extra pair of diffuse maxima could come from a locally intercalated structure. The extra pair of diffuse maxima does not indicate phase biaxiality. X-ray diffraction gives information on the local short range packing of the molecules within the phase. It was therefore concluded in [11] that the occurence of three pairs of diffuse maxima suggests that the local molecular packing is biaxial but that the phase itself could not be conclusively proven as being biaxial. This conclusion was further supported by the observation of the same diffuse rings in the isotropic phase which indicated that the diffraction pattern was produced by local order.

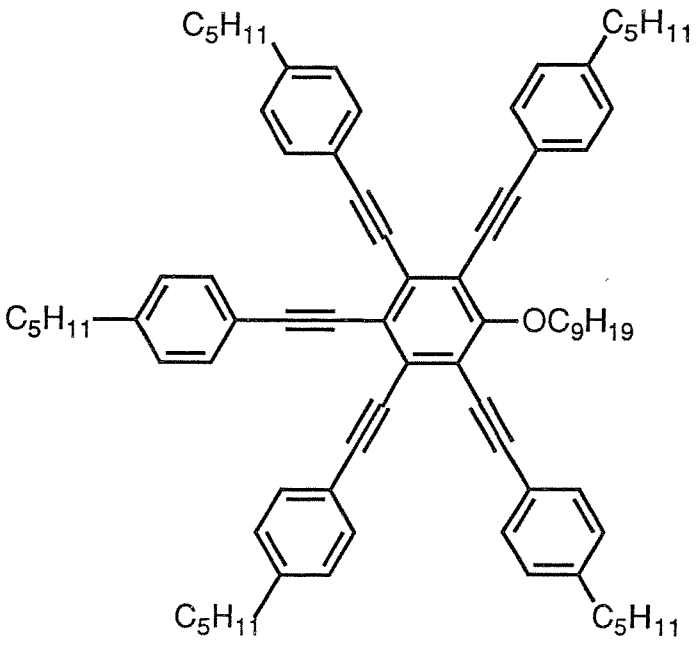

C 86.4°C N_B 109.9°C I

(3)

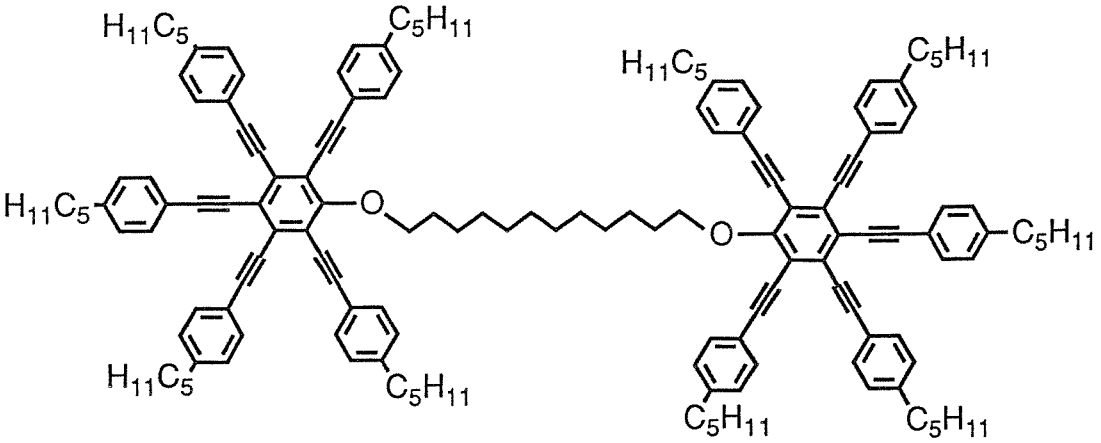

C 121.4°C N_B 156.2°C I

(4)

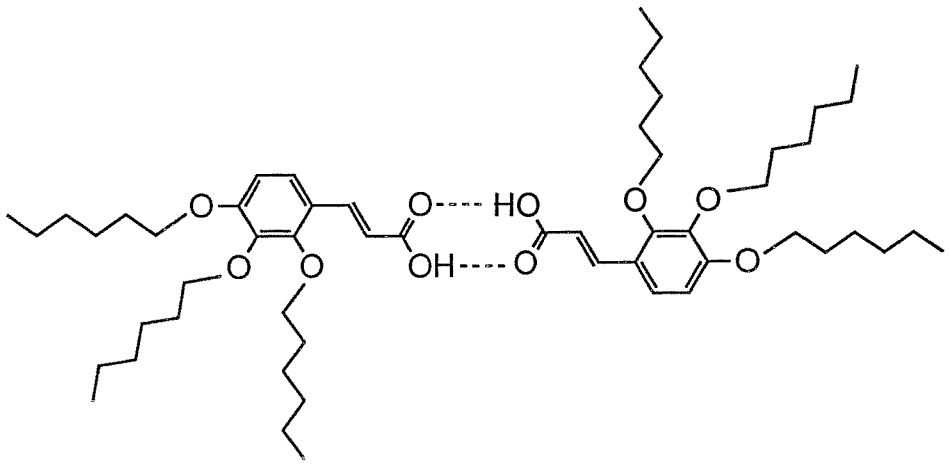

C 51.2°C N_B 59.6°C I

(5)

The characterisation of the majority of thermotropic, biaxial nematic phases reported in the literature has been based almost entirely on a combination of X-ray diffraction

and conoscopy. However, both fail to quantify the degree of phase biaxiality. X-ray diffraction gives us information only on the local order within the phase and conoscopy, although can identify large phase biaxiality, is prone to surface effects which can lead to unreliable results when considering phases with small optical biaxialities. Deuterium NMR spectroscopy, however, provides a sensitive means of measuring the symmetry of the bulk nematic phase since it enables us to measure simultaneously two of the principal axes in the molecular frame *xyz*. As we shall see with the aid of deuterium NMR spectroscopy it becomes possible to obtain a direct measurement of the degree of phase biaxiality.

It is the main aim of this chapter to report the results of a deuterium NMR study of the symmetry of the nematic phase of 2,3,4-tri-*n*-hexyloxycinnamic acid, which has been characterised as exhibiting a biaxial nematic phase. But first, we examine the effect of lateral chains on the phase behaviour of the trisubstituted 2,3,4-tri-*n*-alkyloxycinnamic acids and compare the results with the well-known, calamitic, 4-*n*-alkyloxycinnamic acids [12]. Before describing the deuterium NMR experiment itself we outline the theory of deuterium NMR spectroscopy and show how the orientation of the director with respect to the magnetic field is of crucial importance in understanding the deuterium NMR spectra of uniaxial and biaxial nematic phases. Finally we show how it is possible to measure directly the phase biaxiality of thermotropic, biaxial nematic phases.

2. Experimental

The scheme shows the reaction pathway to the 2,3,4-tri-*n*-alkyloxycinnamic acids. The corresponding 4-*n*-alkyloxycinnamic acids can be prepared in one step as the 4-*n*-alkyloxybenzaldehydes are all commercially available (Lancaster synthesis). For the purpose of simplification the 2,3,4-tri-*n*-alkyloxycinnamic acids are abbreviated to T*n*O.CA, where T denotes trisubstitution, *n* is the number of carbon atoms in the alkyloxy chain and CA is cinnamic acid. Similarly the mnemonic for the monosubstituted 4-*n*-alkyloxycinnamic acids is *n*O.CA. Here we give the synthesis of

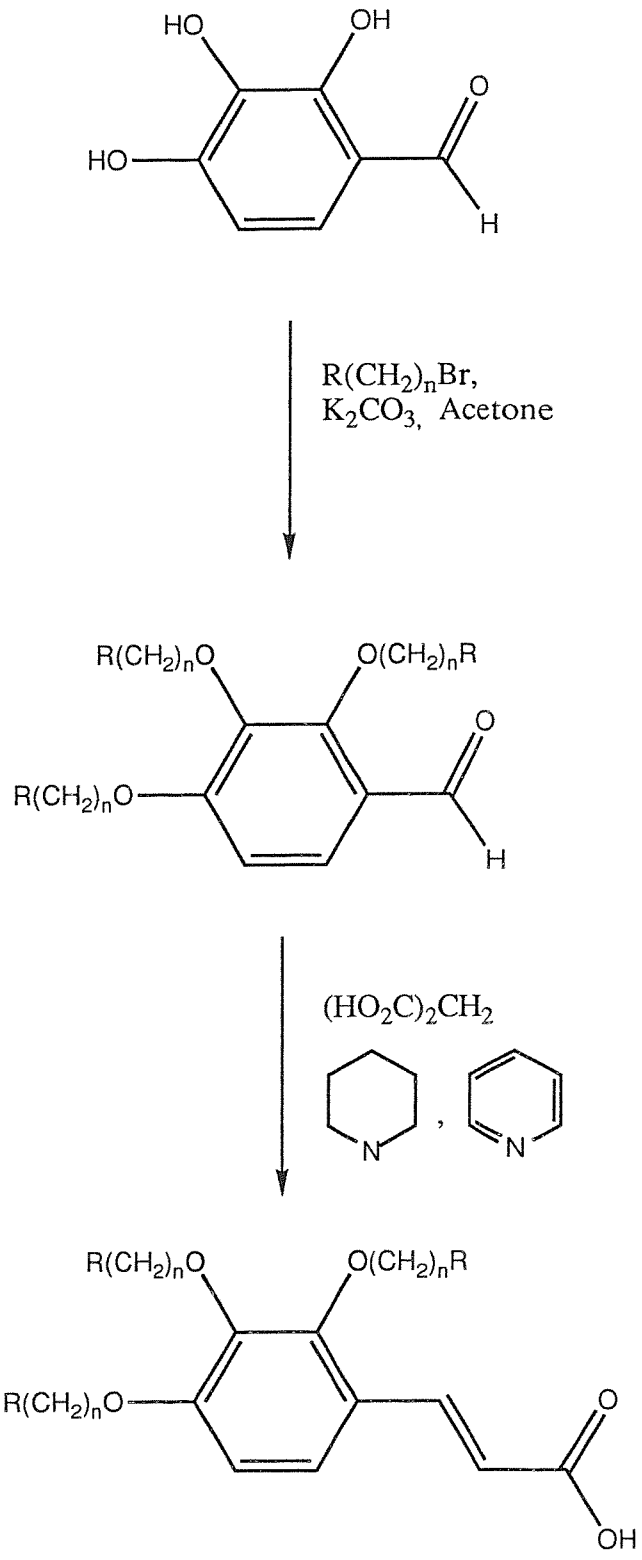

The synthetic pathway to the 2,3,4-tri-*n*-alkyloxycinnamic acids.

2,3,4-tri-*n*-hexyloxycinnamic acid as an example.

2.1. *Synthesis of 2,3,4-tri-n-hexyloxybenzaldehyde*

2,3,4-Trihydroxybenzaldehyde (5g; 3.25 x 10^{-2}mol), 1-bromohexane (32g; 1.95 x 10^{-1}mol) and anhydrous potassium carbonate (81g; 5.85 x 10^{-1}mol) were refluxed in 300ml of Analar acetone for 24h in a 500ml, conical flask. The excess potassium carbonate and any potassium bromide formed were filtered off and washed with hot acetone. The acetone was removed on a rotary evaporator and the unreacted 1-bromohexane was distilled off under reduced pressure (≈88°C, 1mb). The remaining oil was purified using column chromatography (silica gel 60) and dichloromethane as eluent to give a pale yellow liquid. Yield 5.94g (45%). All the other homologues were also pale yellow liquids and their yields were all in excess of 40%.

IR (NaCl disc, neat): ν 1682.4, 1741.6 (Aldehyde C=O), 1372.8, 1467.3, 2956cm^{-1} (Al. C-H).
^{1}H NMR ($CDCl_3$): δ 0.8-1.1 (t, 9H), 1.2-2.0 (m, 24H), 3.8-4.2 (m, 6H), 6.7-6.8 (d, 1H), 7.4-7.6 (d, 1H), 10.1 (s, 1H).

2.2. *Synthesis of 2,3,4-tri-n-hexyloxycinnamic acid*

2,3,4-Tri-*n*-hexyloxycinnamic acid (3.06g; 7.54 x 10^{-3}mol) and malonic acid (1.63g; 1.51 x 10^{-2}mol) were dissolved in 20ml of pyridine. Six drops of the base piperidine were added to initiate the reaction and the mixture was then heated on an oil bath at 100°C for 3h. The mixture was cooled and then poured with care into a mixture of ice and concentrated hydrochloric acid which was stirred for about 30min. The resultant precipitate was filtered off and recrystallised twice from acetonitrile to give white, needle-shaped crystals which were dried *in vacuo*. Yield 1.93g (57%). All the other homologues were white crystals and their yields were in excess of 55%.

IR (NaCl disc, film): ν 1680.6 (Acid C=O), 2860.2, 2932.0 (O-H).

^{1}H NMR ($CDCl_3$): δ 0.9-1.0 (t, 9H), 1.3-1.9 (m, 24H), 3.9-4.1 (m, 6H), 6.4 (d, 1H, J=16Hz), 6.7 (d, 1H), 7.3 (d, 1H), 8.1 (d, 1H, J=16Hz).

MS (EI): 178, 448 (M^+).

2.3. *Synthesis of 2,3,4-tri-n-hexyloxycinnamic acid-d_1*

The synthesis of 2,3,4-tri-*n*-hexyloxycinnamic acid-d_1 was carried out in the same way as in section 2.2 where perdeuteriated malonic acid (Aldrich Chemical Co.) was used as the source of deuterium. The synthesis of 4-*n*-hexyloxycinnamic acid-d_1 was carried out in a similar way. Figure 3 shows the site of deuteriation for the trisubstituted compound. ^{1}H NMR spectra of this compound show the degree of deuteriation to be $\approx$70% as indicated by the difference in the heights of the peaks for the olefinic protons (see figure 4(*a*)). Figure 4 shows the difference in the ^{1}H NMR signals at the olefinic bond for the protonated and deuteriated 2,3,4-tri-*n*-hexyloxycinnamic acids.

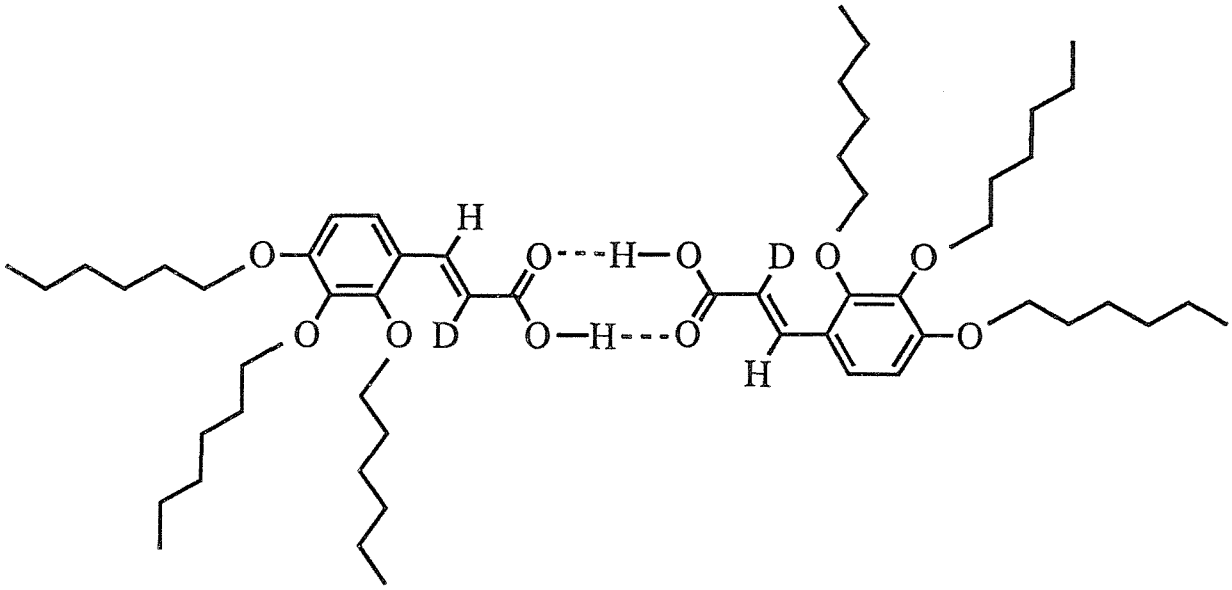

Figure 3. The site of deuteriation for 2,3,4-tri-*n*-hexyloxycinnamic acid-d_1.

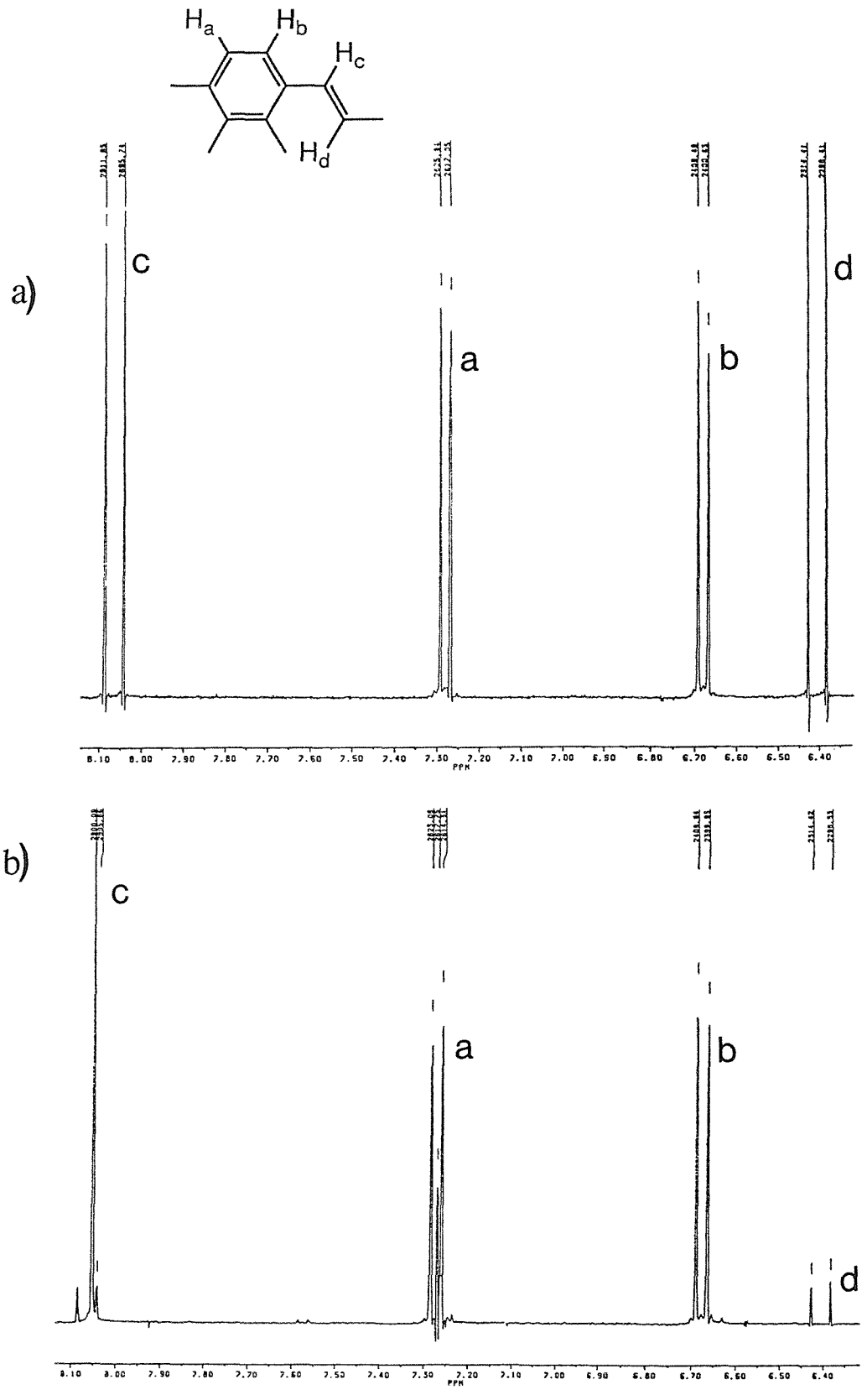

Figure 4. The ^{1}H NMR spectra of the aromatic and ethylenic protons for (*a*) 2,3,4-tri-*n*-hexyloxycinnamic acid and (*b*) 2,3,4-tri-*n*-hexyloxycinnamic acid-d_1.

3. Results and discussion

Table 1 summarises the transition temperatures, enthalpies and entropies of the T*n*O.CA series and table 2 gives the analogous data for the *n*O.CA series. Figures 5 and 6 show the influence of the length of the terminal alkyl chain(s), *n*, on the transition temperatures for the T*n*O.CA and *n*O.CA series, respectively. From comparison of the two figures we see that mesophase behaviour exists for every homologue of the *n*O.CA series whereas only homologues n=4-10 of the T*n*O.CA series are liquid crystalline. All the liquid crystalline compounds exhibit a nematic phase which flashed when subjected to mechanical stress. The n=9 and 10 homologues of the *n*O.CA series also possess a smectic C phase which was characterized by its focal-conic fan and schlieren textures. Interestingly the melting points of the n=1 and 2 homologues are the same in both series. The difference in the melting points for the remaining homologues of both series diverge quickly, those of the T*n*O.CA series levelling off at around 50°C, while those of the *n*O.CA series remain high at around 140°C. The nematic to isotropic transition temperatures of the *n*O.CA series show no real odd-even effect as the terminal chain length is extended. For the T*n*O.CA series only the n=4-7 homolgues show an odd-even effect. The n=6 and 7 homologues of the T*n*O.CA series are enantiotropic nematogens whereas all the homologues of the *n*O.CA series are enantiotropic.

Figures 7 and 8 show the influence of the length of the terminal alkyl chain ,*n*, on the nematic to isotropic entropy change for the T*n*O.CA and *n*O.CA series, respectively. The most striking observation between the two figures is the difference in the magnitude of the entropy of transition. For the *n*O.CA series the $\Delta S/R$ values fluctuate between 0.60 and 1.12 which are large for low molar mass liquid crystal compounds which are typically 0.2-0.6 but are similar to those found for other hydrogen-bonded dimers [13]. Conversely the nematic to isotropic entropy changes for the T*n*O.CA series are considerably smaller and this reflects the increased molecular biaxiality created by the inclusion of the two lateral chains which indictates that the phase could be biaxial.

Table 1. The transition temperatures, enthalpies and entropies of the 4-*n*-alkyloxycinnamic acids.

n	*T*/°C			Δ*H*/kJmol^{-1}			Δ*S*/R		
	C-N †C-S_C	S_C-N	N-I	C-N †C-S_C	S_C-N	N-I	C-N †C-S_C	S_C-N	N-I
1	173		191	22.5		2.3	6.1		0.6
2	196		201	25.2		4.4	6.5		1.1
3	170		186	15.2		3.1	4.1		0.8
4	150		176	20.0		3.6	5.7		1.0
5	143		181	19.2		2.7	5.6		0.7
6	150		180	23.0		3.1	6.5		0.8
7	145		175	19.3		2.3	5.6		0.6
8	143		176	21.2		3.5	6.1		0.9
9	†132	153	171	†18.2	1.98	3.0	†5.4	0.6	0.8
10	†137	145	172	†19.1	2.24	3.3	†5.6	0.6	0.9

Table 2. The transition temperatures, enthalpies and entropies of the 2,3,4-tri-*n*-alkyloxycinnamic acids.

n	*T*/°C		Δ*H*/kJmol^{-1}		Δ*S*/R	
	C-I †C-N	N-I	C-I †C-N	N-I	C-I †C-N	N-I
1	173		32.2		8.7	
2	197		46.3		11.9	
3	127		25.1		7.6	
4	76	(68)	18.6	(0.8)	6.4	(0.3)
5	62	(51)	10.0	(0.8)	3.6	(0.3)
6	†51	60	†14.1	0.9	†5.2	0.3
7	†45	53	†29.7	0.6	†11.3	0.2
8	54	(51)	48.7	(0.5)	17.9	(0.2)
9	57	(41)	45.6	(0.4)	16.6	(0.2)
10	53	(37)	36.3	(0.6)	13.4	(0.2)

Parentheses indicate a monotropic transition.

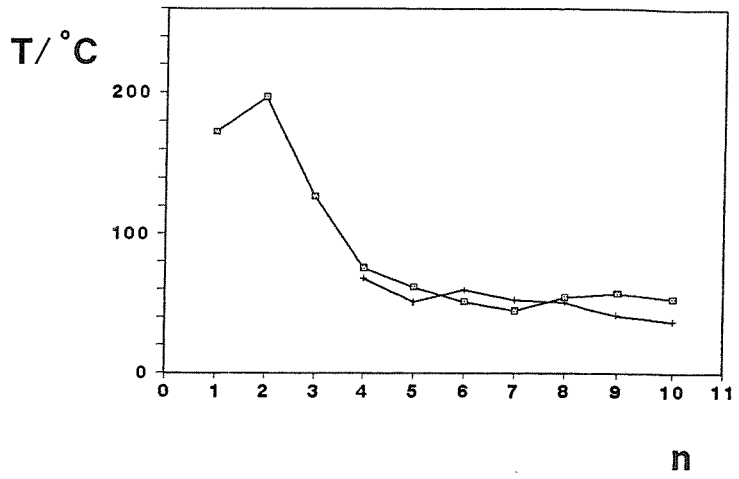

Figure 5. The influence of the terminal alkyloxy chain length, *n*, on the transition temperatures for the 2,3,4-tri-*n*-alkyloxycinnamic acids. C- (■), N-I (+).

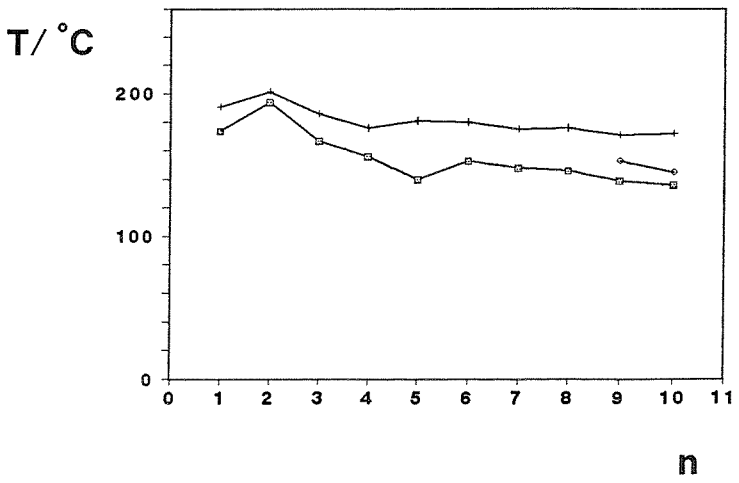

Figure 6. The influence of the terminal alkyloxy chain length, *n*, on the transition temperatures for the 4-*n*-alkyloxycinnamic acids. C- (■), N-I (+), S_C-N (◇).

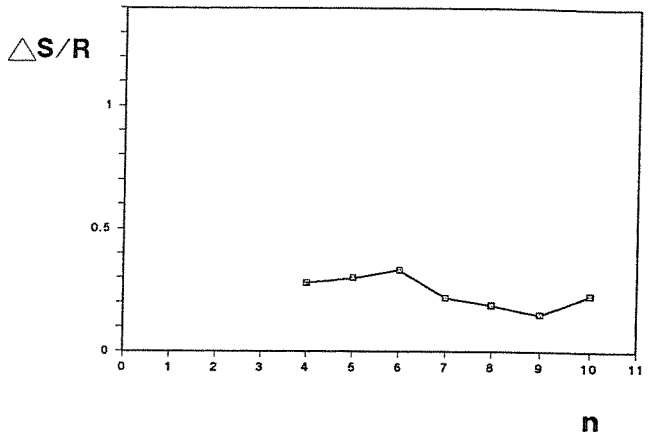

Figure 7. The influence of the terminal alkyloxy chain length, *n*, on the nematic to isotropic entropy change for the 2,3,4-tri-*n*-alkyloxycinnamic acids.

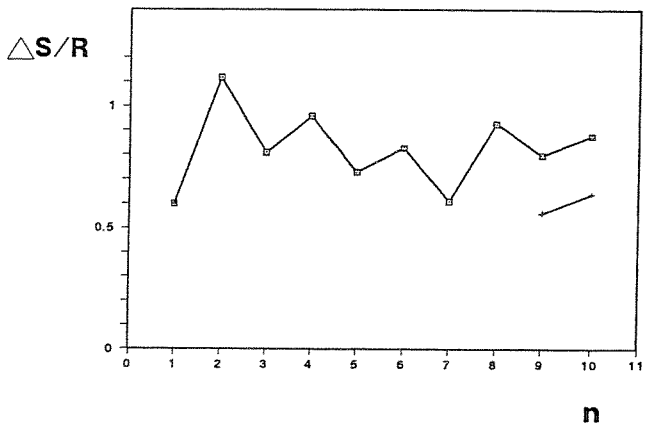

Figure 8. The influence of the terminal alkyloxy chain length, *n*, on the nematic to isotropic (■) and smectic C to nematic (+) entropy changes for the 4-*n*-alkyloxycinnamic acids.

4. Deuterium NMR spectroscopy of liquid crystals

4.1. *Theory*

Certain nuclei possess a characteristic property called spin denoted by the letter I; for hydrogen $I=½$ and for deuterium $I=1$. Such nuclear spin has $2I+1$ spin states which are labelled with a nuclear spin quantum number m. m takes values from I to -I and so for a single deuteron $m=1,0$ or -1. In the absence of an external field these spin states are degenerate. Nuclei are charged and those with a spin possess a magnetic moment, the magnitude of which depends on the value of m. The nuclear magnetic moment can interact with the magnetic field (Zeeman coupling) of the spectrometer and remove the degeneracy of the spin levels. The resultant energy difference is

$$E(m) = -\gamma_n \hbar mB, \tag{1}$$

where $E(m)$ is the energy difference of the spin states m, γ_n is the nuclear magnetogyric ratio, $\hbar$ is the Planck constant divided by 2π and B is the magnetic flux density. The selection rule, $\Delta m=\pm 1$, means that there are only two allowed transitions. From figure 9(a) we see that the energy involved for the two transitions is the same and the spectrum contains a single line at a frequency ν known as the Larmor frequency where

$$\nu = (\gamma_n B)/2\pi. \tag{2}$$

The position of the line depends upon the environment of the nucleus in the molecule, an effect called the chemical shift, and so equation (2) becomes

$$\nu = (\gamma_n B(1-\sigma))/2\pi, \tag{3}$$

where σ is the chemical shift.

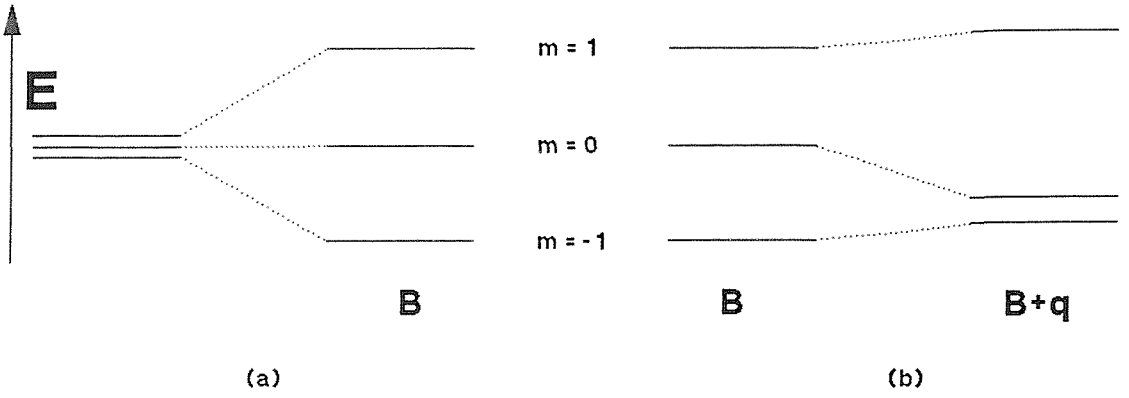

Figure 9. The removal of spin degeneracy for deuterium by (*a*) the Zeeman coupling and (*b*) the quadrupolar coupling.

The deuterium nucleus has $I=1$ and therefore it also possesses a quadrupole moment which can interact with a magnetic field gradient. This quadrupolar coupling to the magnetic field removes the degeneracy of the three spin states (see figure 9(*b*)). The spin states corresponding to $m=1$ and -1 are raised in energy by this interaction by a constant amount which depends on $(3m^2\text{-}2)q$, where q is the quadrupolar coupling tensor in the direction of the magnetic field, while that of $m=0$, also dependent on $(3m^2\text{-}2)q$, is lowered. The energy involved for the two transitions is now unequal and the spectrum consists of a doublet centred at ν, the separation of which depends on the strength of the quadrupolar coupling, that is the degree of orientational order. The coupling is averaged to zero when the molecule tumbles rapidly in an isotropic fluid, but in a liquid crystal mesophase the averaging is not complete and the separation between the lines gives important information on the ordering within the phase. The peak separation is given by

$$\Delta\tilde{\nu} = 3/2 q_{CD} S_{CD}, \quad (4)$$

where ~ denotes an average value for the liquid crystal phase, q_{CD} is the quadrupolar coupling constant for the deuteron in the C-D bond and S_{CD} is the order parameter for the C-D bond axis which is given by

$$S_{CD} = \overline{(3\cos^2\beta - 1)/2}, \quad (5)$$

where β is the angle made by the C-D bond axis with the magnetic field. The bar denotes an ensemble average. For liquid crystals with a positive diamagnetic susceptibility, $\Delta\tilde{\chi}$, the director aligns parallel to the magnetic field and the maximum uadrupolar splitting is observed. However, if the sample is now rotated with respect to the magnetic field the quadrupolar splitting becomes

$$\Delta\tilde{\nu}(\beta) = \Delta\tilde{\nu}(0)\ (3\cos^2\beta - 1)/2. \quad (6)$$

On rotating the sample the splitting decreases until the so-called magic angle of $\approx 55°$ is reached when just a single line is observed as the peaks superimpose corresponding to the degeneracy of the two transitions. As β increases further the single peak splits into a doublet again and the peak splitting continues increasing to a value $\Delta\tilde{\nu}(0)/2$ when the director is orthogonal to the field.

5. The determination of mesophase symmetry by deuterium NMR

Here we recall the principal difference between uniaxial and biaxial phases. In the case of a uniaxial phase the order parameter along the x and y directions is the same but different along the z direction. For a biaxial phase the order parameter along the x, y and z directions is different. We can visualise four ways in which these three axes, or directors, can be distributed with respect to a magnetic field. As the order parameters along the x, y and z axes are different for uniaxial and biaxial phases different deuterium NMR spectra result depending on the phase symmetry and

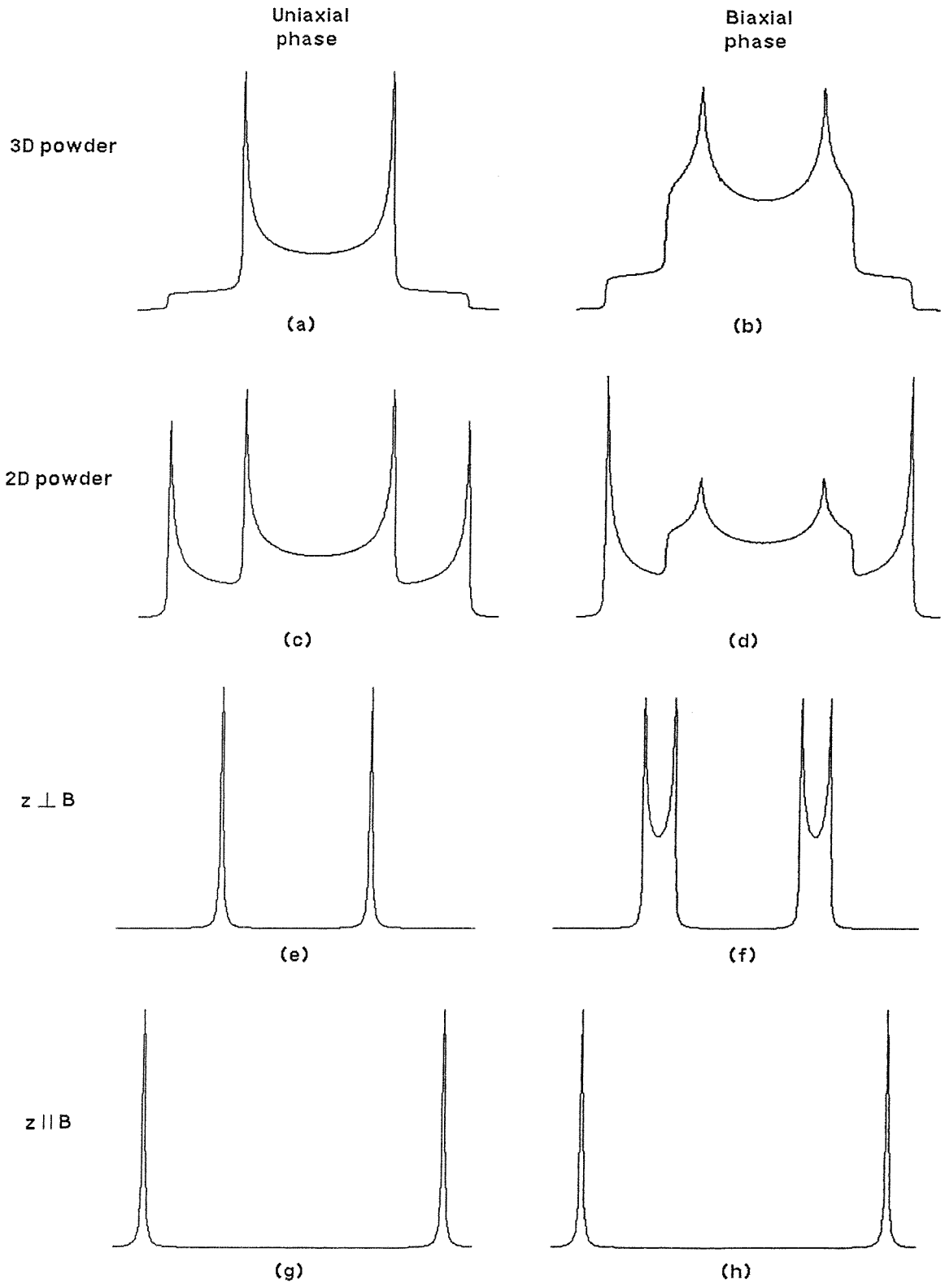

Figure 10. The computer simulated deuterium NMR spectra of the different director distributions for uniaxial and biaxial nematic phases.

director distribution (see figure 10). We now give a qualitative description of the four possible director distributions.

5.1. *3D powder director distribution*

Figure 10(*a*) shows the deuterium NMR spectrum for a 3D powder director distribution for a uniaxial phase which corresponds to a 3D, random director distribution. We see that the spectrum consists of a pair of outer wings and an inner doublet. The separation between the outer wings is twice that of the inner doublet as the wings come from domains in which the major axis (z axis) is parallel to the magnetic field and the inner doublet corresponds to the situation in which the z axis is perpendicular to the field, that is the x and y axes are parallel to the field. As the order parameter along the z axis is twice that along the x and y axes the separation between the outer wings is twice that of the inner wings. The intensity of the inner doublet is twice that of the outer wings since in a 3D isotropic distribution there are two ways for the z axis to be perpendicular and only one way for it to be parallel to the magnetic field.

In a biaxial phase the order parameter along the x and y axes is different and the inner doublet of figure 10(*a*) is split into two doublets (see figure 10(*b*)). As well as the extreme director distributions, that is $z \perp B$ and $z \parallel B$, all the other possible director distributions also exist in a 3D powder distribution and so the overall lineshape consists of a pair of outer wings, an inner doublet and a pair of shoulders mounted on the inner doublet which correspond to the order parameters along the z, x and y (or y and x) axes, respectively.

5.2. *2D powder director distribution*

Figure 10(*c*) shows the deuterium NMR spectrum for a 2D powder director distribution in a uniaxial phase. In this situation the liquid crystal directors are

distributed randomly in a plane containing the magnetic field. This is easily achieved by spinning the sample. The spectrum contains two pairs of doublets with the inner doublet corresponding to the case where the z axis is perpendicular to the magnetic field, that is the x or y axis is parallel to the magnetic field, and the outer doublet corresponds to the situation where the z axis is parallel to the field. As the ordering along the x or y axis is half that along the z axis, the inner doublet has a separation which is equal to half the separation of the outer doublet. The outer doublet has the same intensity as that of the inner doublet since the probability of the z axis being perpendicular to the magnetic field is the same as for it being parallel in this distribution.

For a biaxial phase we know the order parameter is not the same along the x and y axes and as a result the inner doublet of figure 10(c) has an additional pair of shoulders (see figure 10(d)). Here we assume the x and y axes are randomly distributed and so, in two dimensions, have the same probability of being parallel to the field. In a special situation in which not only the director (z axis) but also one of the minor axes, for example the x axis, is confined to a plane containing the magnetic field, the y axis will be perpendicular to the field and the deuterium NMR spectrum of a biaxial phase will consist of only two pairs of doublets representing the different orderings along the x and z axes. The spectrum will thus be very similar to that of a 2D powder distribution for a uniaxial phase except that the separation of the inner doublet will not be half that of the outer doublet as for a uniaxial phase. The phase biaxiality has a direct effect on the appearance of a 2D powder distribution for a biaxial phase. Figure 11 shows the effect of the phase biaxiality on the expected deuterium NMR spectra. (The simulated spectra were taken from [14].) Figure 11(a) shows a planar distribution in which both the z and x axes are in the plane of the magnetic field. The outer doublet corresponds to the ordering along the z axis and the inner doublet corresponds to the ordering along the x axis. As the y axis is orthogonal to the field its quadrupolar splitting is not shown in the spectrum. Figure 11(b) shows the spectrum of the planar director distribution for the case when the z and y axes are contained in the plane of the magnetic field. The outer and inner doublets correspond to the quadrupolar splittings for the z and y axes, respectively.

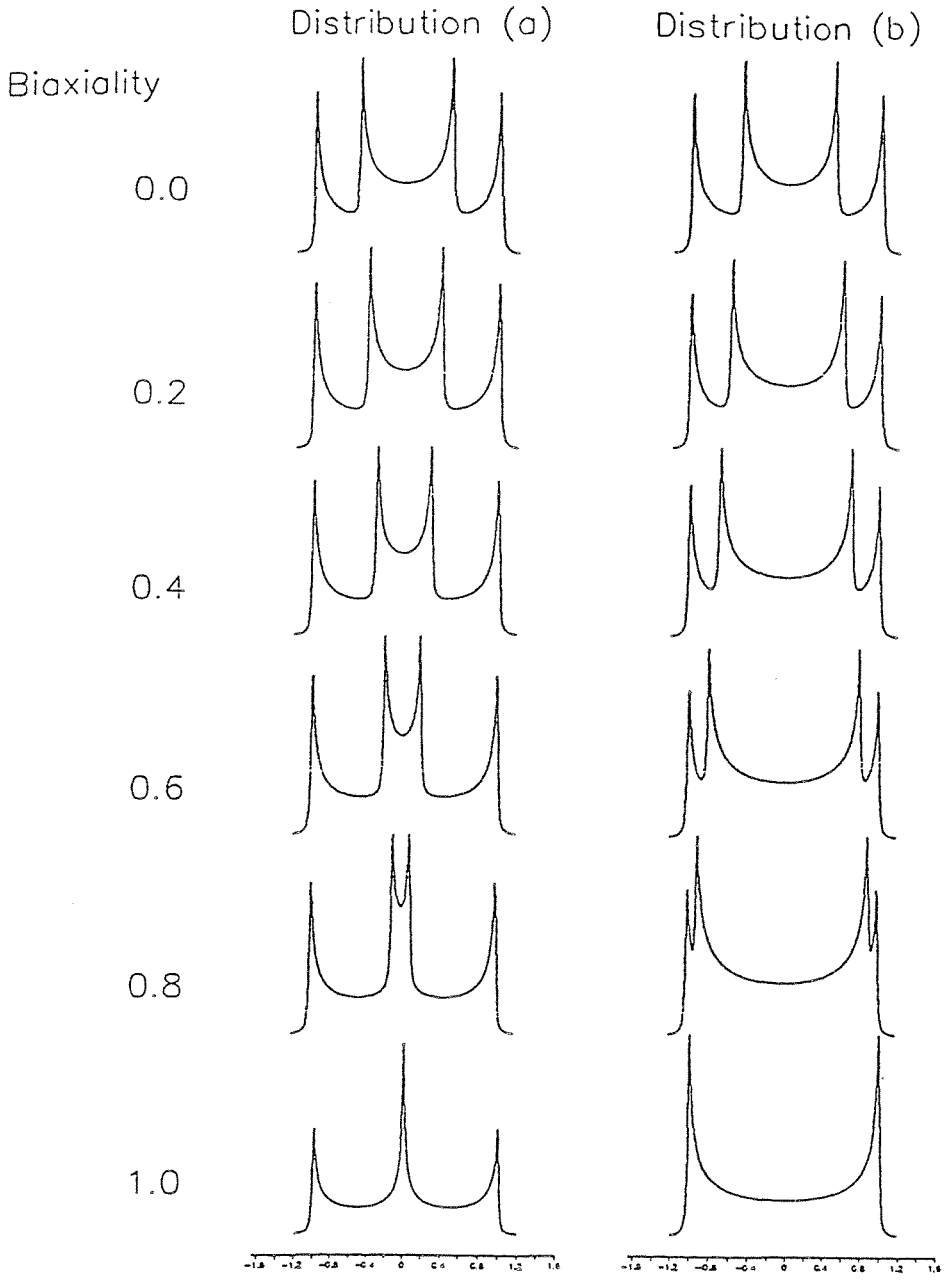

Figure 11. The computer simulated deuterium NMR spectra of two special 2D powder distributions. (*a*) The 2D powder distribution in which both the *z* and *x* axes are confined in the plane containing the magnetic field. (*b*) The 2D powder distribution in which both the *z* and *y* axes are confined in the plane.

In this case the quadrupolar splitting along the x axis is not presented. We see from figure 11 that as the phase biaxiality increases, the inner doublet moves together for the director distribution in figure 11(a) and apart for the distribution in figure 11(b) which corresponds to a decrease in the quadrupolar splitting for the x axis and an increase in the quadrupolar splitting for the y axis, respectively. When the maximum phase biaxiality of 1.0 is reached the quadrupolar splitting for the y axis has the same value as that for the z axis and the quadrupolar splitting for the x axis must vanish since the quadrupolar tensor ordering matrix is traceless, that is if

$$q_{xx} + q_{yy} + q_{zz} = 0 \tag{7}$$

then at maximum phase biaxiality

$$q_{yy} = -q_{zz} \tag{8}$$

and so it follows that

$$q_{xx} = 0. \tag{9}$$

5.3. $z \perp B$

Figure 10(e) shows the deuterium NMR spectrum for a monodomain, uniaxial phase when the z axis is orthogonal to the magnetic field. The spectrum contains a doublet and this can be understood as follows. When the z axis is orthogonal to the field its quadrupolar splitting is not revealed in the spectrum, instead the x and y axes now lie parallel to the field. Since for a uniaxial phase the quadrupolar splitting for the x and y axes is the same the spectrum contains a doublet. As the quadrupolar splittings for the x and y axes are half that for the z axis the peak separation is half of that when the z axis is parallel to the field.

The simulated deuterium NMR spectrum for $z \perp B$ for a biaxial phase is shown in

figure 10(*f*). As the order parameter along the *x* and *y* axes is different the spectrum contains two doublets. A measure of the phase biaxiality is indicated by the difference in the peak separation between the two doublets. In this case we assume that the probability of either the *x* or *y* axis being parallel to the magnetic field is the same and as a result the intensities of the two doublets is the same. However, there exists the probability that one axis is preferentially aligned parallel to the magnetic field and then only one doublet appears in the spectrum. In this situation the spectrum resembles that of a uniaxial phase. However, the confusion can be clarified since the separation of the doublet for a biaxial phase is not half the separation when the *z* axis is parallel to the magnetic field.

5.4. $z \parallel B$

In a monodomain liquid crystal phase in which the *z* axis is parallel to the magnetic field the deuterium NMR spectrum for either a uniaxial or a biaxial phase consists of a doublet (see figures 10(*g*) and (*h*), respectively). The two spectra are not distinguishable as the phase symmetry is not detected. However, if the sample is spun about an axis orthogonal to the magnetic field a two dimensional, powder director distribution is obtained which can be used to distinguish between uniaxial and biaxial phases (see section 5.2).

6. Deuterium NMR analysis of the nematic phase of 2,3,4-tri-*n*-hexyloxycinnamic acid

6.1. *Experimental set-up*

The variable temperature deuterium NMR spectra were recorded on a Bruker MSL 200 Fourier transform spectrometer at 30.7MHz with a horizontal solenoid probe. Approximately 200mg of sample was used in a 5mm o/d NMR tube. Each spectrum was obtained by averaging approximately 5000 transients. The 2D powder deuterium

NMR spectra were measured on a Bruker MSL 300 spectrometer operating at 46.1MHz using a home-made probe fitted with a device to spin the sample about an axis orthogonal to the magnetic field [15]. The sample was rotated using a permanent magnet DC motor and a mechanical drive; the spinning rates were measured with photodiode sensors connected to a Hameg frequency counter. The spinning speed did not vary by more than ±0.1Hz. The spectra were measured using a quadrupolar echo sequence $(\pi/2)_x$-τ-$(\pi/2)_{\pm y}$-τ acquired at the top of the echo. The dwell time was 2μs, the $\pi/2$ pulse length was 3.5μs and the pulse spacing was 50μs. For the static sample 1000 transients were averaged to obtain the spectra while for the spinning sample 5000 transients had to be recorded to achieve comparable signal-to-noise ratios. The temperature was controlled using a Bruker VT unit and was constant to within ±0.2°C; the temperature gradient across the sample was less than 1°C.

6.2. *Results and discussion*

Figure 12 shows the temperature dependence of the quadrupolar splitting for the ethylenic deuteron (see figure 3) in 2,3,4-tri-*n*-hexyloxycinnamic acid-d_1 (the data are listed in table B1 in Appendix B). The quadrupolar splitting is large at T_{NI} in comparison to the 5OCB-d_2 system (≈4kHZ at T_{NI} for a deuteron *ortho* to the pentyloxy chain); these splittings might be expected to be comparable because they make an angle of 60° with the *para*-axis. Given this unusual result it was decided to synthesise the monosubstituted analogue in order to see if its quadrupolar splitting was also anamolously large. The values of this splitting for 4-*n*-hexyloxycinnamic acid-d_1 are also shown as a function of temperature in figure 12 and are consistently larger than those of its trisubstituted analogue (the data are listed in table B2 in Appendix B). Thus the anamolous behaviour of the quadrupolar splitting for the ethylenic deuteron seems not to result from the presence of three hexyloxy chains. In an attempt to understand the large splittings found for the ethylenic deuterons in both mesogens we have to recall that the splitting depends not only on the overall order of the molecule but also on the orientation of the C-D bond within the molecule. Thus for a cylindrically symmetric molecule (either rod-like or disc-like)

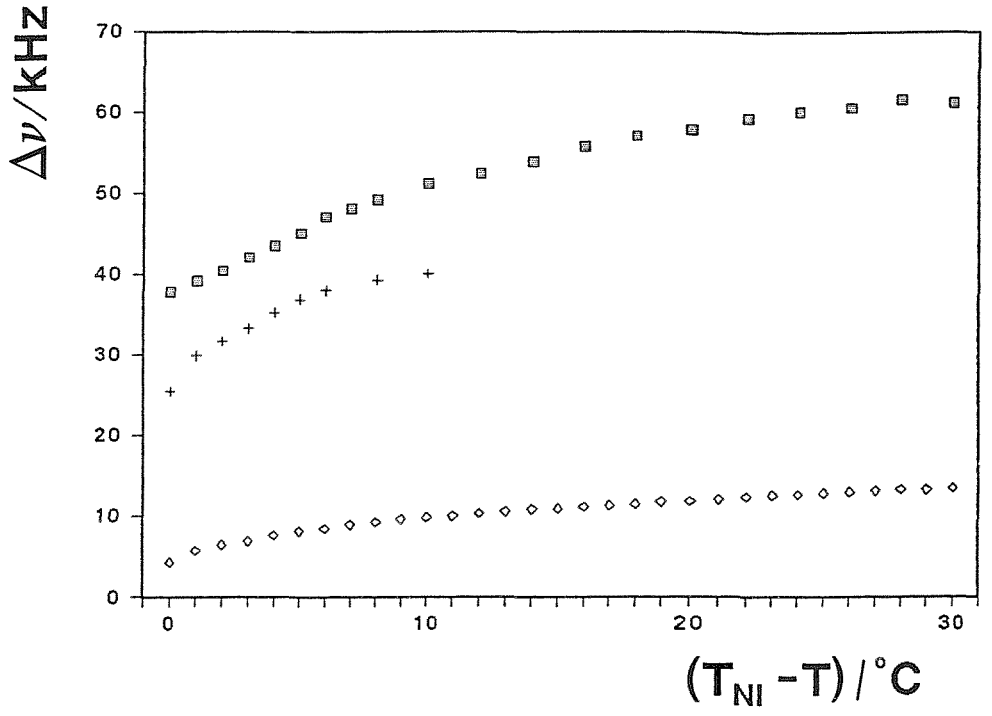

Figure 12. The temperature dependence of the quadrupolar splitting for the 4-*n*-hexyloxycinnamicacid-d_1(■), 2,3,4-tri-*n*-hexyloxycinnamicacid-d_1(+) and 4-pentyloxy-4'-cyanobiphenyl-d_2 (◇) systems.

the quadrupolar splitting is a maximum when the C-D bond axis is parallel to the symmetry axis, decreases to zero as the angle between these two axes increases and then increases to one half the original value when the axes are orthogonal. The situation is more complex when the molecule deviates from cylindrical symmetry for now the order parameters associated with the three principal axes must be known together with the angles made by the C-D bond with these. The calculation of such

quantities is a non-trivial task especially as the shape of the molecules of interest here can change with the conformations adopted by the hexyloxy chains. To overcome this we assume that the chains adopt their lowest energy configuration and we then locate the orientation of the principal axes by evaluating the so-called surface tensor for this molecular conformation [16]. A knowledge of this second rank tensor when combined with the molecular field approximatiom can yield the principal components of the ordering matrix of the nematic to isotropic transition. In principle the surface tensor approach assumes that molecules tend to organise themselves so that they have as much of their surfaces in common. A consequence of this is that for calamitics the molecules are arranged so that the maximum surface is parallel to the director whereas for discotics it is perpendicular.

The first step in the evaluation of the surface tensor is the determination of the molecular structure; since these are not available from X-ray crystallographic studies we have calculated them using the CHARMM molecular mechanics program which minimises the internal energy as a function of the nuclear coordinates. Given these the molecular surface is then constructed by adding a van der Waals sphere to each nuclear site. The surface tensor is then transformed to its principal axis system by diagonalising its cartesian form. This then gives the angles made by the C-D bond with the principal axes. The next step is to evaluate from the surface tensor together with the molecular field approximation the principal components of the Saupe ordering matrix. These can then be used to calculate the order parameter for the C-D bond. We now consider the results of this approach for the two cinnamic acids of primary interest here.

We begin with the monosubstituted acid whose structure is shown in figure 13 together with the superimposed van der Waals spheres. The two views of the molecule clearly show that it has a rod-like shape with a relatively large biaxiality. This is confirmed by the surface tensor whose components are given in table 3; thus the largest component is positive confirming the rod-like character while the biaxiality is 0.31 which is not significantly larger than for typical calamitics. The orientation of

the C-D bond in the principal axis system is also given in table 3 and we see that the C-D bond makes an angle of essentially 90° to the major principal axis. The major order parameter S_{zz}^{NI} at the transition is predicted to be about 0.2 which results from the relatively large biaxiality of the surface tensor and is also revealed by the biaxiality of the ordering matrix. Combination of the ordering matrix and the angle made by the major principal axis then gives the order parameter for the C-D bond as 0.04. We now consider the trisubstituted case which is shown in figure 14 with the superimposed van der Waals spheres. The two views of the molecule show that it has a disc-like shape. Indeed the largest value of the surface tensor, whose components are listed in table 3, is negative indicating the disc-like nature of this compound while the biaxiality is 0.21. The orientation of the C-D bond in the principal axis system is also shown in table 3 and we see that it makes an angle of approximately 60° with respect to the major principal axis. The major order parameter S_{zz}^{NI} at the transition is predicted to be about 0.3 which is a result of the relatively smaller biaxiality of the surface tensor for this compound. A combination of the ordering matrix and the angle made by the C-D bond and the major pricipal axis gives the order parameter of the C-D bond as 0.02. If we assume that both compounds have a positive diamagnetic susceptibility the quadrupolar splitting at T_{NI} is predicted to be 11kHz and 6kHZ for the mono- and trisubstituted compounds, respectively. In summary the model has predicted the correct order of magnitude for the quadrupolar splitting at T_{NI} for both compounds and further their relative magnitude is also correct. The magnitude of the quadrupolar splitting at T_{NI} is also predicted to be larger than that of 5OCB. However, whether the model would predict a similar order parameter to that of 5OCB-d_2 for the C-D bond *ortho* to the hexyloxy chain in the 4-position for either cinnamic acid derivative is as yet unknown.

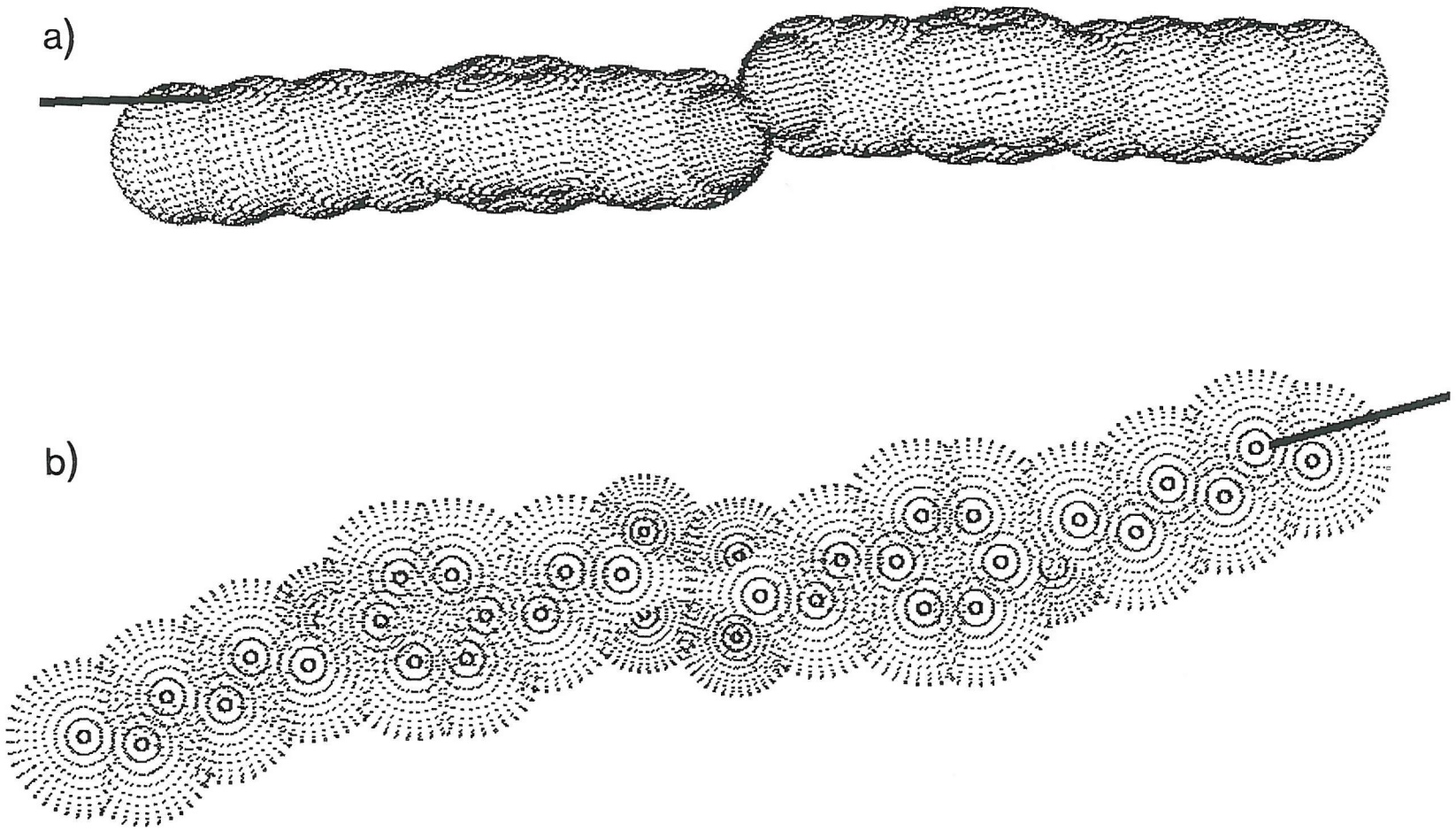

Figure 13. The structure of 4-*n*-hexyloxycinnamic acid together with the superimposed van der Waals spheres. The black line represents the position of the major principal axis. (*a*) Side-on, (*b*) face-on.

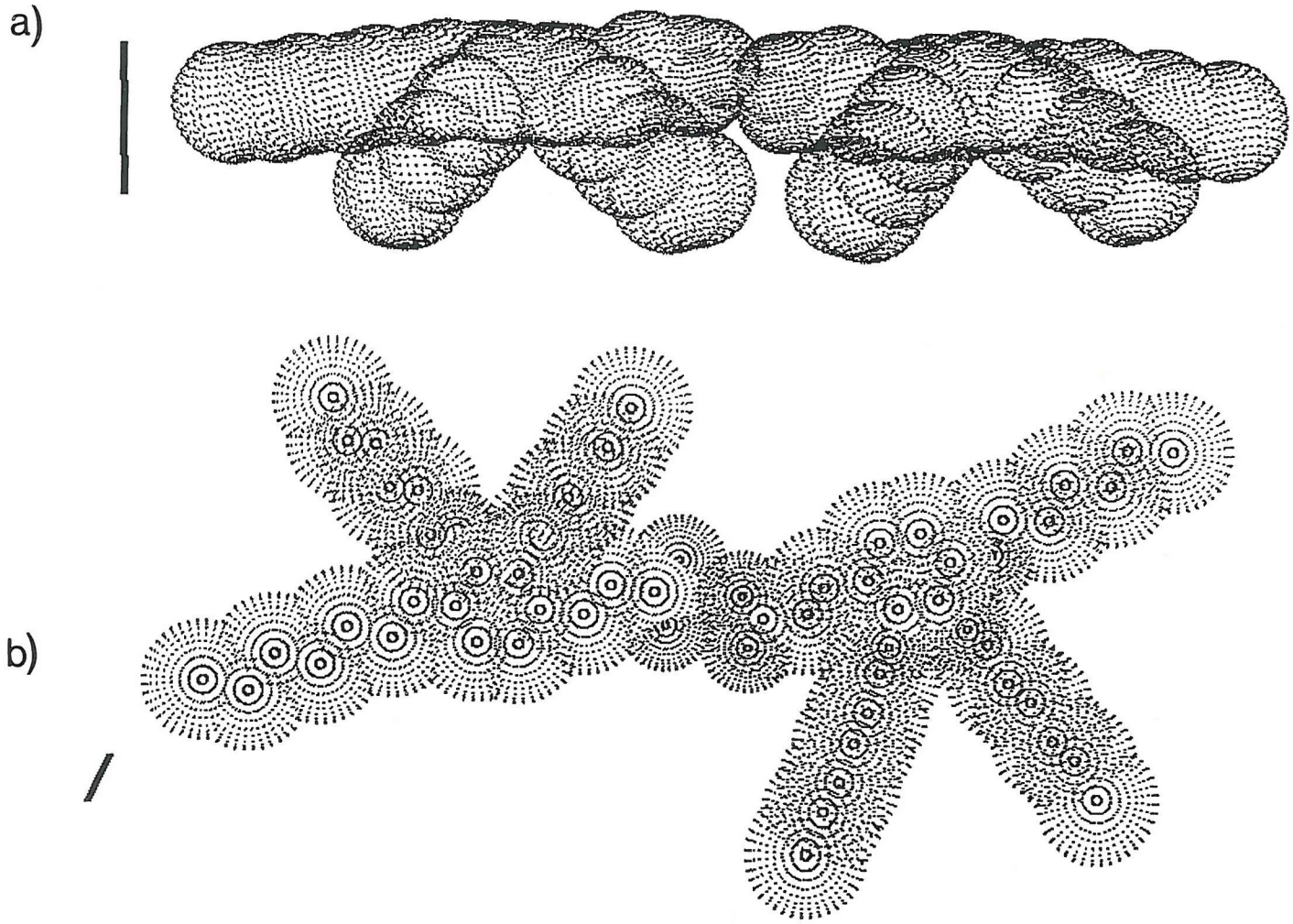

Figure 14. The molecular structure of 2,3,4-tri-*n*-hexyloxycinnamic acid together with the superimposed van der Waals spheres. The black line represents the position of the major principal axis. (*a*) Side-on, (*b*) face-on.

Table 3. The surface tensor in the principal axis system, T_{xx}, T_{yy}, T_{zz}, the symmetry axis order parameter, S_{zz}^{NI}, the biaxiality order parameter, $(S_{xx}^{NI}-S_{yy}^{NI})$, the direction cosines, l_x, l_y, l_z, and the order parameter for the C-D bond at T_{NI} for 4-*n*-hexyloxycinnamic acid and 2,3,4-tri-*n*-hexyloxycinnamic acid.

T_{xx}	T_{yy}	T_{zz}	S_{zz}^{NI}	$(S_{xx}^{NI}-S_{yy}^{NI})$	l_x	l_y	l_z	S_{CD}^{NI}
4-*n*-Hexyloxycinnamic acid								
-15.2	-106.3	121.5	0.2	0.1	0.99	0.05	0.15	0.04
2,3,4-Tri-*n*-hexyloxycinnamic acid								
98.0	30.8	-128.9	0.3	0.1	0.18	0.84	0.52	0.02

We now turn to the discussion of the 2D powder deuterium NMR spectra of 2,3,4-tri-*n*-hexyloxycinnamic acid-d_1. The sample was studied at three temperatures, one at a shifted temperature (T_{NI}-T) of 3°C; one at a shifted temperature of 6°C and one in a supercooled sample at a (T_{NI}-T) of 9°C. The behaviour of the sample at these three temperatures was qualitatively the same and so we shall confine our analysis to the sample at the middle shifted temperature of 6°C. The deuterium NMR spectrum for the static sample consists of just a doublet and is shown in figure 15(*a*). At this temperature the splitting of 37.5kHz is large; indeed at the nematic to isotropic transition temperature the splitting is 24.0kHz which indicates the strength of the first order nature of the transition (typically this is 6-12kHz). The linewidth is large, typically 4kHz, which is consistent with the high viscosity of the nematic phase. A 2D director distribution was achieved by spinning the sample at 2.3Hz and the resultant spectrum is shown in figure 15(*b*); increasing the spinning speed did not alter the appearance of the spectrum. The observation that a 2D powder pattern is

produced by sample spinning indicates that the major axis is alligned parallel to the magnetic field in the static sample which implies that the anisotropic diamagnetic susceptibility is positive in contrast to that reported in [10].

The 2D powder pattern in figure 15(*b*) consists of two quadrupolar doublets; the spacing between the outer doublet corresponds to that observed for the static sample. The outer splitting comes from the main director lying parallel to the magnetic field; the spacing between the inner pair comes from the situation when the main director is orthogonal to the field, that is when one of the minor directors is parallel to the field. The ratio of the inner to the outer spacing is approximately 1:2 which is what is expected for a uniaxial phase. In order to confirm the symmetry of the nematic phase of 2,3,4-tri-*n*-hexyloxycinnamic acid the powder pattern shown in figure 15(*b*) has been simulated with the assumption that the quadrupolar tensor q has cylindrical symmetry. In this case the quadrupolar splitting depends only on the angle β between the magnetic field and the director according to

$$\Delta\tilde{\nu}(\beta) = (3/2)\,\tilde{q}_{zz}\,P_2\,(\cos\beta), \tag{10}$$

where the label *zz* indicates the component parallel to the director and $P_2\,(\cos\beta)$ is the second Legendre function. The positions of the lines in the spectrum corresponding to the director at a particular angle to the field are then

$$\tilde{\nu}(\beta) = \nu_0 \pm (3/4)\tilde{q}_{zz}\,P_2\,(\cos\beta), \tag{11}$$

where the central frequency ν_0 is independent of β because of the negligible anisotropy in the chemical shift compared with the quadrupolar splitting. The 2D powder pattern is a sum of spectra from all director orientations in the plane orthogonal to the spinning axis, namely

$$L(\nu)=1/\pi\int_0^{\pi} T_2/\{1+4\pi^2T_2^2[\nu-\tilde{\nu}(\beta)]^2\}d\beta. \tag{12}$$

Here T_2 is the deuterium spin-spin relaxation time for the sample. In the spectral

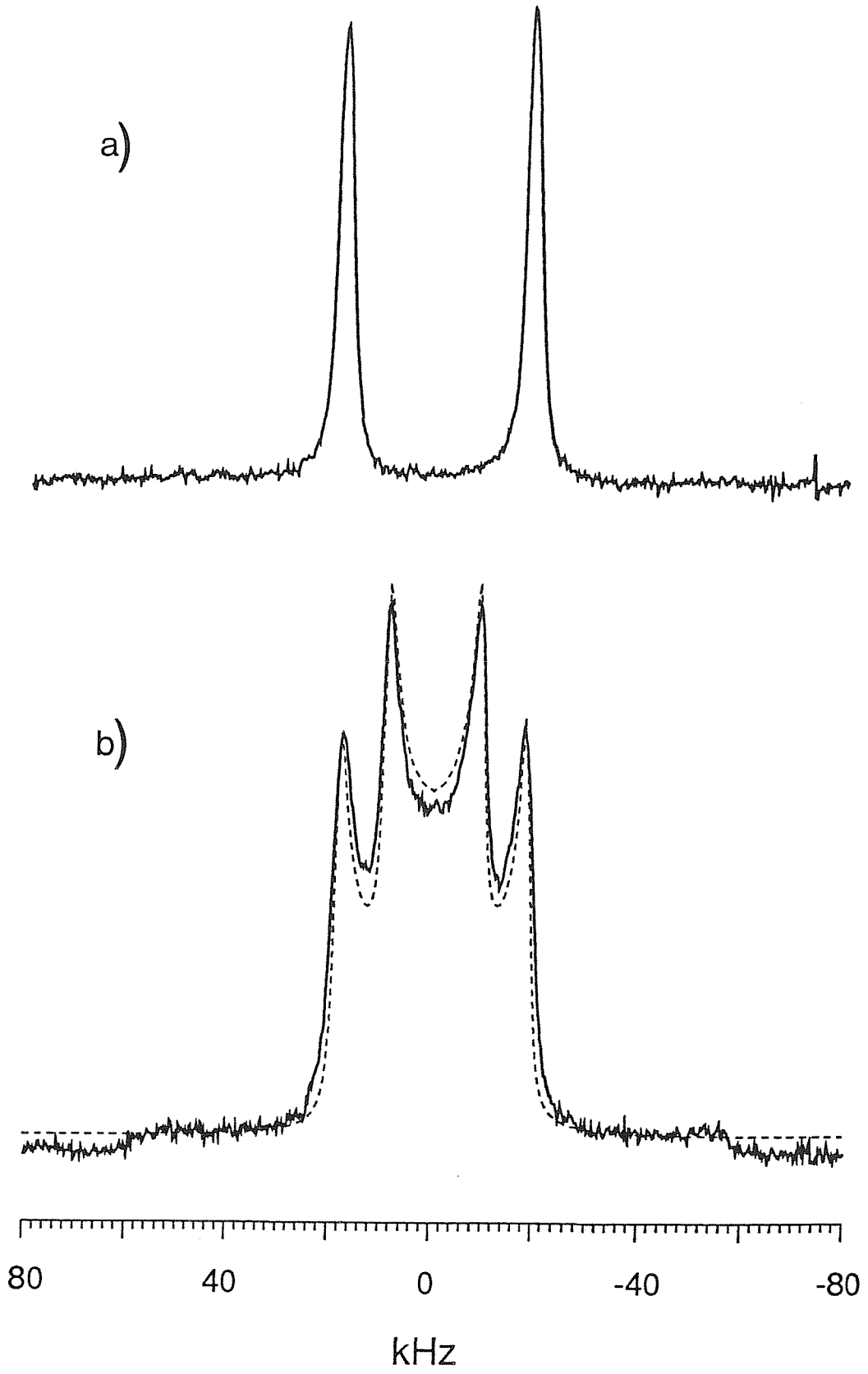

Figure 15. The deuterium NMR spectra of 2,3,4-tri-*n*-hexyloxycinnamic acid-d_1 at a shifted temperature (T_{NI}-T) of 6°C. (*a*) Static and (*b*) spinning. The two dimensional powder pattern calculated for a uniaxial phase ($\tilde{\eta}$=0) is shown as the dashed line.

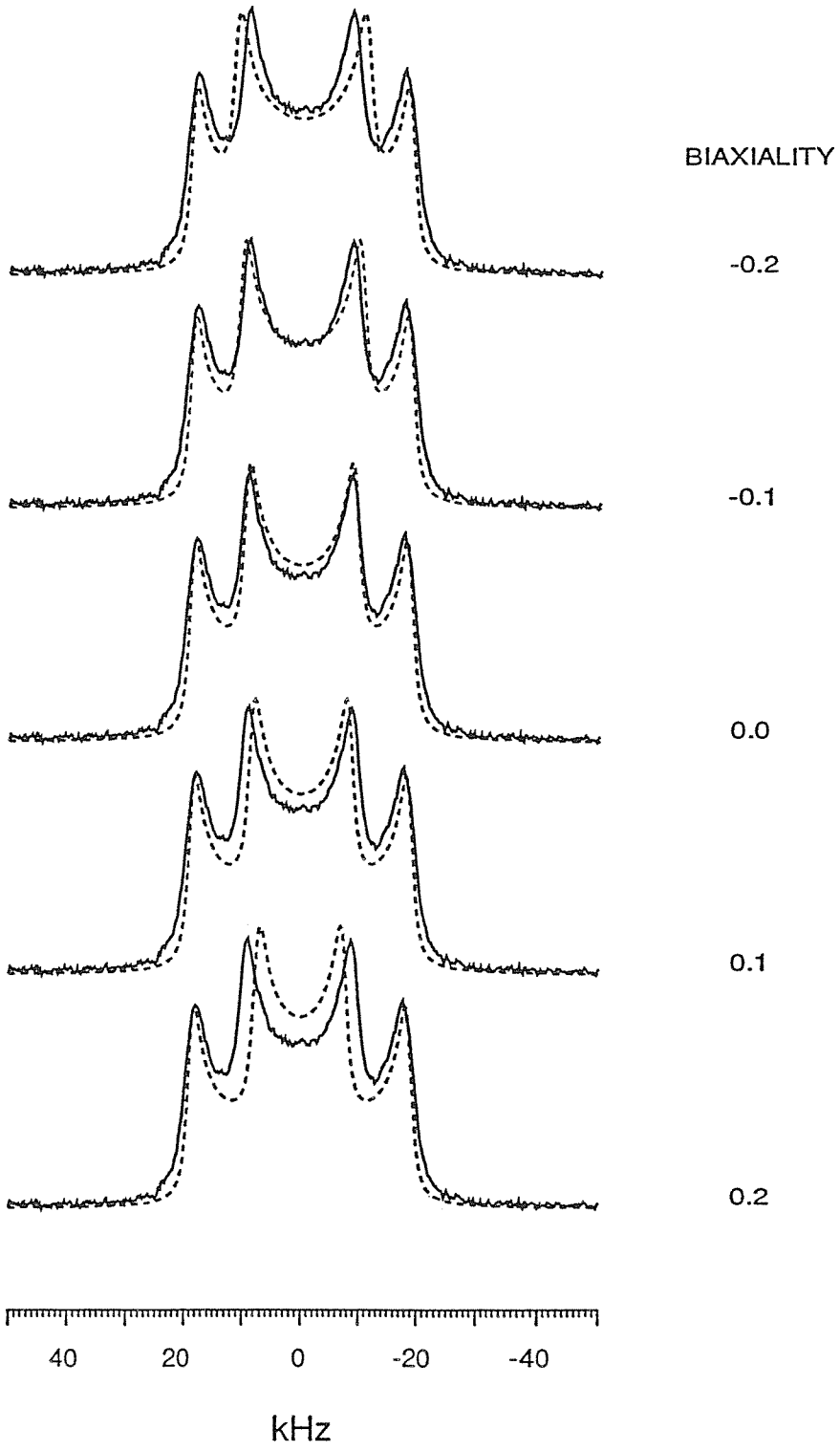

Figure 16. The two dimensional powder patterns simulated from equations (12) and (13) for differing values of the quadrupolar biaxiality parameter $\tilde{\eta}$ (these are shown as the dashed lines). Superimposed on each of the simulated spectra is the experimental spectrum.

simulations $\tilde{q}_{zz}$ and the lineshape parameters were obtained by fitting the spectrum of the spinning sample; they were q_{zz} = 25.0kHz, T_2 = 200μs and $\Delta\nu_0$ = 0.95kHz. The 2D powder pattern calculated with these parameters is shown as the dashed line in figure 15(*b*). The agreement between the two spectra is good and further confirms the assumption that the symmetry of the phase is uniaxial.

To gain an indication of the upper limit of the phase biaxiality $\tilde{\eta}$ ($\tilde{\eta}=(\tilde{q}_{xx}-\tilde{q}_{yy})/\tilde{q}_{zz}$) which would be consistent with the observed spectrum 2D powder patterns for different values of $\tilde{\eta}$ have been simulated. It is assumed that one of the minor axes (for example *y*) of the partially averaged quadrupolar tensor is parallel to the spinning axis and hence orthogonal to the field. The angular dependence of the resonance frequencies is given by

$$\tilde{\nu}(\beta) = \nu_0 \pm (3/4)\,\tilde{q}_{zz}\,[P_2(\cos\beta) + 1/2\tilde{\eta}\,\sin^2\beta], \qquad (13)$$

when $\tilde{\eta}$ vanishes we recover equation (10) for $\tilde{\nu}(\beta)$. The spectra were calculated with $\tilde{\eta}$ equal to 0, ±0.1, ±0.2 and with all of the other parameters given their original values. The spectra are shown in figure 16 with the experimental spectrum superimposed on each. The simulated spectra show that changes in $\tilde{\eta}$ have no influence on the spacing between the outer pair of lines but they do on the inner pair. Increasing $\tilde{\eta}$ causes the inner spacing to decrease so that the ratio of the outer to the inner splitting deviates from the value of 2 for a uniaxial phase. When $\tilde{\eta}$ takes its maximum value of 1.0 the inner pair of lines collapses to a single line. For negative values of $\tilde{\eta}$ the splitting between the inner pair of lines increases until $\tilde{\eta}$ takes its minimum value when the splitting between the outer and inner pair of lines is the same and a single doublet results. If we compare the simulated spectra with the experimental spectrum we see that when $\tilde{\eta}=\pm0.2$ there is a clear disagreement with experiment. The disagreement is obvious when $\tilde{\eta}=0.1$ but not so apparent when $\tilde{\eta}=-0.1$. The differences become clearer when we compare the simulated spectrum for $\tilde{\eta}=0$ with experiment. These simulations suggest, therefore, that the nematic phase is uniaxial but they do not rule out the possibility that there may exist a small biaxiality parameter less than 0.1.

7. Conclusions

In this chapter we have studied the phase transition temperatures and entropies of the T*n*O.CA series and compared them with their monosubstituted analogues (*n*O.CA). We have seen that both the nematic to isotropic transition temperatures and the associated transitional entropies are significantly lower for the trisubstituted T*n*O.CA series. The nematic phase of T6O.CA has been reported to be biaxial, although it shows a weak, first order entropy change for the clearing transition [10]. This appears to be a contradiction as theory predicts the biaxial nematic to isotropic transition to be second order. A deuterium NMR study of T6O.CA and 6O.CA showed the quadrupolar splitting for the ethylenic deuteron to be large; the splitting for 6O.CA was consistently larger than that of T6O.CA as the temperature was varied. By evaluating the surface tensor for these two compounds we have been able to gain an insight as to why the quadrupolar splittings are so large and why they are larger for 6O.CA than T6O.CA. We have shown that it is possible to probe the symmetry of the nematic phase of a thermotropic liquid crystal using deuterium NMR by spinning the sample orthogonal to the magnetic field. In this way an NMR spectrum of a 2D powder director distribution is achieved allowing us to measure simultaneously the order parameter along one of the minor axes (x or y) and that of the major axis. Using this technique a monodeuteriated sample of T6O.CA indicated that the biaxiality of the nematic phase for this material is less than 0.1. This value is for the upper limit and is very small when compared with those found for lyotroic, biaxial nematic phases where the smallest value of $\tilde{\eta}$ reported is 0.51 and the largest is the maximum value of 1 [17]. These observations for the nematic phase of T6O.CA-d_1 suggest that if the phase is biaxial then the extent of this is very small. Such an observation is not necessarily inconsistent with the conoscopic observations of T6O.CA which indicated a small optical biaxiality [10].

References

[1] Freiser, M.J., 1970, *Phys. Rev. Lett.*, **24**, 1041.

[2] Luckhurst, G.R., and Romano, S., 1980, *Molec. Phys.*, **40**, 129.

[3] Allen, M.P., 1990, *Liq. Crystals*, **8**, 499.

[4] Yu, L.J., and Saupe, A., 1980, *Phys. Rev. Lett.*, **45**, 1000.

[5] Malthête, J., Liebert, L., Levelut, A.-M., and Galerne, Y., 1986, *Compt. Rend. Acad. Sci. Paris II*, **303**, 1073; Malthête, J., Tinh, N.H., and Levelut, A.-M., 1986, *J. chem. Soc., chem. Commun.*, 1548.

[6] Galerne, Y., and Liebert, L., 1985, *Phys. Rev. Lett.*, **55**, 2449.

[7] Praefcke, K., Kohne, B., Gündogan, B., Singer, D., Demus, D., Diele, S., Pelzl, G., and Bakowsky, U., 1991, *Molec. Crystals liq. Crystals*, **198**, 393.

[8] Chandrasekhar, S., Sadashiva, B.K., Ratna, B.R., and Raja, V.N., 1988, *Pramāna - J. Phys.*, **30**, L491; Chandrasekhar, S., Ratna, B.R., Sadashiva, B.K., and Raja, V.N., 1988, *Molec. Crystals liq. Crystals*, **165**, 123.

[9] Praefcke, K., Kohne, B., Singer, D., Demus, D., Pelzl, G., and Diele, S., 1990, *Liq. Crystals*, **7**, 589.

[10] Praefcke, K., Kohne, B., Gündogan, B., Demus, D., Diele, S., and Pelzl, G., 1990, *Molec. Crystals liq. Crystals Lett.*, **7**, 27.

[11] Taylor, L., 1991, Ph.D. Thesis, Southampton University.

[12] Gray, G.W., and Jones, B., 1954, *J. chem. Soc.*, 1467.

[13] Howell, O.T., 1992, Ph.D Thesis, Southampton University.

[14] Fan, S.M., 1992, Ph.D. Thesis, Southampton University.

[15] Heaton, N., Reimer, D., and Kothe, D., 1992, *Chem. Phys. Lett.*, **195**, 448.

[16] Ferrarini, A., Moro, G.J., Nordio, P.L., and Luckhurst, G.R., 1992, *Molec. Phys.*, **77**, 1.

[17] Nicoletta, F.P., Chidichimo, G., Golemme, A., and Picci, N., 1991, *Liq. Crystals*, **10**, 665.

CHAPTER 6

Chemically induced liquid crystalline phases

1. Introduction

Molecules which form thermotropic liquid crystal phases have a high degree of shape anisotropy associated with them. Between the molecules repulsive forces exist at short range such that each molecule occupies an exclusion volume. In addition there are specific attractive forces which are necessary for the formation of smectic phases by rod-like molecules. In consequence liquid crystal molecules tend to be polar or easily polarisable. Intermolecular forces, such as dipole-dipole interactions, can be easily varied by the addition of a dopant which can be used to modify the liquid crystalline properties of a compound. For example the formation of smectic phases in binary mixtures of calamitic compounds is well-known [1]. Thus when nematic, biforked compounds are mixed with derivatives of 4,4'-bis-*n*-alkyloxy-azoxybenzene (also nematic) a smectic A phase is formed which results from the so-called space-filling effect [2] (see figure 1). Furthermore, smectic A phases can also be stabilised by electronic interactions in binary mixtures of 4,4'-diacylbiphenyl derivatives with *N*,*N*'-dialkyl-4,4'-diaminobiphenyl compounds [3]. The molecules form electron donor-acceptor complexes which are further attracted to one another through hydrogen bonds (see figure 2). We must, however, be careful when talking about such effects in the context of mesophase induction. In binary mixtures mesophase induction is the raising of the clearing point above that of the pure components. It should not be confused with eutectic behaviour where a lowering of the melting point can reveal new mesophases. Thus there have been many reports of the occurence of smectic phases in binary mixtures of nematogens but in many instances mesophase induction does not occur.

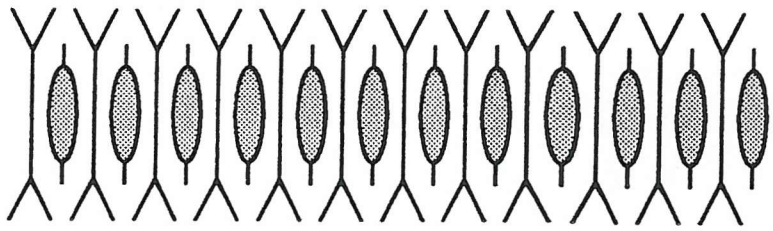

Figure 1. A schematic representation of the space-filling effect which is thought to be responsible for the formation of a smectic A phase when nematic biforked compounds are mixed with derivatives of 4,4'-bis-*n*-alkyloxyazoxybenzene.

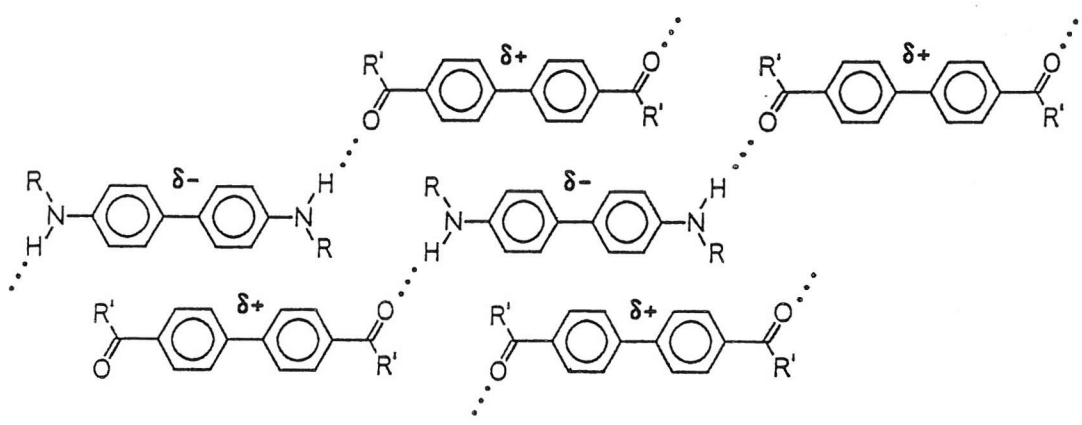

Figure 2. The electron donor-acceptor complexes of 4,4'-diacylbiphenyl derivatives and *N*,*N*'-dialkyl-4,4'-diaminobiphenyl compounds which are thought to be responsible for the formation of the smectic A phase.

In the last few years much interest has focussed on binary mixtures of large, electron-rich, disc-like molecules and electron deficient compounds such as 2,4,7-trinitro-9-fluorenone (TNF) [4-7]. Mixtures of [(1,2,3,5,6-pentakis(phenylethynyl))benzene-4'-oxy]nonane or tridecane with TNF led to the discovery of the columnar nematic phase (N_c) [5] (see figure 3). This phase is stabilised by charge transfer interactions between the two components as indicated by the yellow to deep red colour change that occurs when the two components are mixed together. The phase is formed from columns of alternating electron donor and acceptor molecules. The assignment of this phase as a columnar nematic can only be based on its X-ray diffraction pattern as its schlieren optical texture is typical of that for any nematic phase and its clearing entropy change is not sufficient evidence. Thus at small angle it has a diffuse reflection (16.6Å) which is reported to correspond to the intercolumnar packing and a sharp reflection at wide angle (3.5Å) which corresponds to the intracolumnar separations. Therefore, the columns have long range orientational order but no positional order. It has also been shown that depending on the relative amounts of the donor and acceptor compounds in the binary mixture more ordered phases, such as discotic hexagonal ordered (D_{ho}), can be formed (see figure 4). As a result of the charge transfer interactions the TNF molecules help to assemble the molecules into columns which depending on steric interactions may self-organise into a hexagonal array.

Large, electron-rich, disc-like molecules are interesting not only because of their novel behaviour with electron acceptors, such as TNF, but also because when they are substituted with a long alkyl chain or linked together via an alkyl spacer they have been reported to exhibit a biaxial nematic phase [8,9]. The existence of biaxial nematic phases has been predicted for mixtures of rod-shaped and disc-shaped molecules [10]. Experimentally this prediction has yet to be realised as the two components phase separate [11]. One way of circumventing this problem is to link both the disc-like and rod-like units together via a flexible spacer. To date there are very few reports in the literature which describe the properties of such compounds. One by Kreuder *et al.* [12] reported the compounds shown in figure 5. When the rod was linked laterally to the discs (see figure 5(*a*)) no mesophase was found even after

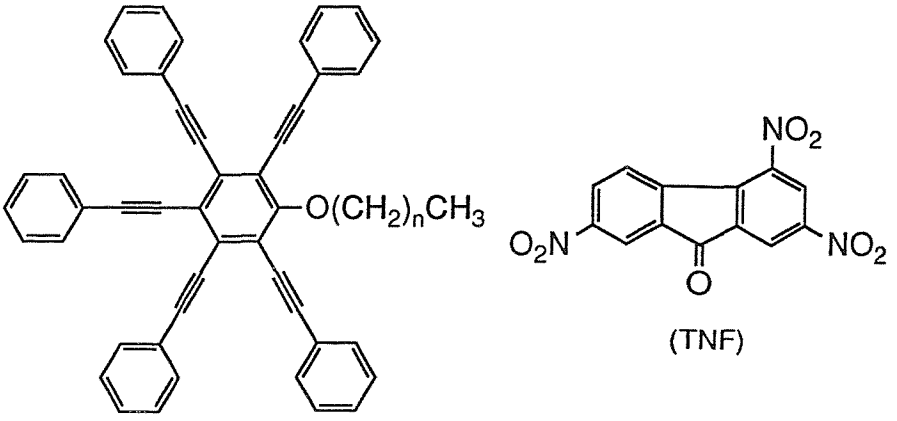

Figure 3. The structures of the [1,2,3,5,6-pentakis(phenylethynyl)benzene-4-oxy]alkanes and 2,4,7-trinitro-9-fluorenone (TNF).

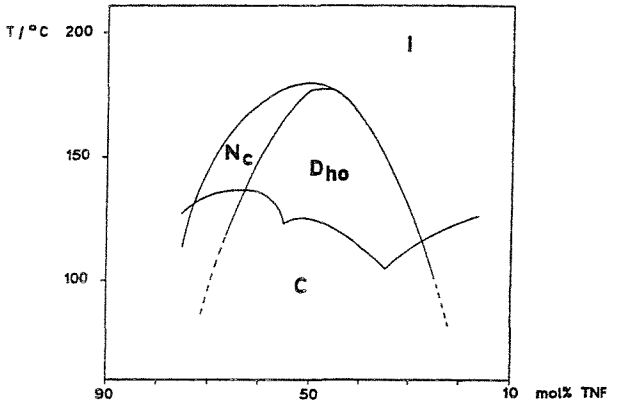

Figure 4. The simplified phase diagram of the binary mixture of [1,2,3,5,6-pentakis(phenylethynyl)benzene-4-oxy]nonane and 2,4,7-trinitro-9-fluorenone.

(*a*)

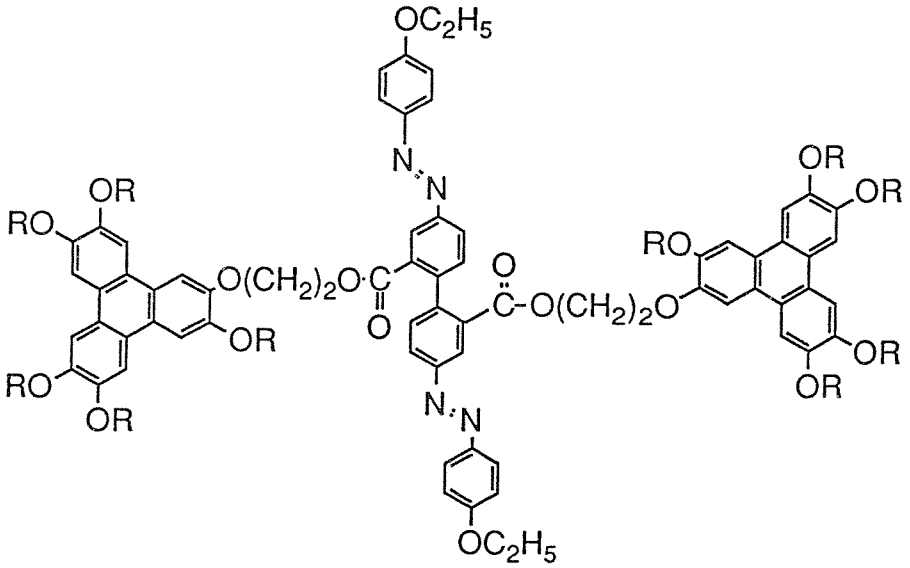

$R = -C_5H_{11}$.

(*b*)

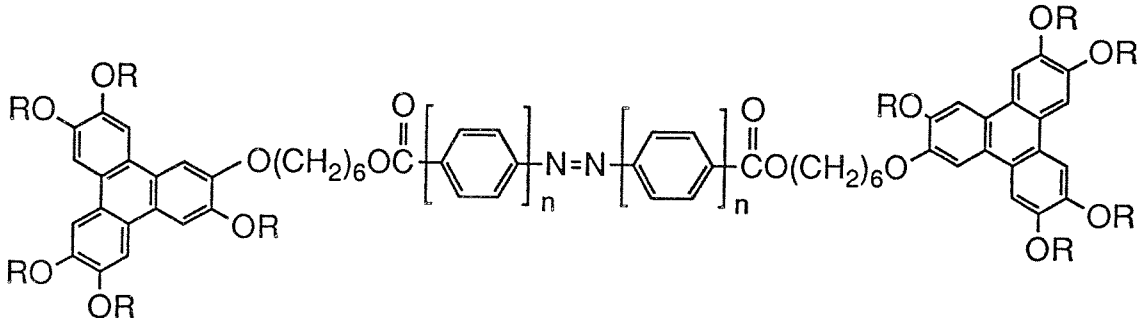

$R = -C_5H_{11}$, $n=2$.

Figure 5. The discotic twin with (*a*) a laterally bound and (*b*) a terminally bound rod-like unit reported by Kreuder *et al.* [12].

extensive supercooling. However, when the rod was terminally linked (see figure 5(*b*)) an exotic mesophase was formed in which the discs were arranged in columns and the rods were arranged in layers.

To explore further the liquid crystalline properties of compounds composed of rod-like and disc-like units linked together via a flexible alkyl spacer we present in this chapter a new series of compound, the α-[(1,2,3,5,6-pentakis(4-pentylphenyl-ethynyl))benzene-4'-oxy]-ω-(4'-cyanobiphenyl-4-yloxy)alkanes. We have also doped these compounds with TNF to examine their charge transfer behaviour and compared the results with the α-[(1,2,3,5,6-pentakis(4-phenylethynyl))benzene-4'-oxy]-ω-(4'-cyanobiphenyl-4-yloxy)alkanes which are not expected to be liquid crystalline. In this way it was possible to compare the effect of the terminal alkyl chains on the phase behaviour of the binary mixtures. Homologues with six to twelve carbon atoms in the flexible alkyl spacer were synthesised as it has been shown that shorter chains do not extend beyond the diameter of the super-disc (see figure 6) [5]. Finally we have also examined the effect of mixing TNF with some symmetric dimeric, discotic compounds, the α,ω-bis[(1,2,3,5,6-pentakis(4-pentylphenylethynyl))benzene-4'-oxy]alkanes and the α,ω-bis[1,2,3,5,6-pentakis(4-phenylethynyl)benzene-4'-oxy]alkanes. It was envisaged that the addition of TNF would help stabilise an extended molecular network by organising the dimers into interlinked columns.

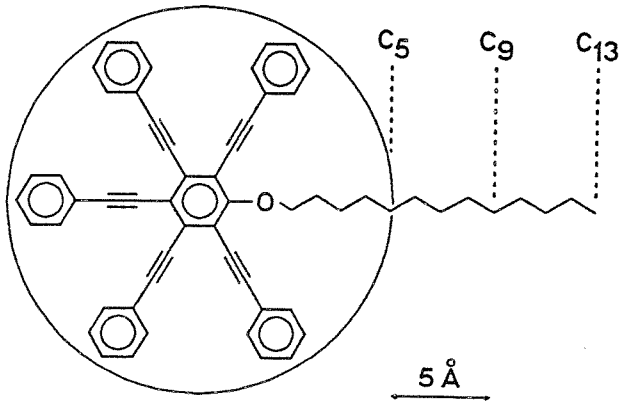

Figure 6. A schematic representation of a disc based on [pentakis(4-phenylethynyl)]benzene and an alkyloxy chain exiting from its centre.

2. Experimental

For simplicity the α-[(1,2,3,5,6-pentakis(4-pentylphenylethynyl))benzene-4'-oxy]-ω-(4'-cyanobiphenyl-4-yloxy)alkanes and the α-[(1,2,3,5,6-pentakis(4-phenylethynyl))benzene-4'-oxy]-ω-(4'-cyanobiphenyl-4-yloxy)alkanes, are abbreviated to 5D.O*n*O.CB and D.O*n*O.CB, respectively, where 5 denotes pentyl, D disc, CB cyanobiphenyl and *n* is the length of the alkyl spacer. Similarly the dimeric compounds, the α,ω-bis[(1,2,3,5,6-pentakis(4-pentylphenylethynyl))benzene-4'-oxy]alkanes and the α,ω-bis[(1,2,3,5,6-pentakis(4-phenylethynyl))benzene-4'-oxy]alkanes, are abbreviated to 5D.O*n*O.5D and D.O*n*O.D, respectively. The synthetic paths for the non-symmetric and symmetric dimers are given in schemes 1 and 2, respectively. Here we outline the synthetic routes and structural characterisation of 5D.O6O.CB, D.O6O.CB and D.O10O.D in detail.

2.1. *Synthesis of 4-pentylacetophenone*

Pentylbenzene (52.16g; 3.45 x 10^{-1}mol) was added dropwise to a stirred mixture of anhydrous aluminium (III) chloride (55.35g; 4.1 x 10^{-1}mol) and acetyl chloride (78.70g; 3.8 x 10^{-1}mol) in carbon tetrachloride (200ml) in a 500ml, three neck, round bottom flask fitted with a Leibig condenser and calcium chloride guard tube in an ice bath. During the addition the temperature of the reaction mixture was kept between 0-5°C to prevent the formation of the *ortho* derivative. The ice bath was removed and the mixture was strirred for an additional hour at room temperature. The mixture was then poured cautiously into a beaker containing concentrated hydrochloric acid (250ml) and ice (500g). A heterogeneous mixture resulted of which only the lower, organic layer was kept. This was washed with 2M hydrochloric acid to remove the aluminium salts, then with sodium carbonate (100ml), distilled water (100ml) and dried overnight with 4Å molecular sieves. The solvent was removed on a rotary evaporator and the residue distilled. The colourless fraction which distilled at 108°C (1mb) was collected. Yield 65.6g (89%).

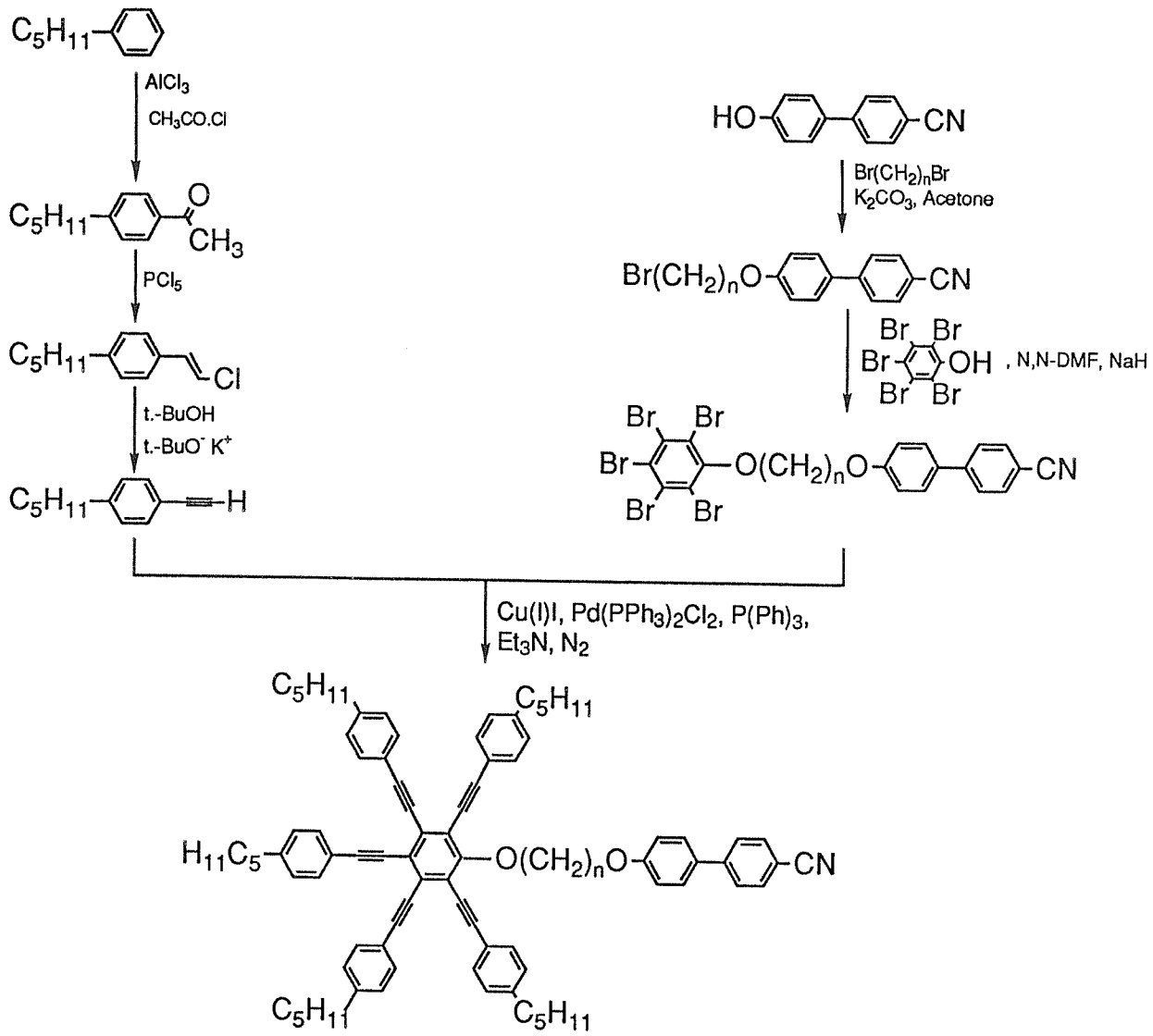

Scheme 1. The synthetic route to the 5D.O*n*O.CB series (the route to the D.O*n*O.CB series is essentially the same).

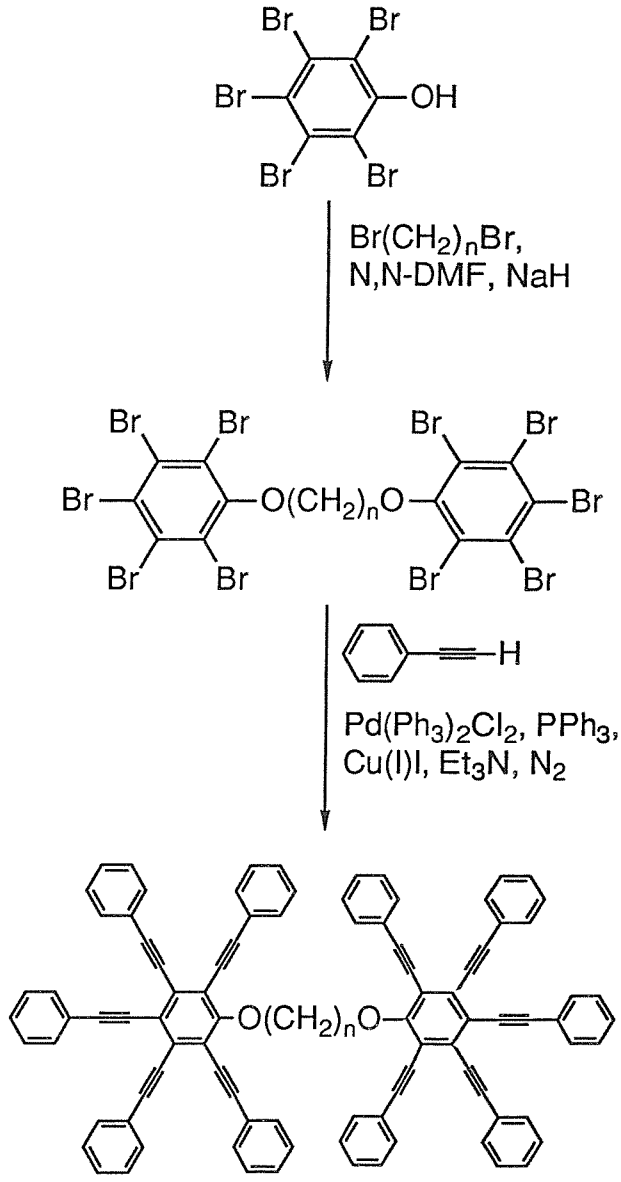

Scheme 2. The synthetic route to the D.O*n*O.D series (the route to the 5D.O*n*O.5D series is essentially the same).

IR (NaCl disc, neat): ν 1682cm^{-1} (C=O).
^{1}H NMR ($CDCl_3$): δ 0.8-1.0 (t, 3H), 1.2-1.8 (m, 6H), 2.5-2.75 (m, 5H), 7.2-7.3 (d, 2H), 7.8-7.9ppm (d, 2H).

2.2. *Synthesis of 1-(4-pentylphenyl)-2-chloroethene*

Phosphorus pentachloride (69.8g; 2.83 x 10^{-1}mol) was placed in a 500ml, two neck, round bottom flask fitted with a calcium chloride guard tube and dropping funnel cooled in an ice/sodium chloride/water bath. 4-Pentylacetophenone (59g; 3.11 x 10^{-1}mol) was added dropwise to this over an hour and then the mixture was stirred for a further 12h at room temperature. Phosphorus oxychloride, a by-product of the reaction, was removed by distillation under water vacuum for two hours at 90°C. The remaining orange-brown liquid was purified by distillation (98°C, 1mb) to give a colourless liquid. Yield 42.3g (65%).

IR (NaCl disc, neat): ν 734.0, 778.7 (C-Cl), 1611.5cm^{-1} (C=C).
^{1}H NMR ($CDCl_3$): δ 0.8-1.0 (t, 3H), 1.1-1.8 (m, 6H), 2.6-2.8 (t,2H), 5.5 (d, 1H), 5.8 (d, 1H), 7.1-7.3 (d, 2H), 7.5-7.7ppm (d, 2H).

2.3. *Synthesis of 4-pentylphenylacetylene*

1-(4-Pentylphenyl)-2-chloroethene (30.2g; 1.5 x 10^{-1}mol) and potassium *tert*-butoxide (59.5g; 0.53mol) were refluxed in *tert*-butanol (650ml) for 36h at 110°C on an oil bath in a litre conical flask fitted with a Leibig condenser. After cooling, the reaction mixture was poured onto an ice/water mixture and extracted with diethyl ether (4 x 100ml). The combined ether extracts were washed with aqueous sodium chloride solution (4 x 100ml) and dried over anhydrous magnesium sulphate. After filtration and evaporation of the solvent the crude product was distilled under vacuum on a Kugelrohr apparatus. The colourless fraction boiling at 110°C (1mb) was collected. Yield 14.8g (57%).

IR (NaCl disc, neat): ν 2108.7 (C≡C), 3296.1cm^{-1} (H-C≡).
^{1}H NMR ($CDCl_3$): δ 0.8-1.0 (t, 3H), 1.1-1.8 (m, 6H), 2.5-2.7 (t, 2H), 3.0 (s, 1H), 7.0-7.2 (d, 2H), 7.3-7.5ppm (d, 2H).

2.4. *Synthesis of α-(1,2,3,5,6-pentabromobenzene-4'-oxy)-ω-(4'-cyanobiphenyl-4-yloxy)hexane*

Sodium hydride (0.29g; 9.6 x 10^{-3}mol) and pentabromophenol (3.87g; 8.0 x 10^{-3}mol) were warmed in 50ml of dry *N,N'*-dimethylformamide (4Å molecular sieves) and then stirred for one hour in a 100ml conical flask fitted with a Leibig condenser. α-Bromo-ω-(4'-cyanobiphenyl-4-yloxy)hexane (4g; 1.12 x 10^{-2}mol), as prepared in chapter 3, was then added and the reaction mixture heated to 80°C with stirring for 26h. After cooling the mixture was added to water and the resulting precipitate was filtered off and dried *in vacuo*. The crude solid was recrystallised twice from acetone to give white crystals. Yield 5.5g (65%); C 150.4°C (N 52.7°C) I. The yields of the remaining homologues were all in excess of 65% and their melting behaviour is shown in table 1.

IR (NaCl disc, film): ν 2224.1cm^{-1} (-C≡N).
^{1}H NMR ($CDCl_3$): δ 1.4-2.0 (m, 8H), 3.8-4.1 (m, 4H), 6.9-7.0 (d, 2H), 7.4-7.5 (d, 2H), 7.6ppm (s, 4H).

Table 1. The phase behaviour of the α-(1,2,3,5,6-pentabromobenzene-4'-oxy)-ω-(4'-cyanobiphenyl-4-yloxy)alkanes.

n	*T*/°C	
	C-I	N-I
6	150	(52)
7	114	
8	122	(52)
9	88	
10	125	
11	102	(33)
12	100	(54)

Parentheses indicate a monotropic transition.

2.5. *Synthesis of α-[(1,2,3,5,6-pentakis(4-pentylphenylethynyl))benzene-4'-oxy]-ω-(4'-cyanobiphenyl-4-yloxy)hexane*

α-(1,2,3,5,6-Pentabromobenzene-4-oxy)-ω-(4'-cyanobiphenyl-4-yloxy)hexane (1.54g; 2.03 x 10^{-3}mol), 4-pentylphenylacetylene (3.5g; 2.0 x 10^{-2}mol), copper (I) iodide (70mg; 3.68 x 10^{-4}mol), triphenylphosphine (120mg; 4.58 x 10^{-4}mol) and bis(triphenylphosphine) palladium (II) chloride (70mg; 9.97 x 10^{-5}mol) were heated in degassed triethylamine (30ml) on an oil bath at 110°C under nitrogen for 15h in a 50ml, three neck, round bottom flask fitted with a Leibig condenser attached to a bubbler and with a nitrogen gas inlet needle. After cooling, the reaction mixture was poured into 5M hydrochloric acid (200ml). This was extracted with dichloromethane (4 x 50ml) and the combined extracts were dried over anhydrous sodium sulphate. Evaporation of the solvent gave a dark brown oil which solidified when washed with petroleum ether. The resultant light brown solid was filtered off and purified by flash chromatography (silica gel 60) using chloroform/petroleum ether (3:2) as eluent. Two recrystallizations from acetone furnished yellow crystals. In organic solvents, such as chloroform, the crystals showed blue flourescence. Yield 0.9g (36%). The yields of all homologues were between 30-40%.

IR (NaCl disc, film): ν 2202.2 (-C≡C-), 2226.7cm^{-1} (-C≡N).

^{1}H NMR ($CDCl_3$): δ 0.8-1.1 (t, 15H), 1.2-2.1 (m, 38H), 2.5-2.8 (m, 10H), 3.8-4.0 (t, 2H), 4.4-4.5 (t, 2H), 6.8-7.0 (d, 2H), 7.1-7.3 (m, 10H), 7.4-7.7ppm (m, 16H).

MS (Argon FAB): 154, 1222 (M^+).

Elemental analysis: calculated C 88.45%, H 7.78%, N 1.15%; found C 87.92%, H 7.81%, N 1.16%. The elemental analyses of two other homologues in this series are listed in table 2.

Table 2. The analytical data for some members of the 5D.O*n*O.CB, D.O*n*O.CB and D.O*n*O.D series. Calculated values are in parentheses.

Compound	Analytical data		
	C	H	N
5D.O6O.CB	87.92% (88.45%)	7.81% (7.78%)	1.16% (1.15%)
5D.O9O.CB	88.05% (88.36%)	8.04% (8.00%)	1.09% (1.11%)
5D.O10O.CB	87.93% (88.33%0	8.11% (8.07%)	1.08% (1.10%)
D.O6O.CB	89.02% (89.55%)	5.21% (5.17%)	1.63% (1.61%)
D.O7O.CB	89.07% (89.49%)	5.29% (5.21%)	1.56% (1.58%)
D.O11O.CB	88.91% (89.23%)	5.91% (5.85%)	1.47% (1.49%)
D.O9O.D	91.86% (92.38%)	5.20% (5.18%)	
D.O10O.D	91.87% (92.13%)	5.26% (5.28%)	

2.6. *Synthesis of α-[(1,2,3,5,6-pentakis(4-phenylethynyl))benzene-4'-oxy]-ω-(4'-cyanobiphenyl-4-yloxy)hexane*

The experimental procedure for the synthesis of this compound is the same as that given in section 2.5. The quantities used in the synthesis were: α-(1,2,3,5,6-

pentabromobenzene-4'-oxy)-ω-(4'-cyanobiphenyl-4-yloxy)hexane(1g; 1.15 x 10^{-3}mol), phenylacetylene (1.2g; 1.15 x 10^{-2}mol), bis(triphenylphosphine)palladium (II) chloride (70mg; 9.97 x 10^{-5}mol), copper (I) iodide (70mg; 3.68 x 10^{-4}mol), triphenylphosphine (120mg; 4.58 x 10^{-4}mol) and triethylamine (30ml). Yield 0.52g (52%). The yields of the other homologues were between 30-40%.

IR (NaCl disc, film): ν 2204.3 (-C≡C-), 2222.6cm^{-1} (-C≡N).
^{1}H NMR ($CDCl_3$): δ 1.2-2.0 (m, 8H), 3.9-4.1 (t, 2H), 4.3-4.5 (t, 2H), 6.9-7.0 (d, 2H), 7.3-7.8ppm (m, 31H).
MS (Argon FAB): 565, 871 (M^+).
Elemental analysis: calculated C 89.55%, H 5.17%, N 1.61%; found C 89.02%, H 5.21%, N 1.63%. The elemental analyses of two other homologues in this series are listed in table 2.

2.7. *Synthesis of α,ω-bis(1,2,3,5,6-pentabromobenzene-4'-oxy)decane*

The experimental procedure for the synthesis of this compound is the same as that in section 2.4. The quantities used in the synthesis were: pentabromophenol (5.13g; 1.06 x 10^{-2}mol), 1,10-dibromodecane (1.5g; 5.04 x 10^{-3}mol), sodium hydride (0.28g; 1.2 x 10^{-2}mol), and 50ml of dry *N,N'*-dimethylformamide (4Å molecular sieves). Yield 3.6g (64%); mp 147.4°C.

IR (NaCl disc, film): ν 1636.0cm^{-1} (Ar. -C=C-).
^{1}H NMR ($CDCl_3$): δ 1.2-2.0 (m, 16H), 3.9-4.1ppm (t, 4H).

2.8. *Synthesis of α,ω-bis[(1,2,3,5,6-pentakis(4-phenylethynyl))benzene-4'-oxy]decane*

The experimental procedure for the synthesis of this compound is the same as that in section 2.5. The quantities used in the synthesis were: α,ω-bis(1,2,3,5,6-pentabromobenzene-4'-oxy)decane (1g; 9.04 x 10^{-4}mol), phenylacetylene (1.84g; 1.81

x 10^{-2}mol), bis(triphenylphosphine) palladium (II) chloride (140mg; 1.99 x 10^{-4}mol), copper (I) iodide (140mg; 7.36 x 10^{-4}mol), triphenylphosphine (240mg; 9.16 x 10^{-4}mol) and triethylamine (30ml). Yield 0.64g (53%).

IR (NaCl disc, film): ν 2206.7cm^{-1} (-C≡C-).
^{1}H NMR ($CDCl_3$): δ 1.1-2.0 (m, 16H), 4.2-4.4 (t, 4H), 7.1-7.7ppm (m, 50H).
MS (Argon FAB): 565, 1327 (M^+).
Elemental analysis: calculated C 92.13%, H 5.28%; found C 91.87%, H 5.26%. The elemental analysis of the n=9 homologue is given in table 2.

2.9. *Synthesis of α,ω-bis[(1,2,3,5,6-pentakis(4-pentylphenylethynyl))benzene-4'-oxy]decane*

The experimental procedure for the synthesis of this compound can be found in [8].

2.10. *Analysis of the phase behaviour of mixtures by contact preparations*

Contact preparations were achieved by first melting the compound with the highest melting point and covering with a cover slip. Then the lower melting compound was placed on the side of the cover slip and melted. Through capillary forces the compound flows under the cover slip and makes contact with the other component. This is clearly seen by the formation of an orange-red band. Across this band exists a concentration gradient making it possible to observe the phase behaviour of different binary compositions with temperature.

2.11. *Preparation of the charge transfer complexes*

The charge transfer complexes were prepared by weighing out calculated, mole percentage amounts of the super-disc derivatives and dry 2,4,7-trinitro-9-flourenone

(anhydrous Na_2SO_4). The two components were mixed by dissolving them in dichloromethane. The formation of the charge transfer complex was indicated by a deep, red-orange colour change. The dichloromethane was first allowed to evaporate by leaving the solution to stand overnight and then finally by placing the samples in a vacuum oven (25°C, 1mb), after which an orange-red solid resulted.

3. Results and discussion

3.1. *The 5D.OnO.CB series*

Table 3 summarises the transitional behaviour of seven members of the 5D.O*n*O.CB series. From the table we see that except for one compound there is no liquid crystalline behaviour exhibited by this series. The $n=6$ homologue, from observation of isolated, isotropic droplets, shows a nematic phase approximately 45°C below the melting point. This overall result is disappointing as results in [9] show that a simple nonyloxy chain protruding from the super-disc core supports liquid crystallinity and yet the strongly mesogenic cyanobiphenyl group destroys it. In these compounds the spacer may cause the organisation of the rod and disc units to be incompatible with that required for the nematic phase. It appears that T_{NI} is lowered as the melting point for 5D.O6O.CB is approximately the same as that for the super-disc compound attached to a nonyloxy chain in [9].

Table 3 also lists the transitional behaviour for binary mixtures of the 5D.O*n*O.CB series and TNF. The 50:50mol% composition was chosen because contact preparations showed the existence of only a nematic phase at all temperatures and compositions. Moreover polarising microscopy observations showed the thermal stability of the nematic phase to be peaked around the 50:50mol% composition point. All seven members gave a very monotropic, viscous nematic phase. The phase had a sanded texture and flashed when subjected to mechanical stress (see plate 1). Figure 7 shows the effect of the length of the alkyl spacer, n, on the transition temperatures for these binary mixtures. We see that there is no odd-even effect and

Table 3. The transition temperatures, enthalpies and entropies of the 5D.O*n*O.CB series and the 5D.O*n*O.CB and TNF 50:50mol% binary mixtures.

n	5SD.O*n*O.CB			5SD.O*n*O.CB + TNF (50:50mol%)					
	T_{CI}/°C	ΔH_{CI}/kJmol^{-1}	ΔS_{CI}/R	T_{CI}/°C	T_{NI}/°C	ΔH_{CI}/kJmol^{-1}	ΔH_{NI}/kJmol^{-1}	ΔS_{CI}/R	ΔS_{NI}/R
6	125†	48.5	14.56	62	(48)	19.5	(0.3)	6.99	(0.13)
7	111	52.8	16.59	77	(42)	19.9	(0.3)	6.83	(0.10)
8	98	56.5	18.28	76	(37)	26.9	(0.3)	9.27	(0.10)
9	85	43.2	14.51	76	(12)	24.4	(0.3)	8.40	(0.14)
10	65	47.0	16.73	46	(29)	22.8	(0.3)	8.59	(0.11)
11	76	51.2	17.67	41	(18)	19.6	(0.6)	7.51	(0.23)
12	63	45.1	16.06	41	(24)	20.9	(1.0)	8.00	(0.42)

† From polarizing microscopy a nematic phase was observed at 79°C by supercooling isolated droplets.

Parentheses indicate a monotropic transition.

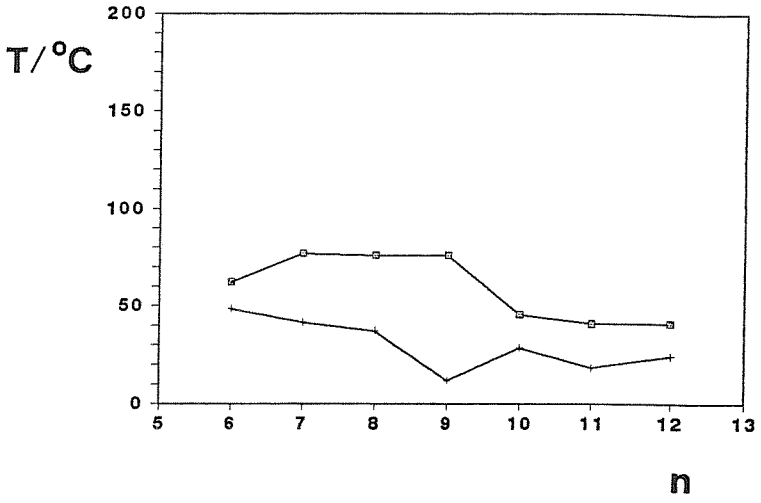

Figure 7. The influence of the length of the alkyl spacer,*n*, on the transition temperatures of 50:50mol% mixtures of the 5D.O*n*O.CB series and TNF. C-I (■), N-I (+).

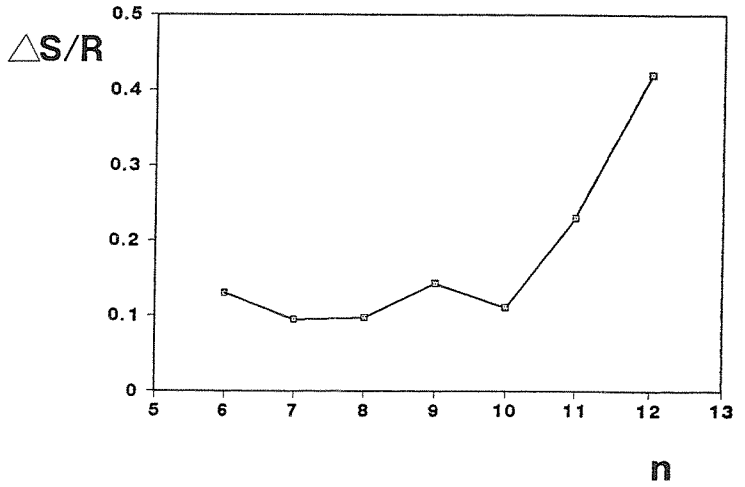

Figure 8. The influence of the length of the alkyl spacer, *n*, on the nematic to isotropic entropy change for 50:50mol% mixtures of the 5D.O*n*O.CB series and TNF.

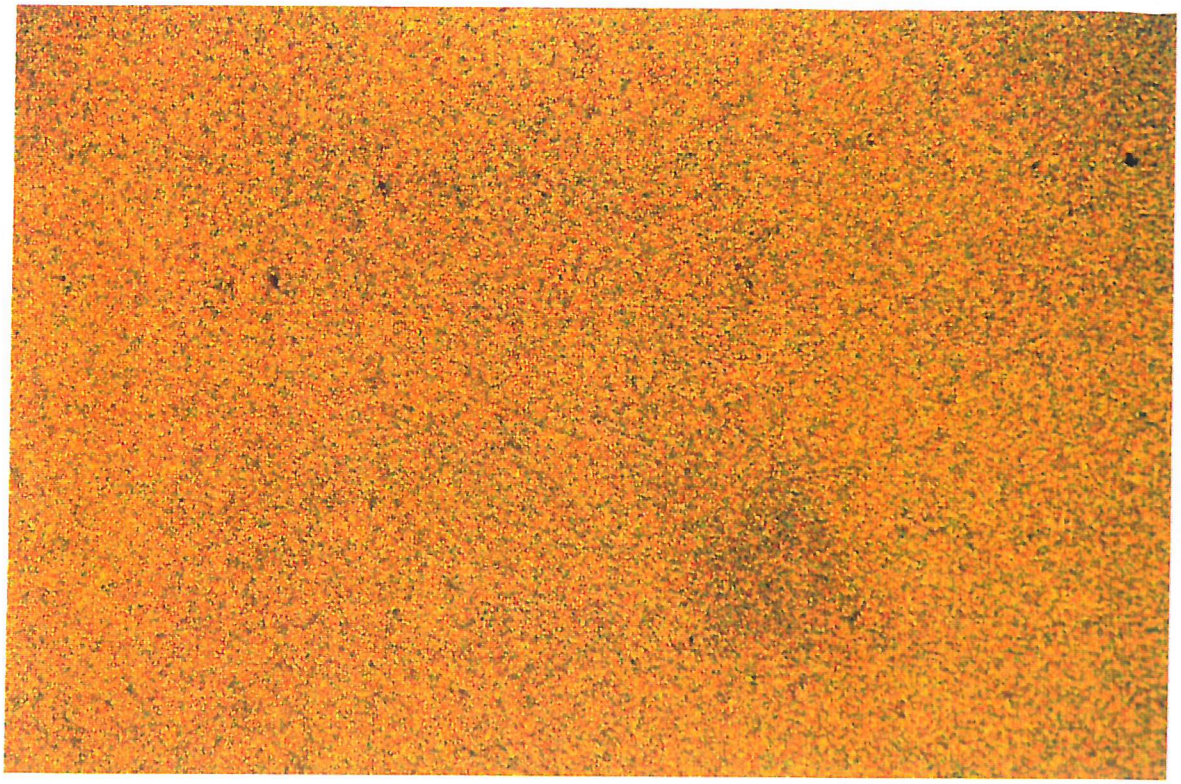

Plate 1. The sanded texture of the nematic phase of the equimolar mixture of 5D.O6O.CB and TNF on cooling from the isotropic phase. 47°C, magnification x100.

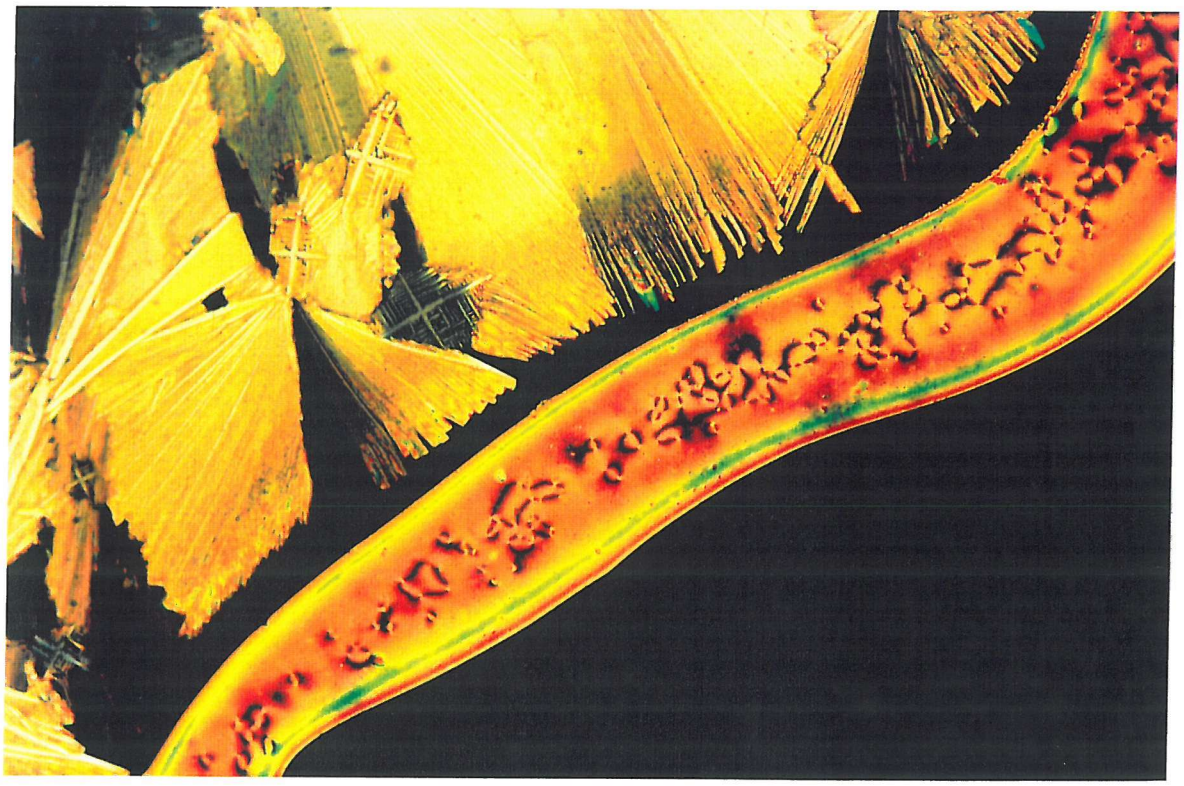

Plate 2. The contact preparation of D.O6O.CB and TNF on cooling from the isotropic phase. From left to right: crystalline D.O6O.CB, nematic phase texture, and isotropic TNF. 122°C, magnification x100.

that there is a gradual decrease in T_{NI} with increasing spacer length. Figure 8 shows the effect of the length of the alkyl spacer, n, on the entropy change for the nematic to isotropic transition for the binary mixtures. For homologues n=6-10 the entropy change is very low ($\Delta S/R \approx 0.1$) indicating the weakness of the transition and is similar in magnitude to that for a discotic nematic to isotropic transition [9]. Homologues n=11 and 12 show a larger clearing entropy change ($\Delta S/R = 0.2$ and 0.4, respectively) and suggest the occurence of new phase behaviour. This new behaviour could be indicative of a columnar nematic phase since the entropy changes for the columnar nematic phases of [(1,2,3,5,6-pentakis(phenylethynyl)benzene-4'-oxy]nonane and tridecane systems were $\Delta S/R = 0.4$ and 0.2, respectively. Unfortunately it was not possible to characterise further the liquid crystalline phase exhibited by the 5D.O*n*O.CB series as during X-ray diffraction and deuterium NMR experiments the sample crystallised.

3.2. *The D.OnO.CB series*

Table 4(*a*) presents the transition temperature, enthalpy and entropy data for seven members of the D.O*n*O.CB series. As expected none was liquid crystalline. The melting points for these compounds are much higher than those of the analogous members of the 5D.O*n*O.CB series because in the latter compounds the terminal chains tend to dilute the core-core interactions and disrupt the crystal packing. Contact preparations between members of the D.O*n*O.CB series and TNF gave a monotropic nematic phase which clearly showed two and four point singularities and which flashed when subjected to mechanical stress (see plates 2 and 3). For all the homologues the thermal stability of the nematic phase was greatest for the 50:50mol% composition as was the case for the 5D.O*n*O.CB series. Table 4(*b*) lists the transition data for the equimolar mixtures of D.O*n*O.CB with TNF. As for the 5D.O*n*O.CB and TNF binary mixtures all of the nematic phases were very monotropic. However, the nematic to isotropic transition temperatures of the D.O*n*O.CB and TNF mixtures are all much higher than their 5D.O*n*O.CB and TNF counterparts as expected. The terminal pentyl chains help to lower both the melting

Table 4. The transition temperatures, enthalpies and entropies of (*a*) the D.O*n*O.CB series and (*b*) their 50:50mol% binary mixtures with TNF.

(*a*)

n	D.O*n*O.CB		
	T_{CI}/°C	ΔH_{CI}/kJmol^{-1}	ΔS_{CI}/R
6	180	70.3	18.71
7	179	48.0	12.86
8	150	42.3	12.03
9	148	30.5	8.79
10	122	23.8	7.23
11	126	34.7	10.51
12	91	11.9	3.93

(*b*)

n	D.O*n*O.CB + TNF (50:50mol%)					
	T_{CI}/°C	T_{NI}/°C	ΔH_{CI}/kJmol^{-1}	ΔH_{NI}/kJmol^{-1}	ΔS_{CI}/R	ΔS_{NI}/R
6	181	134	35.9	0.1	9.28	0.04
7	157	119	19.3	0.4	5.40	0.11
8	139	123	22.8	0.4	6.66	0.13
9	128	104	25.4	0.4	8.80	0.14
10	124	108	12.6	0.3	4.01	0.09
11	142	110	36.0	0.3	10.51	0.08
12	144	107	36.0	0.2	10.45	0.06

Parentheses indicate a monotropic transition.

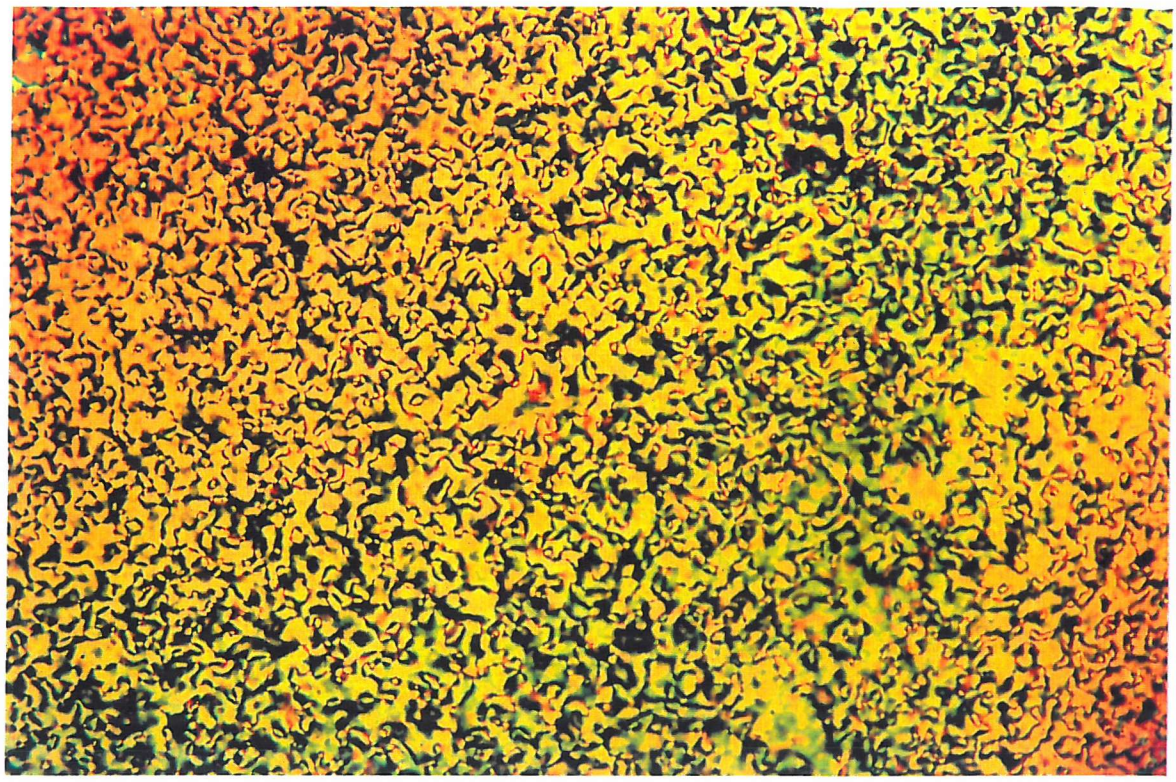

Plate 3. The nematic phase texture of of the equimolar mixture of D.O6O.CB and TNF on cooling from the isotropic phase. 136°C, magnification x100.

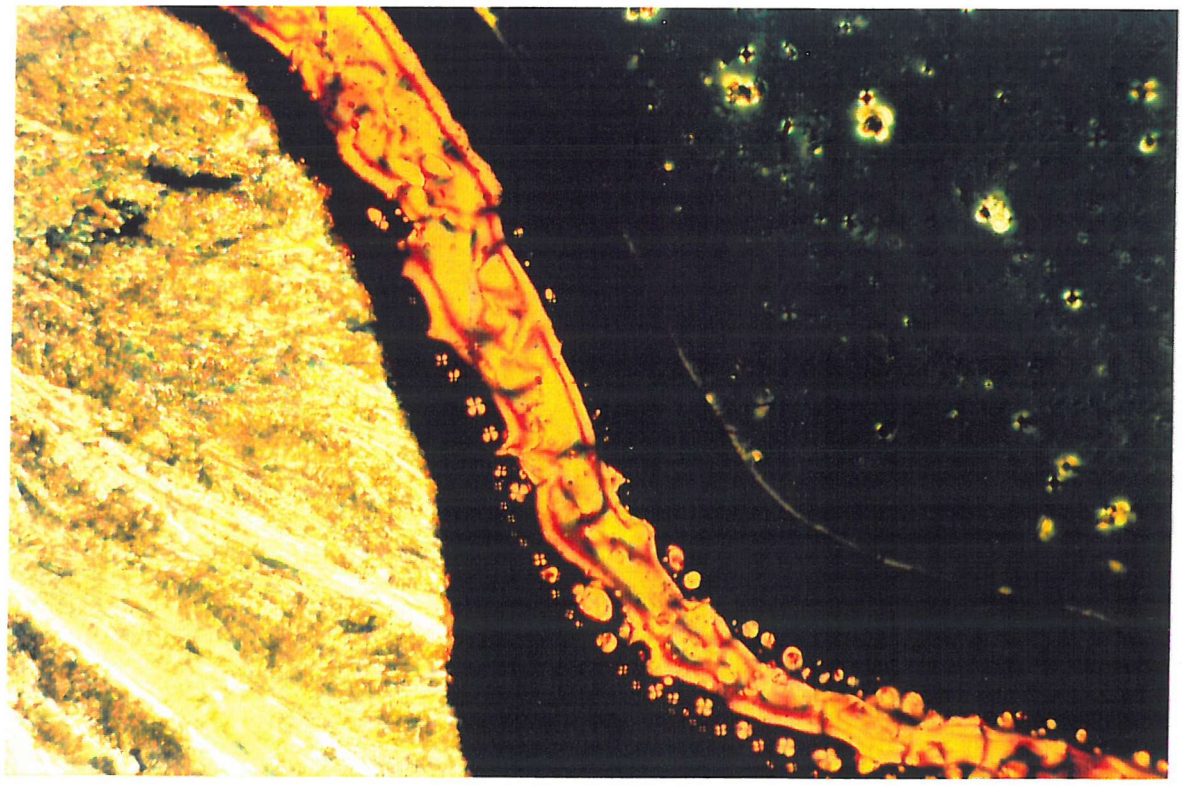

Plate 4. The contact preparation of 5D.O10O.5D and TNF on cooling from the isotropic phase. From left to right: crystalline TNF, nematic phase texture, and the homeotropic nematic phase texture of 5D.O10O.5D. 117°C, magnification x200.

and clearing temperatures by destabilising intermolecular interactions [13]. Figure 9 shows the effect of the length of the alkyl spacer, *n*, on the transitional behaviour of the D.O*n*O.CB and TNF 50:50mol% binary mixtures. There is very little sign of an odd-even effect for the nematic to isotropic transition temperatures of this series. Figure 10 shows the effect of the length of the alkyl spacer, *n*, on the nematic to isotropic entropy change for the equimolar mixtures of D.O*n*O.CB and TNF. The nematic to isotropic entropy changes are all very small and are characteristic of a discotic nematic phase. When n=10-12 the flexible spacer appears to have a different effect on the nematic to isotropic transition entropies compared to the 5D.O*n*O.CB and TNF mixtures. The $\Delta S/R$ values initially rise and peak for the n=9 homologue. On further increasing the spacer length the entropy change decreases again instead of rising as is the case for the 5D.O*n*O.CB series. It appears that a discotic nematic phase persists across the series. Due to the monotropic nature of the nematic phase exhibited by these compounds it was not possible to elucidate the struture of this phase any further.

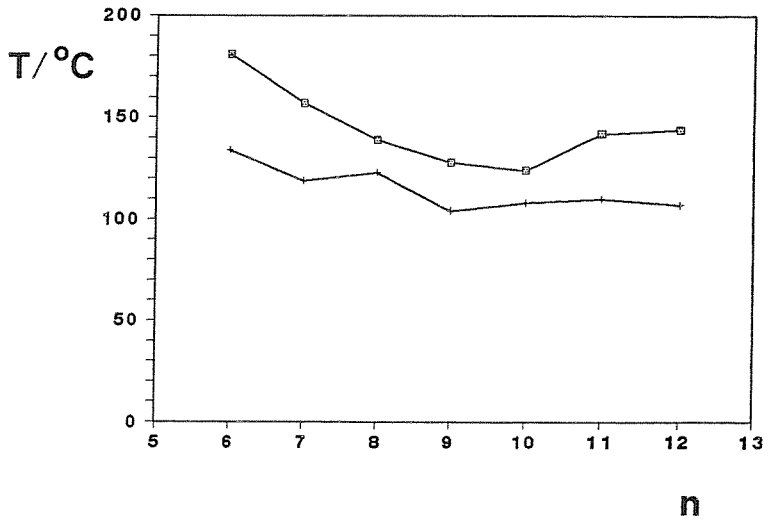

Figure 9. The influence of the length of the alkyl spacer, *n*, on the transition temperatures of 50:50mol% mixtures of the D.O*n*O.CB series and TNF. C-I (■), N-I (+).

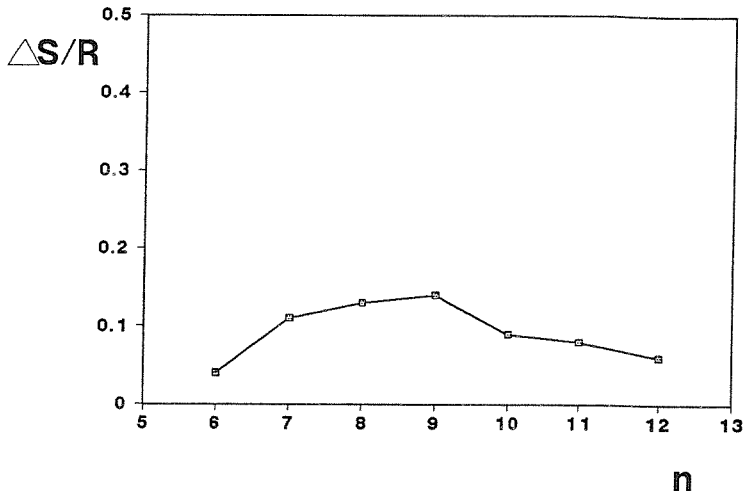

Figure 10. The influence of the length of the alkyl spacer, *n*, on the nematic to isotropic entropy change for 50:50mol% mixtures of the D.O*n*O.CB series and TNF.

3.3. *The 5D.OnO.5D series*

Table 5(*a*) summarises the phase behaviour of two homologues of the 5D.O*n*O.5D series; these data were taken from [8]. Both homologues possess discotic nematic phases: the $n=9$ homologue is monotropic whereas the $n=10$ homologue has a nematic phase range of 24.4°C above the melting point. The nematic to isotropic entropy change for the $n=10$ homologue is very small and the phase was reported as exhibiting a weak optical biaxiality [8]. Contact preparations of both homologues with TNF produced a nematic phase which had a lower T_{NI} value than that of pure 5D.O*n*O.5D (see plate 4). The $n=9$ homologue had the lowest T_{NI} value of the two compounds. The thermal stability of the nematic phase peaked at the 50:50mol% composition. Table 5(*b*) lists the phase behaviour of binary mixtures of 5D.O*n*O.5D

Table 5. The transition temperatures, enthalpies and entropies of the $n=9$ and 10 homologues of (*a*) the 5D.O*n*O.5D series and (*b*) their binary mixtures with TNF.

(*a*)

n	5D.O*n*O.5D					
	$^1T_{CN}$/°C T_{CI}/°C	T_{NI}/°C	$^2\Delta H_{CN}$/kJmol^{-1} ΔH_{CI}/kJmol^{-1}	ΔH_{NI}/kJmol^{-1}	$^3\Delta S_{CN}$/R ΔS_{CI}/R	ΔS_{NI}/R
9	131	(113)†	67.5		20.09	
10	[1]129	154	[2]57.0	0.3	17.06	0.09

† Determined from polarizing microscopy only.

Parentheses indicate a monotropic transition.

(*b*)

n	5SD.O*n*O.5SD + TNF						
	TNF/mol%	T_{CN}/°C	T_{NI}/°C	ΔH_{CN}/kJmol^{-1}	ΔH_{NI}/kJmol^{-1}	ΔS_{CN}/R	ΔS_{NI}/R
9	50	81	84	30.8	0.2	10.53	0.08
10	50	111	114	30.4	0.4	9.52	0.12
10	66	85	113	17.8	0.6	5.98	0.18
10	75	107	112	21.6	1.1	7.43	0.33

and TNF. Both binary mixtures of 50:50mol% TNF and 5D.O*n*O.5D showed an enantiotropic nematic phase. The nematic to isotropic entropy changes for both the $n=9$ and 10 homologues are small and show the transition to be typical of a discotic nematic phase. As the concentration of TNF is increased from 50 to 75mol% in the binary mixture containing the $n=10$ homologue there is a rise in the nematic to isotropic entropy change. This result implies that the ordering in the phase is increasing and that a switchover from discotic nematic to columnar nematic behaviour may be occurring. Interestingly the clearing temperatures for the mixtures containing 50, 60 and 75mol% TNF hardly change.

To understand further the nature of the phases exhibited by the binary mixtures containing 50 and 66mol% TNF we have carried out X-ray diffraction and deuterium NMR studies. First, we shall consider the results obtained from X-ray diffraction experiments. The densitometer traces of the X-ray diffraction patterns of the mixtures containing 50 and 66mol% TNF are shown in figure 11. Discotic compounds have a negative diamagnetic susceptibility and in consequence align with the director orthogonal to the direction of an applied magnetic field. In consequence the director is distributed randomly in a plane which contains the X-ray beam; the scattering pattern is then equivalent to that from a two dimensional powder. The densitometer traces appear therefore to be from an unaligned nematic phase. The small angle and wide angle periodicities for the 50mol% TNF mixture were 17.9Å and 5.4Å, respectively, whereas the respective periodicities for the 66mol% TNF mixture were 17.7Å and 5.0Å (the error in the periodicities is ±0.4Å). In both cases the small angle reflections are more intense than those of the wide angle reflection implying that the face-to-face correlation is low but that the side-by-side periodicity is well-correlated. Thus the local structures of the nematic phases exhibited by both mixtures appear to be the same. The X-ray diffraction studies of pure 5D.O10O.5D carried out in [14] gave the small angle and wide angle periodicities as 19.6Å and 4.5Å, respectively. In this case the wide angle reflection was more intense than that of the small angle. This result is similar to that found for the monomeric hexakis(4-alkyloxyphenylethynyl)benzenes [15]. For the heptyloxy and octyloxy derivatives studied the wide angle was found to be more intense than that of the small angle. In

the octyloxy case the small angle corresponded to a periodicity of 22.6Å and the wide angle to 4.6Å. From the X-ray diffraction results it is clear that the wide angle periodicity corresponds to the face-to-face separation. However, the small angle periodicity does not correspond to the disc diameter or indeed to any of the molecular dimensions. Discrepancy between the molecular dimensions and the periodicities corresponding to the reflections appears to be common for compounds containing multiene discs. Clearly the wide angle reflection can be understood in terms of the spacing created by discs lying on top of each other. However, the small angle reflection does not correspond to the all *trans* molecular length which was calculated to be 47Å from CPK atomic models for 5D.O10O.5D. There have been numerous explanations as to why this is the case and these are addressed in [14].

Thus it appears that the periodicities of the dimer and monomer are very similar and that the spacer does not have an effect on the local order in the discotic nematic phase. Therefore, we should consider the discotic dimer as behaving like two monomers. If we compare the diffraction patterns of 5D.O10O.5D with those of the two binary mixtures we find that the intensities of the small and wide angle reflections are reversed. However, the reflections are centred at approximately the same positions. It appears that the introduction of TNF has the effect of decreasing the face-to-face correlation length and increasing the side-by-side correlation length. It was thought that the nematic phase exhibited by the 66mol% TNF mixture might have a columnar structure, however as described previously the wide angle reflection is broad. The wide angle reflection for columnar nematic phases [4,5] is reported to be sharp and this corresponds to the increased face-to-face correlation length as the molecules stack into columns. Why the 66mol% TNF mixture does not exhibit a columnar nematic phase is not clear but it might be explained in terms of the terminal pentyl chains which hinder the approach of the TNF molecules.

Let us now consider the deuterium NMR study of the 5D.O10O.5D and 50 and 60mol% TNF mixtures. In these experiments 2,4,7-trinitro-9-fluorenone-d_5 was used in which the five deuterons occupy the 1,3,5,6 and 8 positions in the molecule. The synthesis of this compound proceeds via fluorene which is deuteriated in the aromatic

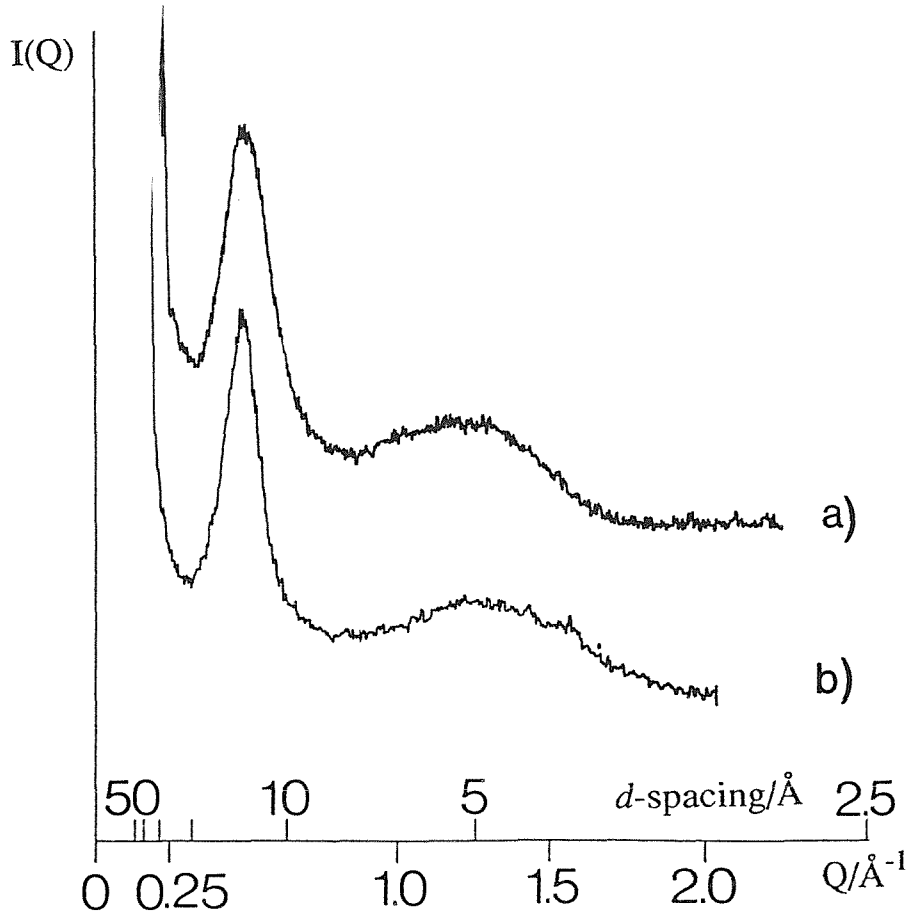

Figure 11. The densitometer traces for binary mixtures of 5D.O10O.5D containing (*a*) 50mol% and (*b*) 66mol% TNF.

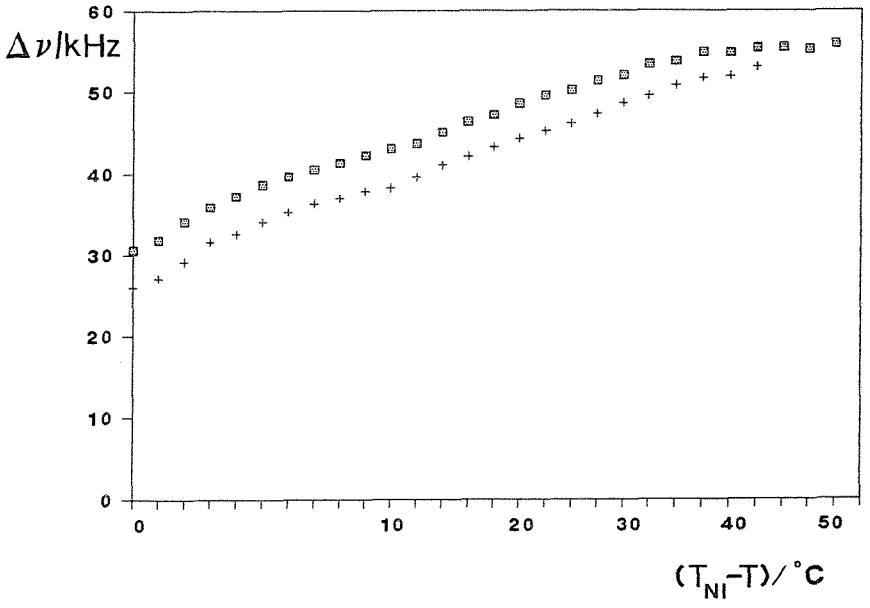

Figure 12. The dependence of the quadrupolar splitting on temperature for the binary mixture of 5D.O10O.5D containing 66mol% TNF (■) and 50mol% TNF (+).

positions by using perdeuteriated benzene and a mixture of triethyl aluminium and aluminium (III) chloride as a catalyst. Subsequent conversion to fluorenone and nitration with a mixture of concentrated sulphuric acid and nitric acid yields 2,4,7-trinitro-9-fluorenone-d_5. The deuterium NMR spectra contain only a single pair of peaks even though the deuterons are not equivalent by symmetry. This can be explained as follows. When TNF-d_5 is dissolved in a discotic liquid crystal phase it tends to behave as a disc in that the Saupe ordering matrix has cylindrical symmetry. At a qualitative level we can think of the TNF molecule as being sandwiched between the disc-like mesogens. Thus the plane of the TNF molecule is essentially orthogonal to the director and along this axis the quadrupolar coupling constant is the same for all deuterons. Since the TNF molecule can spin freely about an axis parallel to the magnetic field all five deuterons become equivalent. Figure 12 compares the quadrupolar splittings for both mixtures (the data are given in tables C1 and C2 in Appendix C) which are large indicating a high orientational order in these systems. The quadrupolar splitting at T_{NI} is 30.6kHz for the 66mol% TNF mixture whereas it is 25.9kHz for the 50mol% mixture. The difference in the quadrupolar splittings is approximately 4kHz across the entire temperature range measured. The order parameter for the effective symmetry axis, orthogonal to the molecular plane, is 0.45 at T_{NI} (rising to 0.81 at T_{NI}-T=40°C) for the 66mol% TNF mixture and 0.40 (rising to 0.77 at T_{NI}-T=40°C) for the 50mol% TNF mixture. These order parameters at T_{NI} are typical for calamitic nematic liquid crystals. These results reflect the difference in the entropy change for the 50 and 66mol% TNF mixtures. However, the entropy change for the 66mol% TNF mixture was approximately 50% greater than that for the 50mol% TNF mixture. The difference in the order parameters is about 13% which implies that the change in the orientational order at the nematic to isotropic transition does not account for the overall entropy change. The results obtained from X-ray diffraction and deuterium NMR imply that the nematic phase exhibited by the 50mol% and 66mol% TNF mixtures is discotic but there is no evidence that the phase could be a columnar nematic. Further studies need to be carried out on the 75mol% TNF mixture to understand if a crossover from discotic nematic to columnar nematic behaviour occurs for these binary mixtures. In addition we need to study a mixture of 5mol% TNF to see if low dopant

concentrations have an effect on the local order within the nematic phase exhibited by 5D.O10O.5D.

3.4. *The D.OnO.D series*

The transition temperatures, enthalpies and entropies of two homologues of the SD.O*n*O.SD series are given in table 6. Both homologues are not liquid crystalline as expected. The melting points for the $n=9$ and 10 homologues of the D.O*n*O.D series are higher than their 5SD.O*n*O.5SD counterparts as expected. Contact preparations between the two homologues and TNF led to the induction of a discotic hexagonal phase (see plates 5 and 6). The clearing transition of the mixture was, in both cases, much higher than the melting points of the pure components (see table 5(*b*). The thermal stability of this phase was greatest at the 50:50mol% composition. The melting entropy changes were considerably lower than those for the pure D.O*n*O.D compounds and this reflects the transition to a highly ordered phase. The mixture of the $n=10$ homologue and TNF had the highest clearing temperature. Unfortunately it was not possible to measure the entropy change for the D_h-I transition as the 50:50mol% binary mixtures of the $n=9$ and 10 homologues and TNF were seen to decompose by DSC analysis at ≈230°C and ≈240°C, respectively. To characterise the discotic hexagonal phase further an X-ray diffraction study was performed on the $n=9$ homologue. The densitometry trace of a powder sample of the $n=9$ homologue, obtained by heating directly into the discotic hexagonal phase is shown in figure 13. The small angle reflection is sharp and corresponds to a periodicity of 13.7Å whereas the wide angle reflection is diffuse and corresponds to a periodicity of 5.2Å (the error in the measured periodicities is ±0.4Å). Thus the side-by-side correlations persist over a much larger distance than those of the face-to-face periodicity. The X-ray diffraction pattern of the discotic hexagonal ordered phase in [5] gave a small angle reflection of considerably higher intensity than that of the wide reflection. However, the wide angle reflection was sharper than that obtained for D.O9O.D and suggests that the columns are more ordered. The periodicity of 5.2Å is similar to that found for the 5D.O10O.5D and TNF mixtures

Table 6. The transition temperatures, enthalpies and entropies for (*a*) the n=9 and 10 homologues of the D.O*n*O.D series and (*b*) their 50:50mol% binary mixtures with TNF.

(*a*)

	D.O*n*O.D		
n	T_{CI}/°C	ΔH_{CI}/kJmol^{-1}	ΔS_{CI}/R
9	190	42.9	11.23
10	216	51.4	12.74

(*b*)

	D.O*n*O.D + TNF (50:50mol%)					
n	T_{CDh}/°C	T_{DhI}/°C	ΔH_{CDh}/kJmol^{-1}	ΔH_{DhI}/kJmol^{-1}	ΔS_{CDh}/R	ΔS_{DhI}/R
9	92	266	16.5	†	5.44	†
10	206	280	15.6	†	3.92	†

† DSC analysis showed the sample to decompose before reaching the clearing temperature.

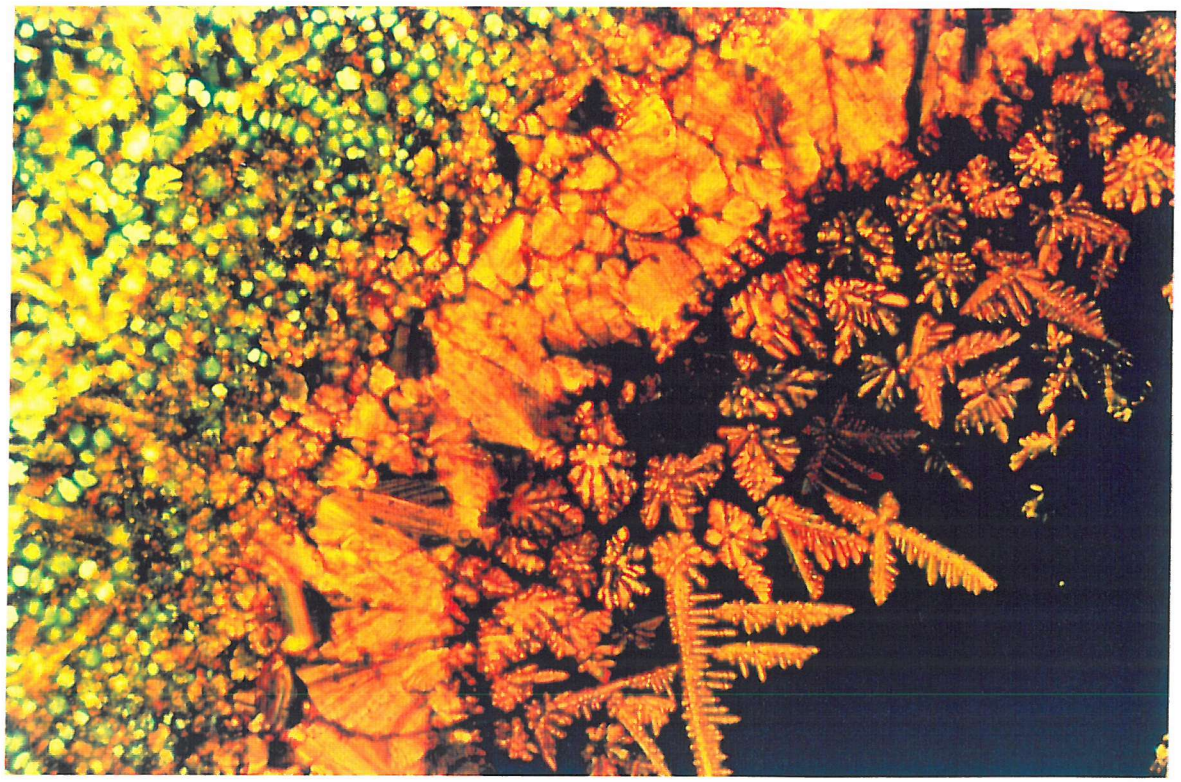

Plate 5. The contact preparation of D.O10O.D and TNF on cooling from the isotropic phase. From left to right: crystalline D.O10O.D, the discotic hexagonal phase texture, and isotropic TNF. 159°C, magnification x200.

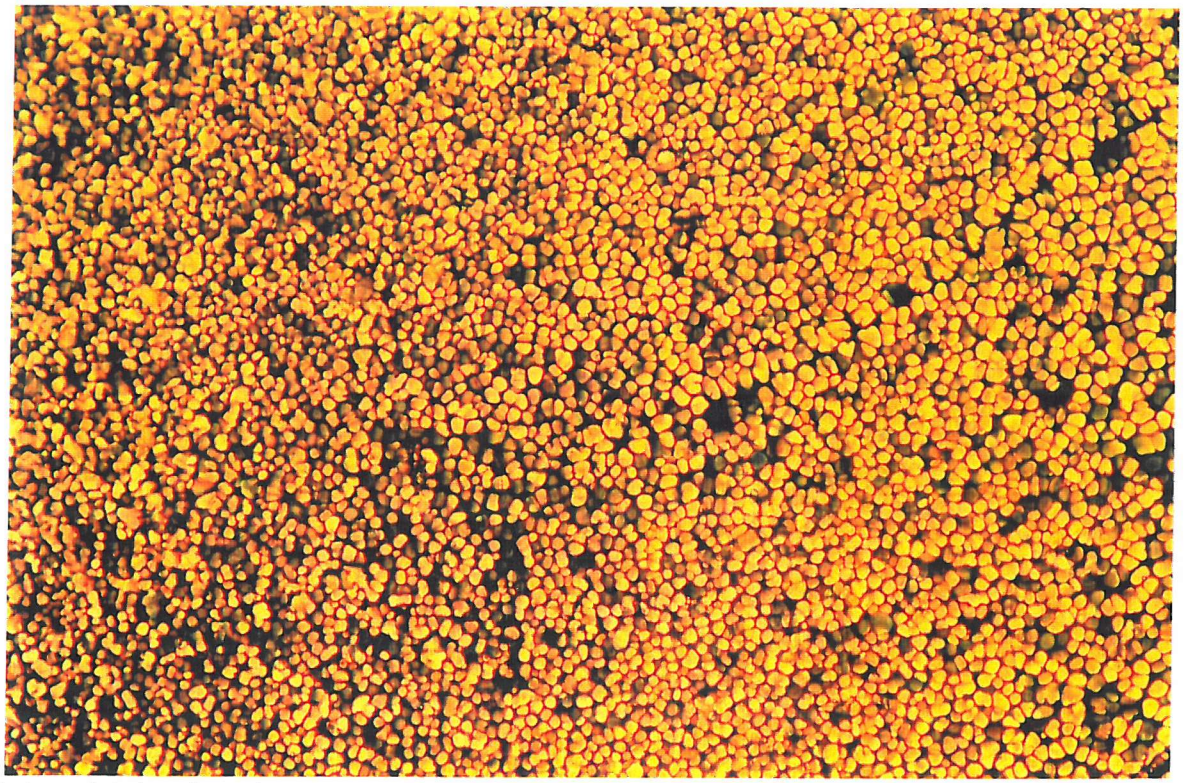

Plate 6. The discotic hexagonal phase texture of the equimolar mixture of D.O10O.D and TNF on cooling from the isotropic phase. 270°C, magnification x100.

mentioned previously. However the periodicity corresponding to 13.7Å is hard to account for since the all *trans* molecular length is 33Å as measured from CPK atomic models. The fact that the small angle reflection corresponds to such a small distance may again result from the fact that the two discs in the dimer should be regarded as individual units and that the spacer does not influence the local order within the phase. Clearly the rationalisation of the X-ray diffraction patterns of such charge transfer mixtures containing TNF is difficult and before we have a real understanding of their phase behaviour much more work needs to be carried out.

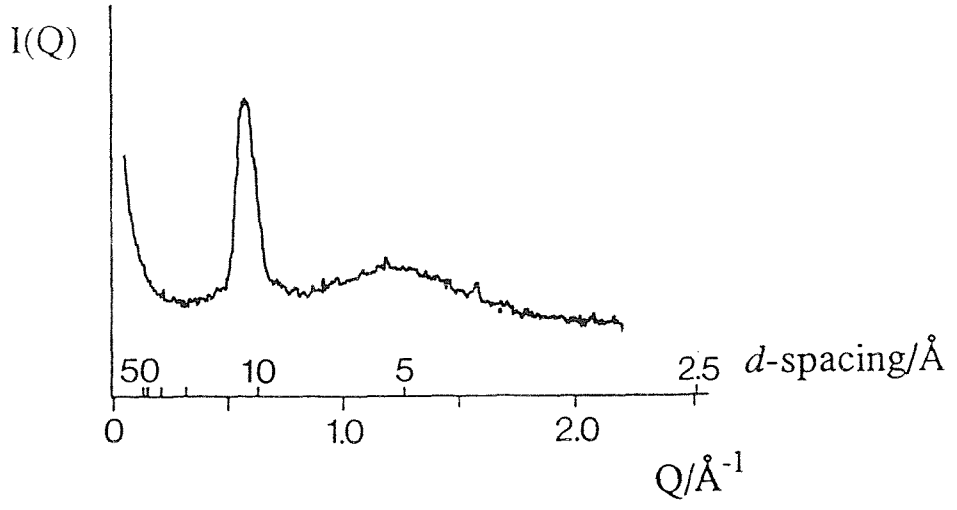

Figure 13. The densitometer trace of the 50:50mol% binary mixture of D.O*n*O.D and TNF.

4. Conclusions

In this chapter we have presented two series of non-symmetric dimers composed of rod-like and disc-like units. The 5D.O*n*O.CB series were not liquid crystalline and when mixed with TNF gave a very monotropic liquid crystalline phase which had a very indistinct optical texture. However, it flashed when mechanically stressed and

was thus nematic-like. On the basis of the very low clearing transitional entropy changes for the n=6-10 homologues of this series we can tentatively assign this liquid crystalline phase as being discotic nematic. The n=11 and 12 homologues were also nematic-like and had, respectively, clearing transitional entropy changes two and four orders of magnitude higher than those of the other homologues. Unfortunately, the possibility that these phases were columnar could not be examined owing to their monotropic nature. The D.O*n*O.CB series of compounds were, as expected, not liquid crystalline. When mixed with TNF they exhibited a very monotropic nematic phase which was characterised by a well-defined schlieren texture. The clearing transitional entropy changes were very low for all members of this series and thus the nematic phase was assigned as being a discotic nematic. The effect of mixing a discotic dimer with TNF was examined with the 5D.O*n*O.5D compounds. An enantiotropic nematic phase with a characteristic schlieren texture was exhibited for equimolar mixtures. However, the clearing temperature of the mixture was found to be markedly lower than that of pure 5D.O*n*O.5D. As the concentration of TNF in the mixture with the n=10 homologue increased, so the entropy change for the nematic to isotropic transition was found to increase. Mixtures of 5D.O10O.5D and 50 and 66mol% TNF were studied by both X-ray diffraction and deuterium NMR. X-ray diffraction showed the local structure of both phases to be very similar. It was found that the introduction of TNF led to an increase in the side-by-side correlation but to a decrease in the face-to-face correlation distance compared to the diffraction pattern of pure 5D.O10O.5D from [14]. The deuterium NMR studies showed both phases to be similar such that the order parameter at the nematic to isotropic transition was 0.45 and 0.4 for the 66mol% and 50mol% TNF mixtures, respectively. To be sure if a crossover from discotic nematic to columnar nematic phase behaviour is occurring we must examine the 75mol% TNF mixture by deuterium NMR as well as by X-ray diffraction. In addition at present we do not know the phase behaviour of the entire composition range of 5D.O10O.5D and TNF and so the phase diagram of this system needs to be studied in detail. In comparison to the 5D.O*n*O.5D compounds the effect of mixing TNF with homologues from the D.O*n*O.D series is striking. For both the n=9 and 10 homologues a liquid crystalline phase was formed which had an optical texture characteristic of a discotic hexagonal phase. Further, in

both instances the clearing temperature of this phase was well above that of the pure components such that this phase can be regarded as being induced and not revealed due to eutectic behaviour as for the 5D.O*n*O.CB, D.O*n*O.CB and 5D.O*n*O.5D compounds. We have studied the local order of the discotic hexagonal phase of the $n=9$ homologue. The powder X-ray diffraction pattern, which showed the presence of a strong side-by-side correlation and a relatively weaker face-to-face correlation, is similar to that observed for the discotic hexagonal ordered phase reported in [5]. As was the case with the X-ray diffraction studies of the 5D.O10O.5D and TNF mixtures the small angle distance did not correspond to any of the molecular dimensions. This appears to be a common feature of compounds which contain multiene disc-like units. Clearly work on charge transfer mixtures of highly unsaturated discotic compounds and electron acceptors such as TNF is still in its infancy. Before we can begin to understand their phase behaviour much more research is required.

References

[1] de Jeu, W.H., Longa, L., and Demus, D., 1986, *J. chem. Phys.*, 84, 6410.

[2] Diele, S., Pelzl, G., Weissflog, W., and Demus, D., 1988, *Liq. Crystals*, 3, 1047.

[3] Kolbe, A., and Pelzl, G., 1982, *Adv. Molec. Relax. Interact. Proc.*, 24, 251.

[4] Bengs, H., Karthaus, O., Ringsdorf, H., Baehr, C., Ebert, M., and Wendorff, J.H., 1991, *Liq. Crystals*, 10, 161.

[5] Praefcke, K., Singer, D., Kohne, B., Ebert, M., Liebmann, A., and Wendorff, J.H., 1991, *Liq. Crystals*, 10, 147.

[6] Gündogan, A., Liebmann, A., Praefcke, K., Singer, D., and Wendorff, J.H., 1992, *Presented at the 14th International Liquid Crystal Conference*, Pisa June 21-26, Italy; *Liq. Crystals* (in the press).

[7] Praefcke, K., Singer, D., and Kohne, B., 1993, *Liq. Crystals*, 13, 445.

[8] Praefcke, K., Kohne, B., Gündogan, B., Singer, D., Demus, D., Diele, D., Pelzl, G., and Bakowsky, U., 1991, *Molec. Crystals liq. Crystals*, 198, 393.

[9] Praefcke, K., Kohne, B., Singer, D., Demus, D., Pelzl, G., and Diele, S., 1990, *Liq. Crystals*, 7, 589.

[10] Alben, R., 1973, *J. chem. Phys.*, 59, 4299.

[11] Tinh, N.H., Destrade, C., and Gasparoux, H., 1979, *Phys. Lett.* A, 72, 251.

[12] Kreuder, W., Ringsdorf, H., Hermann-Schönherr, O., and Wendorff, J.H., 1987, *Angew. Chem. Int. Ed. Engl.*, 26, 1249.

[13] Gray, G.W., 1974, *Liquid Crystals and Plastic Crystals*, Vol. 1, edited by G.W. Gray and P.A. Winsor (Ellis Horwood, Ltd., Chichester), Chap. 4.

[14] Taylor, L., 1991, Ph.D. Thesis, Southampton University.

[15] Ebert, M., Jungbauer, D.A., Kleppinger, R., Wendorff, J.H., Kohne, B., and Praefcke, K., 1989, *Liq. Crystals*, 4, 53.

Appendix A

The structural characterisation of the synthesised materials

Compounds were structurally characterised by means of IR spectroscopy (Perkin-Elmer 1600 series FTIR spectrometer) and ^{1}H NMR spectroscopy (JEOL FX90Q Fourier transform NMR spectrometer) as well as with a Bruker AM 360MHz NMR spectrometer for fine structure analysis. End-products were also characterised by mass spectroscopy (VG 70-250) and in some instances elemental analysis was also employed to ensure the determined compounds were obtained.

Appendix B

Table B1. The dependence of the quadrupolar splitting on temperature for 2,3,4-tri-*n*-hexyloxycinnamic acid-d_1.

$(T_{NI}-T)$/°C	$\Delta\nu$/Hz
0	25349
1	29805
2	31595
3	32714
4	34586
5	36783
6	37902
8	39164
10	39978

Table B2. The dependence of the quadrupolar splitting on temperature for 4-*n*-hexyloxycinnamic acid-d_1.

$(T_{NI}-T)$/°C	$\Delta\nu$/Hz
0	37825
1	39124
2	40418
3	41039
4	43422
5	45017
6	47091
7	47482
8	49115
10	51147
12	52386
14	53817
16	55748
18	57015
20	57729
22	59281
24	60032
26	60554
28	61564
30	61147

Appendix C

Table C1. The dependence of the quadrupolar splitting on temperature for the 5D.O10O.5D and 50mol% TNF-d_5 binary mixture.

$(T_{NI}-T)$/°C	$\Delta\nu$/Hz	$(T_{NI}-T)$/°C	$\Delta\nu$/Hz
0	25451	23	45431
1	27120	24	46163
2	29154	25	46509
3	31616	26	46956
4	32552	27	47384
5	34078	28	47607
6	35258	29	48462
7	36316	30	48665
8	37028	31	48950
9	37862	32	49703
10	38249	33	49886
11	39612	34	49601
12	40100	35	50191
13	41077	36	50863
14	41382	37	51412
15	42134	38	51758
16	42440	39	51737
17	43294	40	51656
18	43772	41	52205
20	44312	42	53080
21	44881	43	52286
22	45227		

Table C2. The dependence of the quadrupolar splitting on temperature for the 5D.O10O.5D and 66mol% TNF-d_5 binary mixture.

$(T_{NI}-T)$/°C	$\Delta\nu$/Hz
0	30619
1	31860
2	34139
3	35909
4	37231
5	38696
6	39673
7	40548
8	41321
9	42257
10	43070
11	43742
13	45085
15	46407
17	47241
20	48604
22	49601
24	50212
27	51432
30	52063
34	53507
36	53833
38	54911
40	54850
42	55440
44	55501
46	55278
48	55928